Base-level fall, knickpoint retreat and transient channel morphology: The case of small bedrock rivers on resistant quartzites (Isle of Jura, western Scotland)

Miguel E. Castillo-Rodríguez
(M.Sc, National Autonomous University of Mexico)

Thesis submitted for the degree of Doctor of Philosophy

School of Geographical and Earth Sciences

University of Glasgow

March 2011

Dedication

To Esperanza and my familiy.

Abstract

Understanding the link between tectonics and climate and their consequences in landscape evolution is a major current issue in Earth sciences. Bedrock rivers are an important component of the landscape because they transmit changes in tectonic and/or climatic conditions by setting bed rock incision rates to which the landscape must be adjusted. Nevertheless, there remain unresolved issues in relation to bedrock river processes and response to perturbation. The effects caused by propagation of a knickpoint triggered by a sudden drop in base-level remain to be fully clarified. Questions about rates of knickpoint recession, the control exerted by structure and lithology, the morphological response of rivers after knickpoint recession and whether bedrock incision rates are re-established after the passage of a knickpoint, as theory predicts, are all issues that need to be clarified. Moreover, the estimation of bedrock incision, which is key to understand transience in landscapes, has relied on the stream power model, mainly tested on large fluvial settings. Whether the stream power model is valid for small bedrock rivers is not well understood. Some of these questions are tackled in this research, by studying small bedrock river catchments. The case of a knickpoint propagation on a homogeneous resistant lithology (quartzite), triggered by an instantaneous base-level lowering (18 m in 13.6 ka), is evaluated here, as well as the effect of structure and the morphological response of rivers to base-level fall. Two approaches were followed: (1) stream profile analysis using slope-area and distance-slope plots and (2) the analysis of terrestrial cosmogenic nuclides to obtain erosion rates. The Isle of Jura, located in the west coast of Scotland, was selected as natural laboratory because bedrock rivers incise the landscape and rapid rock uplift resulting from glacio-isostatic rebound after the Last Glacial Maximum has left the Jura landscape in transience. The present research is organised in seven chapters. In chapter 1, the motivation for this research is presented. In chapter 2, a review of theory underpinning research on bedrock rivers, landscape evolution and knickpoint generation, is detailed. The relevant studies in the field are also reviewed. The physical setting of Jura is characterised in chapter 3, as well as the morphometry of catchments, stressing the

effect of Quaternary glaciation on the landscape of Jura. Unpublished exposure ages and analysis of the resultant raised beaches ($\sim$ 35 m OD) of Jura's west coast are used to demonstrate a sudden drop in base-level in Jura $\sim$13.6 ka. Chapter 4 details how stream long-profiles were extracted and how the slope-area (SA) and distance-slope (DS) analyses were undertaken. This chapter 4 shows that the Jura rivers have strong imprints related to glacial processes and base-level fall, making it difficult to use SA and DS models to estimate channel incision as has been done for large fluvial settings. Chapter 5 is explains how the base-level fall knickpoints were identified and it is shown that stream discharge is a first-order control on knickpoint propagation. Structure and lithology, on the other hand, are not first-order controls on knickpoint recession. Chapter 5 also evaluates the vertical distribution of knickpoints and morphological response of rivers after knickpoint migration, with the results indicating that stream power controls the vertical distribution of knickpoints and the morphological response of rivers to base-level fall. A threshold of $\sim$5 km^2, where rivers' ability to modify their channel, resulting in a channel convex profile, is also identified. In chapter 6 the problem of bedrock incision and the role of sediment is tackled. Based on the sampling of sediment in fieldwork, it is demonstrated that the median fraction in the rivers of Jura is $\approx$ 45 mm and grain-size neither fines nor increases with stream discharge and channel slope, strongly indicating that detachment-limited conditions are likely to control bedrock incision. In the second part of chapter 6, the incision rates upstream and downstream of the base-level fall knickpoint are obtained to test whether incision rates are re-established after knickpoint propagation. Incision rates were obtained from the concentrations of cosmogenic ^{10}Be in samples extracted from the river bed. The results indicate that incision rates are not re-established at an expected value of $\approx$ 0.1 m/k yr after knickpoint migration. Rather, incision rates below the knickpoint remain somewhat elevated ($\approx$ 0.5 m/k yr) reflecting: (1) ongoing base-level fall, and/or (2) the propagation of younger knickpoints ($<$ 13.6 ka) in those transient reaches. The cosmogenic-derived incision rates were tested with different bedrock incision rules. The results indicate that the stream power model is a good

predictor for channel incision, even for the case of small catchments. In chapter 7 the conclusions of this research are provided.

Contents

List of Figures

List of Tables

Acknowledgements

My postgraduate research at the University of Glasgow would not be possible without the trust of my first supervisor Prof. Paul Bishop, who has always been supportive, enthusiast and helpful and guided me into the roots of the fascinating world of geomorphology. Thank you very much Paul. Special thanks also goes to my sponsor, The National Council of Science and Technology of Mexico (CONACYT), who awarded me with a scholarship (Ref. 207555) to pursue a PhD degree in the UK.

I also want to express my gratitude to my other supervisors Dr. Derek Fabel and Dr. John Jansen, who have always been helpful, patient and were in the will to discuss with me the bunch of doubts that came during my research. Also I want to thank Prof. Susan Waldron for her administrative support, especially during the last part of my research. I want to give thanks to Maria Miguens for her support during my stay at SUERC.

I also want to thank to the academics and postgraduate students of the Department of Geographical and Earth Science (now School) who always were helpful and gave me an enriching feedback during the multiple presentations of my PhD research.

I want to thank Esperanza, for her support in my personal life and in the academia. Also lot of thanks go to Delia Gheorghiou, Dr. Tibi Codiliean, Reka Fülop, Dr. Leah Gibbs and Dr. Alberto Perez-Huerta, for their friendship and the moments we shared in our transit in Glasgow.

Author's declaration

The material presented in this thesis is the result of independent research carried out by myself during three and a half years at the School of Geographical and Earth Sciences of the University of Glasgow. The research was supervised by Prof. Paul Bishop, Dr. Derek Fabel and Dr. John Jansen. The intellectual arguments presented here represent my own research. The published or unpublished work by other authors have been given full acknowledgement in the text. This work has not been submitted for any degree or academic qualification.

Miguel Castillo

March, 2011

Chapter 1

Introduction

1.1 Motivation

Geomorphology aims to understand the processes that modify the landscape on Earth and how landscapes evolve in time and space. Traditionally, research on landscape evolution has focused on understanding the way that fluvial processes operate in the landscape. Moreover, the nature of rivers as agents of erosion and transport of sediments, makes them specially important agents of modification of surfaces uplifted by tectonic forces, by mobilising sediments generated by weathering and/or other erosional processes (e.g., glacial, mass wasting, aeolian) (Leopold et al., 1964; Selby, 1985; Summerfield, 1991; Burbank and Anderson, 2001). The dynamics of alluvial rivers and their relationship with tectonics is more or less known (Holbrook and Schumm, 1999). However, for the case of bedrock rivers, the dynamic, behaviour, evolution and response to tectonics are not yet fully understood (Seidl and Dietrich, 1992; Tinkler and Wohl, 1998). Consequently, in the last twenty years bedrock rivers have become a central topic in research on landscape evolution.

Bedrock rivers are important components of the landscape because they set a primary control on the erosion of mountainous topography. Erosion and landscape evolution in large mountain ranges of regions experiencing high rates of rock uplift, including the Himalaya (Leland et al., 1998; Kirby and Whipple, 2001; Lavé and Avouac, 2001; Seong et al., 2008), the mountain range of Taiwan (Stolar et al., 2007;

Turowski et al., 2008) or in relatively steady tectonic areas such as the west coast of USA, including California (Stock et al., 2005a; Clark et al., 2005), Washington (Wegmann and Pazzaglia, 2002; Tomkin et al., 2003), and Oregon (Montgomery, 2001; VanLaningham et al., 2006), are mostly driven by the incision of bedrock rivers. Nonetheless, incision is not confined to areas of highly active crustal deformation, but is also a key element in the evolution of old mountain ranges, such as the Appalachians (Hack, 1957; 1973; Frankel et al., 2007), landscapes in passive margins like in southeast Australia (Goldrick and Bishop, 1995; 2007), in young volcanic terrains like in Alaska (Whipple et al., 2000b) or in the Hawaiian volcanic slopes (Seidl et al., 1994).

Many papers have been published in the last two decades aimed at estimating channel incision in bedrock rivers and its response in different tectonic settings (e.g., Wohl and Ikeda, 1997; 1998; Stock and Montgomery, 1999; Whipple et al., 2000b; Montgomery, 2001; Snyder et al., 2000; Duvall et al., 2004). Other aspects are starting to be addressed including the importance of strath-terraces as geomorphic markers to estimate channel incision (Leland et al., 1998; Hancock and Anderson, 2002; Wegmann and Pazzaglia, 2002; Pan et al., 2003; Montgomery, 2004; Wohl, 2008), and bedrock rivers downstream hydraulic geometry (Montgomery and Gran, 2001; Wohl, 2004; Finnegan et al., 2005; Amos and Burbank, 2007; Whittaker et al., 2007; Wobus et al., 2008).

A major issue in landscape evolution research is if it is possible to achieve a steady-state condition in the landscape (Whipple, 2001; 2004). The steady-state is reached when landforms are in equilibrium with the erosional system and these become time-independent (Hack, 1960; 1975), transience is in contrast, a phase of disequilibrium in the erosional system (Whipple and Tucker, 1999). Bedrock rivers studies have used the stream power model, assuming that erosion is dominated by detachment-limited conditions where plucking is the main processes causing bedrock incision, in order to test for the presence of equilibrium in a channel (Whipple

and Tucker, 1999). Some studies have demonstrated that some landscapes are not in steady-state (Whipple, 2001; Clark et al., 2005; Harkins et al., 2007; Whittaker et al., 2007; Reinhardt et al., 2007a; Attal et al., 2008; Cowie et al., 2008). Apparently, reaching the condition where tectonic uplift is balanced with the erosion requires high rates of both rock uplift and erosion, as has been observed for the case of the mountain range of Taiwan (Whipple, 2001; Dadson et al., 2003; Stolar et al., 2007) and in the coast range of Oregon (Montgomery, 2001). The dynamic interaction between tectonics, relief, and climate reduces the possibility of maintaining a long duration of a steady-state (Whipple, 2001). Moreover, sudden tectonic movements, eustatic sea level changes or a combination of both, generate fluctuations in base-level (Snyder et al., 2002; Whipple, 2004). A drop in base-level generates a disequilibrium in the fluvial system and may trigger knickpoints that propagate through the fluvial network (Leopold et al., 1964; Burbank and Anderson, 2001; Whipple, 2004; Bishop et al., 2005; Reinhardt et al., 2007a). Understanding transience by the knickpoint propagation is therefore fundamental to understand equilibrium in the landscape and, ultimately, the landscape's evolution.

The presence of knickpoints in rivers was recognised early in geomorphology (e.g., Gilbert, 1877; Davis, 1932; von Engeln, 1940). Flume experiments and further modelling of their behaviour and evolution have been proposed for alluvial and bedrock beds (e.g., Holland and Pickup, 1976; Gardner, 1983; Wolman, 1987; Howard, 1998; Haviv et al., 2010). However, the formation and propagation of knickpoints on bedrock rivers remains poorly understood (Crosby and Whipple, 2006). The case of knickpoints generated by a drop in base-level have re-captivated the attention of geormophologists recently (e.g., Whipple, 2004; Bishop et al., 2005; Crosby and Whipple, 2006; Berlin and Anderson, 2007; Frankel et al., 2007). Knickpoints are key elements of rivers because they contain and send information about changes of base-level to which the landscape must be adjusted (Whipple and Tucker, 1999; Bishop et al., 2005). Understanding the so called bottom-up processes in a fluvial system (i.e., knickpoint propagation and its effects, Bishop, 2007) is essential in

order to understand disequilibrium.

Understanding landscape transience is not an easy task. There are still missing pieces which need to be fitted in the puzzle of bedrock rivers and the propagation of knickpoints. One missing piece is the role of lithology and structure in relation to knickpoint propagation. Erosion rates in bedrock channels also need to be quantified empirically. Moreover, understanding the evolution of bedrock rivers in transience is crucial to test the theory that predicts that a concave-upward profile is indicative of steady-state (Howard, 1994; Whipple and Tucker, 1999).

Inspired by the necessity to explore and understand the role of bedrock rivers in a transient landscape, in this research I focus on the propagation of knickpoints triggered by a drop in base-level, its morphological response and estimation of bedrock incision rate after the knickpoint propagation for the case of small bedrock river catchments ($< 100\text{km}^2$). The isle of Jura (west coast of Scotland) has been selected as a natural laboratory because a sudden drop in base-level has presumably occurred caused by the rock uplift driven by a glacio-isostatic rebound initiated ~ 16 ka (Lambeck, 1993b; Peltier, 1996). The landscape in Jura is mostly mountainous and lithology is relatively homogeneous with well defined structure. Quaternary landscape changes due to climatic and lithospheric processes are therefore, ideal to evaluate the propagation of knickpoints in small bedrock rivers in transience.

The present research is organised in seven chapters. In Chapter 2 a review of the studies focused on bedrock rivers in different settings is provided. In the same chapter the theoretical framework that underpins the research of bedrock rivers is also introduced. In Chapter 3 are provided the details of the physical setting and geology of Jura, the Quaternary processes (i.e., glaciations, deglaciation and sea-level change) that generated the fall of rivers' base-level are also detailed. Chapter 4 explains the approach followed here to study the Jura bedrock rivers. The base-level fall knickpoints are treated in Chapter 5, and it is also analysed the morphology

of the reaches downstream of these base-level fall knickpoints. Chapter 6 provides an analysis of bed sediment and cover and bedrock exposure as well as the results of the erosion rates using measurements of *in situ* produced cosmogenic ^{10}Be. The details of the strategy followed and the hypothesis tested are also explained. The final results and the conclusions are presented together in Chapter 7. The appendices show at the end, present the data used and/or produced in this research.

Chapter 2

The role of bedrock rivers in landscape evolution

2.1 Introduction

The importance of bedrock rivers as components controlling the erosion of landscape was recognised early by Gilbert (1877) who wrote about bedrock rivers in his report of the Henry mountains. Gilbert discussed the role of sediment size and sediment supply as well as channel slope (declivity in Gilbert's terminology) as factors controlling the rate of incision into bedrock. He also foreshadowed principles that later came to constitute the notion of dynamic equilibrium that was formally introduced by Hack (1960). Interest in bedrock channels following Gilbert's report remained somewhat minor with most of the studies focused on understanding alluvial and gravel rivers, with an increasing number of studies in the middle of the twentieth century which resulted in the formulation of the concept of the hydraulic geometry (Leopold et al., 1964; Chorley et al., 1984; Knighton, 1998). The renewed interest in bedrock rivers was initiated by Hack (1957) who proposed the dynamic equilibrium concept as an alternative explanation for landscape evolution, and contesting the Davisian approach (Hack, 1960; 1975). Hack implicitly set the concept of dynamic equilibrium on streams by proposing the use of the stream gradient index to assess the adjustment of channel gradient to incision on a different lithology and under the effect of diastrophic forces (Hack, 1973).

Undoubtedly, the emergence of plate tectonic theory gave rise to new explan-

ations in the Earth sciences, becoming its new, and still current central paradigm (Thorn, 1988). Plate tectonics provide a solid framework to investigate landscape evolution because tectonic uplift and climate can be coupled together in a systematic approach that provides a solid explanation for long-term landscape evolution. The last decade of the twentieth century marks a milestone for landscape evolution studies because several questions concerning the link between tectonics and climate began to emerge. Thus, the paradox posed by Molnar and England (1990) concerning mountain uplift, incision and its effect on the denudational uplift with possible feedback to climate. Another important contribution was the recognition that mountain erosion enhances rock uplift caused by an isostatic response to mass removal (e.g., England and Molnar, 1990; Gilchrist et al., 1994; Montgomery, 1994) which have further implications in the denudation of post-orogenic settings (Baldwin et al., 2003; Bishop, 2007).

The landscape evolution studies (Bishop, 2007; Tucker and Hancock, 2010) have been benefited by major advances in the geochronological techniques, such as the measurement of terrestrial cosmogenic nuclides (Cerling and Craig, 1994; Cockburn and Summerfield, 2004; Bishop, 2007) and the development of Surface Processes Models (Codilean et al., 2006; Bishop, 2007; Tucker and Hancock, 2010) explaining the research of the long-term erosion in the landscape. Because bedrock rivers drive the incision of the landscape (Hancock et al., 1998; Whipple and Tucker, 1999), they have become central to the research on landscape evolution. As a result, an increasing number of papers have appeared since the 1990s aimed at understanding the dynamics, forms and long term incision of these important components of the landscape. Interestingly, most of the research during this period has been oriented (1) to test the presence of steady-state in a landscape, (2) to evaluate the effects of base-level fall and (3) to detect tectonic signals in streams. In contrast, less effort has been given to the effect of lithology on bedrock incision and channel morphology; incision in landscapes in transience has only received attention quite recently (e.g., Crosby et al., 2007; Finnegan et al., 2007; Harkins et al., 2007).

Although there has been increasing interest in the study of bedrock rivers, as confirmed by the number of papers published on this topic, some processes in bedrock rivers remain poorly known (Tinkler and Wohl, 1998). Few studies have provided estimation of bedrock incision *in situ* (e.g., Hancock et al., 1998; Whipple et al., 2000b; Hartshorn et al., 2002; Montgomery, 2004; Stock et al., 2005b) and the influence of sediment has started to be evaluated more recently (e.g., Sklar and Dietrich, 1998; 2004; Turowski et al., 2007; Finnegan et al., 2007; Cowie et al., 2008). The spatial and hydraulic geometry limits of bedrock channels are not well constrained although some proposals have already made (Turowski et al., 2008; Wohl, 2004). The role of channel width and its relation to slope and channel incision have started to capture the attention of some researchers (e.g., Finnegan et al., 2005; Amos and Burbank, 2007; Whittaker et al., 2007; Yanites and Tucker, 2010) providing novel results and suggesting that bedrock rivers may have different hydraulic geometry than that in alluvial and gravel rivers. Bedrock rivers are still a challenging topic, requiring the attention of geomorphologists.

It is not surprising that most of the research in bedrock rivers has been focused on large rivers where bedrock incision has been addressed by analysing longitudinal profiles as well as the propagation of knickpoints (e.g., Kirby and Whipple, 2001; Duvall et al., 2004; Bishop et al., 2005; Larue, 2008). The case of small bedrock river catchments has been somewhat neglected. It could be argued that low drainage area bedrock rivers might not contribute as much as large rivers and may operate anyway in the same way as the tributaries of large rivers. However, there are some questions that have not been addressed yet for both small bedrock channels and tributaries. For example, does the rate of bedrock incision are the same in all reaches according to the concept of equilibrium?, Do small bedrock rivers develop a full concave profile?, Are small bedrock rivers capable of transmitting changes in tectonic and climate conditions? What are the rates of propagation of a knickpoint resulting from a drop in a small rivers base-level? Does the rock plucking control

channel incision in small bedrock rivers or are these streams controlled by sediment cover and tools?

In this research I address some of these questions. For this purpose the Isle of Jura, located on the west coast of Scotland, has been selected as a natural laboratory to study the case of small bedrock rivers. The glacial history of Jura indicates that a rapid base-level fall occurred as a consequence of a glacio-isostatic rebound (Lambeck, 1991). In this situation: (1) knickpoint propagation can be evaluated as predicted from theory, and (2) the morphological response of rivers to base-level fall can be assessed. Also the role of sediment is evaluated and bedrock incision is estimated by measuring concentrations of cosmogenic ^{10}Be in channel bedrock samples. In this chapter the theory underpinning bedrock channels research is presented.

2.2 Quantifying the bedrock channel incision

Gilbert's (1877) valuable and interesting observations and hypothesis on bedrock river dynamics encompass the role of channel slope as a factor enhancing or reducing incision rates, the resistance offered by lithology to incision and the effect exerted by sediment flux on rivers. On this last point, Gilbert noted that fine and medium size particles are likely to be more easily transported by rivers than the large ones. This observation was later quantified, confirming the importance of medium size particles in bedrock abrasion (Sklar and Dietrich, 1998; 2004). Gilbert (1877) also indicates that the local stream power (declivity and discharge, in his terminology) increases incision when the channel slope is steep and incision diminishes on gentler slopes. He also indicated that there is a tendency in rivers to equalise the 'work' they do leading to a grading of streams (Gilbert, 1877).

The first attempts to quantify bedrock incision were probably obtained in flume experiments (e.g., Shepherd, 1972; Shepherd and Schumm, 1974; Holland and Pickup, 1976; Gardner, 1983). Such studies not only explored incision in cohesive material but also evaluated the propagation of knickpoints (e.g., Holland and Pickup, 1976; Gardner, 1983). Exploring incision into bedrock and meander formation and cutting, Shepherd and Schumm (1974) noted that the bedrock incision is controlled by the shear force acting on the channel floor (τ) where:

$$\tau = \gamma R S \tag{2.1}$$

where γ is the weight of water, R the hydraulic radius and S is the slope or energy line grade. These authors propose that the erosion index (ω) can be obtained by the product of τ and the velocity (V) thus:

$$\omega = \tau V \tag{2.2}$$

The form of equation 2.2 indicates that incision increases where slope and stream discharge is greater and perhaps this model is the first attempt to estimate bedrock

incision. Similar formulations were subsequently used to model bedrock incision (e.g., Gardner, 1983; Howard and Kerby, 1983).

Perhaps one of the most influential papers on bedrock incision was that of Howard and Kerby (1983) who surveyed bedrock incision in the badlands of Virginia (USA) for seven years. By regressing the rate of lowering of the channel elevation ($\delta z/\delta t$) versus the drainage area (A) and the channel gradient (S), these authors modelled channel incision according to:

$$\delta z/\delta t = -0.11 A^{0.4} S^{0.7} \tag{2.3}$$

In equation 2.3 the constant becomes a factor (K) that incorporates the stream discharge, the shear-stress and the rock erodibility (Howard and Kerby, 1983). This model bedrock incision was later expressed in its general form as (Howard et al., 1994):

$$\delta z/\delta t = K A^m S^n \tag{2.4}$$

Equation 2.4 is known as the stream power model and the channel lowering depends on values of m and n (Sklar and Dietrich, 1998; Whipple and Tucker, 1999; Bishop et al., 2005) and it is based on the assumption that bedrock incision occurs once an excess of shear stress that initiates incision is overcome. The derivation of equation 2.4 can be found in Howard et al. (1994); Whipple and Tucker (1999) and Sklar and Dietrich (1998) also provide the details on the derivation.

The estimation of bedrock incision according to the model of equation 2.4 largely depends on the values assigned to m, n and K. It should be born in mind that equation 2.4 was derived empirically and changes on climate and lithology can then result in a change of exponents and in the term K. This issue was latterly analysed by Stock and Montgomery (1999) who found found that m and n vary according to base-level stability. Stable base-level settings were found to be predominantly

dependent on drainage area (the A term) and the values of exponents (~ 0.7) approximate those used by Howard et al. (1994). In contrast, settings where changes in the base-level drive knickpoint propagation, the exponent of area is ~ 1 and from 0 to 2 for slope (Stock and Montgomery, 1999). Other studies suggest that bedrock incision can be approximated by the product of area and the local slope (thus $m = 1$ and $n = 1$) (Seidl and Dietrich, 1992).

One of the major outstanding issue for the broad applicability of equation 2.4 is calibrating the values of K, m and n (Stock and Montgomery, 1999; Sklar and Dietrich, 2006). K is difficult to parametize since it captures the erodibility of the channel, stream discharge and climate as well as the effect of sediment (Howard and Kerby, 1983) which vary according to lithology and climate. Nevertheless, equation 2.4 or different versions of it (Whipple and Tucker, 1999) are widely used to assess fluvial incision into bedrock in which it is assumed that incision is dominated by detachment-limited conditions in which plucking imposes the rate of channel lowering.

A further point related to the bedrock incision rule expressed in equation 2.4 is that the effects of sediment flux and abrasion are not explicitly defined but are implicit in K (Sklar and Dietrich, 1998). The first attempt to quantify rates of abrasion in bedrock rivers was by Foley (1980). Based on an aeolian abrasion model, Foley proposed that for bedrock rivers the abrasion rate (y_t) results from the sum of the rate of rock lowering by deformation (y_d) and by cutting wear (yc). The model of Foley (1980) accounts only for a condition where particles are colliding on a bedrock surface but neglects the effect of suspension and cover by sediment. This aspect was integrated to the bedrock abrasion model proposed by Sklar and Dietrich (2004) in which the effect of sediment is accounted for. The model of these authors is detailed in chapter 6. Other methods to quantifying bedrock incision are based on field techniques using erosion pins (Hartshorn et al., 2002; Montgomery, 2004; Stock et al., 2005b) and the dating of geomorphic markers, such as strath-terraces

(Leland et al., 1998; Schaller et al., 2005; Reusser et al., 2004) and a single case reported by Hancock et al. (1998) where cosmogenic nuclides were extracted from the riverbed to obtain incision rates.

Several models for bedrock channels incision have been proposed in the last twenty years (see Whipple and Tucker (1999); van der Beek and Bishop (2003); Sklar and Dietrich (2006) for details) and at least two groups can be distinguished: (1) the detachment-limited models which is driven by shear stress on the channel (e.g., Howard et al., 1994; Seidl et al., 1994; Whipple and Tucker, 1999; van der Beek and Bishop, 2003; Goldrick and Bishop, 2007), and (2) the sediment transport-based models which incorporate the effect of sediment, to estimate bedrock abrasion (e.g., Foley, 1980; Beaumont et al., 1992; Kooi and Beaumont, 1996; Sklar and Dietrich, 1998; Whipple and Tucker, 2002; Sklar and Dietrich, 2004). Tomkin et al. (2003) evaluated different bedrock abrasion models in the Clear Water River (NW of USA) to assess which produces a better explanation for incision rates observed. The authors indicate that none of the existing models fully reproduce the observed rates and they also debate the use of the stream discharge and channel width scaling, arguing that by assuming a simply hydraulic geometry the processes related to channel incision are not fully captured.

Van der Beek and Bishop (2003) examined the bedrock incision in the upper Lachlan catchment (SE Australia) to test five different models of bedrock incision and assessed which of them best captures the observed fluvial incision. Their results indicate that the detachment-limited derived models seem the best at capturing the fluvial incision observed. Sklar and Dietrich (2006) evaluated the effect on sediment (tools and cover) for different bedrock incision models by parametizing a generic bedrock incision equation using a a site in the Eel River in California (USA) (Sklar and Dietrich, 2006, their Equation 20). Their results indicate that the shear stress models do not fully capture the effect by abrasion and this only occurs when sediment transport capacity and sediment flux are considered in a model. The results

obtained by van der Beek and Bishop (2003) and Sklar and Dietrich (2006) suggest that bedrock river incision can can be controlled by either plucking or abrasion or a combination of both.

2.3 Stream Long Profile Analysis: Searching for a steady-state landscape

The concept of steady-state in landscapes is deeply rooted in the study of bedrock rivers and in research on landscape evolution (Montgomery, 2001; Bishop, 2007). The principles surrounding this idea can be found on the works of Gilbert and Davis (Hack, 1960; Montgomery, 2001) which are tightly related to the notion that a graded river is a condition of equilibrium in rivers (Mackin, 1948; Yatsu, 1955; Hack, 1960; Snow and Slingerland, 1987). A steady-state landscape was formally defined by Hack (1960) through the definition of dynamic equilibrium. This states that " ... with a single erosional system all elements are mutually adjusted so that they are downwasting at the same rate. The forms and processes are in a steady state of balance and may be considered as time independent " (Hack, 1960, page 85).

Hack (1960) described the case where a steady-state may be achieved in the landscape without necessarily involving changes in the base-level. However, the idea that a steady-state can be attained with ongoing tectonic uplift is probably a notion that is very attractive to many geomorphologists. Dynamic equilibrium is not only an opposing model[1] to the Geographic Cycle proposed by Davis (1889) but it also offers a framework which may help to explain the topography observed in tectonic areas that were not considered in the model of Davis (1889).

The steady-state landscape has been conceptualised as a condition in which tectonic uplift is balanced by erosion in any part of the landscape (Howard, 1994; Montgomery, 2001; Whipple, 2001). This condition was firstly evaluated for transport-limited rivers (Willgoose et al., 1991; Tarboton et al., 1992; Howard, 1994) and later for detachment-limited settings. Long profile evolution incorporating the rock uplift for a bedrock river has then been expressed as (Howard, 1994; Whipple and Tucker,

[1]Hack expressed that dynamic equilibrium should be seen as a concept rather than a model (Hack, 1975). However, the rivers in steady-state are tested in the models of bedrock incision converting this into a model of landscape evolution

1999; Kirby and Whipple, 2001):

$$\delta z/\delta t = U(x,t) - KA^m S^n \tag{2.5}$$

where z is the channel elevation, U is the rock uplift, x is the distance downstream and t refers to time. Equation 2.5 is derived from the stream power model expressed in equation 2.4. Under conditions of steady-state, exponents in equation 2.5, as well U and K, are expected to remain constant and the steady state can be assessed by solving the equilibrium channel slope (S_s) (Whipple and Tucker, 1999; Kirby and Whipple, 2001; Duvall et al., 2004) thus:

$$S_s = (U/K)^{1/n} A^{-m/n} \tag{2.6}$$

The first term or equation 2.6 captures the channel steepness resulting from the interplay of rock uplift and erosion, and the exponent of A dictates the rate of change of channel slope with drainage area (Duvall et al., 2004). The form of equation 2.6 is similar to the power law function empirically found by other authors (e.g., Hack, 1957; Flint, 1974; Howard and Kerby, 1983) and this equation has been reduced to a simple power law function of channel gradient as a function of the drainage area which is a surrogate of stream discharge (e.g., Kirby and Whipple, 2001; Snyder et al., 2002; Duvall et al., 2004) thus:

$$S = k_s A^{-\theta} \tag{2.7}$$

Equation 2.7 has been used to evaluate whether rivers adjust to a condition close to equilibrium (e.g., Whipple, 2001; Kirby and Whipple, 2001; Duvall et al., 2004; Wobus et al., 2006b; Cyr et al., 2010). A similar form of equation 2.7 has been used by Goldrick and Bishop (2007). These authors assessed the approach followed by (Hack, 1975; 1973) noting the insensitiveness of Hack's model to differentiate disequilibrium reaches from those where there is adjustment to lithology. Their alternative model incorporates hydraulic geometry into the long profile by substituting stream discharge or its proxy A with the distance downstream (D). Thus, a

river in equilibrium can be assessed through the following expression (Goldrick and Bishop, 2007):

$$S = kL^{-\lambda} \tag{2.8}$$

where k captures the stream power, bedrock erodibility and rock resistance per unit length and L is the distance downstream and λ marks the channel concavity. Goldrick and Bishop (2007) also indicate that this form not only allows the detection of a graded stream but can be used to detect changes in bedrock incision with lithology and the presence and propagation of disequilibrium. Equations 2.7 and 2.8 are similar because the drainage area and the distance from the divide are both related to stream discharge (Goldrick and Bishop, 2007).

The analysis of several stream profiles in different settings indicate that a condition of a steady-state of the landscape as predicted from equation 2.7 or equation 2.8 is difficult to observe in either neotectonic or post-orogenic settings because of transient features on profiles may be resulting from changes in base-level and a different incisional response to lithology (e.g., Snyder et al., 2000; Baldwin et al., 2003; Duvall et al., 2004; Goldrick and Bishop, 2007; Whittaker et al., 2007). Moreover, it may be difficult for steady state to be developed because of rapid changes in climate and tectonics (Montgomery, 2001; Whipple, 2001). Landscapes in stead-state have only been confirmed in mountainous settings like in Taiwan (Whipple, 2001; Stolar et al., 2007), the southern Alps of New Zealand (e.g., Hovius et al., 1997; Willet, 1999; Crosby and Whipple, 2006), the mountain of Oregon Coast Range (USA) (Montgomery, 2001) although the latter has been debated by VanLaningham et al. (2006) who proposed a transient state for the central part of the mountain range. Quasi-state state has been proposed for the eastern margin of the Tibetan Plateau (Ouimet et al., 2009) and the mountains of central Italy (Cyr et al., 2010). Shortcomings in using slope-area regressions have been identified by Montgomery (2001); Tomkin et al. (2003); Stolar et al. (2007); Whittaker et al. (2008) and Attal et al. (2008) and so, other analyses instead of the slope-drainage area regression, have been used to characterise steady-state landscapes (Montgomery, 2001; Stolar et al.,

2007).

Even though it has been argued that slope-area regressions may not be appropriate to characterise a steady-state landscape (Montgomery, 2001), and approaches using shear stress or stream power have been debated (e.g., Humphrey and Konrad, 2000; Tomkin et al., 2003), such analyses have been used to evaluate other processes related to bedrock incision, tectonic forcing, lithology effect and base-level fall signals (e.g., Snyder et al., 2000; Duvall et al., 2004; Goldrick and Bishop, 2007; Snyder et al., 2003; Whittaker et al., 2007; DiBiase et al., 2010). Arguments against the stream power or shear stress model point to an oversimplification of the representation of the processes involved in channel incision, especially the neglect of discontinuities in channel width as well as the variability in stream discharge (Montgomery, 2001; Tomkin et al., 2003). On the other hand, the long-term incision rates determined by observing former streams or straths terraces, point to a relatively fair approximation of the stream power model (Stock and Montgomery, 1999; van der Beek and Bishop, 2003). One problem in bedrock channels research that has further implications for assessing the steady-state of landscapes is the paucity of data on bedrock channel incision obtained *in situ*. And whether the steady-state concept is accepted or not, the quantification of bedrock incision is required in different settings and on streams with different size to test the validity of the stream power and shear stress formulations.

Independently of the approach followed in the research of landscape evolution and in particular on bedrock rivers and whether the steady-state condition is accepted or not, the notion of steady-state is still the main starting point for research on landscape evolution. The concepts of disequilibrium and landscape transience assume *a priori* that equilibrium is at least attainable in the landscape. For the case of bedrock rivers, the notion of equilibrium is still the starting point for assessing the response of incision to any external change (i.e., tectonic and climate). In this sense, the stream power model can not be dismissed and it is still a powerful tool

that can also be used for studies interested in disequilibrium (Schoenbohm et al., 2004; Goldrick and Bishop, 2007; Berlin and Anderson, 2009).

2.4 Transient landscapes: Base-level fall and knickpoint propagation

The likelihood of a landscape reaching steady-state in some settings is unclear mainly because the response time required for landscape to keep a balance between rock uplift and incision is likely to be larger than changes in the climatic or tectonic conditions which perturb the landscape. Reaching a steady-state in landscape requires (1) persistent stability in climate or (2) rapid response of streams to absorb any change imposed by tectonics (Whipple, 2001). Several studies in tectonically active areas suggest that steady-state may not be easily achieved because new pulses of incision may occur due to an increase in rock uplift and subsequent base-level fall (e.g., Stock et al., 2005a; Harkins et al., 2007; Reinhardt et al., 2007a). Other mechanisms generating transience in the landscape have been attributed to river capture (Clark et al., 2004b; Harkins et al., 2007) and climate changes (Whipple and Tucker, 1999; Wegmann and Pazzaglia, 2002; Finnegan et al., 2007; Fuller et al., 2009). Interaction between tectonics and climate, as well as the local controls in the landscape (e.g drainage area, lithology, structure), can cause a permanent state of transience (Bishop, 2007).

The transient response of rivers caused by a tectonic forcing is expressed in two mechanisms (Whipple and Tucker, 1999): (1) a rapid drop of base-level which triggers a knickpoint that migrates headwards and (2) an increase in the rock uplift rate which results in channel steeping and the migration of a knickzone. If faulting occurs, a knickpoint may be formed. However, this type of knickpoint has received less attention (Burbank and Anderson, 2001), although its effect has been evaluated (e.g., Brocard and van der Beek, 2006; Whittaker et al., 2007; Larue, 2008). Several studies in natural settings have confirmed knickpoint propagation generated by a drop of base-level (e.g., Bishop et al., 2005; Crosby and Whipple, 2006; Anthony and Granger, 2007; Loget and van den Driesseche, 2009) and the knickzones related to an area of high rock uplift zones have been detected using term k_s of equation 2.7 (e.g., Snyder et al., 2000; Harkins et al., 2007; DiBiase et al., 2010).

The forcing imposed by climate and its effect on a transient landscape are less understood. Forcing by climate in river dynamics has been linked to sediment production and subsequent increases or decreases in sediment flux (Tucker and Bras, 2000; Whipple, 2001; Wegmann and Pazzaglia, 2002; Fuller et al., 2009; Finnegan et al., 2007). Whipple (2001), evaluating the response time of rivers in steady-state landscapes, simulated a scenario where channel incision increases due to an increasing orographic precipitation and subsequent sediment mobilisation. He showed that the fluvial response time shortens meaning that the steady-state condition is likely to be reached more rapidly. Whipple's simulation (2001) did not account for the effect of sediment (both tool and cover) since he used a shear stress model. Flume experiments (Finnegan et al., 2007) indicate that, depending on sediment supply and the amount of cover on the bed, the incision acts on the bed or on the lateral margins of channels. Increases in sediment supply not only may increase or dramatically reduced the incision rates on channel (Sklar and Dietrich, 1998; 2004; Turowski et al., 2008) but may inhibit any incision as has been theoretically proposed (Stark et al., 2009).

Sediment supply changes driven by a change in climate need to be quantified and incorporated in landscape evolution research and, more importantly, in the study of bedrock channels. Because rates of bedrock incision may increase or dramatically decrease depending on the sediment flux and sediment size, the rate of sediment production and how the sediment flux varies over time needs to be clarified. Moreover, because sediment transport is related to rainfall intensity and distribution, it is necessary to elucidate how any change in climate affects sediment supply and the sediment production rate. In this sense, glaciations are an important factor leaving the landscape in transience by (1) modifying and reshaping the pre-existing topography which in most of the cases result in the presence of deep gorges, hanged valleys and steps on rivers (Selby, 1985) and (2) leaving an important source of sediment which are latter transported by rivers (Church and Slaymaker, 1989).

There remain significant gaps related to tectonics and transience that have not been fully solved. The rates and effect of knickpoint propagation caused by base-level fall are not fully understood, even though such features were recognised early in geomorphology (e.g., Davis, 1932; von Engeln, 1940; Philbrick, 1970). Loget and van den Driesseche (2009) have argued that knickpoint migration can last ~ 1 Ma, meaning that such knickpoints may extend the duration of transience in landscape as knickpoints are transmitted to the fluvial network (Bishop et al., 2005; Crosby et al., 2007; Berlin and Anderson, 2009) and other secondary processes such as landslides, may directly relate to knickpoint migration headwards as some flume experiments indicate (e.g., Hasbargen and Paola, 2000; Bigi et al., 2006). Even in the case of rapid knickpoint propagation, the response of the landscape is not the same in all parts. Fluvial incision may rapidly propagate the base-level fall but the response of hillslopes may be slower (Reinhardt et al., 2007a). The asynchronous response of landscapes has also been demonstrated by the formation of hanging valleys related to a base-level fall (Wobus et al., 2006a; Crosby et al., 2007) and the increase of sediment flux due to change in the climate (Pratt-Sitaula et al., 2004; Goode and Burbank, 2009).

Transient landscapes where bottom-up processes (Bishop, 2007) dominate need to be fully understood. Particular emphasis should be placed on rates of knick-point migration generated by base-level lowering and the effects related to lithology and structure. The role of lithology and structure has been explored in flume experiments (e.g., Shepherd and Schumm, 1974; Holland and Pickup, 1976; Gardner, 1983) but field-based models are scarce (Hayakawa and Matsukura, 2003; Bishop et al., 2005; Hayakawa and Matsukura, 2009; Haviv et al., 2010). The change caused in the hydraulic geometry of the reaches downstream of a knickpoint are not well known, but the effects observed in faulted stream by Whittaker et al. (2007) indicate that breaks in scaling occur as well as changes in sediment size which also notably increase the stream power in high incision zones. The side effects caused by the knickpoint migration have not been fully addressed, but instability of hillslopes is

likely to occur which may result in an increase of landslide activity (Hasbargen and Paola, 2000; Bigi et al., 2006; Reinhardt et al., 2007b).

As briefly mentioned in the first chapter and in the paragraphs above, the main goal of this research is to evaluate the knickpoint migration caused by a rapid base-level fall. The natural laboratory chosen here is, however, different from the theoretical case where a steady-state or quasi steady-state landscape is perturbed. Jura, is a particular setting which has been highly perturbed by glaciations that have modified substantially the topography, therefore, streams are likely to be far from a steady-state. The cutting of Jura rivers into a relatively homogeneous quartzite and the recent base-level fall ($\sim$ 13.6 ka) induced by a glacio-isostatic rebound are important conditions that allow to evaluate the knickpoint propagation caused by a rapid rock uplift in a hard homogeneous lithology. Moreover, testing whether the knickpoint propagation is likely to occur in already transient small bedrock rivers, widens the gap of in the understanding the role of bedrock rivers in landscape evolution.

Chapter 3

The Jura landscape

3.1 Introduction

The rate of incision of rivers depends on several factors including the lithology, structure and topography over which rivers flow. The tectonic and climatic conditions are a primary control that can promote or dampen fluvial incision. One way to promote incision is by lowering the base-level (Hack, 1975; Whipple, 2001; Snyder et al., 2002). Due to its geographical location, the landscape of Jura has experienced major climatic and glacio-tectonic changes during the Quaternary. A glacially eroded landscape was formed during the Last Glacial Maximum (LGM) which started ∼26 ka and ended ∼19 ka and fully culminated in the Younger Dryas event (∼11 ka) in the latest Pleistocene (Chiverrell and Thomas, 2010). Since then, fluvial processes have not only been reshaping the inherited glacial landscape, but they are also transmitting the effect caused by the drop in river base-level which resulted from rapid post-glacial isostatic rebound (Lambeck, 1995; Shennan et al., 2006).

In order to understand river response to tectonics and climate in Jura, it is necessary to document the glacial chronology of the landscape as well as the lithology and structure in which rivers are incising. This chapter characterises the physical setting of Jura focusing on its lithology, structure and climatic conditions. The ice sheet that covered most of Scotland and north of England is briefly introduced. The

evidence of the post-glacial rebound provided by the abandoned shorelines is also treated in this chapter and in the final part, the specific case of the base-level fall as a consequence of the post-glacial rebound is presented. The morphometric analysis done for 34 streams of Jura is presented here. In chapter 4 the approach followed to obtain the stream long profiles is presented. The main purpose of this chapter is to provide a comprehensive framework to elucidate the main processes that triggered the propagation of base-level fall knickpoints on the isle of Jura.

3.2 Physical setting

The isle of Jura (55°57′ N, 5°54′ W), located on the west coast of Scotland, is one of the set of isles known as the Inner Hebrides. Jura has an elongated shape oriented north-east to south-west and is characterised by a moderate to steep topography over all the isle. The topography of Jura exhibits strong contrasts north and south of Loch Tarbert. North of Loch Tarbert the landscape is characterised by hills that have more or less the same elevation. The scenery changes dramatically south of Loch Tarbert. On the south-western coast a continuous cliff-line surrounds the coastline overlaid by an abandoned rock platform that is tilted seaward (Figure 3.1). The rock platforms is overlaid by a wide piedmont below the mountainous massifs known as 'The Paps of Jura' (Figure 3.1), which reach an altitude of 780 m OD (Ballantyne, 1999) and dominate the topography of the southern half of the isle.

The British Ordnance Survey 50 m resolution DEM (available from EDINA[1]) was processed in the Ilwis 3.3 Academic GIS (ITC, 2005) to produce two cumulative percentage frequency curves of elevation and slope (Figure 3.2). The results indicate that elevation changes rapidly from sea level to approximately 400 m OD (Figure 3.2A), such elevation range represents $\sim 90\%$ of the elevation values observed for the isle. The cumulative distribution of slope also indicates that most of the topography in Jura is dominated by moderate ($\sim 20°$) to steep terrain ($> 30°$) (Figure 3.3). Slopes increase rapidly from flat areas to slopes of $\sim 20°$ which represents $\sim 90\%$ of the values observed for the isle. The remaining 10% represent the steepest slopes ($> 20°$) on the isle. Although the cumulative curve of the elevation values indicates that the landscape is mostly characterised by a mountainous terrain, the lack of steeper slopes ($> 30°$) (Figure 3.2B) indicates that the landscape is smoothed, such effect presumably being related to intense glacial processes that generated an intense smoothing of landforms (Ballantyne, 1999).

[1]The service is provided by National Academic Data Centre based in Edinburgh. The website is: http://www.edina.ac.uk

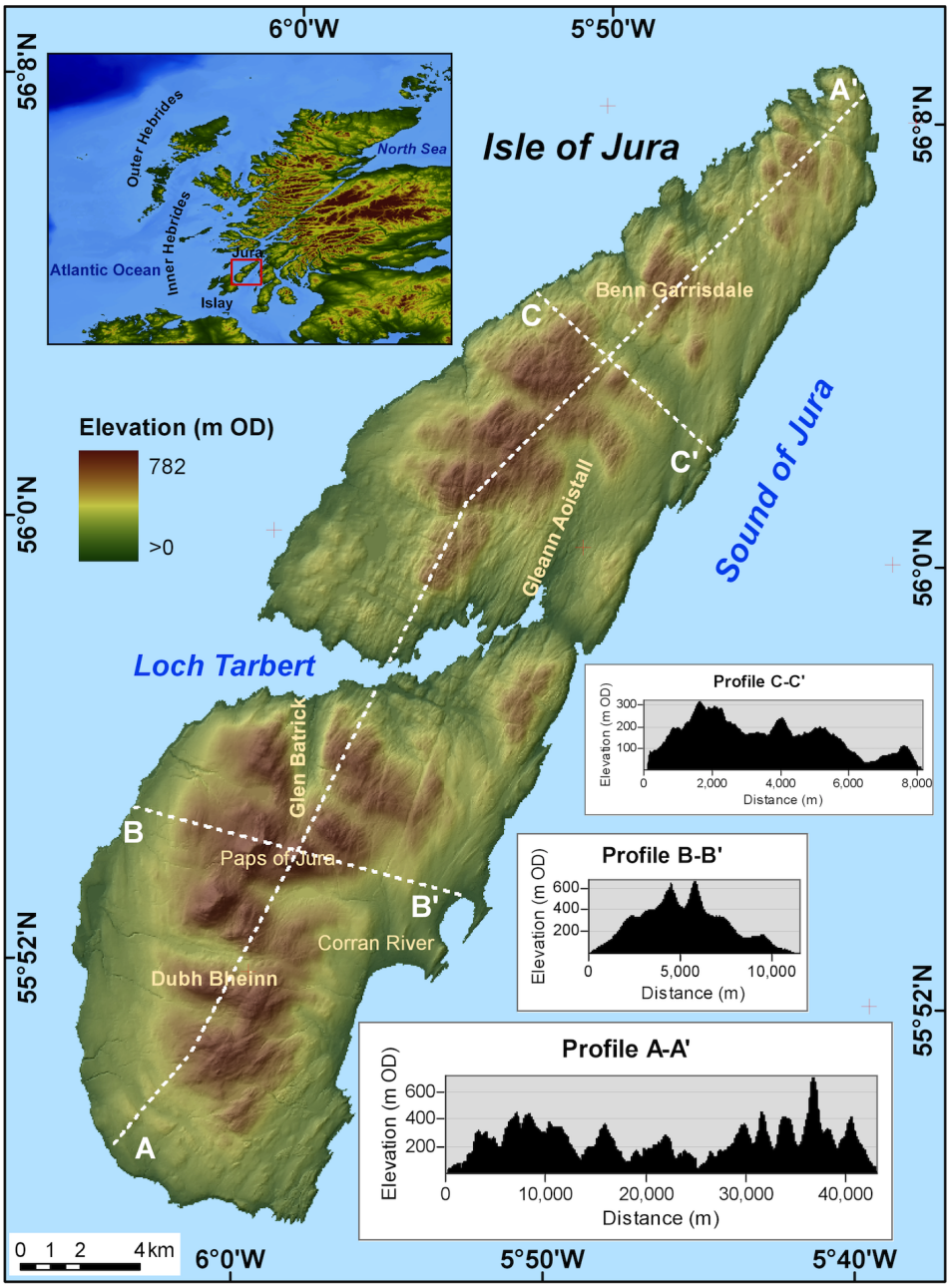

Figure 3.1: Location map of the Isle of Jura (west coast of Scotland, UK). The hypsometric values (see legend) and the topographic profiles indicate that a mountainous terrain characterises the topography of the isle.

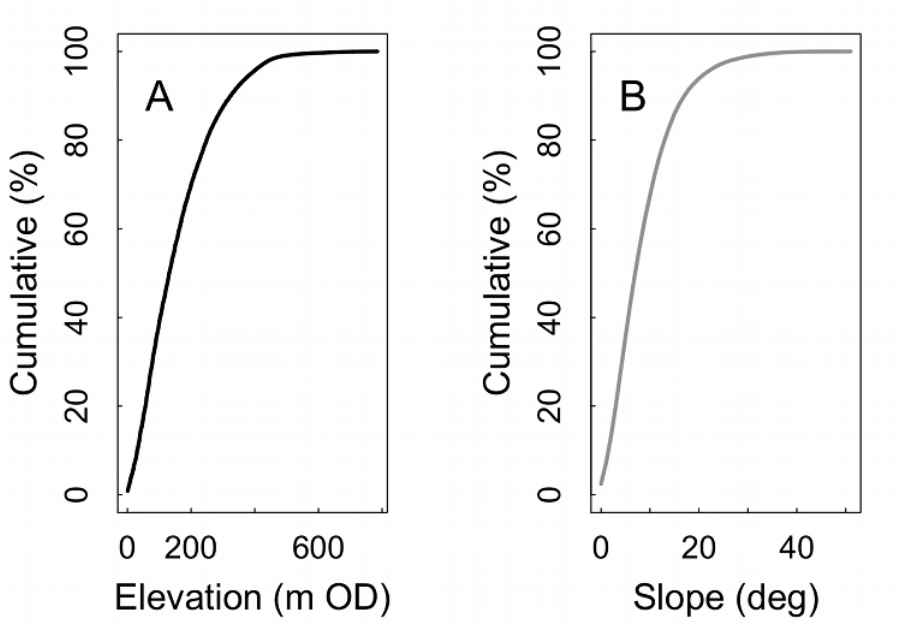

Figure 3.2: A. Cumulative graph of the elevation values of Jura. The steeper gradient of the curve in A indicates a rapid changes in elevation for the first 400 m OD. B. Cumulative graph of slope values, indicating that the landscape is characterised by a moderate to steep slopes.

Jura has a surface area of approximately 368 km^2 and the distance from the north tip to south tip of the isle is $\sim$ 44 km. The approximate distance between the west and east coast is $\sim$ 10 km. The relatively small area and the elongated shape along with the presence of mountainous massifs, makes Jura a high-relief setting which also exerts control over the distribution of rainfall.

The climatic conditions in Jura are mostly controlled by the regional climatic pattern observed for the Inner Hebrides and the west coast of Scotland (Lopez, 1995). The principal climatic control on the west coast of Scotland and for most of the west coast of the British Isles is the North Atlantic Drift (NAD) which serves as a thermo-regulator that generally prevents temperatures falling below 0°C (Stamp and Beaver, 1971). The NAD produces climate characterised by mild temperatures on land and a coast free of ice even though the British Isles are located at

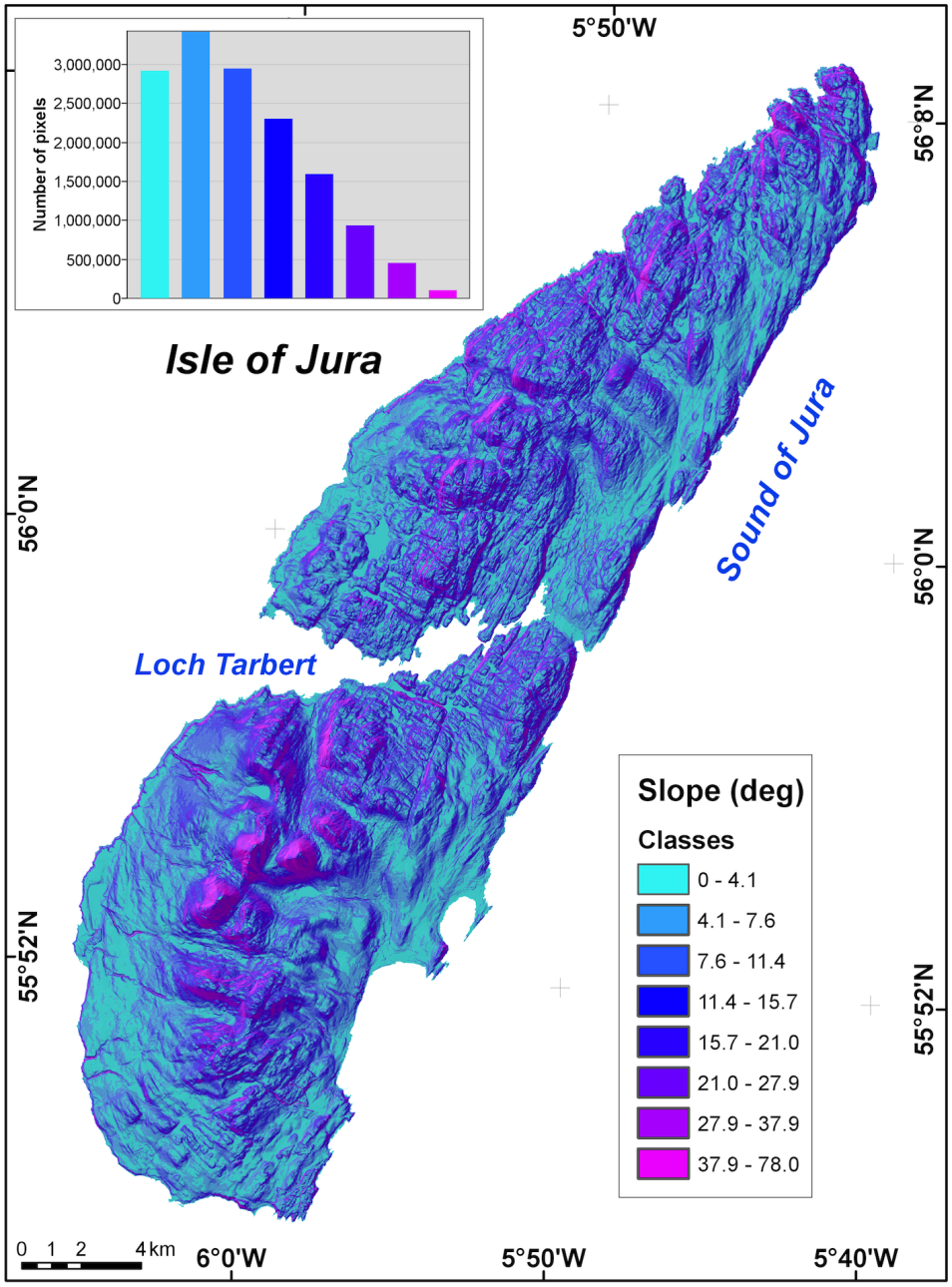

Figure 3.3: Slope map and slope histogram of the isle of Jura. Note that steep slopes are confined to the mountainous massifs of Jura and moderate to flat slopes characterise most of the topography of the Isle.

high latitudes (Stamp and Beaver, 1971). Cool summers and mild winters mark the seasonality on the west coast. The NAD also controls the spatial distribution of rainfall. The highest records of rainfall are concentrated at the north-west of Scotland and south of Wales where mountains enhance cloudiness and precipitation. There are no meteorological station registered by the MetOffice on Jura. The only information available is through regional maps published by the MetOffice on its website (MetOffice, 2010). According to this information, the minimum mean annual air temperature in Jura ranges from 5°C and 7°C on summit areas. Mean annual temperature increases slightly to 8°C and 10°C in the lowlands (MetOffice, 2010). Rainfall occurs in most months of the year and its spatial distribution is somewhat related to topography. In the west of Scotland, the highest rainfall values are concentrated on the western Scottish Highlands. Such pattern is observed in Jura where the mean annual rainfall is $1,700$ mm to $2,200$ mm on the mountain summits, dropping to $1,400$ mm to $1,700$ mm in the lowlands (Figure 3.4). In order to obtain a record of the seasonal trend for air temperature and rainfall, data from the closest regional station located at Paisley were used (Figure 3.5A). The Paisley station is considered to be representative of the climate prevailing on the west of Scotland (MetOffice, 2010).

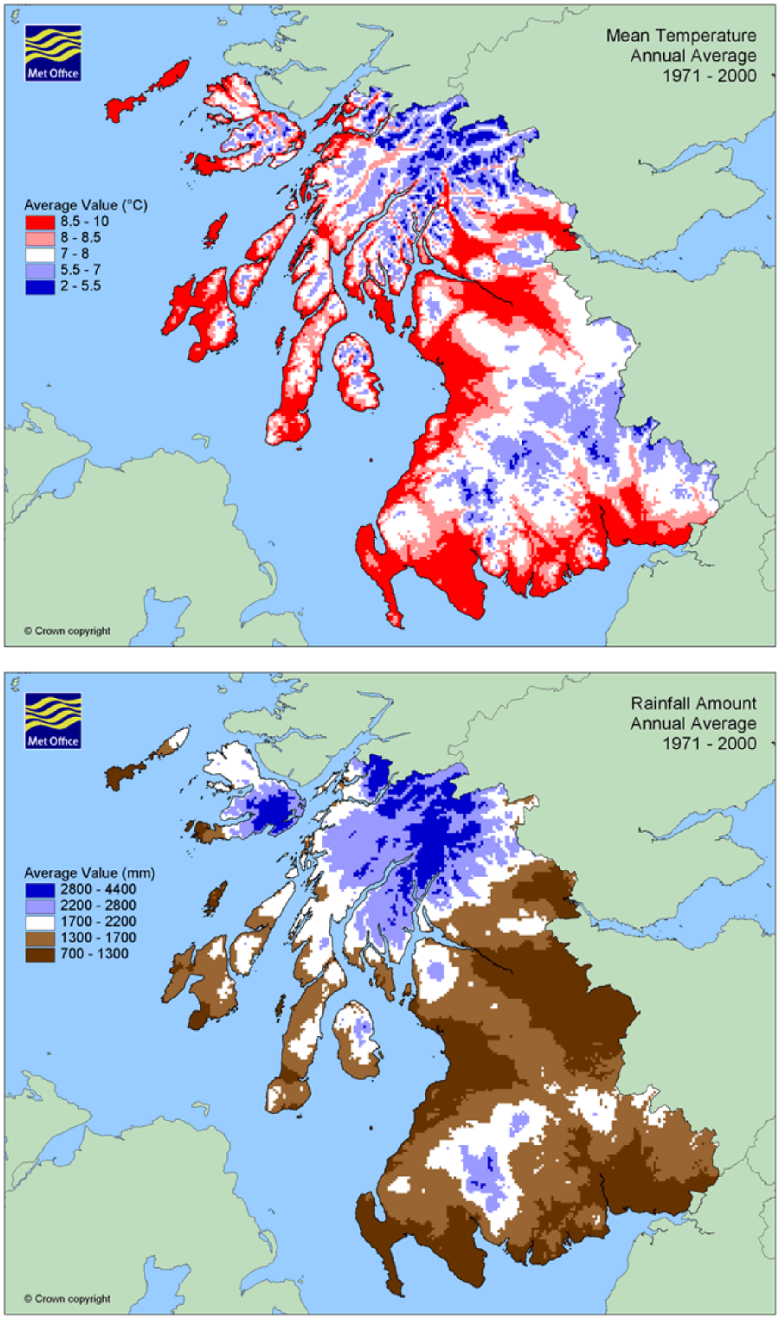

Figure 3.4: Maps of mean annual temperature and total rainfall published by in the Metoffice (©Crown copyright 2011,the Met Office) webpage (MetOffice, 2010). Note that the changes in temperature and rainfall are related to the topography of Jura (see Figure 3.1).

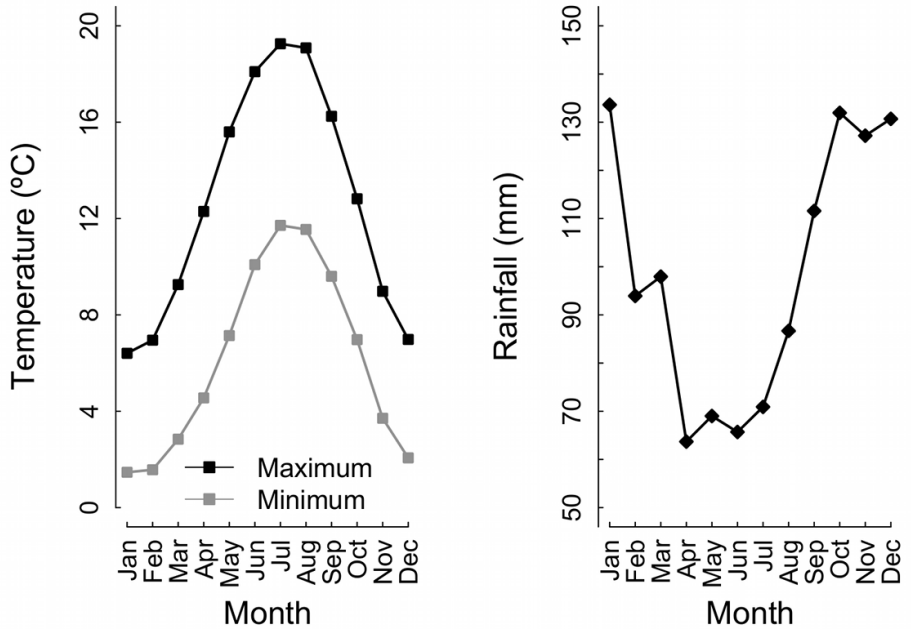

Figure 3.5: Maximum and minimum air temperatures and mean monthly rainfall. Data from Paisley station ($55°, 50'$N, $4°, 24'$W) obtained for 50 years period (1959-2008). Source: MetOffice website (MetOffice, 2010).

The warmest months in the west of Scotland are July and August when maximum and minimum temperatures are $\sim$ 18°C and $\sim$ 11°C respectively (Figure 3.5A). Winter maxima and minima drop to $\sim$ 6°C and $\sim$ 2°C respectively (Figure 3.5A). The rainfall season roughly coincides with changes in the mean temperature, which means that as temperature increases, rainfall decreases. Winter is the wettest season, the highest record is January when rainfall exceeds 130 mm (Figure 3.5B).

3.3 Lithology and Structure

Lithology and structure are important controls on river processes since lithology constitutes the material on which bedrock rivers must incise and structure can control river location. The rocks that crop out in Jura belong to the Argyll Group, which in turn, is part of the Dalradian Supergroup (Anderton et al., 1979; Johnson, 1991). The Argyll Group consists of rocks from late Precambrian to Lower Paleozoic in age (Johnson, 1991) and four formations have been established (Table 3.1). The rocks of the Argyll Group have been studied for more than a century (Anderton, 1985). However, some interpretations of the depositional environments and evolutionary models are still in debate (Anderton, 1985).

The Argyll Group rocks are distributed in parallel belts oriented from north-east to south-west (Anderton, 1985, his Figure 2). The Argyll Group is in contact in the north with rocks of the Grampian Group and Appin Group south of the Great Glen Fault. The southern limit of the Argyll Groups occurs at the contact with the rocks of the Southern Highland Group, which crop out on the northern side of the Highland Boundary Fault. The geology of the western isles of Scotland and for most of the Dalradian terrain is complex (Anderton, 1985). Although the lithology in Jura is mostly represented by a single unit (i.e., the Jura Quartzite), other outcrops have been recognised and mapped for the isle such as the Port Ellen Phyllites (Bailey, 1916) and its formation is related to other rock outcrops observed on the isles of Islay, Scarba, Colonsay and the west of coast of Scotland. Anderton (1985) provides the most recent review of the stratigraphy and the sedimentation of the Dalradian Supergroup and includes an evolutionary tectonic model, which had not been considered in previous pre-Plate Tectonics models.

The first detailed map of the stratigraphy and lithology of Jura was published by Bailey (1916) (Anderton, 1977). Bailey (1916) recognised and mapped four lithological units in Jura. The most widespread unit corresponds to a quartzite termed the 'Main Quartzite' (Bailey, 1916). Bailey's map includes several measurements

Table 3.1: Stratigraphy of the Argyll Group, part of the Dalradian Supergroup (After Anderton, 1985).

Group	**Subgroup**	**Formation**	**Depositional environment**
	Tayvallich	Tayvallich Limestone	Turbidite basin with volcanism
		Tayvallich Volcanics	Turbidite basin with volcanism
	Crinan	Crinan Grits	Submarine fan
ARGYLL	Easdale	Craignish Phyllites	Tidal flat to low energy shelf
		Easdale Slates	Turbidite basin
		Scarba Conglomerate	Turbidite basin
	Islay	**Jura Quartzite**	**Tidal shelf**
		Bonahaven Dolomite	Nearshore shelf to tidal flat
		Port Askaig Tillite	Tidal to glacial shelf

of dip which is $\sim 30^\circ$ towards the east with slight variations in the south-west where layer dips are $\sim 10^\circ$ to $\sim 15^\circ$ to the south-west (Bailey, 1916). Bailey's data are consistent with later measurements by Anderton (1976) who notes that the quartzite dips 20° to 40° eastwards. The strong structural control of the Jura quartzite is also evident on a three-dimensional view of the isle where the dip-slope and scarp-slope layers can be distinguished by the texture of the landscape (Figure 3.6). Other important rock units recognised by Bailey (1916) are the 'Jura Slates' which are two types of slates distinguished by their black and grey colours. Some minor outcrops of epidiorite sills have been found in the south west of the Isle and the rocks related to the Scarba Conglomeratic Group are exposed on the north tip of the isle. With exception of the Jura Quartzite, all the units mentioned crop out on the east coast forming a narrow strip oriented from north-south.

In the geological map published by the British Geological Survey (BGS), a network of volcanic dykes that intrude the quartzite delineated (Figure 3.7). Anderton et al. (1979) and Graham and Borradaile (1984) have correlated these dykes as members of the Tayvallich Formation.

The most up-to-date geological data for the Inner Hebrides are available through the BGS mapping. The lithology, stratigraphy and age for all the units recognised by the BGS on Jura are summarised in Table 3.2 and presented in a map in Figure 3.7 The units are briefly described below in chronological order.

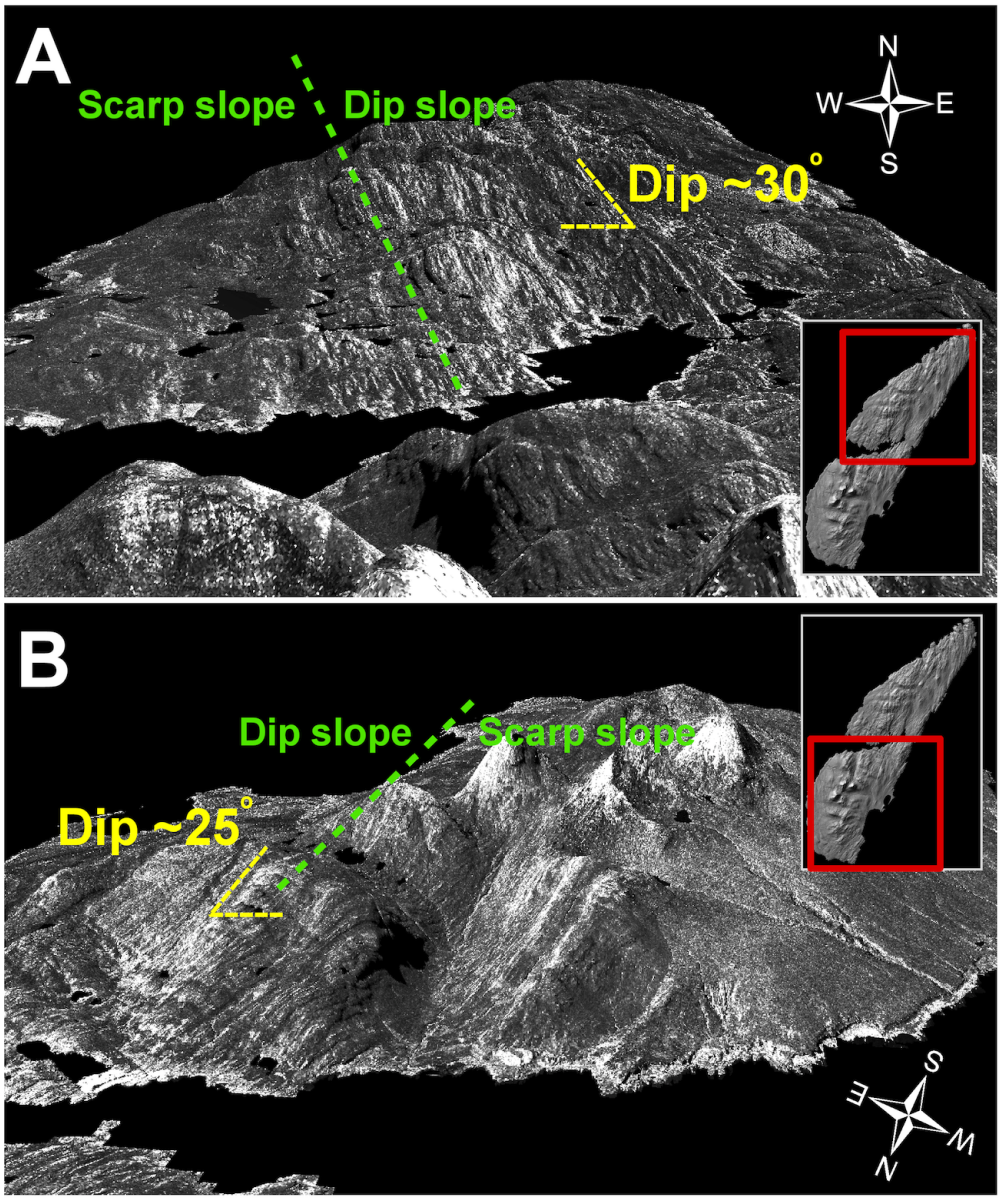

Figure 3.6: Two 3D perspectives of the isle of Jura, highlighting the structural control given by the eastward dip of quartzite. Images were obtained from a SAR image overlaying a 5m resolution DEM from NEXTMAP©. Vertical exaggeration 2.5.

Table 3.2: Stratigraphy of Jura according to the BGS map (BGS, 2010). The Jura Quartzite Formation crop out entirely on the isle. The youngest rocks are the olivine dykes, that intrude the quartzite (see text for further details).

Rock type	**Stratigraphy**	**Maximum age (Ma)**	**Minimum age (Ma)**
Olivine-Dolerite	Palaeogene Dyke	65	24
Olivine-Dolerite	Mull Dyke-Swarm	65	24
Dolerite	Palaeogene Dyke Suite	65	24
Quartz-Dolerite	Late Carboniferous to Permian Alkali Dyke Suite	327	248
Olivine-Basalt	Glas Eilean Lava Formation	290	256
Quartz-Dolerite	Late Carboniferous Tholeiitic Dyke Swarm	327	290
Lamprophyre	Siluro-Devonian Calc-Alcaline Dyke Suite	443	354
Andesite	Siluro-Devonian Calc-Alcaline Dyke Suite	443	354
Felsite	Siluro-Devonian Calc-Alcaline Dyke Suite	443	354
Minette	Siluro-Devonian Calc-Alcaline Dyke Suite	443	354
Vogesite	Siluro-Devonian Calc-Alcaline Dyke Suite	443	354
Amphibolite	Dalradian Supergroup	1000	545
Quartzite	Jura Quartzite Formation	1000	545
Pelite-Graphitic	Jura Slate Member	1000	545
Metalimestone	Ardrishaing Phyllite Formation	1000	545
Pelite-Semipelite	Jura Slate Member	1000	545
Metalimestone	Port Ellen Phyllite Formation	1000	545
Psammite-Gritty	Port Ellen Phyllite Formation	1000	545
Semipelite	Port Ellen Phyllite Formation	1000	545
Metaconglomerate	Scarba Conglomerate Formation	1000	545
Quartzite and Conlogmerate	Scarba Conglomerate Formation	1000	545
Quartite and Metaconglomerate	Scarba Conglomerate Formation	1000	545

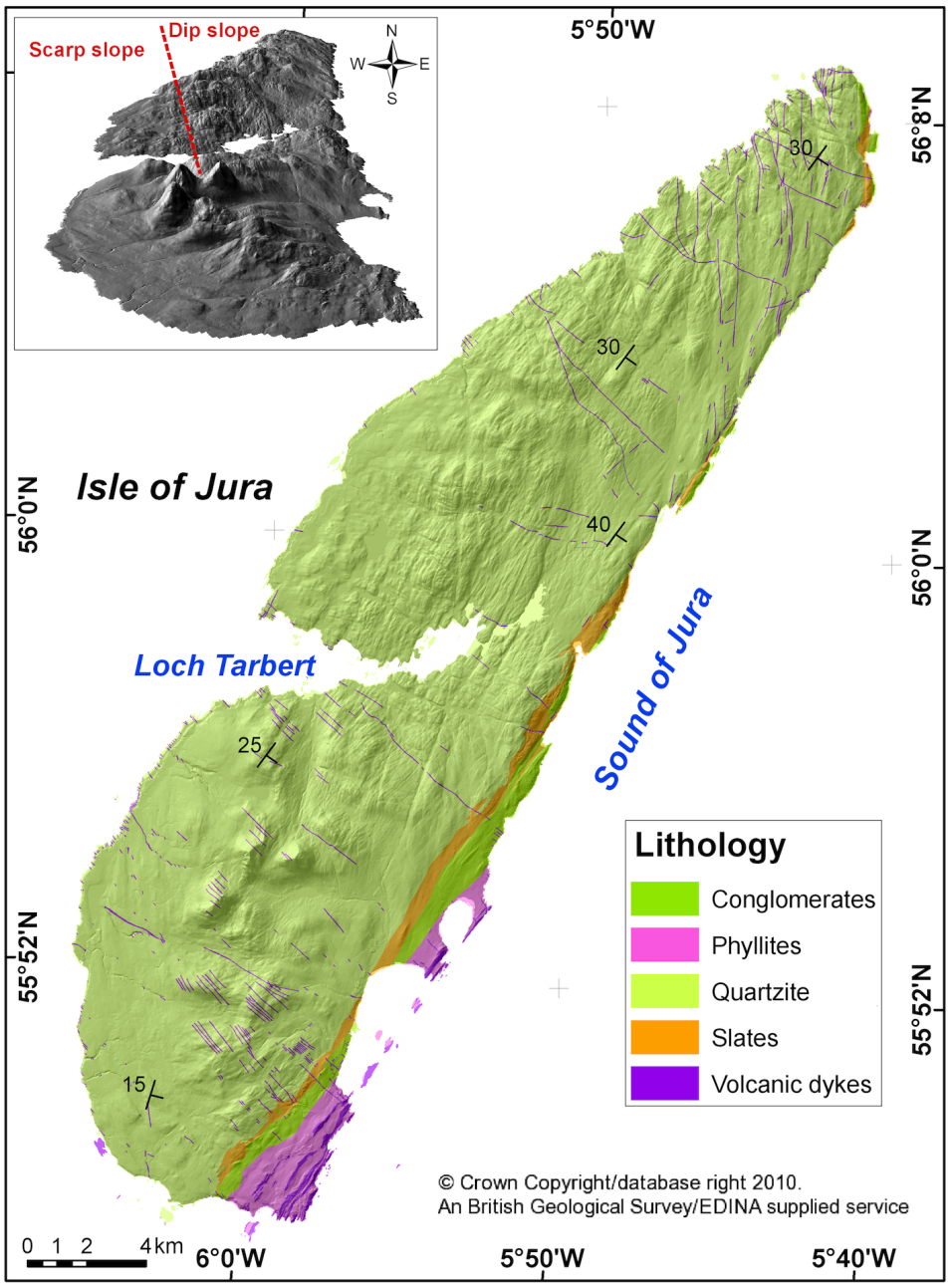

Figure 3.7: Geological map of the Isle of Jura. The quartzite is the predominant lithology with some intrusions (volcanic dykes) and a minor outcrop of other metasedimentary units on the south-east sector of the isle.

3.3.1 Jura Quartzite

Depositional processes for the Jura Quartzite (Anderton, 1985) named by Bailey (1916) as The Main Quartizite, have been discussed by Anderton (1971; 1977; 1985). Anderton suggests the Jura Quartzite in Jura is the result of deposition of sediments on a shallow tidal-shelf environment (Anderton, 1971; 1976), he supports his interpretation by analysising several facies in the quartzite layers (Anderton, 1976). He concludes that "...the bulk of the coarse facies was deposited in a subaqueous environment where deposition of coarse sediment from powerful flows and the migration of large bedforms, mainly dunes, alternated periods of erosion and the deposition of silt. Such conditions are found in some large rivers, estuarine and shallow tidal seas." (Anderton, 1976, p. 439). The source of the quartzite has been related to the erosion of a quartzo-feldespatic land located to the east of Jura (Johnson, 1991, his Figure 4.5).

3.3.2 Scarba Conglomerate

The quartzite-conglomerate rock unit that outcrops on southeast corner of Jura (Figure 3.7) is a continuation of the metasediments found on the isle of Scarba (Tables 3.1 and 3.2) to the north of Jura. The Scarba Conglomerate was deposited in a deep-water turbidite basin (Anderton, 1985). Stratigraphically, the quartzite-conglomerates overlie the Jura Quartzite. Anderton (1985) proposed that the Scarba Conglomerate on Jura resulted from the deposition of sediments at the base of large fans at the face of fault scarps (Anderton, 1985, his Figure 5D).

3.3.3 Easdale slates

The rock units mapped by the BGS as semipelites and pelites (Figure 3.7) correspond to the black and grey slates identified by Bailey (1916). The slates of the east coast of Jura are differentiated by the (BGS, 2010) as: (1) the Port Ellen Phyllite Formation and (2) the Jura Slates Member. The stratigraphical classification of

the slates of the west coast of Jura of Bailey (1916), used by BGS (2010), differs from the stratigraphy of Anderton (1985, his Figures 1, 2, 5A and 5D). Anderton groups the slates rocks as part of the Easdale formation and he correlates them with the Craignish Phyllites (Table 3.1). The Craingnish Phyllites were deposited in a shallow marginal marine environment dominated by stormy conditions (Anderton, 1985). In the BGS map the outcrops of slates is intercalated with minor outcrops of volcanic amphibolites (Figure 3.7) that are classified as part of the Dalradian Supergroup (Table 3.2). Bailey (1916) recognised the volcanic rocks on the east as Epidiorite sills, and explained them as a result of an isoclinal folding. The volcanic character of the slate units was also recognised by Anderton (1985) who regarded this as a reflecting reworking of volcanic detritus from the Easdale Group. The stratigraphic correlation of the Jura Quarzite, the Scarba Conglomerate the Easdale Slates and the Craignish Phyllites can be traced following the rock outcrops from the north of Easdale to the south of Islay (Anderton, 1985, his Figures 5A and 5B).

3.3.4 Tayvallich volcanics

The youngest rocks mapped by the BGS as cropping out in Jura correspond to numerous volcanic dykes intruding the Jura Quartzite (Figure 3.7). The correlation of the volcanic dykes with the volcanism in the Loch Awe area (West of Scotland) has not been fully confirmed (Graham and Borradaile, 1984) but the wide distribution of volcanic rocks grouped in the Tayvallich Formation (Table 3.1) seems to be related to the intrusion of dykes in Jura (Anderton, 1976; Johnson, 1991). Detailed geochemical analyses of the Jura dykes show that the dykes are the same in their chemistry as other metabasaltic rocks in other Dalradian volcanic rocks and that the extrusion of volcanic material was partially through sills (Graham and Borradaile, 1984). These authors explained the intrusion of dykes in Jura as a consequence of a change in tensional stresses to the NE-SW. The volcanic rocks of the Tayvallich Formation were formed in deep marine basin environment (Anderton, 1985; John-

son, 1991), and experienced metamorphism during the Grampian and Caledonian orogenies (Anderton et al., 1979; Graham and Borradaile, 1984). The rocks of the Argyll Group were metamorphosed during the Grampian Orogeny (Anderton et al., 1979).

3.4 The Quaternary glaciations

Most of the Scottish landscape on mainland and on its isles, is characterised by a set of glacial landforms that started (or continued) to form $\sim 120,000$ yr ago when the Devensian glacial stage was initiated (Boulton et al., 1991). There is a scant record for older glaciations in Scotland and only the recent glaciation is well documented and its evidences are imprinted on the landscape (Boulton et al., 1991; Gordon and Sutherland, 1993). The climax of glaciation in Scotland occurred more or less contemporaneously with the global LGM and ended during the Windermere interstadial with a subsequent short-lived pulse of glacial processes that reshaped the landscape $\sim 11,000$ yr B.P. during the Loch Lomond Readvance (LLR). The glaciation finally ended with the Flandrian interstadial age (Boulton et al., 1991; Golledge, 2010).

During the LGM ($\sim$20 ka) an ice sheet, conventionally termed the British Ice Sheet (Bowen, 1989; Boulton et al., 1991; Bradwell et al., 2008b) or more recently the British-Irish Ice Sheet (BIIS) (e.g., Hubbard et al., 2009; Chiverrell and Thomas, 2010), covered most of Ireland, Scotland and the north of England (Boulton et al., 1991; Hubbard et al., 2009; Chiverrell and Thomas, 2010). The BIIS substantially modified the landscape and the deposits associated with it (mainly till) are widely distributed across Scotland.

The literature of the BIIS is prolific, with around 2,000 papers published about the BIIS and the glaciations in UK (Clark et al., 2004a). In the last twenty years, there has been notable emphasis on the limits and evolution of BIIS (e.g., Bowen,

1989; Boulton et al., 1991; Lambeck, 1991; 1993b; Ballantyne et al., 1998; Ballantyne, 2009). However, the time of formation, dynamics and limits of the BIIS have not been determined precisely. Moreover, some issues related to the merging of the BIIS with the Fennoscandinavian Ice Sheet (FIS) and the ice thickness and limits remain controversial (e.g., Sissons, 1981b; Lambeck, 1995; Bradwell et al., 2008b; Chiverrell and Thomas, 2010). The presence and approximate limits of the BIIS have been demonstrated by the analysis of glacio-marine sediments collected inland (Bowen, 1989) and the observation of eroded features in the landscape (e.g., Ballantyne et al., 1998; Ballantyne, 1999). Geophysical and numerical modelling have also been used to explore the extent and thickness of the BIIS (e.g., Lambeck, 1993b; 1995).

More recently, the surveying of the sea floor in the northern and north-western sector of the British Isles has been useful to obtain a detailed map of those areas affected by BIIS (Bradwell et al., 2008b;a). The detailed mapping of glacial features on the sea floor as well as the identification of mega-grooves in the landscape, have provided new data about the extent and dynamic of the BIIS which has been summarised recently by Bradwell et al. (2008b). These authors' results indicate that the BIIS merged the FIS during one of its phases, associated with the development of an ice stream on the Norwegian Channel (Bradwell et al., 2008b, their Figure 10). Their results also suggest that the thickness of the BIIS and its limits have been underestimated in previous interpretations. Their data seem to be consistent with recent results obtained from numerical modelling (e.g., Boulton and Hagdorn, 2006; Hubbard et al., 2009) which support the hypothesis of a merging of the BIIS and the FIS during its maximum growth and the development of ice streams in the Norwegian Channel and in the Celtic Sea (Sejrup et al., 2005; Boulton and Hagdorn, 2006; Hubbard et al., 2009).

Two papers published recently, contain the most up-to-date review of the BIIS and the mapping of glacial landforms of the UK. Clark et al. (2004a) published

an explicative text of a map at scale of $1 : 625,000$ which contains all the glacial features associated with the BIIS in mainland UK and on the continental shelf. These authors' mapping is based on a compilation of a large dataset of published papers and theses. Chiverrell and Thomas (2010) have published a review of the BIIS limits and dynamics with special emphasis on the northern sector and the ice sheet advances and retreats during the LGM. In this paper the authors provide the most up-to-date version of the BIIS including the recent results of Bradwell et al. (2008b;a) who have mapped geomorphic features on the sea floor in the north and north-west of Scotland. The work of Chiverrell and co-workers is used here to describe the timing and limits of the BIIS.

The deposits and extent of the LLR are more or less well documented in multiple sites in the western and south-western Highlands, the southern Grampians, the Isle of Mull and Skye (Boulton et al., 1991; Gordon and Sutherland, 1993). Very few data are available for the Scottish isles but it is believed that the ice was concentrated in glacial cirques or corries in the isles (Sissons, 1983). It is accepted an ice cap was formed on the Scottish Highlands (Sissons, 1981a; Boulton et al., 1991; Gordon and Sutherland, 1993; Ballantyne et al., 1998; Golledge et al., 2007), and the lateral extent of glaciers during the LLR has been established by the presence of moraines (Boulton et al., 1991; Golledge et al., 2007). Nevertheless, the ice thickness at the crest of the Scottish mountains is less known, but recent results suggest that this could be higher than the trimline previously interpreted by Thorp (1981) as the limit of the ice cap. Thus, LLR ice thickness could be underestimated in previous studies (Golledge et al., 2007).

The glaciers during the LGM and LLR have dramatically transformed the Scottish landscape. The glaciers in Jura have formed cirques, gorges and have left several steep reaches on the rivers of Jura which are the focus of the present study. Although the chronology of glaciations in Jura is not yet known in detail, the inherited landforms related to glacial processes of the BIIS and the LLR over the Scottish

landscape can be extended to account for most of the Quaternary landforms of Jura.

3.4.1 The British-Irish Ice Sheet

As mentioned above, the precise time of formation of the BIIS has not been satisfactorily stated. At least two cold periods related to the formation of the BIIS have been recognised $\sim 70,000$ yr B.P. and $\sim 20,000$ yr. B.P. (Boulton et al., 1991). Although sediments indicate that the Scottish landscape was glaciated $\sim 70,000$ yr B.P. and some eroded landforms also seems to support this, it is generally agreed that the BIIS was completely formed $\sim 20,000$ yr B.P. when it reached its maximum extent (Boulton et al., 1991; Chiverrell and Thomas, 2010).

Many authors have attempted to establish the limits of the BIIS (e.g., Bowen, 1989; Boulton et al., 1991; Shennan et al., 2006) but, none of them with exception of Chiverrell and Thomas (2010), have included recent data from glacial landforms mapped on the sea floor on the north of Scotland. The limits of the BIIS in Figure 3.8 are based on the map published by Chiverrell and Thomas (2010); the chronology and details are provided therein. It is important to note that the limits shown here must be considered as preliminary since recent discussions and research have raised the possibility of an asynchrony of the BIIS (Bradwell et al., 2008a; Ballantyne, 2009; Chiverrell and Thomas, 2010) which makes difficult to establish one deterministic limit for the BIIS.

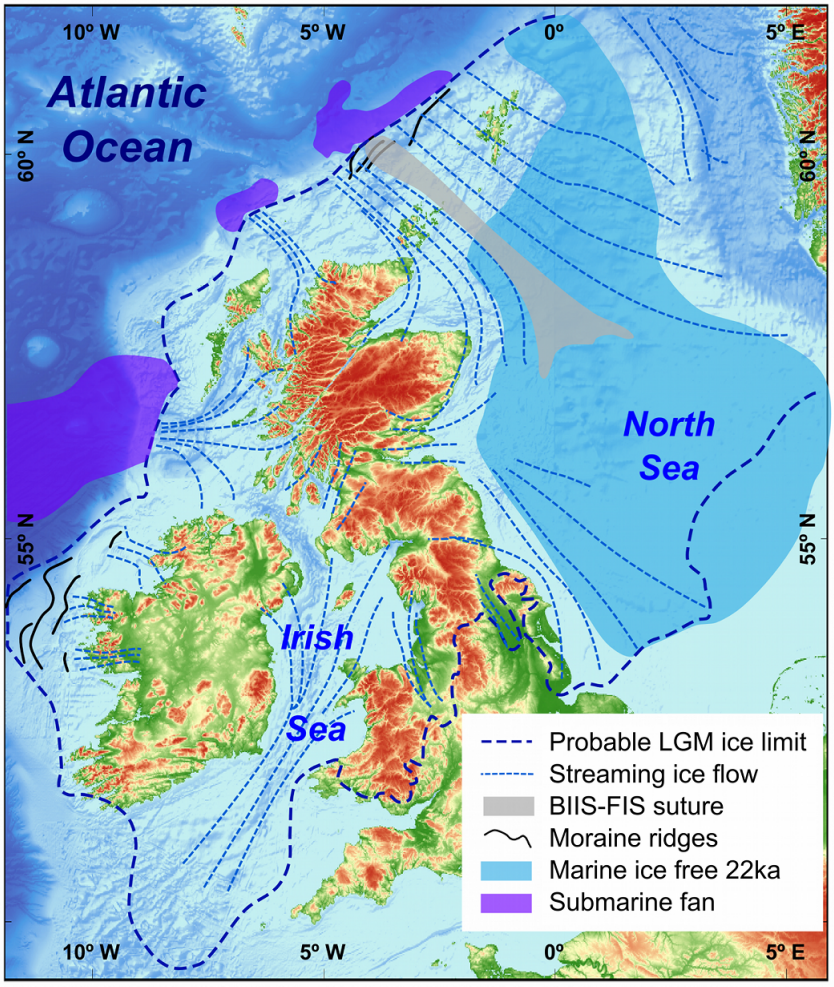

Figure 3.8: Limits and principal features associated to the BIIS (Modified from: Chiverrell and Thomas, 2010). Base map obtained from the General Bathymetric Chart of Oceans (GEBCO) website (http://www.gebco.net)

The chronology of the deglaciation of the BIIS is still incomplete (Boulton et al., 1991). Deglaciation ages in Ireland and in the north and north-west of Scotland indicate that between the Late glacial and the LLR some periods of cooling prevented the total melting of the ice sheet in Scotland (Sissons, 1983; Bradwell et al., 2008a; Ballantyne, 2009; Hubbard et al., 2009). At least one cold period previous to the LLR known as the Killard Point Stade has been related to the advance of glaciers

in the eastern Scotland (Ballantyne, 2009). Deglaciation started in the Irish Sea sea $\sim$ 18 ka (Ballantyne, 2009) and for the North Sea the ice-free conditions started $\sim$ 22 ka (Sejrup et al., 2005; Chiverrell and Thomas, 2010). In general it is believed that the marine ice-free conditions occurred $\sim$ 16 ka (Boulton et al., 1991; Bradwell et al., 2008a) but this has been debated (Bradwell et al., 2008a). The deglaciation onshore of the British Isles has been obtained by the collection of pollen samples (Boulton et al., 1991) and the dating of landforms on the northern isles of Scotland (Ballantyne, 2009). The interpretation of landforms and ages suggests that the ice associated with the BIIS remained until the initiations of the LLR (Boulton et al., 1991; Ballantyne, 2009) implying that some glaciers were simply re-activated during this stage.

The effects of the BIIS glaciations on Jura are scarcely documented. The most detailed work has been done by Ballantyne (1999) who suggested a vertical ice distribution on Jura and Mull and confirmed the ice motion based on geomorphic makers such as striae and ice moulded rock outcrops (*roches moutonnées*) (Ballantyne, 1999, his Figure 2). The geomorphic markers indicate that Late Devensian ice on Jura reached an altitude of $\sim$ 600 m to $\sim$ 700 m. Higher altitudes might be expected and there is a possibility that the BIIS covered the mountainous massifs of Jura (Ballantyne, 1999). The geomorphic markers strongly indicate that ice flowed westward of the British Isles as other authors have suggested (e.g., Sissons, 1983; Gordon and Sutherland, 1993; Boulton and Hagdorn, 2006).

Besides the geomorphic markers identified by Ballantyne (1999) in Jura, perhaps the most compelling evidence of the presence of BIIS and its movement upon the landscape of Jura is given by the presence of a medial moraine located at the foot of Beinn an Oir, which continues westwards and terminates close to Loch na Sgrioba (Dawson, 1979) (Figure 3.9).

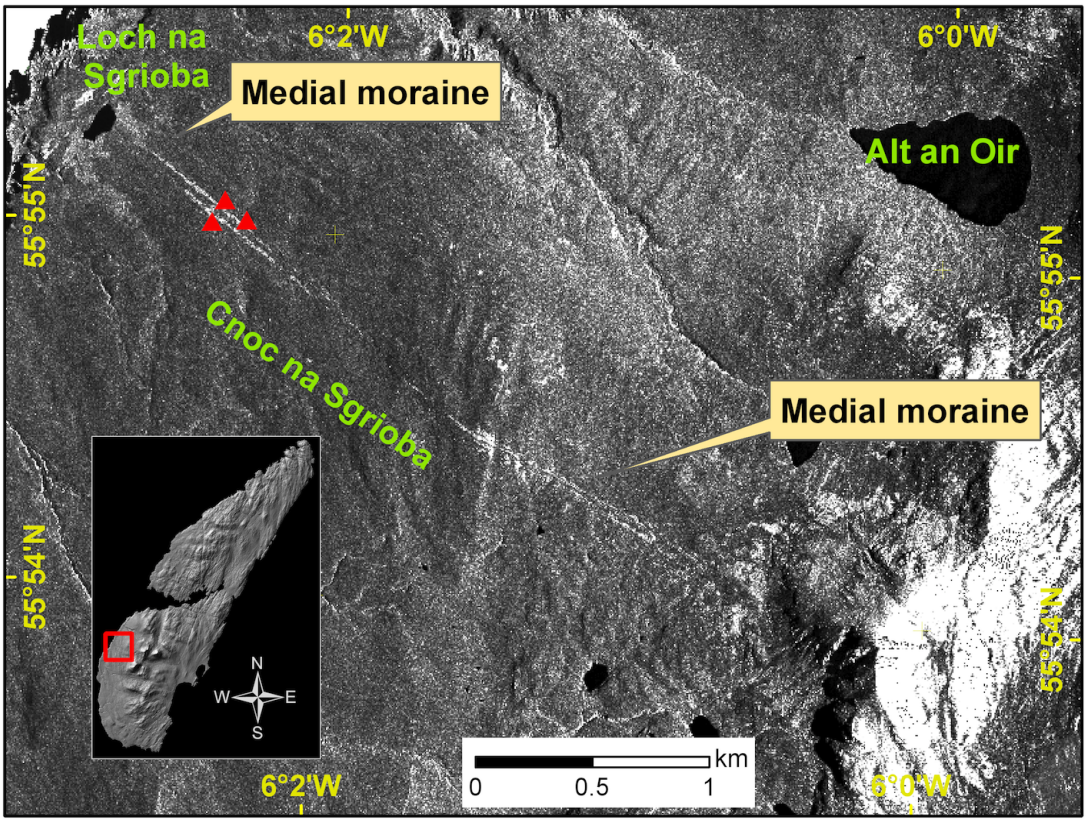

Figure 3.9: Location of the medial moraine of Jura (white stripped line). Note the end of the moraine at Loch na Srioba. The red triangles show the location of the cosmogenic samples obtained by Bishop and co-workers (pers. comm).

The moraine was reported in detail by Dawson (1979) who suggests that it resulted from the transportation of supra-glacial debris of the BIIS during its waning stage. The moraine is mostly composed of quartzite clasts that are not striated (Dawson, 1984). Dawson hypothesised that the debris source is found at the Benn an Oir (785 m OD) and Beinn a Chaolais (733 m OD). The hypothesis of Dawson for debris production of the moraine in Jura is consistent with the findings of Ballantyne (1999) for the same area in which no signs of glacial erosion were found on mountains summits and rock sliding and scree slopes dominate the landscape (Ballantyne, 1999). The medial moraine of Jura not only evidences the effect of BIIS

on the landscape but its preservation suggests that the deglaciation was probably fast. The time of formation and abandonment of the medial moraine of Jura is not known, but unpublished cosmogenic exposure ages of three samples extracted from the moraine by Bishop and co-workers (pers. comm.) yield an age of $\sim$ 13 ka to $\sim$ 15 ka (Table 3.3). The oldest age obtained by Bishop and co-workers is consistent with the time of deglaciation of the BIIS as some authors have proposed (e.g., Boulton et al., 1991; Lambeck, 1991; Shennan et al., 2006).

Table 3.3: Cosmogenic exposure ages of the medial moraine of Jura. Unpublished data of Bishop and co-workers.

Sample	**Coordinate (DD)**	**Elevation (m OD)**	**^{10}Be (atoms/gr/yr)**	**Age † (yr)**
S1	55.9176, -6.0509	106	87600	$15,616 \pm 1,506$
S2	55.9172, -6.0512	106	78983	$14,656 \pm 1,426$
S3	55.9176, -6.0522	92	72564	$13,330 \pm 1,336$

† Samples were processed at the Scottish Universities of Environmental Research Centre (SUERC), UK.

3.4.2 The Loch Lomond Readvance

The Late glacial period was characterised by the melting of the BIIS $\sim$ 16 ka; contemporaneously eustatic sea level started to rise (Boulton et al., 1991). A warmer period characterised by the growth of vegetation and fauna commenced $\sim$ 13 ka in the Windermere interstadial, which ended with the LLR (Boulton et al., 1991). Although the environmental conditions were characterised by a milder temperature with expansion of vegetation and fauna (Boulton et al., 1991; Sissons, 1979) the climate prior to LLR was unstable and there may have been re-advance of glaciers associated with the Older Dryas event (Boulton et al., 1991; Hubbard et al., 2009;

Ballantyne, 2009).

The LLR was marked by an important drop in global mean air temperature of $\sim$ 8°C to $\sim$ 10°C (Golledge, 2010) that resulted in reactivation of glaciers $\sim$ 11 ka that lasted for almost 1,000 years (Sissons, 1983; Boulton et al., 1991; Golledge et al., 2007). The Younger Dryas in Scotland has been confirmed by the dating of hummocky moraines, boulders and drift limits, complemented by sedimentary cores, pollen analysis and radiocarbon ages from organic matter (Sissons, 1983; Golledge, 2010).

The re-advance of glaciers during the LLR and subsequent retreat have been demonstrated on the isles of Mull and Arran located north and south of Jura respectively. It is highly probable that glaciers re-advanced during the LLR. Ballantyne (1999) recognised the presence of moraines related to the LLR at the foot of Beinn a Chaolais and Beinn and Oir (Ballantyne, 1999, his Figure 2). In previous interpretations it was assumed that during the LLR glaciers flowed over valleys towards the approximate limit of the actual sea level (Charlesworth, 1955 in Dawson, 1979; 1997). Dawson (1979) questioned the interpretations of Charlesworth, arguing that there are not visible signs of full glaciation in the valleys of Jura. Moreover, the presence of a fossil rock glacier and the periglacial deposits on scree slopes identified by Dawson (1997) indicate that periglacial processes acted on system of valleys of Jura at $\sim$11ka.

The high elevation topography of Jura means that periglacial activity is likely during the LLR (Dawson, 1997; Ballantyne, 1999). Moraines have been recognised in the south-east (Ballantyne, 1999), indicating that glaciers were located at the foot of the mountains, without reaching the coast. The topography at the foot of the Paps of Jura exhibits the classical glacial cirque morphology (Figure 3.10) and the geomorphology of southern Jura as well as the presence of lochs supports the argument of Dawson (1979) that LLR ice was confined to small cirques.

A simple model of the re-advance of glaciers and the deglaciation for the LLR seems difficult to obtain for Scotland because ages on different samples indicate that the ice growth has not been synchronous and in some areas the ice stagnated at the onset of the LLR (Golledge, 2010). For the particular case of Jura it is unknown if the ice could have lasted from the melting of the BIIS until the LLR. The apparent absence of recessional moraines and eskers may be consistent with recent interpretations of an abrupt melting of ice during the LLR as Golledge (2010) has recently suggested for the observations made throughout Scotland.

Summarising the Quaternary glacial history of Jura, it can be said that the BIIS strongly modified the landscape of Jura causing the smoothing of most of the landforms observed today. The BIIS covered most of Jura's landscape as the medial moraine found on the west coast indicates. The precise deglaciation age for Jura is unknown but the unpublished exposure ages obtained by Bishop and co-workers on the medial moraine are arguments in favour of a deglaciation age of $\sim$ 16 ka. The impact caused by ice in the landscape has also been imprinted in the stream long profiles of Jura as will be shown in the next chapter. Whether Jura remained ice-free before LLR is unknown, but it is possible that some glaciers have persisted at glacial cirques. The LLR re-activated the glacial activity but its effects on Jura are not well documented. However, it is possible that glaciers activity remained limited to glacial cirques modifying the topography which resulted in a the perturbation of the longitudinal profiles of rivers.

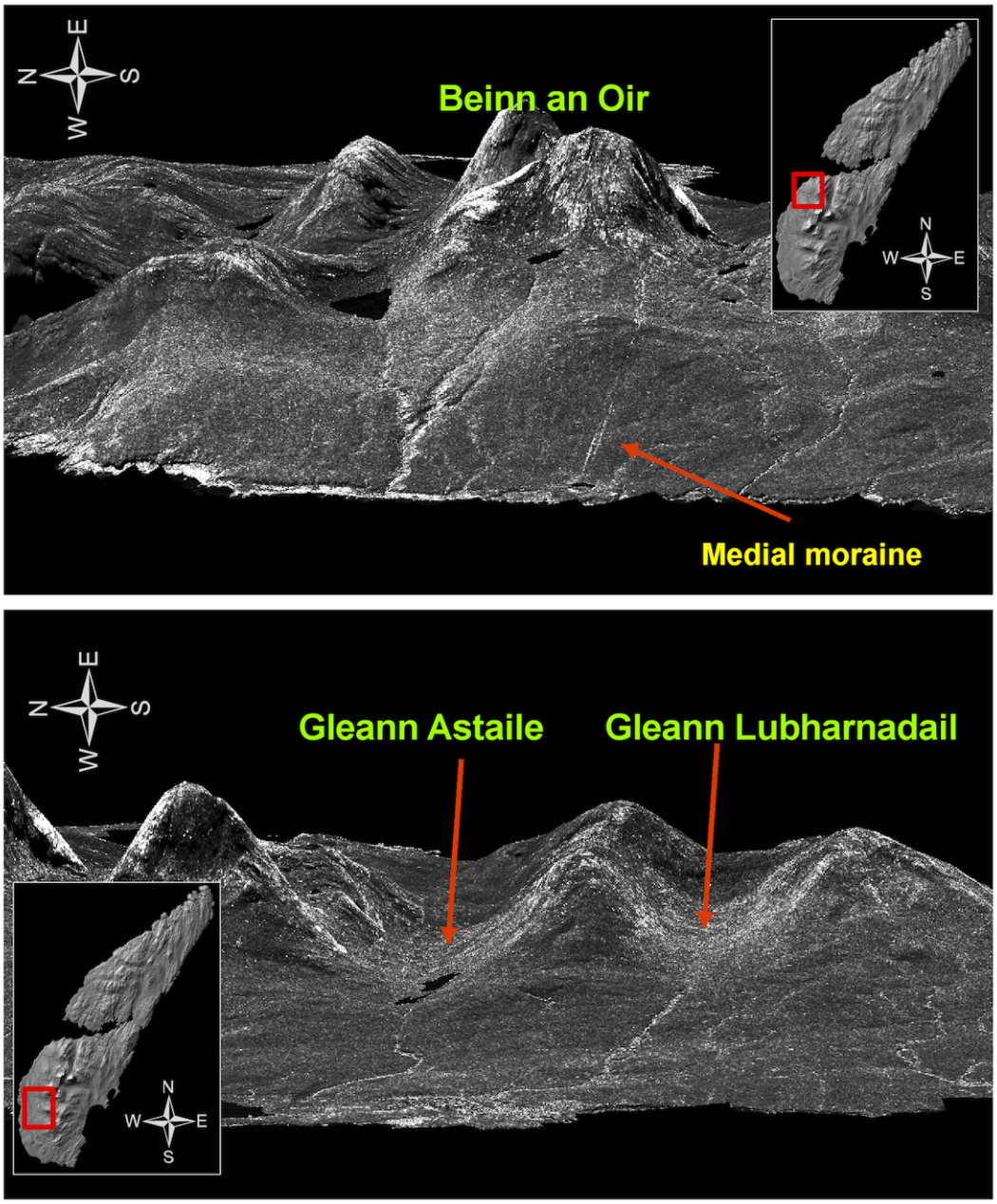

Figure 3.10: Glacial cirques (front) formed at the foot of Beinn an Oir (foreground at centre, upper photograph) located on the west flank of the mountains of Jura. The white strip that appears at the foot of the Beinn an Oir is the medial moraine reported by Dawson (1979). In the lower photograph, the Gleann Astaile (left) and Gleann Lubharnadail (right) valleys. Both valleys exhibit U-shaped morphology, which suggests that glaciers during the LLR were confined to the bottoms of valleys. Images were obtained from a SAR image overlaying a 5 m resolution DEM (NEXTMAP©). The vertical exaggeration for both pictures is of 2.5.

3.5 The glacio-isostatic rebound and the sea-level change

The melting of ice sheets after the LGM due to the increasing temperatures during the interglacial period produced a twofold effect: (1) a rapid rise in eustatic sea-level ~ 17 ka (Moran and Bryson, 1969; Fairbanks, 1989) and (2) in regions glaciated by ice-sheets, a glacio-isostatic rebound due to the flexural response of the lithosphere to the removal of the load imposed by an ice mass (Walcott, 1973). At the end of the LGM ($\sim$19 ka) sea level was approximately 120 m below its current level (Peltier and Fairbanks, 2006). The change in global glacio-eustatic sea-level after the LGM has been reconstructed from several sites (Figure 3.11) and in some way it is more or less well recorded by oxygen isotope (δ^{18}O) record. It has been estimated that eustatic-sea level rise after the LGM was $\sim$ 10 mm/yr (Alley et al., 2005) and at least two pulses occurred $\sim$ 19 ka and 14.5 ka in which the rate exceeded 50 mm/yr (Alley et al., 2005). At $\sim$ 6 ka the rate substantially slowed and eustatic sea-level stabilised (Moran and Bryson, 1969; Walcott, 1973).

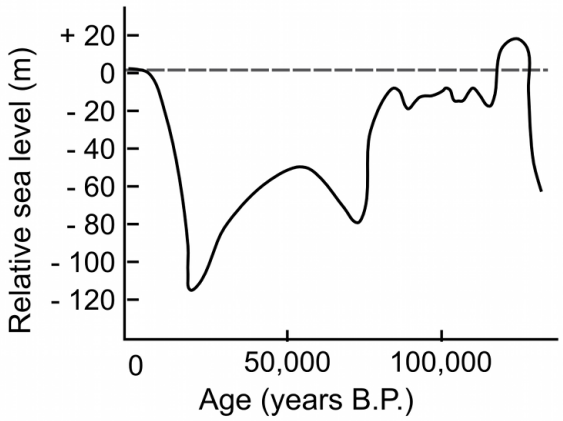

Figure 3.11: Curve of the glacio-eustatic sea level rise reconstructed from cores extracted in the Pacific, Barbados and New Guinea (Modified from: Shackleton and Opdyke, 1973). Note the minimum at $\sim$ 18 ka (LGM) when sea level was at ~ -120 m. The rise of eustatic sea level slowed dramatically at $\sim 6,000$ yr B.P. as can be see on the far left slope of the curve.

In regions covered by ice-sheets during the LGM (e.g., North America, Scandinavia, British Isles) the accumulation of ice and its subsequent melting generated an isostatic rebound due to the lithosphere's flexural response to the unloading being accommodated by elastic properties of the mantle (Walcott, 1973; Peltier and Fairbanks, 2006). The crustal uplift resulting from a glacio-isostatic rebound has been estimated by the dating of geomorphic markers such as raised beaches and strandlines on beaches and lakes (Walcott, 1973; Emery and Aubrey, 1985; Peltier and Fairbanks, 2006). The resultant relative sea level (RSL) are incorporated into geophysical and numerical models (e.g., Lambeck, 1993a; Lambeck et al., 2000; Peltier and Fairbanks, 2006).

Although the geomorphic markers have been found useful to evaluate glacio-isostatic rebound, a high precision estimate of uplift is made difficult by differential vertical movements of the crust which also causes difficulties in defining eustatic curves (Walcott, 1973; Sissons and Cornish, 1982). More recently, Global Positioning System (GPS) monitoring in areas subject to glacio-isostasy has been useful in estimating rates of crustal uplift accurately (e.g., Sjöberg et al., 2000; Dietrich et al., 2010).

For the particular case of the British Isles, the rate of post-glacial uplift has been estimated in two ways: (1) by the recognition of former shorelines, dating of raised beaches and through the stratigraphical record used for the delineation of isobases; and (2) through geophysical and numerical modelling using the data collected empirically (Lambeck, 1991; Shennan et al., 2002; Milne et al., 2006). The copious number of papers published in these two areas has brought confusion in the names used for different shorelines and marine landforms (Rice, 1977) and many interpretations and ages have been debated (Sissons, 1982; Dawson, 1984; Gray and Ivanovich, 1988). Also, inconsistencies in height of the RSL curves produced for some sites of the British Isles have been found (Shennan and Horton, 2002). The research on the sea-level change and the glacio-isostatic rebound for the British

Isles is prolific but not conclusive since new data are being produced continually and existing models require modification. The next subsections present the main evidence in relation to Quaternary post-glacial uplift and sea level change in the west of Scotland, with an emphasis on Jura. The last part of this chapter details how the timing of knickpoint initiation in Jura was constrained.

3.5.1 The sea-level change and the raised shorelines of Jura

Early studies of the raised beaches of the west coast of Scotland can be traced back to the work of Wright (1911). He identified at least three levels of beaches that were termed pre-glacial (> 30 m OD), late-glacial (30 m OD) and post glacial (7.6 m OD)[2]. His study mentions the presence of a continuous rock platform backed by a cliff which can be traced all along the west coast of Scotland. Wright (1911) interpreted the cliff as evidence of an old shoreline stating that " The continuity of the old cliff and platform along stretches of coast many miles in extent, and the manner in which the latter maintains a uniform level independently of, and often in spite of, the rock structure, are sufficient proof that we are dealing with an old shoreline" (Wright, 1911, p. 107). The rock platform was found to be eroded by ice and this led Wright to date it as pre-glacial in age.

McCann (1964) studied the raised beaches in north Islay and south-west coast of Jura and confirmed the presence of the 'Pre-glacial' rock platform identified by Wright which McCann termed as 'inter-glacial'. McCann (1964) also identified a younger cliff which was related to the 'post-glacial' beach which is exposed at $\sim$ 7.6 m OD. The deposits of a raised shingle beach overlying the so-called 'Preglacial Rock Platform' are characterised by several ridges. McCann found that the ridges are exposed between $\sim$ 36 m OD to 12 m OD and he interpreted them as markers of a retreating sea formed during the greatest submergence by the Late-glacial sea (McCann, 1964, his Figure 8). One portion of the raised beaches of the west coast

[2]In the text published by Wright (1911) the values of altitude are given in feet.

of Jura is shown in Figure 3.12.

Several authors continued the work on the raised beaches of the west of Scotland during the 1960s. Synge and Stephens (1966) analysed the altitudes of the raised shorelines, differentiating between a Late Glacial and the Post-Glacial shoreline in which they included data from Islay. They established a relation between the raised beaches of east and west Scotland and Ireland. They attributed the tilting of shorelines to glacio-isostatic uplift. In the 1970s numerous studies of sea-level change and associated landforms were published (e.g., Sissons, 1974; Gray, 1975; 1978). However, different interpretations began to arise in regard to the age and formation of some landforms like the 'Preglacial' rock platform identified by Wright (1911) (Sissons, 1982; Gray and Ivanovich, 1988).

No detailed studies of the raised beaches of Jura are then found until the work of Dawson, who focused on the study of the beaches of the Inner Hebrides, especially in Islay, Jura and Scarba (e.g., Dawson, 1980; 1982; 1997; Dawson et al., 1999). Dawson (1982) identified three shorelines in Islay and Jura which were differentiated by their heights. The altitudes of the three shorelines along with the so called 'Main Postglacial Shoreline' were found to be aligned to the centre of maximum uplift (Dawson, 1980; 1982) (Figure 3.13).

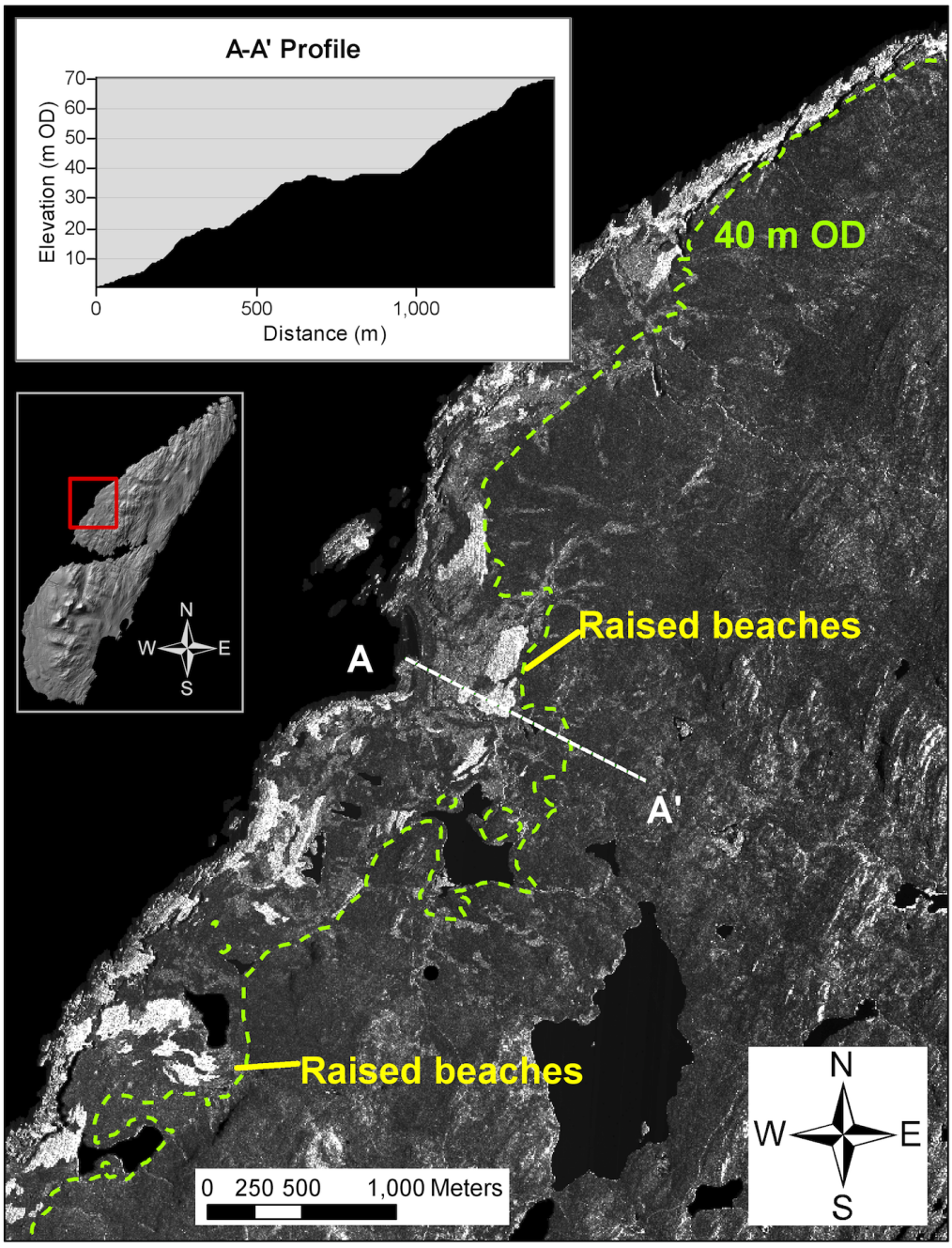

Figure 3.12: Image of one portion of the raised beaches exposed on the west coast of Jura. The beach deposits (white patches) are exposed at ∼40 m OD. Note also the flat surface at ∼ 40 m OD shown in the topographic profile).

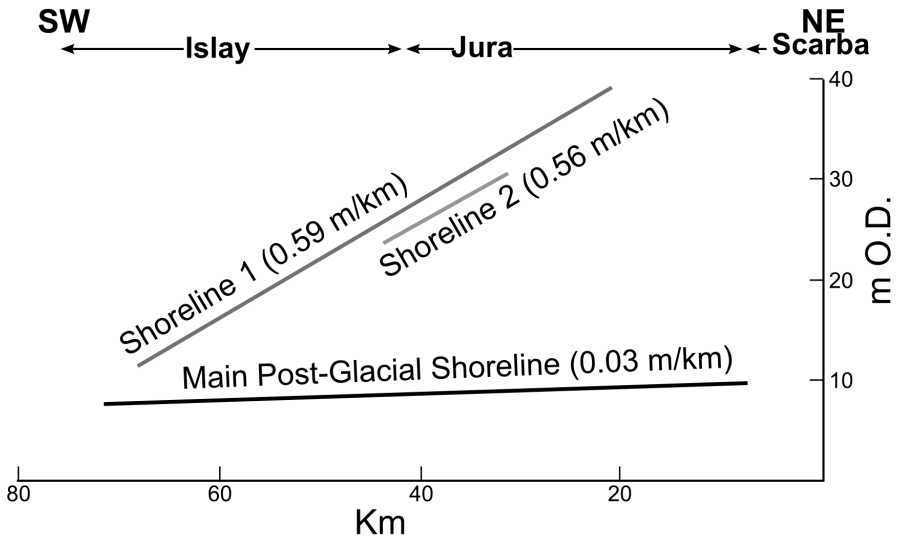

Figure 3.13: Regression lines of the shorelines identified by Dawson (1982) for the Inner Hebrides. Shorelines 1, 2 and the 'Main Post-Glacial Shoreline' decrease in height from the center of maximum uplift located east of Scarba. The difference in gradient between the 'Main Post-Glacial Shoreline' and shorelines 1 and 2 suggest a rapid change in sea-level (Modified from: Dawson, 1982)

The raised beaches ridges on the west coast of Jura were also surveyed by Dawson (1982) who recognised 55. However, the ridges and raised beaches of Jura were considered of limited value for reconstructing the sea level change due to their exposure to coastal erosion (Dawson, 1982). The lack of organic datable material in the shingle beaches also made dating difficult and, so sea-level curves have not been proposed (Dawson, 1982; Jardine, 1982). The rock platforms identified by Wright (1911) and re-named by McCann (1964) were analysed and discussed in detail by Dawson (1980). The cliff platform located $\sim$ 7 m OD mapped by McCann (1964) was surveyed in other sites of west Scotland by Gray (1978) and he used the term 'Main Rock Platform' for this feature. This platform is exposed at $\sim$ 11 m OD in Oban and to $\sim$ 5 m OD in the middle of Mull (Sissons, 1974; Gray, 1978; Dawson, 1980). The Main Rock Platform is tilted to the west and its declivity was related to the isostatic uplift located at the east (Gray, 1978; Dawson, 1980).

Dawson (1980) suggested that the origin of the Main Rock Platform was different from the lowermost fragments of the intertidal platform found on the west coast of Scotland. He surveyed the lowest platforms below the Main Rock Platform on the isles of Islay, Jura, Colonsay, Oronsay and Scarba and found that the level of the platforms was $\sim$ 1.8 m OD (Dawson, 1980, his Table 1). The lowermost platform was termed the 'Low Rock Platform' which according to Dawson (1980) is unrelated to the Main Rock Platform in that it does not exhibit any tilting but its age is thought to be inter-glacial due to evidence of glacial erosion on it (Dawson, 1980). The Main Rock Platform of the west coast of Scotland and in Jura, has been referred to by many authors (e.g., McCann, 1964; Sissons, 1974; Dawson, 1984). The main problem in regard to the interpretation of the platforms relate to their genesis and age. The preglacial age proposed by Wright (1911) has been contested by many authors (e.g., McCann, 1964; Dawson, 1980; Sissons, 1982; Sissons and Dawson, 1981). Sissons (1982) reviewed the existing literature in regard to the 'Preglacial' rock platforms and based on observations made on shorelines surveyed in Wester Ross suggested a younger age for the rock platform, emphasising its complex history and implying a polycyclic genesis.

Uranium ages of speleothems in the 'Main' rock platform in Lismore have yielded late glacial ages younger than 25 ka (Gray and Ivanovich, 1988) but it was suggested that the youngest platforms recognised might have formed some time before in polycyclic genesis. Later Stone et al. (1996) dating the rock platform in Lismore using ^{36}Cl cosmogenic exposures ages suggested a rapid erosion of the rock platform occurred $\sim 11ka$ which suggest a rapid erosion of the rock platform induced by rapid changes in climate. The formation of the rock platforms on the west coast of Scotland still await resolution.

The ridges formed on the raised shingle beaches on the west coast of Jura have been interpreted as a result of a retreating sea which was attributed to an isostatic

uplift (Dawson, 1982; Sissons, 1983). Although the ridges are well preserved, they have not been used to estimate the pattern of glacio-isostatic uplift as has been proposed for other sites (Andrews and Dugdale, 1970). Dawson (1982) reported a regular spacing of ridges of ~ 0.3 m, and suggested that the preservation of ridges can be interpreted as a period of continuous uplift or a steady sea-level retreat with no signs of transgression.

The height of the highest beach deposits found for shorlines 1 and 2 in Jura and Islay (Figure 3.13) approximates to beach deposits found on east coast of Scotland and conform to the Main Perth Shoreline identified by Sissons et al. (1966). The Main Perth Shoreline is tilted easterly (Sissons et al., 1966 , their Figure 1) and because of its similarity with the Late glacial Shoreline Jardine (1982) has suggested that this may be the counterpart of shorelines 1 and 2 found in western Scotland (i.e., Jura and Islay). Jardine (1982) proposed that the Main Perth Shoreline was probably formed $\sim$ 13 ka. The age proposed by Jardine (1982) approximates the unpublished cosmogenic ages obtained by Bishop and co-workers (pers. comm.) in samples extracted from the shingle beaches of west Jura. The ages obtained by Bishop and co-workers, will be presented in the final section of this chapter.

According to Sissons (1983), after the Late Glacial and during the LLR the sea level was low and the Main Late-Glacial Shoreline was eroded. This interpretation has not been well documented due to the limited exposure of sediments in few local sites found on the west coast of Scotland (Dawson, 1984). The Main Late-Glacial Shoreline is thought to have been formed during the Younger Dryas event (Dawson, 1984, his Figure 4).

The location and distribution of the deposits related to the Main Post-Glacial Shoreline are well documented in the west coast (e.g., Gray, 1978; Sissons, 1982; Dawson, 1984) and east coast (Sissons et al., 1966; Jardine, 1982; Dawson, 1984). The chronology of the deposits on the east coast has been used to reconstruct sea-

level changes during the Holocene (Dawson, 1984). By contrast, the chronology of the west coast is somewhat incomplete and ages have been correlated to the region of the Solway Firth (Jardine, 1982; Dawson, 1984). The reconstruction of the Main Post-Glacial shoreline on the west coast of Scotland is based on the identification of terraces related to the deposition of the Main Postglacial Transgression (Dawson, 1984). The approximate age of the Main Post-Glacial Shoreline has been set at $\sim$ 7 ka to 6 ka (Dawson, 1984). This shoreline in Jura has been related to the raised beaches found at Inver in south-west of Jura (Sissons, 1983; Dawson, 1984). The deposits related to this shoreline exhibit a regional variation that has been related to the glacio-isostatic uplift (Dawson, 1984, his Figure 8). In Oban the deposits crop out at $\sim$ 11 m OD and the highest deposit reach an altitude of 14 m OD (Jardine, 1982; Dawson, 1984).

In Table 3.4 is presented a synthesis of the shorelines recognized for the west of Scotland. The Main Post-Glacial shoreline overlies the deposits of the modern shoreline. Information on Late Holocene sea-level changes is still preliminary and a call to complete the existing information has been explicitly made (e.g., Jardine, 1982; Dawson, 1982). In the last fifteen years, an increasing number of studies have focused on the acquisition of a detailed record of Holocene sea-level changes. The data obtained have been used to estimate the rates of post-glacial uplift and major eustatic for Scotland and most of the British Isles (e.g., Firth and Stewart, 2000; Smith et al., 2000; Shennan and Horton, 2002).

3.5.2 The glacio-isostatic rebound in Jura

The glacio-isostatic rebound of the British Isles has been evaluated by: (1) the reconstruction of shorelines to produce isobases and/or (2) the use of RSL to constrain the geophysical modelling (Jardine, 1982; Milne et al., 2006). Several isobases maps have been produced for most of Scotland and north of England showing the altitudes of the different shorelines recognized for the Brith Isles (e.g., Gray, 1978;

Table 3.4: Quaternary shorelines formed in Islay and Jura recognized by Dawson (1982) .

Shoreline	**Age (ka)**	**Altitude (m OD)**	**Site**
L1	~ 13	$\sim 40 - 32$	West coast of Jura
L2	< 13	$\sim 30 - 22$	West coast of Jura
Main Late-Glacial	~ 11	~ 12	Loch Maol, Jura
Main Post-Glacial	$\sim 6 - 7$	~ 9	Blackrock, Islay

Sissons, 1981a; Dawson, 1984; Jardine, 1982; Smith et al., 2000). In a relatively recent paper, Smith et al. (2006), discussed the errors derived from interpolation of isobases and evaluated the goodness of fit obtained when using two different statistical interpolating methods (i.e., polynomial trend surface and gaussian trend surface). Based on the interpolation of several sites in the British Isles, these authors obtained a better fit using the gaussian trend surface model when compared to results from geophysical models.

The records of RSL change and the rates of uplift for most Scotland are restricted to the height obtained from the Main Post-glacial Shoreline. Unfortunately data on the rate of crustal uplift using empirical data for most of Scotland are scarce and results are restricted to isobase maps of the Main Post-Glacial shoreline. Firth and Stewart (2000) used RSL data to estimate some rates of crustal uplift for the last 18.5 ka at a few sites in Scotland. Their results suggest an exponentially declining in the rate of uplift with time (Figure 3.14).

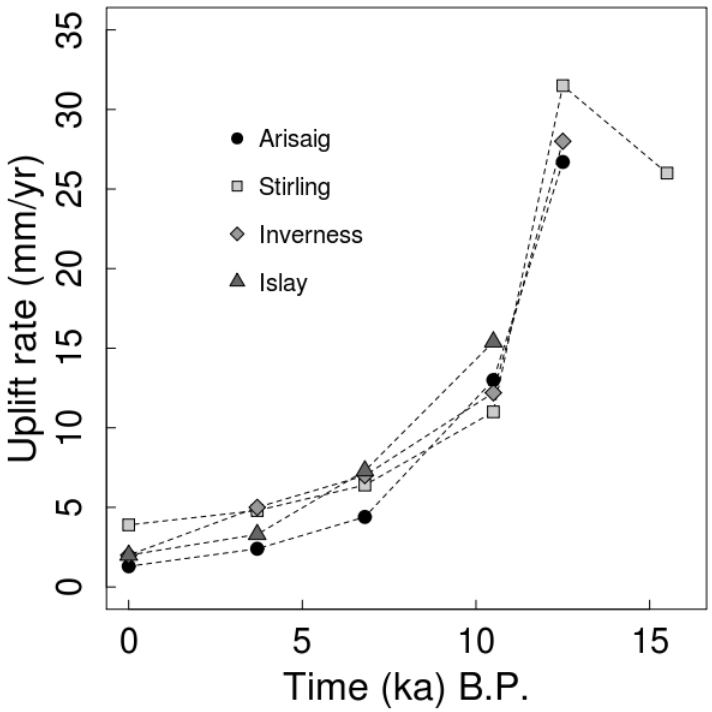

Figure 3.14: Crustal uplift from different sites of Scotland. A decrease in the rate occurred $\sim$ 7 ka. (Data extracted from Firth and Stewart, 2000)

The rates of Firth and Stewart (2000) on Islay can crudely approximate the rate of glacio-isostatic uplift in Jura. However, higher rates of uplift are expected in north of Jura because this section is closer to the area of maximum uplift ($\sim$ 90 km) when compared to Islay. Also, the exposure of shorelines L1 and L2 documented by Dawson (1982) suggest higher rates of uplift in Jura. Shennan and Horton (2002) used the RSL data with tidal corrections to obtain the rates of uplift and subsidence of British Isles for the last 4 ka. The values estimated for Islay were $\sim$ 1.46 mm/yr and a best fit estimated of 1.52 mm/yr (Shennan and Horton, 2002 , their Table 1). The rates of uplift in Islay (Figure 3.14), suggest a declining rate of uplift during the last 7 ka. This behaviour is expected since the rebound is faster during the first stage of deglaciation and decreases exponentially with time (Walcott, 1973; Sharma,

1984).

Research on the post-glacial uplift in the British Isles using geophysical modelling was started by Lambeck (Peltier et al., 2002; Milne et al., 2006) who produced a family of RSL curves for the last 18 ka in various UK sites (e.g., Lambeck, 1991; 1993b;a). Peltier et al. (2002) proposed an alternative model (ICE-4G) and questioned the values used by Lambeck (1993b) for mantle viscosity (i.e., 10^{25}Pa s), arguing that an average viscosity of 2×10^{21}Pa s fits better for the relaxation times of the isostatic rebound as has been observed in other sites. The lower viscosity is also representative of the viscosity of the upper part of the lower mantle. Using the model of Peltier and co-workers Shennan et al. (2002) evaluated the RSL for the last 16 ka in the whole British Isles.

Milne et al. (2006) highlighted limitations of the geophysical models arguing that they do not have any correction for topography. Thus, an overestimation of ice thickness is introduced, specially in mountainous terrains such as north-west Scotland. Also, variations in geophysical parameters such as lithospheric thickness and mantle viscosity, can produce different results. However, Shennan et al. (2006) evaluation of the models of Lambeck and Peltier using data from several sites of the British Isles, suggests that different values of lithosphere thickness, do not introduce significant differences in the models' RSL predictions.

The RSL prediction for the British Isles implementing the geophysical modelling has produced a good approximation of what has been recorded from the RSL index points (Shennan et al., 2002, their Figure 2). For the west coast of Scotland, Arisaig ($56°, 54'$N, $5°, 50'$ W) provides the most complete record of RSL (Shennan et al., 2006). Arisaig thus, provide a first estimate of the pattern of RSL in the west of Scotland but it is important to note that some variations are expected due to the location of sites relative to the area of major isostatic uplift (Shennan et al., 2006, their Figure 7).

Lambeck (1991) obtained the first curve of the RSL rise in western Scotland for the last 15 ka (Lambeck, 1991, his Figure 4D). In this curve the RSL drops constantly until $\sim$ 12 ka where the fall slows; positive values of RSL ocurred $\sim$ 7 ka, which might be related to the glacio-isostatic uplift after the LLR but a sea-level rise at this time is found in other far-field sites (Bird et al., 2010).

The family of predicted RSL curves for the west of Scotland presented by Shennan et al. (2006) varies slightly from Lambeck's curve. The curves of Shennan et al. (2006) for Islay and Knapdale (Figure 3.15) indicate that $\sim$ 17 ka the RSL descended steadily until 14.5 ka when a positive RSL took place. The RSL fell again $\sim$ 13.5 ka until 11 ka when a second rise of RSL occurred. At $\sim$ 6 ka the rise of the RSL ended and the fall of RSL started, and the drop continues to the present. Because Jura lies between Islay and Knapdale, its RSL curve would be expected to follow the trends of the Islay and Knapdale curves, whith the RSL in Jura expected to be higher than Islay but less than Knapdale due to the distance of Jura from the centre of isostatic uplift (Jardine, 1982). The RSL curves for the west of Scotland strongly suggest that the shorelines L1 and L2 found by Dawson (1982) were raised $\sim$ 13.5 ka and an estimation of the isostatic rebound can be obtained from such curves.

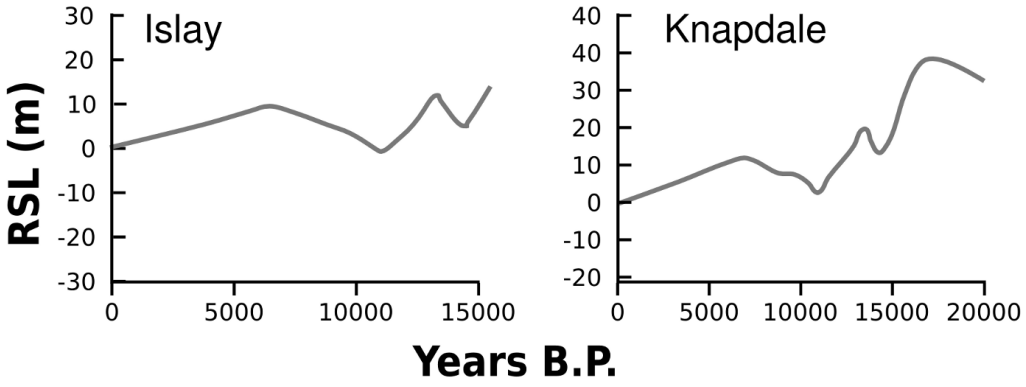

Figure 3.15: Predicted RSL curves produced by Shennan et al. (2006) for Islay and Knapdale. The curves shown here were obtained using a lithospere thickness of 71 km on a thick ice model.(Modified from: Shennan et al., 2006)

3.6 The base-level fall in Jura

The raised shingle beaches of the west coast of Jura (Dawson, 1982), their correlation to the Main Perth Shoreline (Jardine, 1982) and trend of the RSL curve obtained for the west coast of Scotland (Lambeck, 1991; 1993b; Shennan et al., 2006) confirm post-glacial glacio-isostatic uplift occurred in Jura $\sim$ 13 ka. Unfortunately, the information available for the glacio-isostatic uplift and its related deposits is incomplete and the published data available are only focused in few sites of the raised beaches of the west coast of Jura and the north of Islay (e.g., McCann, 1964; Dawson, 1982).

Bishop and co-workers (pers. comm.) sampled several shingle deposits in the meridional sector of the west coast of Jura to measure the concentration of *in situ* produced cosmogenic nuclides of ^{10}Be in grains of quartz obtained from quartzite cobbles in order to obtain exposure ages of the raised beaches (Figure 3.16). Their results are presented in Table 3.5 and a plot of the age versus elevation is presented in Figure 3.17.

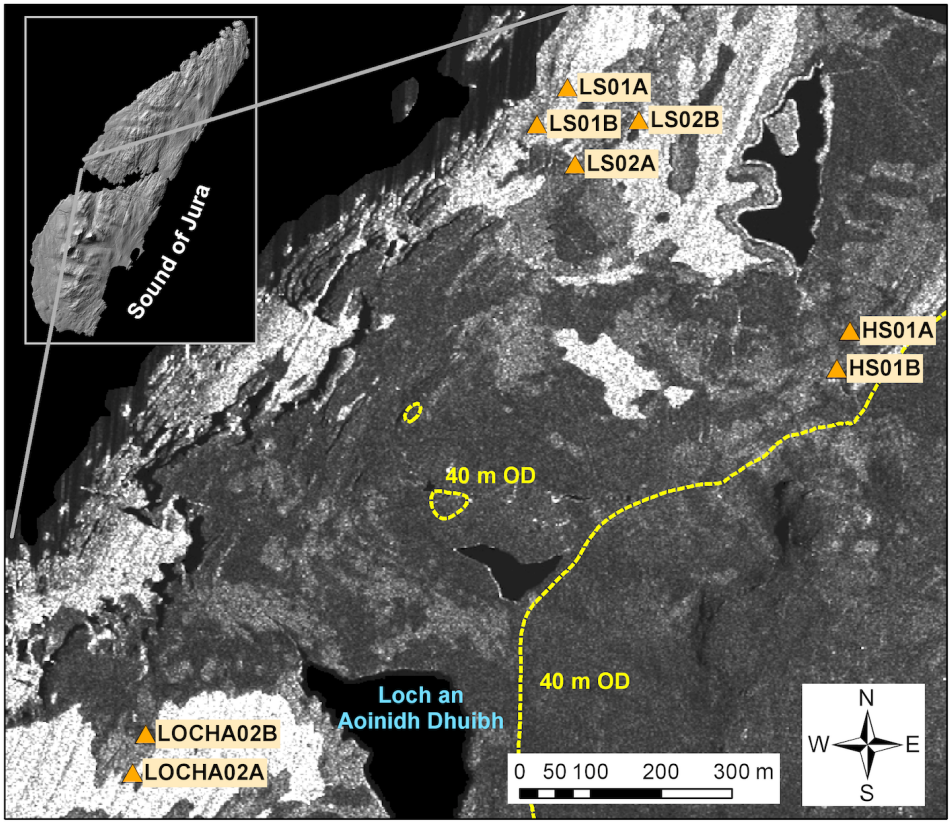

Figure 3.16: Location of the sites sampled by Bishop and co-workers to obtain the cosmogenic exposure ages of the raised beaches of Jura

Table 3.5: Exposure ages of shingle beaches samples of the west coast of Jura. Unpublished data of Bishop et al.

Sample	**Coordinate (Decimal degrees)**	**Elevation †** **(m OD)**	**^{10}Be (atoms/gr/yr)**	**Age §** **(yr)**
LS01A	56.0079, -5.9758	5.6	6822±1419	1,386± 311
LOCHA04B	55.9999, -5.9885	11.4	14237±1480	2,886± 387
LS02A	56.0071, -5.9754	9.1	20631±1678	4,168± 489
LS01B	56.0079, -5.9758	5.6	20634±1684	4,197± 493
LS02B	56.0071, -5.9754	9.1	29101±2986	5,882± 782
HS01B	56.0047, -5.9692	30.2	66393±3201	13,026± 1,269
LOCHA02B	55.9995, -5.9845	23.4	68150±3082	13,641± 1,309
LOCHA01B	55.9959, -5.9813	38.2	68828±3255	13,671± 1,326
LOCHA02A	55.9995, -5.9845	23.4	68488±3155	13,709± 1,321
HS01A	56.0047, -5.9692	30.2	71040±3652	13,942± 1,381

† The elevation values were extracted from a 5 m resolution DEM of NextMap©.

§ Samples were processed at the Scottish Universities of Environmental Research Centre (SUERC), UK.

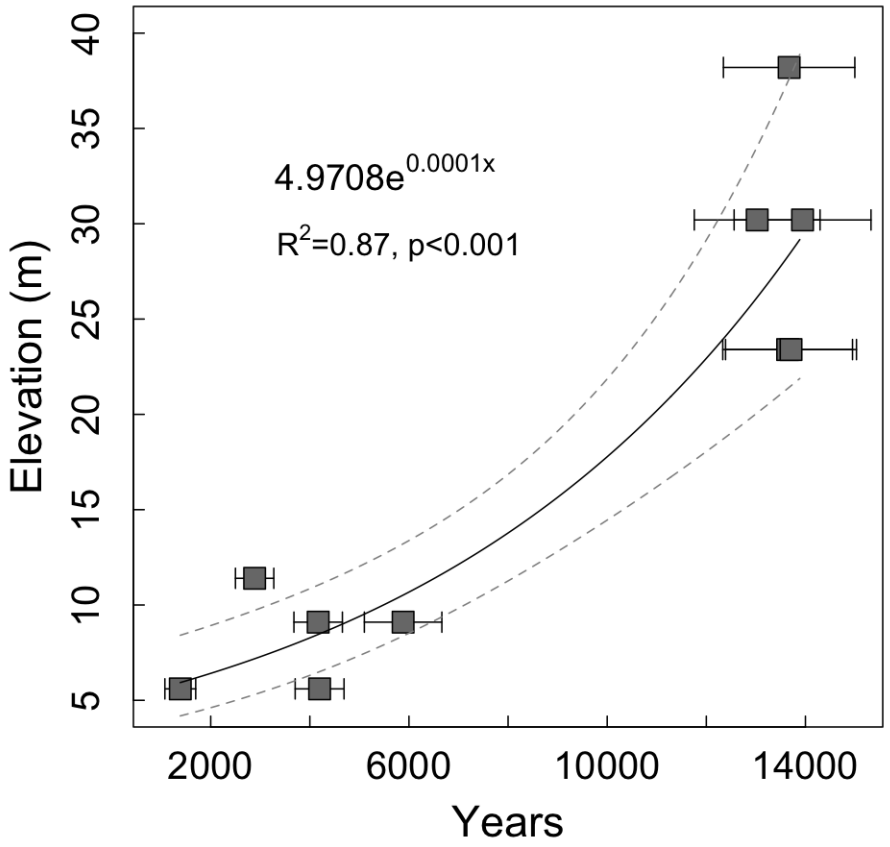

Figure 3.17: Plot of the ^{10}Be cosmogenic ages of the raised beaches of Jura versus elevation. The best curve fitting was obtained by an exponential function. The grey dashed lines indicate the confidence limits at 95%

The age of the highest shingle beaches obtained by Bishop and co-workers (pers. comm.) is of $\sim$ 13.6 ka (Table 3.5). The overall ages of samples located $\sim$ 23 to $\sim$ 38 m OD, are consistent with the altitude and age of the Main Perth Shoreline as Jardine (1982) previously inferred. The younger shingle raised beaches were sampled below 12 m OD and their ages indicate a shoreline formed after the LLR. The age obtained for the 12 m OD shoreline correspond reasonably with the interpretations of Dawson (1984) and Sissons (1983) for their Main Post-Glacial shoreline.

An exponential age-elevation relationship for Bishop and co-workers' data (Fig-

ure 3.17) shows that RSL steadily fell after the LGM with a shoreline well developed $\sim$ 13.6 ka. The cosmogenic ages obtained by Bishop and co-workers are consistent with the RSL curve modelled by Lambeck (1991) whereas the RSL curve of Shennan et al. (2006) seems to underestimate altitude of the shorelines for Islay and Jura. Although the cosmogenic ages exhibit some variability (Table 3.5) and the age of some samples located at 23 m OD are slightly higher than other located above, none of them exceeds 14 ka and none of them is younger than 13 ka. The variability in the age of some samples (i.e., 23 m OD) can be attributed to inheritance or erosion in the samples measured (Gosse and Phillips, 2001).

The ages obtained by Bishop and co-workers, contains a gap from 11 ka to 6 ka. The gap in the record strongly suggests a period of stability that formed the cliff of the west coas of Jura. This interpretation along with the evidence of age gap coincides with a marked period of raising of the RSL according to the curves of Shennan et al. (2006) and Lambeck (1993b). It is possible that the marine transgression had effaced the 11 ka to 6 ka record but it did not exceeded the current level of 23 m OD (Table 3.5). The highest beach deposits dated by Bishop and co-workers, correspond to the deposits mapped by McCann (1964) and Dawson (1982) and they represent the clearest evidence of the post-glacial uplift. The similarity in age of the shingles located at $\sim$ 20 m OD to $\sim$ 38 m OD suggest a rapid response of the isostatic uplift. The preservation of the lowest beaches (i.e., $\sim$ 20 m OD) with ages not younger than 13 ka and the RSL curves observed for the west of Scotland (Shennan et al., 2006) strongly suggest that the rapid glacio-isostatic uplift may have induced a drop on rivers base-level of $\sim$ 18 m. The base-level lowering explains the formation knickpoints at stream's outlet and their further propagation upstream as it is predicted from theory (Whipple and Tucker, 1999). Thus, the base-level fall in Jura represents a truly case of a rapid increase in the rate of rock uplift. The mean value of the beaches dated yield an age of 13.6 ka. The absolute age (i.e., 13.6 ka) of the raised shoreline of Jura termed L2 by Dawson (1982; 1984) as L1 will be used in order to avoid confusion with the terminology used for the

shorelines found in Scotland.

In order to identify the precise elevation of the 13.6 ka shoreline, systematic mapping of the highest beach deposits on Jura was undertaken by interpreting air photographs at scale of $1 : 24,000$ (Table 3.6) held at the the office of the Royal Commission of Historic and Ancient Monuments of Scotland (RCHAMS). Only the raised beaches of the west coast were selected because they are clear *in situ* and can be easily identified on air photographs. Also, the available cosmogenic ages of the deposits of the west coast reduce the uncertainty of the shoreline identified on this side of the isle.

The beach deposits recognised on the air photographs (Table 3.7) were introduced as points in the GIS (Figure 3.18). The elevation was subtracted from a 5 m resolution DEM from NEXTMAP©. The distance of every point ($n = 16$) was measured from an arbitrary point control set at the north tip of Jura in order to evaluate any difference in elevation along the isle (Table 3.7). A normality test was carried out to detect if there are significant differences in elevation among the beach deposits recognised. The elevation values of the raised shingles exhibit a wide dispersion ($\sigma^2 = 2.90$ m). The Shapiro-Wilk test of normality performed in the statistical software R (R Development Core Team, 2009) yield values of $W = 0.84$ and p-value: 0.01. Being $p < \alpha : 0.05$, the null hypothesis is rejected and it confirms the non-normal distribution of the elevation values. A density histogram of frequency reveals a bimodal trend in the frequency of the data (Figure 3.19).

Table 3.6: Air photograph lines consulted at the RCHAMS.

Name	Library no.	Sortie no.	Survey date	Altitude (Ft)	Focal length (mm)	Film format	Scale	Copyright
1	C0237	ASS/612/88	May 16 1988	12000ft	152.31mm	BW99	1:24,000	RCAHMS
2	C0237	ASS/612/88	May 16 1988	12000ft	152.31mm	BW99	1:24,000	RCAHMS
3	C0265	ASS/505/88	May 16 1988	12000ft	151.91mm	BW99	1:24,000	RCAHMS
4	C0265	ASS/505/88	May 16 1988	12000ft	151.91mm	BW99	1:24,000	RCAHMS
5	C0272	ASS/512/88	Jun 10 1988	12000ft	151.91mm	BW99	1:24,000	RCAHMS
6	C0272	ASS/512/88	Jun 10 1988	12000ft	151.91mm	BW99	1:24,000	RCAHMS
7	C0274	ASS/514/88	Jun 14 1988	12000ft	151.91mm	CL99	1:24,000	RCAHMS
8	C0237	ASS/612/88	May 16 1988	12000ft	152.31mm	BW99	1:24,000	RCAHMS
9	C0237	ASS/612/88	May 16 1988	12000ft	152.31mm	BW99	1:24,000	RCAHMS
10	C0237	ASS/612/88	May 16 1988	12000ft	152.31mm	BW99	1:24,000	RCAHMS
11	C0237	ASS/612/88	May 16 1988	12000ft	152.31mm	BW99	1:24,000	RCAHMS
12	C0237	ASS/612/88	May 16 1988	12000ft	152.31mm	BW99	1:24,000	RCAHMS
13	C0272	ASS/512/88	Jun 10 1988	12000ft	151.91mm	BW99	1:24,000	RCAHMS
14	C0273	ASS/513/88	Jun 10 1988	12000ft	151.91mm	CL99	1:24,000	RCAHMS
15	C0274	ASS/514/88	Jun 14 1988	12000ft	151.91mm	CL99	1:24,000	RCAHMS
16	C0274	ASS/514/88	Jun 14 1988	12000ft	151.91mm	CL99	1:24,000	RCAHMS
17	C0272	ASS/512/88	Jun 10 1988	12000ft	151.91mm	BW99	1:24,000	RCAHMS

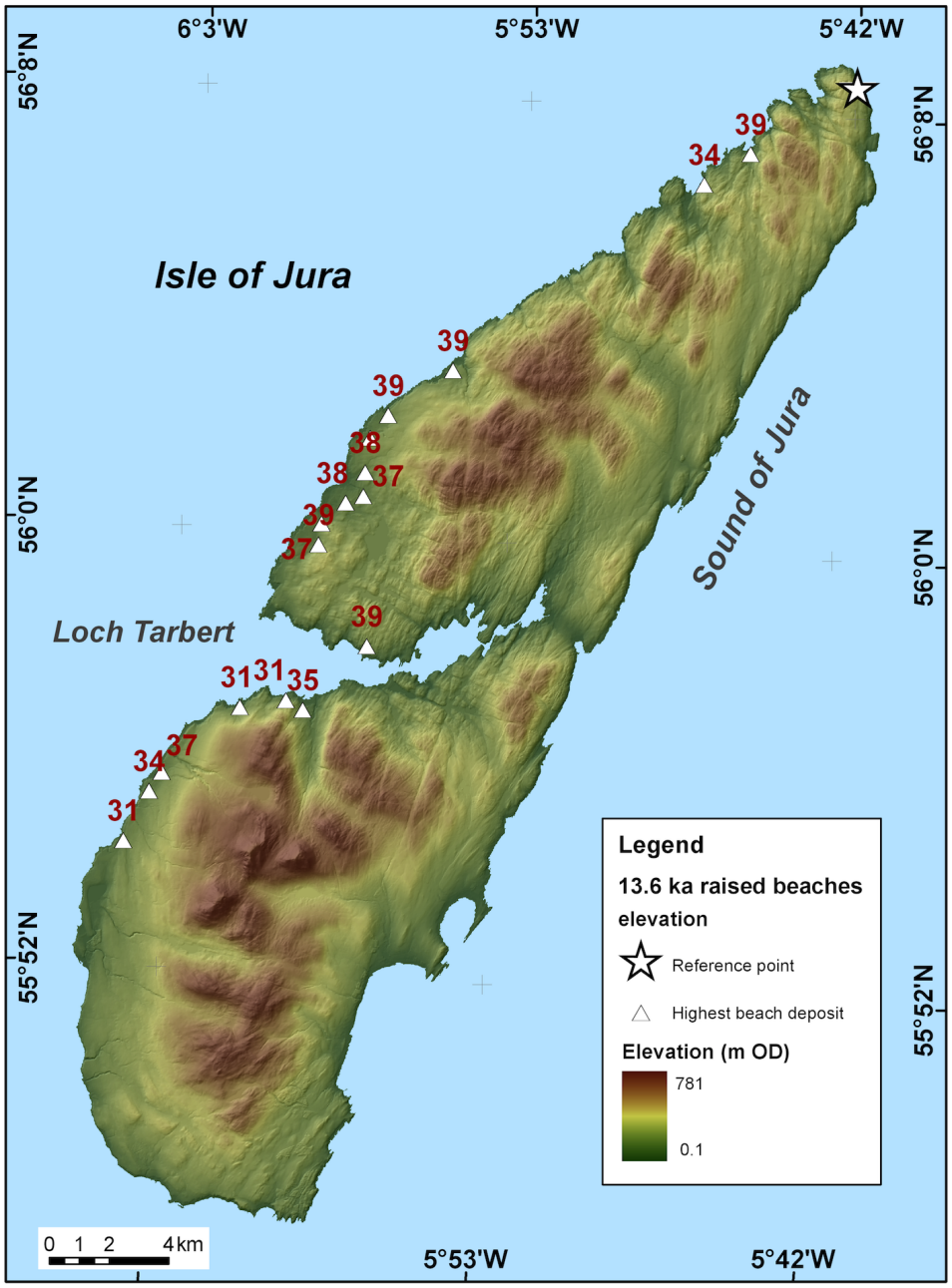

Figure 3.18: Map showing the highest beach deposits identified on the west coast of Jura

Table 3.7: Elevation values of the highest beach deposits recognised in the west coast of Jura. The first row contains the coordinates of the fixed point from which distance was measured.

Coordinate UTM (x,y)	**Elevation (m OD)**	**Distance (km)**
170203, 700640	-	-
154443, 689650	39	19.2
166621, 698427	39	4.2
152102, 685316	39	23.7
156622, 691163	39	16.6
153730, 681901	39	25.0
153016, 686721	38	22.1
153679, 687734	37	21.0
153616, 686937	37	21.5
146842, 677682	37	32.8
152205, 686020	37	23.2
153842, 688903	37	20.1
151577, 679762	35	28.0
146409, 677052	34	33.5
151007, 680097	31	28.1
149467, 679862	31	29.4
145557, 675386	31	35.3

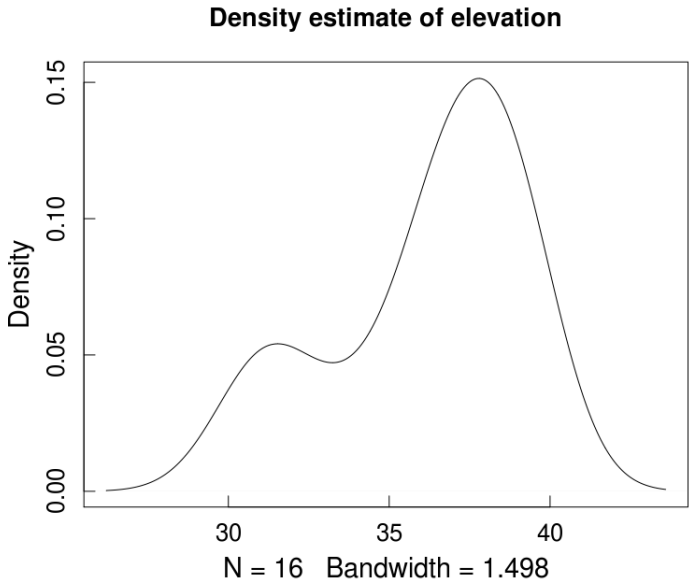

Figure 3.19: Density estimate of the observed high beach deposits of the west coast of Jura. The shape of the curve denotes a bimodal distribution which suggest a non-normality of the elevation values analysed.

The non-normal distribution of the elevation values and $\sigma^2 > 2$ m suggest strong differences among the elevation values of the raised beach deposits. A priori, it was expected that the 13.6 ka shoreline might have some local differences in elevation following the gradient of shorelines L1 and L2 (Dawson, 1982). Variations in elevation might be expected to be higher in the north of Jura and less in the south due to from the centre of maximum glacio-isostatic uplift. This was confirmed by performing a regression of elevation and distance using the values of Table 3.7. The linear regression obtained is shown in Figure 3.20 where it can be observed that the elevation decreases as the distance from the north tip of the isle increases. Although the correlation is weak ($R^2 = 0.27$) the elevation-distance relationship is significant ($p < 0.05$).

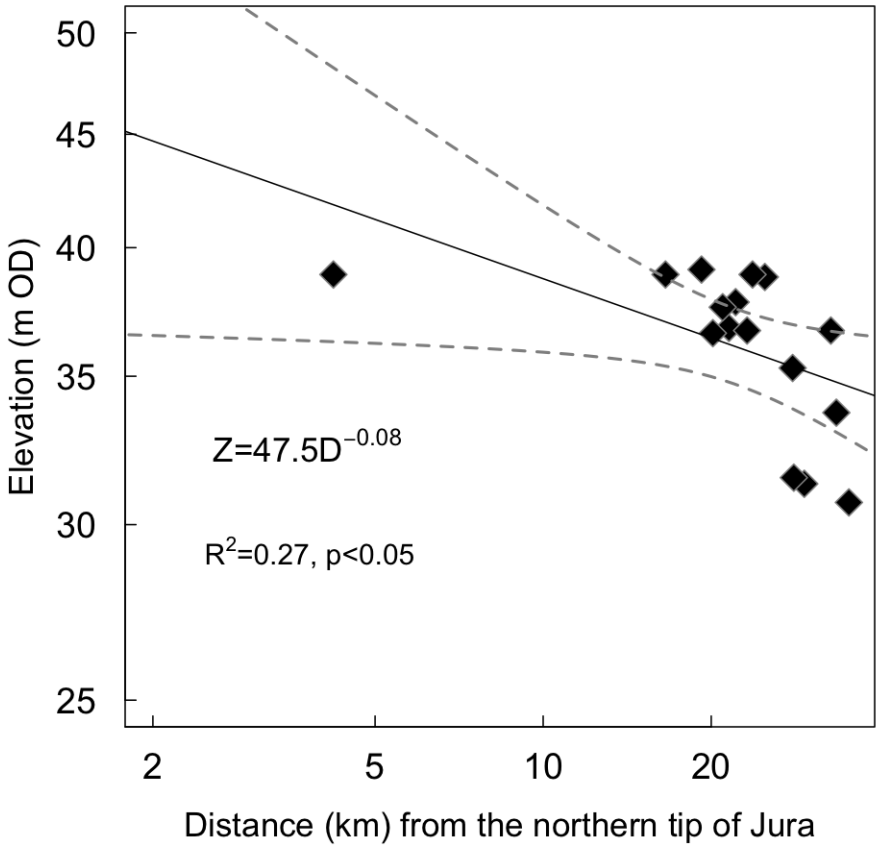

Figure 3.20: Plot of the elevation values of the 13.6 ka raised beaches against the distance to a fixed point in the isle Jura. The power law function indicate that the beach elevation decreases in respect to the distance located at the north of the isle. The change in elevation highlights the local control exerted by a differential response of the glacio-isostatic uplift. The grey lines in the plot indicate the 95% confidence limits.

The power law function observed for the highest beach deposits demonstrate that in Jura the 13.6 ka shoreline is tilted down from north to south with these new data apparently consistent with other observations (e.g., Dawson, 1982; 1984). The data are also consistent with the differential uplift being related to the centre

of maximum glacio-isostatic rebound to the north-est of Jura. The RSL of the 13.6 ka yields a mean elevation of 36 ± 3 m OD. In the analysis of the stream profiles in subsequent chapters the limit of the 13.6 ka was set at 35 m OD. This value lies within the confidence limits of the above value and simplifies the rationale for the DEM analysis to define the point when the drop of the base-level fall started.

3.7 Morphometric analysis

The quantitative characterisation of stream channels and river basins is an old topic of in fluvial geomorphology and the general basis and principles of the fluvial morphometry can be found in many textbooks (e.g., Leopold et al., 1964; Chorley et al., 1984; Knighton, 1998). The morphometry of fluvial basins provides valuable information on basin characteristics of rivers basins as well as basins' geometrical properties, including shape, length and relief. The morphometry of fluvial basins is expected to change from sites according to contrasts in lithology, structure, climate and tectonic activity. The availability of DEMs has re-enhanced efforts in morphometric analysis of the landscape (Pike, 2000) largely because such analysis can now be done more rapidly than by using the traditional cartographic methods. For the purpose of this research, morphometry is used to evaluate the physical properties of Jura rivers and basins. It is expected *a priori* that the glacial inheritance in the landscape of Jura is reflected on the morphometry. Also, the relatively homogeneous lithology of the isle with a well defined structure facilitates the testing of structure on the propagation of knickpoints (cf., Miller, 1991). The morphometric analysis to evaluate the physical properties of Jura are detailed in the sections below.

3.7.1 Strahler's integral

Estimating how eroded the landscape is is a difficult task because it is a result of many processes that modify the landscape. However, for the case of fluvially dominated landscape, one useful way to assess the erosion of river basins is by estimating the missing rock volume of a river basin which can be assessed by integrating the change in area with respect to elevation. This form of analysis was proposed by Strahler (1952) and the method is therefore commonly known as Strahler's hypsometric integral (Pike and Wilson, 1971; Mark, 1975).

Strahler's hypsometric integral is obtained from a definite integral of the catch-

ment area (a) in respect to elevation (h). It is expressed in normalised form as:

$$V = \int_0^1 adh \tag{3.1}$$

where 1 and 0 of the integral sign correspond to the limit of the summit and outlet of the catchments. An alternative form that approximates V is using the values of elevation as follows (Pike and Wilson, 1971):

$$E = \frac{H_{mean} - H_{min}}{H_{max} - H_{min}} \tag{3.2}$$

where E is the relative proportion of the upland and lowland part of the basin and H is the elevation value. Equation 3.2 has been shown to produce a similar result to that of equation 3.1 (Pike and Wilson, 1971) and it is useful since no data on drainage area are required. However, the current availability of DEM and hydrologic tools has made it easier to estimate Strahler's integral from its original form (equation 3.1).

Strahler (1952) used the hypsometric integral to evaluate quantitatively the age of the landscape as related to stage of equilibrium and disequilibrium. Strahler used this approach as a more objective classification of the youth, maturity and old-age of landscape as in the Davisian model of landscape evolution (Davis, 1889). Because the hypsometric integral is dimensionless, the values provide information of the existing volume of rock of a basin therefore, the missing volume is assumed to be eroded from the landscape. Thus, values close to 1 indicate that most of the underlying rock is still present in a less eroded terrain. In contrast, hypsometric values close to 0 strongly indicate that an effective mass removal has occurred in a fully eroded basin. The hypsometric integral is however, valid for certain landscapes in which the erosion has been dominated by fluvial processes and where basins have more or less the morphology.

The hypsometric integral is used here to assess the morphology characterising the basins of the bedrock rivers of Jura. It is also expected that the hypsometric integral would indicate those basins where glaciers have removed most of the existing rock volume. A priori it is expected that in the large basins, the action of glaciers would be more intense. The hypsometric integral was calculated for 34 catchments using equation 3.1 from the 5 m DEM data, the elevation and drainage area data were processed in a script generated for Matlab© program (MathWorks, 2007). The streams were also differentiated according to their main orientation for further analysis of the effect of structure. The results are summarised in Table 3.8 and the spatial distribution of the basis is shown in Figure 3.21.

The mean hypsometric value for the Jura catchments of 0.34 indicates that most of the basins have a reduced volume of rock thus, $\sim 30\%$ for the underlying rock is still present. Results in other settings like those of Brocklehurst and Whipple (2004) suggest that for the glaciated rivers in the Sierra Nevada of California, USA, the hypsometric values are lower in comparison to the fluvially eroded basins. The low values of the hypsometric integral on the glaciated basins suggest an effective erosion caused by glaciers.

For the particular case of Jura, the low mean values suggest that glacial processes occurred during the LGM and LLR may have resulted in the removal of large volumes or rock. A close examination of the data indicates that there is some variability in the values obtained. A t-test indicates that ($t = 14.29$) the null hypothesis is rejected and it is interpreted that there are catchments which does not fall close to the mean value. The hypsometric values were compared against the drainage area to explore if there is an effect in the erosion of landscape related to the basin size. The analysis was performed separately on the dip-slope, scarp-slope and strike flowing rivers. The equations obtained and the regression statistics are presented in Table 3.9 and graphically in Figure 3.22.

Table 3.8: Hypsometric integral values and structural characteristics Jura streams

Stream ID†	Strahler's integral	Structure
1	0.39	Scarp-slope
2	0.47	Scarp-slope
3	0.26	Scarp-slope
4	0.53	Scarp-slope
5	0.41	Scarp-slope
8	0.66	Scarp-slope
10	0.15	Scarp-slope
11	0.30	Dip-slope
12	0.53	Scarp-slope
13	0.23	In-strike
14	0.25	In-strike
15	0.28	Scarp-slope
16	0.45	In-strike
17	0.37	Scarp-slope
18	0.20	In-strike
19	0.41	Scarp-slope
20	0.25	Scarp-slope
21	0.41	Dip-slope
22	0.23	Scarp-slope
23	0.34	Dip-slope
24	0.31	Dip-slope
25	0.21	Scarp-slope
26	0.44	Scarp-slope
27	0.58	Scarp-slope
28	0.57	In-strike
29	0.28	In-strike
30	0.26	Dip-slope
32	0.57	Dip-slope
33	0.27	In-strike
34	0.39	In-strike
35	0.18	In-strike
36	0.20	Dip-slope
37	0.17	In-strike
38	0.14	Scarp-slope

†The streams ID, location and names are detailed in chapter 4.

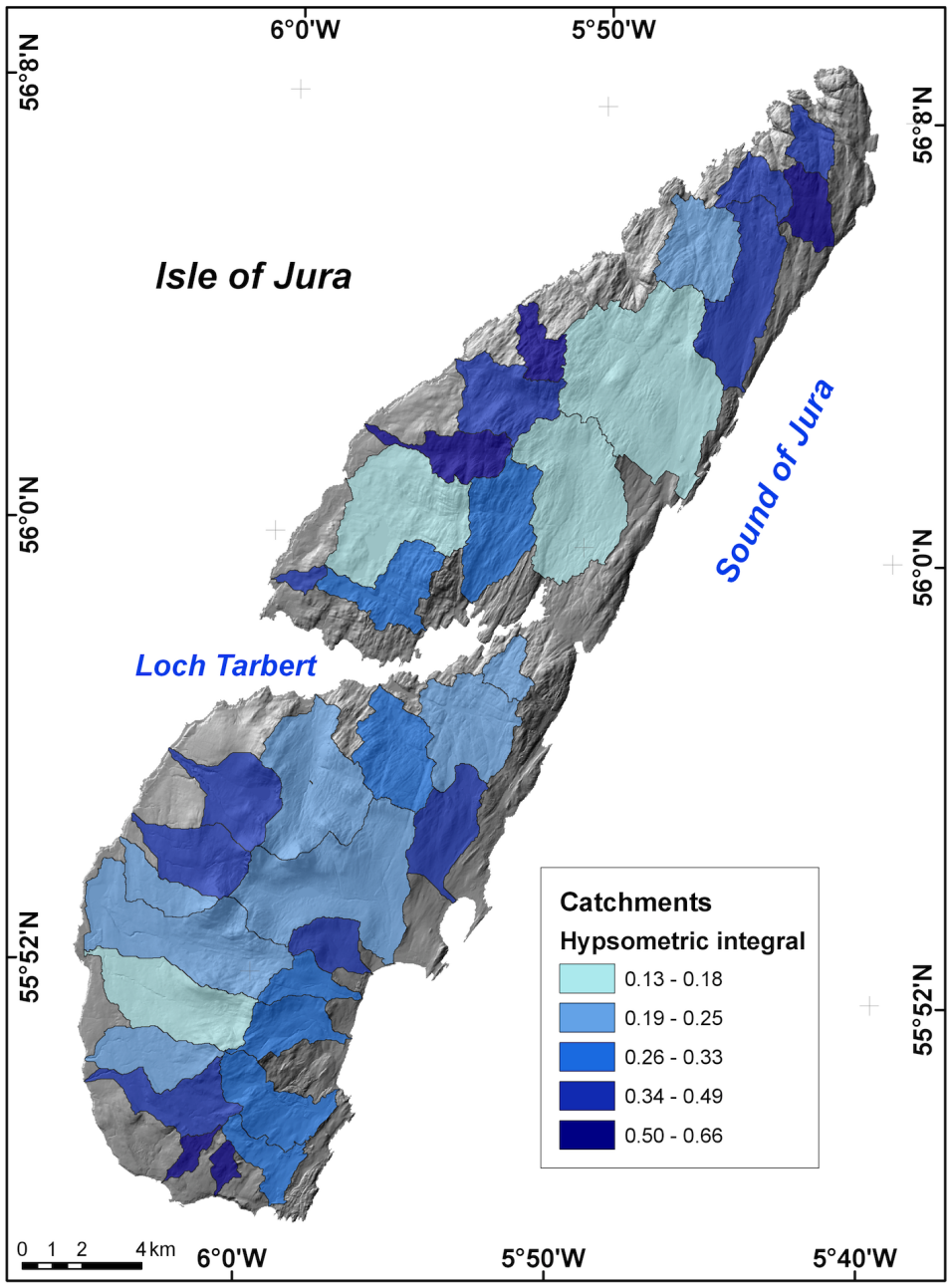

Figure 3.21: Map of the hypsometric integral of 34 basins of Jura. The map shows a trend where large basins have low hypsometric integral value. The highest hypsometric integral values are related to the small basins.

Table 3.9: Equation and summary of the regression statistics of the hypsometric integral against drainage area

Streams	**Equation**	$\mathbf{R^2}$	**RSE**	**p-value**
Dip-slope	$S_{int} = 0.66A^{-0.42}$	0.96	0.2036	2.32×10^{-2}
Scarp-slope	$S_{int} = 0.63A^{-0.37}$	0.55	0.3203	6.12×10^{-4}
In-strike	$S_{int} = 0.46A^{-0.26}$	0.42	0.3255	4.42×10^{-2}
Full	$S_{int} = 0.58A^{-0.35}$	0.52	0.2937	1.2×10^{-6}

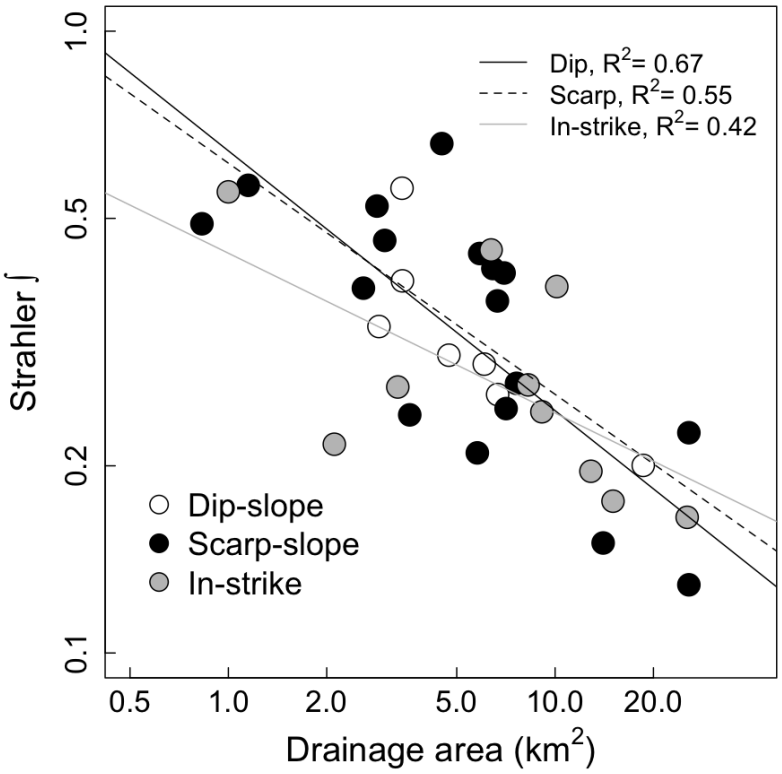

Figure 3.22: Relationship of hypsometric integral and drainage area. The slope of the three regression lines are similar, suggesting that structure is not a first-order control of erosion of landscape.

The results strongly indicates that the drainage area is closely related to the values of the hypsometric integral. As a general rule it can be noted that the larger the catchments, the more concave is the basin. Interestingly, the correlation values were only moderate for the three types of structural settings rivers, with drainage area explaining $\sim$ 50% of the total variance. The drainage area on itself cannot fully explain the values of the hypsometric integral since past glacial processes have eroded the landscape and have probably increased the drainage areas as well as lowering the relief of Jura.

In order to evaluate if there were any significant difference between the regression lines of the different relationships between the drainage area and the hypsometric integral, an analysis of covariance (ANCOVA) was performed in R (R Development Core Team, 2009) and the results are presented in Table 3.10. The examination of the p-values of the ANCOVA indicate that structure does not seem to generate an important effect on the erosion of the the rivers catchments. This also indicates that the erosional form of landscape is more or less similar regardless of structure.

Table 3.10: ANCOVA summary for the regression of drainage area and the hypsometric integral per structure.

Coefficients	**Estimate**	σ	**T value**	$Pr(>\|t\|)$
Intercept	-0.41411	0.34637	-1.196	0.2419
Log(Drainage area)	-0.42237	0.19563	-2.159	0.0396
Structure: Scarp-slope	-0.04379	0.37987	-0.115	0.9091
Structure: In-strike	-0.36019	0.40958	-0.879	0.3867

3.7.2 Hack's law

In a fluvially eroded landscape, the drainage area is tightly related to drainage density (Hack, 1957; Knighton, 1998) and because fluvial processes are responsible for modifying the topography, the stream network is likely to determine, at least partially, the basin geometry (Hack, 1957). Horton (1945) analysed quantitatively stream networks in relation to the drainage area and Hack (1957) subsequently, introduced the functional relationship between drainage area and stream length to characterise the relation between the shape of the basin and its geometric relation to drainage network. This relation is modelled as:

$$L = cA^x \tag{3.3}$$

where L is the distance measured from the divide to the outlet, A is the drainage area, c is a constant and the x captures the geometry of the basin and its relation to drainage density. The drainage area-length relationship commonly known as Hack's law (Whipple and Tucker, 1999; Willemin, 2000; Crosby and Whipple, 2006) has been tested in different fluvial settings where exponent values range between $x = 0.5$ and $x = 0.6$ (Willemin, 2000; Stolar et al., 2007). Here Hack's law is termed the area-length (AL) model and AL regression for simplicity. Willemin (2000) argued that Hack's law does not necessarily capture basin geometry with distance. Rather, the change in channel geometry in relation to basin area is being captured. Unfortunately, the conclusions of Willemin (2000) are based on the analysis of few catchments and omitted any variation in Hack's law exponent. Thus, there is not enough evidence to discard the drainage area-length relationship as an indicator of channel geometry. Moreover, the empirical and theoretical results of Rigon et al. (1996) indicates that there is a basin elongation for Hack's when $x > 1$. The geometric implications of AL regression is useful because contributing areas from the headwater are integrated into x (Stolar et al., 2007). Here the AL analysis is used to estimate: (1) if Hack's law holds true for the small bedrock rivers of Jura and, if so, (2) to assess if the rivers basins elongates as its is expected from theoretical estimations (Rigon et al., 1996). The AL regression was performed for the 34 Jura streams and the results are shown in Table 3.11 and in Figure 3.23.

A strong correlation exists in the AL regression, which in all cases is significant (Table 3.11). The data indicate that the x exponent is concentrated ~ 0.65 to ~ 0.75 with a mean of 0.73. However, some few rivers ($n = 7$, Table 3.11) have a high value ($x > 0.9$). Hack (1957) reported a value of ~ 0.65 for some of the rivers of the Appalachians and Stolar et al. (2007) in the steady-state landscape of Taiwan obtained 0.53 to 0.63 and a mean of 0.53. If the theoretical estimations of Rigon et al. (1996) are correct, rivers with $x > 1$ are those where the basin does not longer elongate as the distance downstream increases. Lack of elongation would then be related to a lack of an effective river incision in the basin occurring at the

Table 3.11: Constant and exponent of the power law function of the drainage area-length relationship for 34 streams and correlation statistics

Stream ID	Equation	R^2	RSE	p-value
1	$1315L^{0.72}$	0.94	0.183	$2.3\times^{-110}$
2	$1094L^{1.05}$	0.95	0.229	$1.4\times^{-114}$
3	$1604L^{0.57}$	0.91	0.240	$1.6\times^{-104}$
4	$1272L^{0.84}$	0.97	0.147	$1.7\times^{-249}$
5	$1411L^{0.70}$	0.93	0.299	$1.2\times^{-223}$
8	$1055L^{0.89}$	0.94	0.291	$2.7\times^{-191}$
10	$1485L^{0.59}$	0.90	0.388	$5.4\times^{-170}$
11	$1593L^{0.68}$	0.95	0.241	$3.2\times^{-160}$
12	$2351L^{1.02}$	0.95	0.193	$8.9\times^{-81}$
13	$2126L^{0.75}$	0.82	0.358	$3.3\times^{-79}$
14	$1133L^{0.64}$	0.88	0.394	$4.4\times^{-71}$
15	$1454L^{0.73}$	0.92	0.344	$4.8\times^{-176}$
16	$1403L^{0.60}$	0.86	0.561	$1.8\times^{-80}$
17	$1324L^{0.64}$	0.89	0.424	$9.7\times^{-167}$
18	$1390L^{0.64}$	0.92	0.272	$2.5\times^{-230}$
19	$1193L^{0.88}$	0.96	0.218	$1.5\times^{-242}$
20	$2121L^{0.72}$	0.87	0.448	$2.7\times^{-160}$
21	$1596L^{0.56}$	0.92	0.219	$2.8\times^{-160}$
22	$1135L^{0.68}$	0.99	0.137	$5.7\times^{-241}$
23	$1847L^{0.67}$	0.87	0.393	$9.6\times^{-188}$
24	$1953L^{0.53}$	0.85	0.363	$2.7\times^{-167}$
25	$2079L^{0.74}$	0.93	0.306	$4.2\times^{-249}$
26	$1376L^{0.68}$	0.96	0.263	$8.3\times^{-160}$
27	$2021L^{0.81}$	0.93	0.241	$1.8\times^{-95}$
28	$1818L^{1.03}$	0.93	0.321	$3.5\times^{-82}$
29	$1939L^{0.95}$	0.92	0.347	$9.0\times^{-144}$
30	$1592L^{0.61}$	0.88	0.437	$1.0\times^{-156}$
32	$1242L^{0.98}$	0.93	0.255	$2.9\times^{-106}$
33	$1612L^{0.65}$	0.92	0.329	$1.7\times^{-206}$
34	$1363L^{0.65}$	0.94	0.319	$1.1\times^{-108}$
35	$1295L^{0.60}$	0.92	0.286	$7.2\times^{-185}$
36	$1166L^{0.59}$	0.91	0.405	$7.8\times^{-188}$
37	$1474L^{0.61}$	0.84	0.538	$1.4\times^{-109}$
38	$864L^{0.90}$	0.89	0.489	$1.2\times^{-156}$

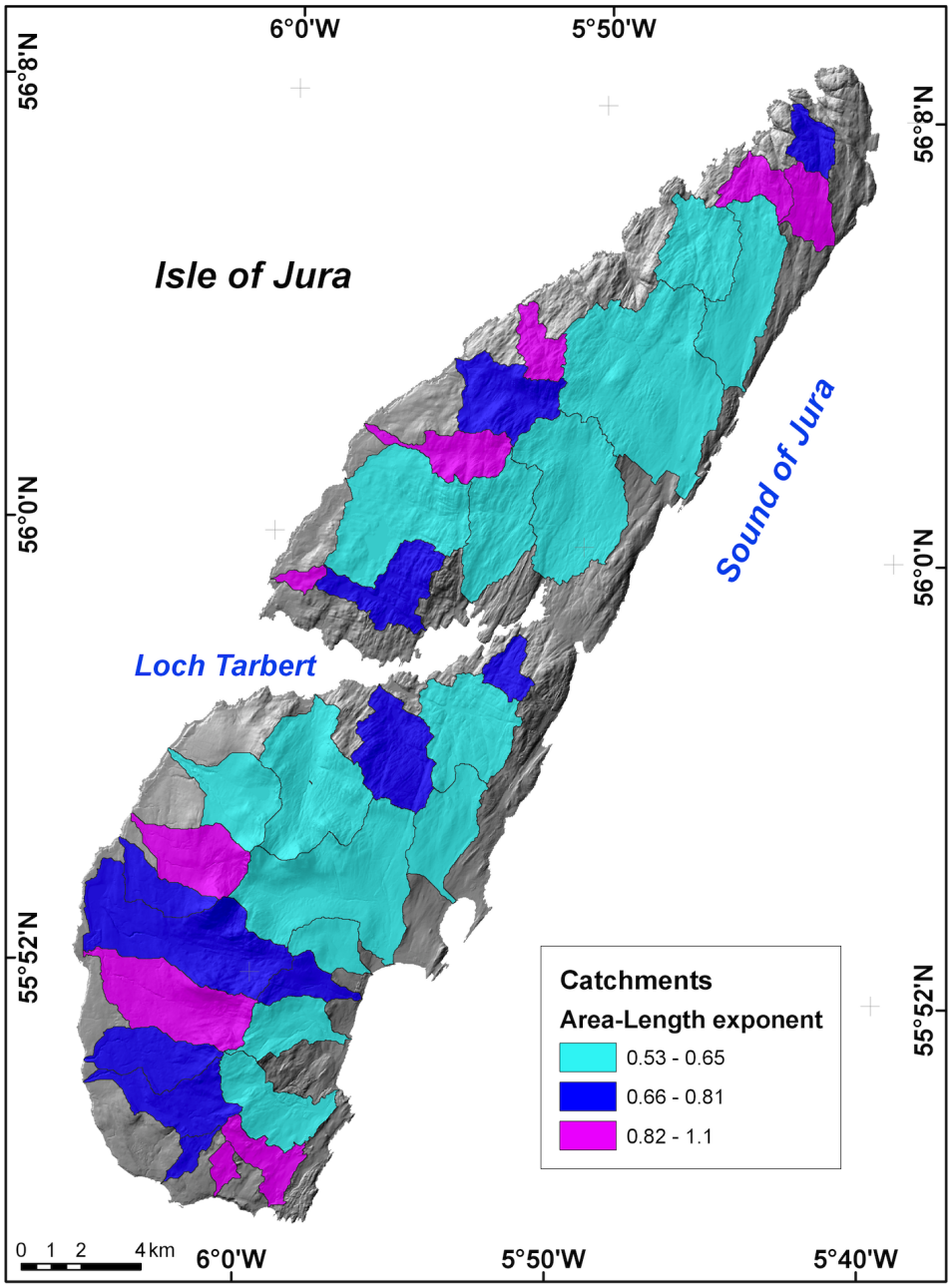

Figure 3.23: The map shows the distribution of the area-length exponent (Hack's law) of 34 basins of Jura. The non-elongated basins have a low area-length exponent and in general, are related to large basins. In contrast, a high area-length exponent is related to a small basin.

headwaters (Rigon et al., 1996).

In order to asses for any spatial pattern and control imposed by structure in the AL exponent, a scaling with the drainage area and with the hypsometric integral was done (Table 3.12). An ANCOVA to assess if structure exerts some control on the AL exponent is also performed. The results indicate that x is a poorly correlated with both drainage area and the hypsometric integral (Table 3.12), with exception of the in-strike rivers however, the ANCOVA indicates that structure does not seems not to exert a control on the AL relationship.

Table 3.12: Equation and regression statistics of Hack's exponent (x) against drainage area and the hypsometric integral for different structures.

Drainage area				
Streams	**Equation**	$\mathbf{R^2}$	**RSE**	**p-value**
Dip-slope	$x = 0.76A^{-0.09}$	0.01	0.2119	5×10^{-1}
Scarp-slope	$x = 0.88A^{-0.08}$	0.20	0.1628	7.3×10^{-2}
In-strike	$x = 0.96A^{-0.96}$	0.72	0.1074	1.7×10^{-3}
Full	$x = 0.88A^{-0.11}$	0.28	0.1662	1.3×10^{-3}
Strahler $\int$				
Streams	**Equation**	$\mathbf{R^2}$	**RSE**	**p-value**
Dip-slope	$x = 0.99S_{int} + 0.32$	0.65	0.1039	3.9×10^{-2}
Scarp-slope	$x = 0.45S_{int} + 0.60$	0.25	0.1235	3.8×10^{-2}
Strike	$x = 0.61S_{int} + 0.52$	0.27	0.1389	1.2×10^{-1}
Full	$x = 0.59S_{int} + 0.53$	0.31	0.1256	6.7×10^{-4}

Table 3.13: ANCOVA summary for the regression of x vs drainage area and x vs strahler's integral per structure.

Drainage area				
Coefficients	**Estimate**	σ	**T value**	$Pr(>\|t\|)$
Intercept	-0.26794	0.18174	-1.474	0.152
Log(Drainage area)	-0.09986	0.10265	-0.973	0.339
Structure: Scarp	0.13890	0.19932	0.697	0.492
Structure: In-Strike	0.23135	0.21491	1.076	0.291
Strahler $\int$				
Coefficients	**Estimate**	σ	**T value**	$Pr(>\|t\|)$
Intercept	0.3196	0.1549	2.063	0.0484
S_{int}	0.9949	0.4310	2.308	0.0286
Structure: Scarp	0.2847	0.1749	1.628	0.1147
Structure: In-strike	0.2084	0.1860	1.120	0.2720

The weak correlation between the AL exponent and drainage area indicates that in some rivers the basins elongation takes place. This type of river has an AL exponent in the range of 0.66 to 1.1 (Figure 3.23) which is in the range of values expected for fluvially dominated landscapes (Rigon et al., 1996). Of particular interest are those rivers where the AL exponent is > 0.80 which in general, correspond to small river basins. However, the low correlation on the AL regression (Table 3.13) indicates that large rivers exceed the theoretical range of Hack's exponent.

The values on Hack's law exponent seem to characterise three types of rivers on Jura: (1) those with low drainage area that are well confined into a valley, (2) those flowing in the transition between strongly contrasted landscape domains (i.e mountain to piedmont) in which the upper valley has been shaped by glacial processes and (3) those wide basins which rivers are not confined to a deep valley (Figure 3.23). Unfortunately, the drainage area and Strahler's integral do not have any apparent functional relationship with Hack's law exponent however, the qualitative

observation of valleys morphology of basins where $x > 0.85$ support the interpretations given above.

The exponents observed from Hack's law in Jura reflect the distribution of fluvial processes which depend on the drainage density and presumably on an effect inherited from glacial processes. Low values of x are found in wide basins where the drainage density is widely distributed on the basin and where presumably, the glacial processes have widen the river basins. In contrast, high values reflect an elongated basin where fluvial processes are more spatially concentrated and where the drainage density lead to the formation of valleys as it is expected for fluvially dominated landscapes. The differences on Hack's exponent are likely to be related with the 'top-down' processes (Bishop, 2009) which may have further implications on the changes in the rates of incision in the landscape (i.e. wide basins vs elongated basins). A priori it is expected high incision rates in elongated basins where rivers and valleys are likely to be better connected to hillslopes than in the case of wide basins. Exploring this relation is out of the goal of this study but it is a situation that needs to be resolved.

3.8 Summary

The results presented in this chapter indicate that the landscape of Jura has been affected by several processes that have resulted in a change of the landscape dynamics that, in the case of the fluvial processes, are explored in subsequent chapters. The most important facts and characteristics of Jura's landscape are summarised below.

- The topography in Jura is mountainous with predominance of hills on the north and massifs at the south. The lithology is homogeneous ($\sim 90\%$) across the isle and is characterised by a Neoproterozoic quartzite formed under tidal shelf conditions. The structure is broadly a simple easterly dip at $\sim 20^{\circ}$ with scarp slope facing to the west.

- The BIIS modified much of Jura's landscape and is clearly evidenced by the presence of till, striaes and a medial moraine located on the west coast. During the LLR it is likely that glacial cirques were developed, indicating restriction of ice growth to the upland areas.

- The melting of the BIIS resulted in a glacio-isostatic rebound which is demonstrated by the raised beaches left $\sim$ 36 m OD on the west coast of Jura and dated in 13.6 ka.

- The RSL curves for the last 20 ka and the cosmogenic ages obtained by Bishop et al., on the west coast indicates that after $\sim$ 14 ka the sea level fell rapidly and a marine still-stand occurred after the LLR. Since then the rate of the the RSL has decreased but the data published to date, suggest that the uplift is still occurring for most of Scotland.

- The glacio-isostatic rebound geologically instantaneous generated a drop in base-level of at least 15m, which is likely to have triggered the knickpoints that modified the long profiles that are the focus of this study.

- As a broad rule, catchment size seems to correlate reasonably with the hypsometric integral suggesting that glacial processes are likely to have modified the river basin morphology. The Hack's law exponent on the other hand, allowed to identified two different type of basins: wide and elongated. The wide basins are probably reflecting the effect of glacial processes imprinted on the headwaters of the rivers of Jura.

- The results of the morphometric analysis reveal an imprint of the past glacial processes in the landscape. Such processes are likely to be present on the longitudinal profile of rivers. This point is treated in detail in chapter 4.

Chapter 4

Stream long profile analysis and morphometry

4.1 Introduction

Stream profile analysis has long be used in geomorphology to evaluate equilibrium in the fluvial system (Rice, 1977). The concept of the 'graded' stream, which denotes a morphological condition of rivers, is the main criterion to assess if there is a state of equilibrium in the fluvial network. The concept of equilibrium, still underpins theoretically the analysis of channel slopes in alluvial and bedrock rivers. Several authors have attempted to define the graded stream (e.g., Gilbert, 1877; Mackin, 1948; Leopold and Bull, 1979) but a single definition is still missing and some inconsistencies and controversies still surround the concept (Merrits et al., 1994). For example, Mackin (1948) defines a graded stream as "... one in which, over a period of years, slope is delicately adjusted to provide... just the velocity required for the transportation of the load supplied from the drainage basin. The graded stream is a system in equilibrium... any change in any of the controlling factors will cause a displacement of the equilibrium in a direction that will tend to absorb the effect of change" (Mackin, 1948, p. 471). He indicates that the longitudinal stream profile of the graded stream tends to have a smooth concave-upward shape but such morphology is not a condition *sine qua non* of a graded stream (Mackin, 1948). Leopold and Bull (1979) indicate that the profile of a graded, then under stable climatic and tectonic conditions, does not experience any rising or lowering of elevation. This last definition suggests a condition of equilibrium (steady-state) but does not spe-

cify any particular morphology. Although some of the definitions of a graded river do not implicitly or explicitly link the concave-up profile with steady-state, there is a widespread idea that concavity is unequivocally linked to equilibrium (Snow and Slingerland, 1987; Sinha and Parker, 1996).

The relationship between graded rivers and equilibrium is well developed for alluvial rivers (e.g., Snow and Slingerland, 1987; Sinha and Parker, 1996; Willgoose et al., 1991). The concept arrived later for the case of bedrock rivers. An influential work related to the study of bedrock rivers has been the paper of Hack (1957) who studied the bedrock rivers of Virginia (USA) and interpreted functional relationships related to channel steepness, drainage density and sediment sorting along stream profiles in terms of the hydraulic geometry of rivers. For Hack (1957) the key point is to understand the stream profiles since these contain information about the incision in the landscape. Hack developed his ideas and observations in a few papers which culminated in the formulation of a stream gradient index used to detect 'anomalies' on a stream long profile (Hack, 1973). Although Hack suggested that the changes in gradient are the key point in understanding the incision and adjustment of slopes, his results and observations indicate that the bedrock rivers tend to develop a concave-up profile in the same fashion as alluvial rivers.

Research in large bedrock river catchments indicates that when rivers are capable of incising in response to base-level fall, they can reach a condition of equilibrium which is tightly related to a concave-up morphology of the stream profile (Merrits et al., 1994). Concavity and its relation to the equilibrium have also been observed and confirmed through numerical modelling of bedrock rivers based on empirical rules (Howard, 1998; Seidl et al., 1994; Whipple and Tucker, 1999). If bedrock rivers can attain a condition of equilibrium, then stream profile analysis is useful and powerful to detect anomalies along the stream long profile. It should be noted, however, that the state-of-the-art in bedrock rivers is mostly based on observations made for the large fluvial settings (drainage area > 100 km^2). Whether small

bedrock rivers (i.e., < 100 km^2) are capable of reaching a steady-state and to propagate the disequilibrium has not been fully addressed. Golden and Springer (2006) evaluated small tributary rivers in the west of Virginia, USA. They found that channel gradient is adjusted in the same way as large fluvial systems with channel slope decreasing as drainage area increases. Phillips and Lutz (2008) have contested the idea that equilibrium is expressed as concave-up morphology along the stream profile. They argued that the convexity observed among some tributary rivers of the coastal plain of Texas and central Kentucky can be interpreted as and effective adjustment of channel slopes and that other processes like local lithological controls (e.g., knickpoints) can produce a convex long profile. The results obtained by some studies done on small bedrock rivers makes them an important and challenging object of study which requires the attention of geomorphologist in order to understand the connection of tributary rivers to the main trunk rivers and its implications on large fluvial systems.

Whether it is accepted that concave-up morphology of rivers denotes a condition of equilibrium or not, the stream profile analysis is a useful and powerful tool to extract information on different processes (i.e., tectonic, climatic or lithological) that control the rate of incision in the landscape and that are recorded in channel morphology. An interesting review of the idea of equilibrium in bedrock rivers can be found in Goldrick and Bishop (2007). Even though the theoretical basis of the stream profile analysis assumes that equilibrium is attainable by bedrock rivers and that this view implies a particular channel morphology, stream profile analysis is useful because it provides a frame of reference to evaluate the disequilibrium given by deviations from a theoretical morphology. Stream profile analysis is central to the present research thus, the stream profile analysis for Jura is presented here. The aim of this chapter is to characterise quantitatively the streams of Jura and to extract information of the geomorphic-processes imprinted on channel morphology.

4.2 The extraction of stream long profiles

The stream long profiles analysis used was based on a high resolution DEM from NEXTMAP© with a pixel size of 5 m. The reported DEM horizontal and vertical accuracies are ±2.5 m and ±1 m respectively. The DEM was processed in the GIS Ilwis Academic 3.3 (ITC, 2005). Although there are other methods for obtaining stream long profiles (e.g., extraction from topographic maps or measuring of channel elevation *in situ*), using a DEM has several advantages. The pixel size used here (5 m) is considered optimum, following the criteria of Zhang and Montgomery (1994) who found that 10 m resolution DEM can reproduce most of the geomorphic and hydrologic processes observed in the landscape. Another advantage is that the DEM used here is a ground truth DEM. This type of DEM has been reported to provide better results than using cartographically derived DEMs (Walker and Willgoose, 1999). The extraction of the stream long profile is summarised in Figure 4.1 and all steps are detailed below.

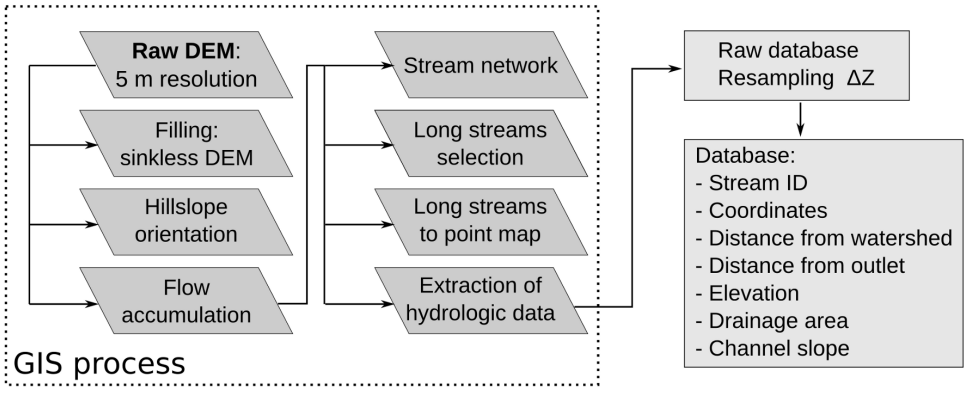

Figure 4.1: Approach followed for extraction of the stream long profiles and the compilation of data. The hydrologic tools provided by the GIS Ilwis Academic 3.3 allowed the hydrologic data extraction. The post-processing of the hydrologic data was done in the statistical software R (R Development Core Team, 2009)

The initial step prior to the extraction of the fluvial network, is the construction

of a sinkless DEM following the normal procedures of the D8 algorithm for fluvial determination (Jenson and Domingue, 1988). Once the filled DEM has been obtained, the raster maps of hillslope orientation and flow accumulation are computed. To extract the fluvial network a threshold area must be assigned to the GIS. The selection of a threshold value not only prevents the formation of artificial channels ('feathering' effect) during the fluvial network extraction but is also related to the critical area for channel initiation (Montgomery and Dietrich, 1989; Montgomery and Foufoula-Georgiou, 1993). Finding the critical drainage area was problematic here since there are no relevant empirical data for channel initiation in rivers in Scotland. Also, the glacial imprint in the upper parts of river catchments complicates the estimation of the critical drainage area because of the large value of drainage area close to the zone of channel initiation. One way to avoid the 'feathering' effect for the fluvial network extraction and which can be useful to set the drainage lines is by choosing lower threshold areas (Montgomery and Foufoula-Georgiou, 1993). Here a value of 25,000 m^2 was used since at this value the fluvial network show not effect of feathering on the flow accumulation map. Because of the prevailing wet conditions over Jura's landscape (mean annual rainfall $\sim 3,000$ mm) and soil saturation during most time of the year, it is likely that the critical drainage area is lower than the value selected. However, for the purpose of this analysis performed, the threshold area selected was considered optimum for the long profile extraction.

Once the stream network was extracted, a stream order map was generated. The fist-order streams were omitted and only the second and third order streams were used to extract the long profile. The hydrologic tools of the GIS and the stream order map were used to extract the longest streams as segments which were transformed to points. The point map is linked to a database containing coordinates in the British National Grid System, stream ID, elevation (m) and drainage area (km^2). Prior to the computation of other hydrologic data, the elevation data were resampled following the procedure described by Wobus et al. (2006b) for an optimum representation of stream profiles obtained from a DEM. The vertical resampling was

done every metre $\Delta Z = 1$ m. After resampling the elevation data, the values of distance (L) from the watershed and from the outlet were calculated using the Pythagoras formula from the x and y coordinates thus:

$$L = \sqrt{(x_u - x_l)^2 - (y_u - y_l)^2} \tag{4.1}$$

where subscripts u and l refers to upper and lower coordinates of the adjacent point. The channel slope was calculated every metre using its dimensionless form (Hack, 1957):

$$S = \Delta Z / \Delta L \tag{4.2}$$

where ΔZ and ΔL are the differential values of elevation and distance of the reaches sampled (Figure 4.3). A total of 34 stream long profiles were obtained for Jura (Figure 4.2 and Appendix A). The stream data are summarised in Table 4.1.

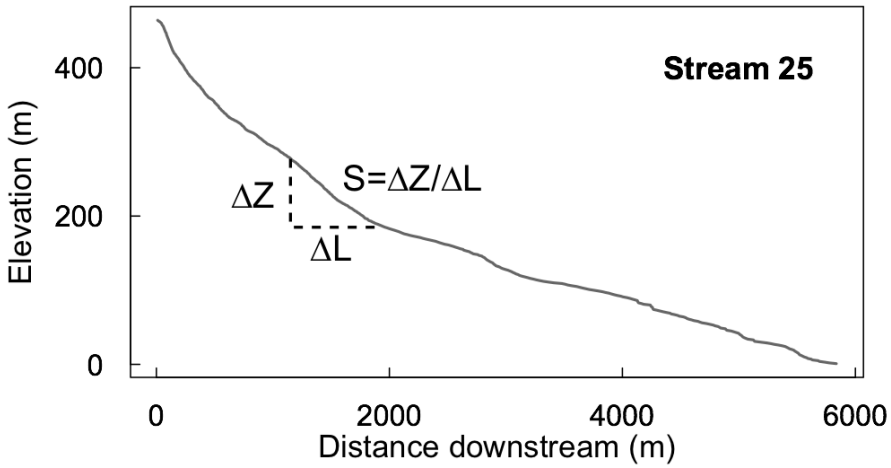

Figure 4.3: Profile of the stream 25 and scheme of how the channel slope has been calculated for the steams of Jura.

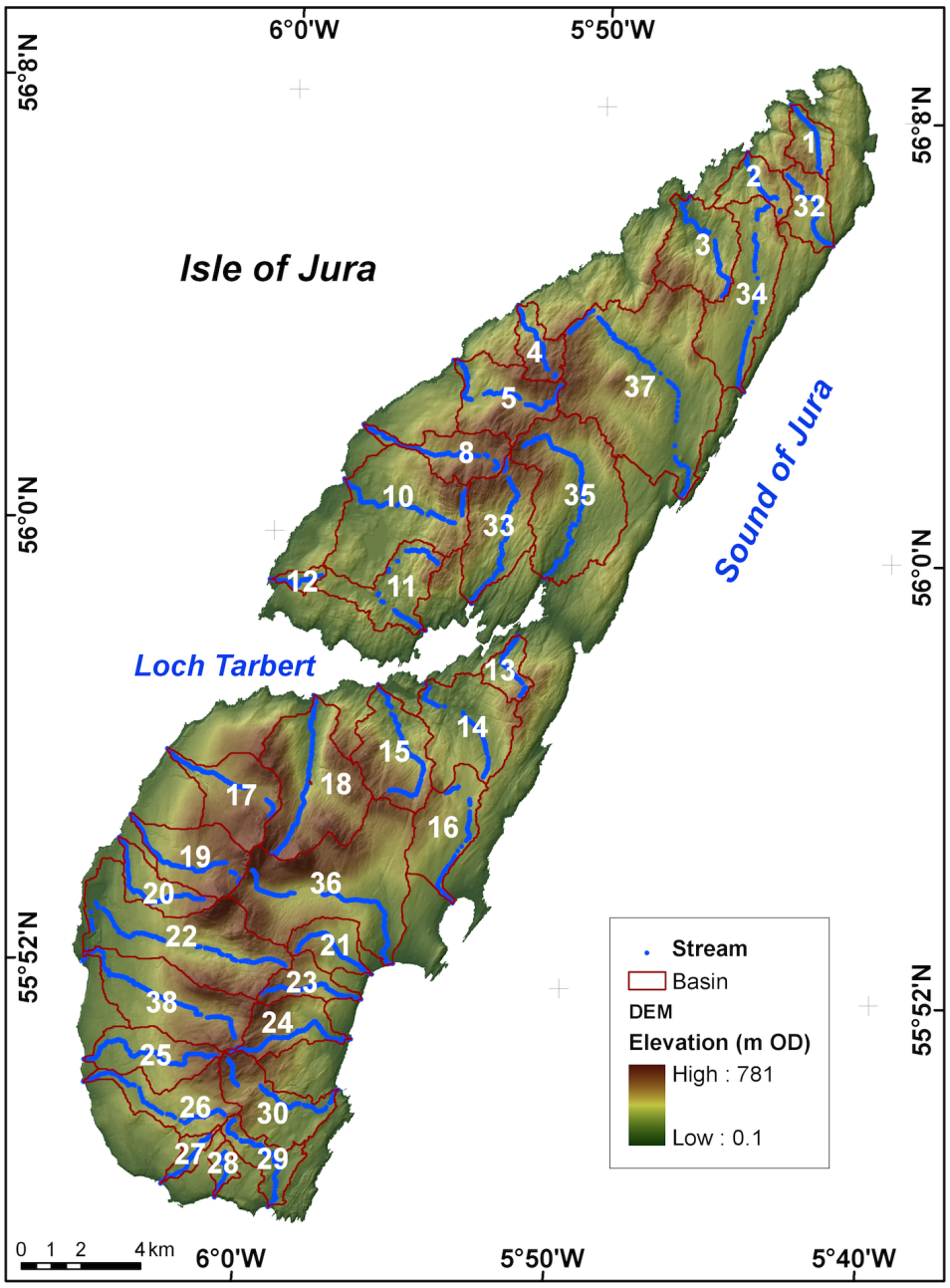

Figure 4.2: Map showing the 34 stream long profiles extracted from the isle of Jura. See Table 4.1 for details about the morphometry of streams.

Table 4.1: Data of the stream long profiles obtained for Jura.

Stream name	ID	Max. coordinate (x, y)	Min. coordinate (x, y)	Drainage area (km^2)	Relief (m)	Distance (m)	Slope† (m/m)
Glac Carn Eachainn	12	152243, 684283	150503, 684153	0.83	126	2073	0.0722
Abhainn Bheag	28	148998, 664903	148633, 663383	1.00	150	1865	0.0960
Allt Glac Eanruigein	27	148488, 665493	146818, 663848	1.15	168	2566	0.0717
Allt Feàrna Mòr	13	158908, 680238	158848, 682278	2.11	268	2736	0.1313
Glentrosdale River	1	169028, 697808	168018, 700118	2.59	189	2836	0.0750
Garbh uisge nan Cad	4	160073, 690958	158858, 693378	2.85	417	3226	0.1540
Alltanan Dubha	23	150218, 670228	153563, 670033	2.89	487	3889	0.1453
Allt Loch na Conaire	2	167653, 696508	166578, 698518	3.01	199	2684	0.0873
Allt a' Bhreac-dhuinain	29	149303, 665963	150423, 663058	3.30	281	4687	0.0903
Allt Garbh	32	167913, 697738	169453, 695348	3.40	206	3469	0.0725
Allt a' Ghlinne Ghrunrunndail	21	151413, 671633	153923, 670868	3.41	300	3639	0.1143
Alltanan Seilich	20	148268, 673398	145418, 675478	3.59	426	4810	0.1207
Allt an Tairbh	8	158048, 687858	153658, 689373	4.50	344	5573	0.0741
Uisge Dearg	24	149203, 668238	153208, 668693	4.73	485	5094	0.1203
Allt nan Ruadhag	25	148688, 668128	144233, 668028	5.78	463	5836	0.1039
Uillt nam Minnean	26	148983, 666143	144218, 667263	5.88	261	5922	0.0533
Garbh uisge	11	156148, 684688	155738, 682433	6.07	262	5366	0.1143
Allt Doir' a' Chlaiginn	16	156403, 676973	156638, 673263	6.37	189	5235	0.0508
Allt an t-Sluic Bhrodaich	19	149428, 673943	145818, 676263	6.45	374	5479	0.0872
Allt na Gile	17	150488, 676198	147053, 678463	6.66	416	4745	0.1011
Allt a' Mhoirt	30	149098, 668003	152798, 666988	6.67	461	5404	0.1202
Abhainn a' Chruaidh ghlinn	5	160303, 690658	156683, 691528	6.98	403	6037	0.1082
Glengarrisdale River	3	165703, 693678	164633, 697048	7.08	216	4792	0.0611
Abhainn Liundale	15	154513, 677048	154143, 680613	7.62	333	5589	0.0929
Abhainn a' Ghlean Duirch	33	158433, 688203	157283, 683333	8.27	420	6216	0.0839
Sruthan na Criche	14	157663, 677498	155728, 680653	9.11	152	4571	0.0411
Lealt Burn	34	167273, 696688	166453, 690443	10.12	175	6854	0.0278
Glenbatrick River	18	150548, 674938	151963, 680258	12.87	467	6299	0.0848
Shian River	10	157113, 687148	153003, 687548	14.03	402	6042	0.0974
Abhainn Ghlean Aoistail	35	159043, 688608	159733, 684163	15.04	361	7404	0.0803
Corran River	36	149918, 674373	154628, 671228	18.61	498	7552	0.0879
Lussa River	37	160573, 692433	164303, 686893	25.36	317	9417	0.0475
Abhainn a' Chnuic Bhric	22	151018, 671158	144203, 671328	25.67	284	9697	0.0417
Abhainn Gleann Lubharnadail	38	149314, 668746	144205, 671325	25.67	384	7343	0.0671

† The slope of the long stream was calculated using the distance from coordinates x and y.

4.2.1 Stream long profiles: A tool for landscape analysis

The changes in channel slope observed on a stream long profile not only provide information about the morphology itself, but they also reflect factors such as lithological contacts and tectonic signals in the landscape which require to be recognised and understood. Careful observation of channel slopes is thus at the core of the stream profile analysis. If the concept of equilibrium is accepted, the stream power predicts that landscapes in steady-state, or in a condition close to it, would have a reasonably good scaling of channel slope with stream discharge (Q) or its proxy, drainage area (Howard, 1994; Whipple and Tucker, 1999; Duvall et al., 2004; Snyder et al., 2003). Observations in different settings show that breaks in the systematic decrease of channel slope with drainage area may reflect processes related to faulting (e.g., Molin et al., 2004; Whittaker et al., 2007; Larue, 2008), contrast in lithology (e.g., Hack, 1973; Goldrick and Bishop, 1995) or base-level fall knickpoints(e.g., Snyder et al., 2000; Bishop et al., 2005; Goode and Burbank, 2009).

Bedrock rivers research has primarily focused on non-glaciated landscapes where fluvial processes are known to be the principal mechanism of incision. Fluvial long profiles in glaciated landscapes have been overlooked in the landscape evolution research, with a few notable exceptions (e.g., MacGregor et al., 2000; Brocklehurst and Whipple, 2002). However, glacial signals may be recorded in channel gradient and this require to be understood. Jura is a challenging setting for stream profile analysis because there is high probability that glacial signals might be inherited in the landscape, especially in controlling the morphology of streams in the upper part of catchments. Also, because Jura is characterised by small bedrock river catchments (Table 4.1) steep channel slopes are *a priori* expected. Here the stream power model known for bedrock rivers has been evaluated using the slope-area and distance-slope regressions with the purpose to evaluate the channel slope and its relation to fluvial processes. These analyses performed are detailed in the next sections.

4.2.2 The drainage area and channel slope analysis

The power law function of equation 2.7 has been used as an empirical formulation of bedrock rivers to test for a steady-steady state condition in the landscape (Whipple and Tucker, 1999; Whipple, 2001). The solution of equation 2.7 can is obtained by performing a linear regression of the logarithm of drainage area against the logarithm of channel slope, I refer to it here as the slope-area (SA) model or SA regression, and to the SA plot as graphical representation. The SA model has been applied in various settings (e.g., Snyder et al., 2000; Duvall et al., 2004; Harkins et al., 2007) and some caution is recommended prior to analysing the result from equation 2.7. Observations based on SA plots in fluvially-dominated landscapes indicate that, at lower drainage area, there is a break in the scaling with channel slope, this breach representing the transition from hillslope and debris processes to fluvial processes (Montgomery and Dietrich, 1989; Montgomery and Foufoula-Georgiou, 1993; Whipple and Tucker, 1999). This transition occurs at $\sim 10^5$ m^2 drainage areas (Montgomery and Foufoula-Georgiou, 1993) and its removal is recommended in SA analysis (Wobus et al., 2006b) which coincides with a slope threshold of 0.1 to 0.2 m/m (Sklar and Dietrich, 1998). The transition between the hillslope and debris flow processes zone of fluvial processes is undocumented for formerly glaciated landscapes. Frequently, glaciated landscapes have wide cirques on their summits and considerable smoothing of valley walls (Selby, 1985; Summerfield, 1991) with the valley cross-section exhibiting a parabolic shape (Graf, 1970). The wide open valleys may result in the disconnection of valley walls where debris flow and hillslope processes predominate from the incising channel. Thus, in these settings, it is likely that the disconnection between hillslope processes and debris flow formation from the main river will occur at very low drainage areas. In such case, the fluvial processes may extend further upstream than in the case of fluvially sculpted landscapes. Because the transition from the hillslope and fluvial processes is not known for glaciated landscapes it is sensible to extend the SA analysis to lower drainage areas if there is evidence of channel incision related to fluvial processes.

A second treatment of data recommended for the SA model is the normalisation of k_s using a reference concavity (θ_{ref}) (Wobus et al., 2006b, their Equations 2 and 3). By normalising k_s it is possible to detect high values of k_s which may characterise zones of high incision rates (Kirby and Whipple, 2001; Wobus et al., 2006a; DiBiase et al., 2010). The normalisation of k_s has been done for fluvially dominated landscape to evaluate the channel steepness and comparing it regionally to detect zones of hight rock uplift (Wobus et al., 2006b) but its suitability for glacial inherited landscapes requires the characterisation of θ and the threshold where fluvial incision starts. The use of the SA model in glaciated landscapes requires the detection of the glaciated reaches and the location of where incision is initiated by fluvial processes. The morphology left by glacial processes on which fluvial processes are operating has been poorly treated and this issue has only been explored through numerical modelling (e.g., MacGregor et al., 2000). Using the SA model, Brocklehurst and Whipple (2002) observed that θ in glaciated catchments on the east of the Sierra Nevada (USA) is ~ 0.16, a little lower than the case for non-glaciated catchments where $\theta \approx 0.27$. These authors used simulations to evaluate the erosion of the glaciated reaches but the implications for debris flow and hillslope processes in the glaciated reaches and the relationship of that to fluvial reaches were not analysed.

In the present research the SA model was implemented following two strategies: (1) evaluating the stream long profile without differentiating a specific minimum drainage area for hillslope and debris flow processes and (2) analysing separately the reaches interpreted as glacial and fluvial based on observations on the stream long profiles. The low drainage area was not isolated because the channel initiation threshold is unconstrained both for the Jura and for the glaciated landscapes in general. However, due to high rainfall on Jura, it is possible that channels might be initiated at low drainage areas of the order of $\sim 10^4$ m^2 as can be observed in the field by the presence of creeks at the headwaters. The glaciated and fluvial reaches were separated by interpreting the basin morphology of the stream long profiles.

The upper reaches characterised by a wide open valley or when the river is not confined to the valley, was interpreted as morphological evidence of a glacial reach which is typical of glacially eroded landscapes (Chorley et al., 1984; Selby, 1985). Where rivers were entrenched and well confined to a valley, these were considered as a fluvial reaches. The streams of the fluvial zone are located close to the mouth of streams meanwhile lochs characterise the glacial reaches (Figure 4.4 and Figure 4.5).

Figure 4.4: Glacial cirque of the river Abhainn Gleann Lubharnadail (stream 38). The flat wide bottom valley indicates that this area has been shaped by glacial processes. Note the distance to valley walls, which promotes the disconnection from hillslope processes to the main channel.

The slope-area and distance-slope regressions were performed for the full longitudinal profile, the glacial reaches and fluvial reaches in the statistical software R (R Development Core Team, 2009). Regressions were run for the 34 streams using the method of the least minimum squares. The results of the regressions and the SA equation obtained are presented in Table 4.2. The SA plots are shown in Appendix

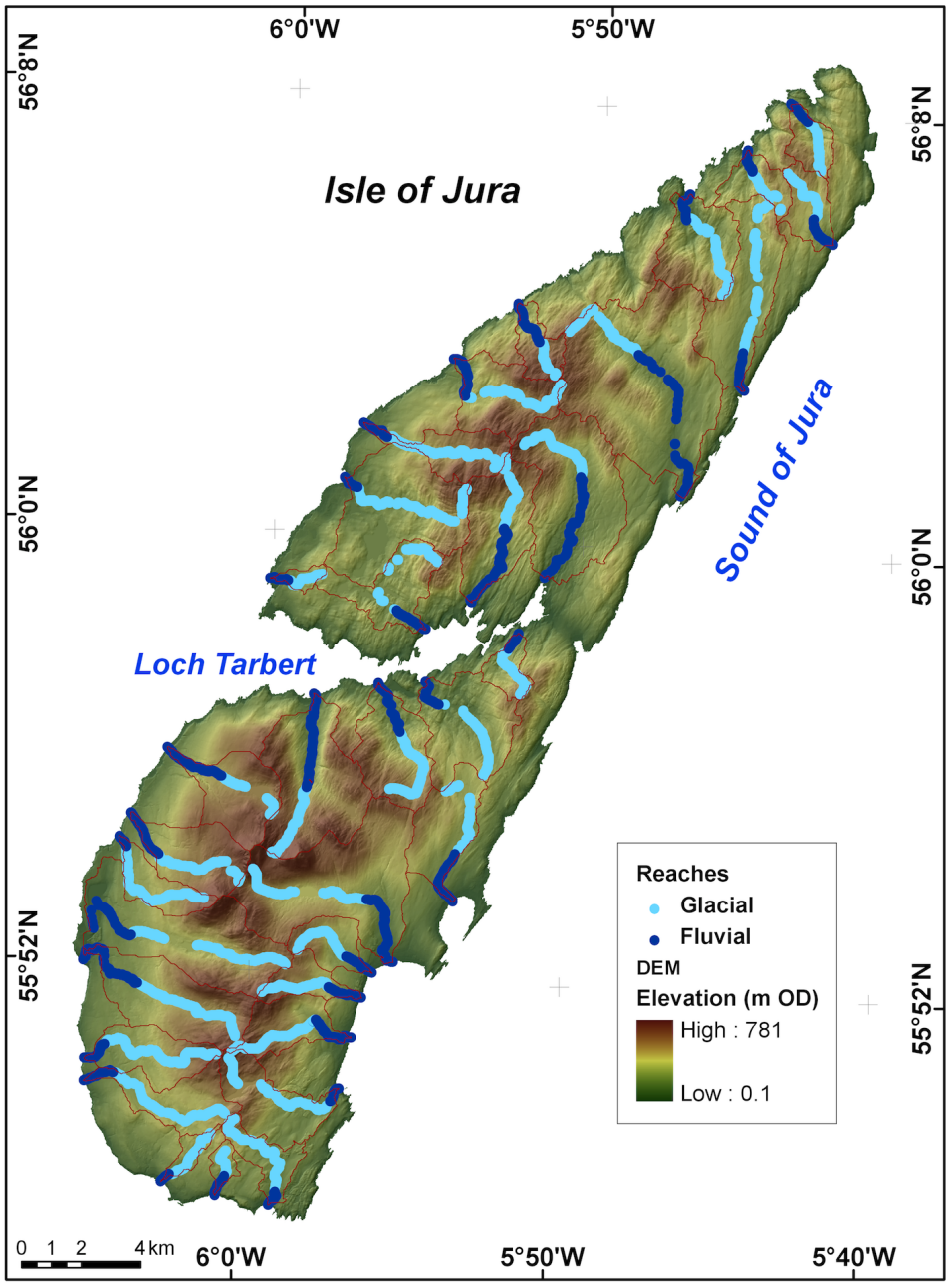

Figure 4.5: Map of the glacial and fluvial reaches interpreted form the SAR image. Note that in all cases the fluvial reaches are concentrated at the low part of the streams.

(B).

The adjusted coefficient of determination for the regression analysis performed indicate that there is only a weak correlation between the drainage area and the channel slope (Table 4.2). Moreover, the SA plots reveal that there are several breaks in channel slope along the steam long profile for each river (Appendix B). Although the channel slope data is scattered in most of the cases, rivers with values of $\theta < 0$ were significant (p-value: < 0.05) on their regression (Table 4.2) in contrasts, rivers with low drainage area (< 3 km^2) (Table 4.1) have positive a value of θ (Table 4.2). This last type of streams are characterised by a convex long profile (Appendix B) and these rivers do not have a significant SA regression (p-value: > 0.05), indicating a poor scale of channel slope against the drainage area.

Only few rivers with $\theta \geq 0.30$ (Table 4.2) tend to have concave-up profile (Appendix A). The lack of fitting in the SA regression model and the scattering in the data of channel slope strongly indicate that the rivers of Jura are not in equilibrium. The variations in channel slope along the long profile of streams are interpreted as a sign of perturbation. Perturbation is remarkable at upper parts of the long profile as well as stream's mouth. It is likely that glacial processes signals might still present on the channel slopes, mainly as a glacial knickpoints, that may cause a disequilibrium on the fluvial network. Another cause related to the prevailing of a convex profile might be due to the post-glacial uplift. Because Jura landscape has experienced a sudden base level fall after the melting of the BIIS, the long profile convexity at the mouth of the rivers might reflect the drop of base-level fall. This last point point will be treated in the next chapter.

Besides the potential effects of glacial processes and the effects of the base-level fall recorded on the streams there still the question if it is possible to detect an area of reference in order to obtained a concavity of reference (θ_{ref}) that represents the regional value of channel concavity in order to normalise the values of k_s and

Table 4.2: Equation of channel slope against drainage area, and regression statistics.

Stream ID	Equation	R^2	RSE†	P-value
1	$8.6 \times 10^{-02} A^{-0.20}$	0.06	0.7781	6.8×10^{-04}
2	$1.0 \times 10^{-01} A^{-0.11}$	0.01	0.7720	6.6×10^{-02}
3	$6.9 \times 10^{-02} A^{-0.11}$	0.02	0.9572	2.9×10^{-02}
4	$1.5 \times 10^{-01} A^{0.02}$	0.00	0.6663	5.7×10^{-01}
5	$9.5 \times 10^{-02} A^{-0.14}$	0.08	0.7323	8.5×10^{-09}
8	$8.4 \times 10^{-02} A^{-0.09}$	0.02	0.7652	6.7×10^{-03}
10	$9.1 \times 10^{-02} A^{-0.33}$	0.43	0.7484	1.3×10^{-42}
11	$8.5 \times 10^{-02} A^{-0.29}$	0.26	0.7797	2.1×10^{-17}
12	$7.7 \times 10^{-02} A^{-0.02}$	0.01	0.6606	8.3×10^{-01}
13	$9.0 \times 10^{-02} A^{-0.31}$	0.14	0.7915	2.9×10^{-08}
14	$5.1 \times 10^{-02} A^{-0.35}$	0.38	0.7474	4.4×10^{-17}
15	$8.1 \times 10^{-02} A^{-0.23}$	0.21	0.7342	8.1×10^{-18}
16	$5.9 \times 10^{-02} A^{-0.23}$	0.31	0.7773	5.8×10^{-17}
17	$1.2 \times 10^{-01} A^{-0.24}$	0.37	0.5947	1.6×10^{-36}
18	$1.1 \times 10^{-01} A^{-0.25}$	0.20	0.7079	2.4×10^{-22}
19	$9.4 \times 10^{-02} A^{-0.15}$	0.05	0.7533	9.5×10^{-06}
20	$7.5 \times 10^{-02} A^{-0.38}$	0.53	0.5752	2.0×10^{-61}
21	$9.7 \times 10^{-02} A^{-0.05}$	0.01	0.6391	6.3×10^{-02}
22	$6.6 \times 10^{-02} A^{-0.21}$	0.11	0.9902	4.1×10^{-08}
23	$1.2 \times 10^{-01} A^{-0.22}$	0.29	0.5166	8.0×10^{-33}
24	$1.0 \times 10^{-01} A^{-0.21}$	0.19	0.7033	1.7×10^{-20}
25	$8.0 \times 10^{-02} A^{-0.33}$	0.46	0.5472	4.7×10^{-58}
26	$6.5 \times 10^{-02} A^{-0.29}$	0.31	0.8011	1.5×10^{-20}
27	$8.2 \times 10^{-02} A^{0.04}$	0.00	0.6710	4.5×10^{-01}
28	$1.0 \times 10^{-01} A^{-0.05}$	0.00	0.7584	3.4×10^{-01}
29	$6.5 \times 10^{-02} A^{-0.41}$	0.35	0.7051	4.6×10^{-26}
30	$1.2 \times 10^{-01} A^{-0.24}$	0.24	0.8186	3.4×10^{-22}
32	$7.2 \times 10^{-02} A^{0.39}$	0.18	0.7598	1.4×10^{-09}
33	$9.5 \times 10^{-02} A^{-0.27}$	0.27	0.7850	4.3×10^{-27}
34	$5.0 \times 10^{-02} A^{-0.24}$	0.21	0.9296	1.2×10^{-10}
35	$8.5 \times 10^{-02} A^{-0.37}$	0.36	0.8124	9.5×10^{-34}
36	$1.1 \times 10^{-01} A^{-0.43}$	0.69	0.6409	9.3×10^{-92}
37	$6.7 \times 10^{-02} A^{-0.40}$	0.44	0.9048	2.6×10^{-36}
38	$9.8 \times 10^{-02} A^{-0.45}$	0.44	0.7681	4.8×10^{-43}

† Residual Standard Error

compare it to detect any effect of base-level fall in the channel steepness of the fluvial reaches. For this purpose, a t-test was performed on the θ values obtained for all the rivers where the SA regression is significant. A priori it is expected that the distribution of the θ would approximate a normal distribution. Thus, the null hypothesis states that $H = \mu$ otherwise $H \neq \mu$. The t-test performed give a value of $t = -13.25$, and the null hypothesis is rejected which means that θ can not be represented by a regional θ_{ref} with a 95% confidence. The mean θ for the streams analysed ($n = 29$) yield a value of -0.26 ± 0.04 at 95% interval confidence. However, $\sigma = 0.10$ suggest a wide variability in the values of channel concavity. The distribution of the k_s values were also analysed, the mean value obtained at the 95% confidence intervals is $86 \times 10^{-3} \pm 7.2 \times 10^{-3}$ and $\sigma = 0.1$. The variability of the constant and exponent of the SA model can be fully appreciated on Figure 4.6.

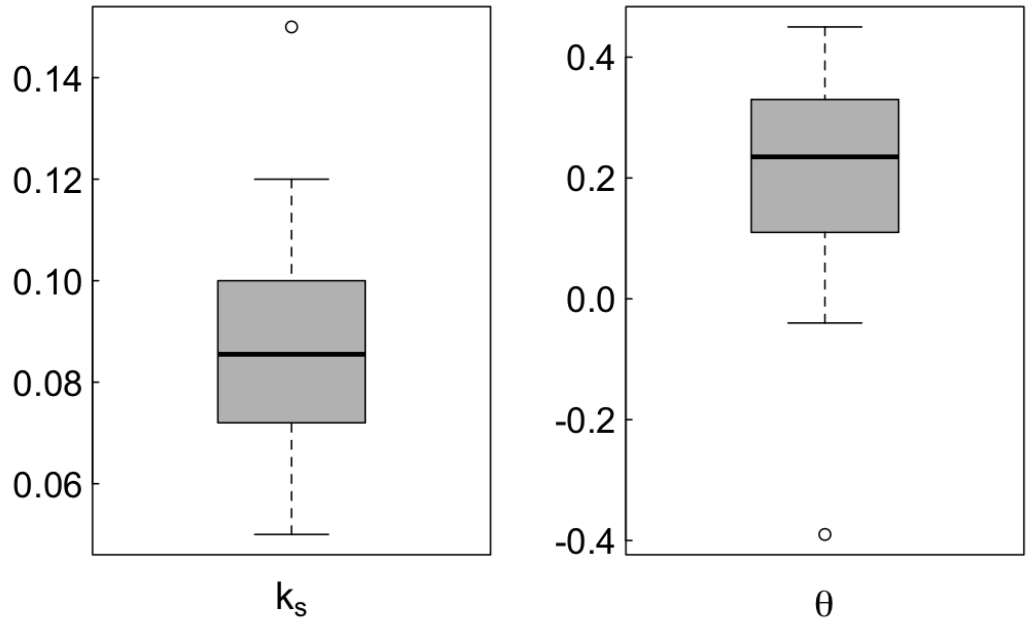

Figure 4.6: Boxplots of θ and k_s obtained from equation 2.7 of 29 stream of Jura. Both coefficient and exponent have a wide variability for all the streams analyzed

To evaluate the difference between the glacial and fluvial reaches obtained from the stream long profiles interpretation, a SA regression was performed for glaciated and non-glaciated reaches. The coefficients and exponents of the SA model are presented in Table 4.3 and the plots are shown in appendices C and D.

A weak to moderate correlation was observed for the SA regression on the glaciated reaches (Table 4.3). Those rivers with a concave profile and where the SA correlation is significant have a mean value of $\theta = 0.21 \pm 0.05$ and a $k_s = 0.079 \pm 0.01$. Whether a regional value of θ can be obtained for the glaciated reaches in order to detect if there is any spatial pattern was assessed in the same fashion as for the full long profiles. In the glaciated reaches θ and k_s are not normally distributed and the t-test applied to $\theta > 0$ yield a value of $t = -10.62$, which rejects the null

Table 4.3: Exponent and coefficient of the power law function of drainage area channel slope for glaciated and non-glaciated reaches of Jura.

	Glaciated				Fluvial			
Stream ID	**Equation**	**R^2**	**RSE**	**P-value**	**Equation**	**R^2**	**RSE**	**P-value**
1	$0.10A^{-0.05}$	0.00	0.7696	0.4970	$9.0E-04A^{4.73}$	0.10	0.7324	0.0270
2	$0.11A^{-0.08}$	0.00	0.6664	0.2150	$1.4E-01A^{-0.57}$	0.02	0.7878	0.1360
3	$0.08A^{0.07}$	0.00	0.8550	0.1990	$8.9E-04A^{1.47}$	-0.06	0.4903	0.6720
4	$0.16A^{0.05}$	0.00	0.4678	0.2010	$1.9E-01A^{-0.31}$	0.00	0.7566	0.1960
5	$0.10A^{-0.12}$	0.06	0.6590	0.0000	$2.6E+03A^{-5.72}$	0.17	0.7123	0.0000
8	$0.08A^{-0.13}$	0.07	0.6810	0.0000	$1.5E+02A^{-5.01}$	0.02	0.8215	0.1510
10	$0.09A^{-0.34}$	0.48	0.6582	0.0000	$1.7E+03A^{-4.13}$	0.00	1.0259	0.3050
11	$0.10A^{-0.21}$	0.13	0.6154	0.0000	$1.2E+00A^{-1.73}$	0.01	0.5397	0.1850
12	$0.06A^{-0.12}$	0.00	0.6848	0.3150	$9.7E-02A^{0.55}$	-0.02	0.6480	0.5920
13	$0.12A^{-0.14}$	0.02	0.7501	0.0310	$1.5E-02A^{2.03}$	0.00	0.7960	0.3430
14	$0.05A^{-0.43}$	0.42	0.6464	0.0000	$3.3E+09A^{-11.81}$	0.16	0.7479	0.0220
15	$0.09A^{-0.19}$	0.15	0.6555	0.0000	$6.6E-03A^{1.04}$	0.02	0.9790	0.1700
16	$0.06A^{-0.27}$	0.58	0.4902	0.0000	$8.8E-05A^{3.58}$	0.50	0.5988	0.0000
17	$0.09A^{-0.36}$	0.74	0.3540	0.0000	$1.4E-01A^{-0.27}$	0.01	0.6253	0.1440
18	$0.13A^{0.02}$	0.00	0.5303	0.3450	$3.8E-01A^{-1.16}$	0.47	0.6522	0.0000
19	$0.09A^{-0.19}$	0.12	0.6600	0.0000	$1.3E-01A^{-0.30}$	0.00	0.8025	0.3310
20	$0.06A^{-0.46}$	0.68	0.4711	0.0000	$9.8E-10A^{14.57}$	0.06	0.8272	0.0940
21	$0.10A^{-0.04}$	0.00	0.6160	0.2910	$4.8E-04A^{4.49}$	0.08	0.6749	0.0060
22	$0.07A^{-0.09}$	0.02	0.9061	0.0210	$1.1E-01A^{-0.54}$	0.02	0.7493	0.1660
23	$0.10A^{-0.29}$	0.39	0.4601	0.0000	$4.2E-03A^{3.28}$	0.06	0.5908	0.0050
24	$0.12A^{-0.15}$	0.08	0.7132	0.0000	$2.6E+00A^{-2.57}$	0.14	0.5693	0.0000
25	$0.08A^{-0.35}$	0.49	0.5116	0.0000	$1.7E-01A^{-0.68}$	0.04	0.7298	0.1070
26	$0.06A^{-0.35}$	0.44	0.7262	0.0000	$6.4E-04A^{2.56}$	-0.02	0.9174	0.7290
27	$0.05A^{-0.16}$	0.07	0.6207	0.0030	$7.6E-02A^{4.31}$	0.03	0.4384	0.1400
28	$0.07A^{-0.24}$	0.10	0.6890	0.0030	$2.5E-01A^{6.52}$	0.56	0.5190	0.0000
29	$0.06A^{-0.47}$	0.40	0.6660	0.0000	$6.4E-06A^{7.85}$	0.13	0.7826	0.0290
30	$0.12A^{-0.23}$	0.21	0.7951	0.0000	$7.2E-38A^{43.84}$	0.19	0.5818	0.0030
32	$0.05A^{-0.11}$	0.00	0.7377	0.2740	$2.6E-02A^{1.62}$	0.27	0.5858	0.0000
33	$0.10A^{-0.26}$	0.22	0.6370	0.0000	$1.1E-01A^{-0.33}$	0.00	1.0322	0.4350
34	$0.04A^{-0.37}$	0.50	0.6759	0.0000	$2.4E-04A^{2.43}$	0.05	0.9429	0.0620
35	$0.11A^{-0.19}$	0.14	0.6878	0.0000	$1.7E-01A^{-0.96}$	0.10	0.8346	0.0040
36	$0.11A^{-0.42}$	0.68	0.6073	0.0000	$3.3E+01A^{-2.71}$	0.52	0.5096	0.0000
37	$0.08A^{-0.32}$	0.26	0.7843	0.0000	$8.2E-03A^{0.36}$	0.02	0.9083	0.1410
38	$0.10A^{-0.40}$	0.36	0.7535	0.0000	$1.1E-01A^{-0.56}$	0.09	0.7168	0.0060

hypothesis and highlights the variability among the glacial reaches, such variability is confirmed by $\sigma = 0.04$. The analysis of $\theta < 0$ could not be performed due to the low number of streams ($n = 6$).

The results obtained for the case on the fluvial reaches indicate a weak correlation on the SA regression (Table 4.3). The value of θ is 1.9 but the uncertainty is higher as estimation of θ done for the 34 fluvial reaches gives $\sigma = 3.00$. The high values of θ reflect oversteepenned reaches. Selecting those streams with a significant correlation ($p < 0.05$) and $\theta > 0$ and (Table 4.2) does not reduce the uncertainty ($\sigma = 1.43$) and a mean value of θ yields a high value (1.57). A regional θ is not suitable on the fluvial reaches because the t-test yield $t = 0.95$, leading to a rejection of the null hypothesis.

To evaluate if both $\theta_{glacial}$ and $\theta_{fluvial}$ have significant differences a two sample t-test was performed for θ on the glacial and fluvial reaches that have a significant (p$<$ 0.05) SA regression and a weak to strong correlation ($R^2 > 0.2$). The t-test gives $t = -1.16$ on 4 degrees of freedom, the null hypothesis is rejected and the alternative hypothesis states that the mean of $\theta_{glacial} \neq \theta_{fluvial}$. It can be noted that $\theta_{glacial}$ has values that denote concavity when compared to $\theta_{fluvial}$ where convexity prevails. For the case of k_s lower values are observed for the glacial and high for the fluvial. Thus, the fluvial reaches are steeper than the glacial reaches (Figure4.7).

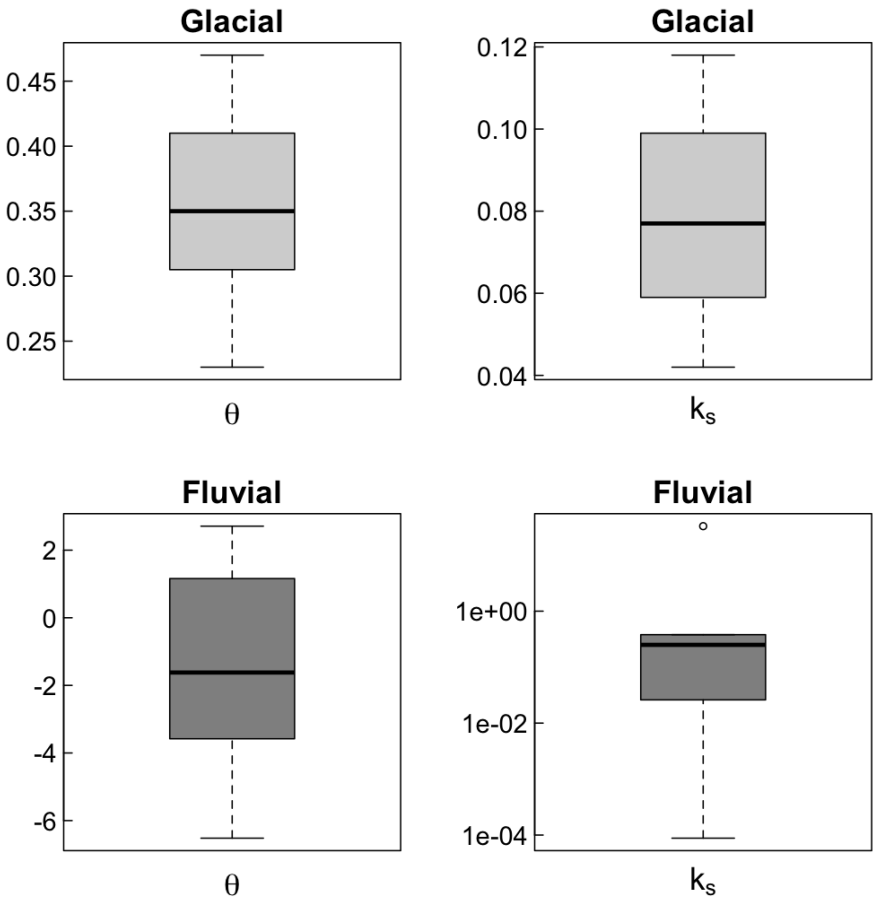

Figure 4.7: Boxplot of θ and k_s values for both glacial and fluvial reaches. A two sample t-test indicate that there are significant differences between the values of θ and k_s. The scale of k for the fluvial is logarithmic.

The differences observed between the glacial and fluvial reaches in terms of θ and k_s suggest (1) that the fluvial reaches tend to be more erosive than the glacial reaches given by the high k_s values of the fluvial reaches and (2) the fluvial reaches are extremely steep. The observed mean $\theta_{glacial}$ is little greater than the values reported by Brocklehurst and Whipple (2002) on the glaciated catchments they analysed. However, the results obtained here confirm that the most glacial reaches do exhibit lower concavity than do the fluvial reaches, as Brocklehurst and Whipple

(2002) indicate. Interestingly, in fluvially incised landscapes θ ranges between 0.35 and 0.6 (Whipple and Tucker, 1999; Snyder et al., 2000; Kirby and Whipple, 2001; Wobus et al., 2006b). These values does not approximate those obtained for Jura. Moreover, the regional mean value of θ and the subsequent normalisation of k_s cannot be done in the study area because there is a high variability among rivers and it is not possible to determine a θ_{ref} at 95% confidence. Those rivers where $\theta > 0$ (Table 4.2) have a convex profiles (Appendix A) and these may be related with a slow response of erosion that cannot absorb the impact of the base-level fall thus, the rock uplift is higher than the bedrock incision. The difference between the glacial and fluvial reaches determined by the SA regression are not trivial and highlights how perturbed are the rivers of Jura. In a condition of equilibrium, the SA regression might be equal for the upstream and downstream reaches because of the scale invariance of the power law function, or in other words the values of k_s and θ are not expected to change if they are estimated from a reach downstream or upstream. The SA model proof its usefulness since the evidences of the perturbed channels of Jura could be evaluated quantitatively and are an unequivocal proof of disequilibrium that is not necessarily by related to the base-level fall.

4.2.3 The distance-slope analysis

The analysis of channel slopes using equation 2.8 is solved in the same fashion as the SA model but in this case, the drainage area is replaced by the distance from the divide. The distance-slope regression, referred here as DS model, DS regression and a DS plot for its graphical representation (Goldrick and Bishop, 2007), is an alternative form of SA. It has been argued that it is easier to estimate because the DS plot lacks important effects imposed on distance by the DEM resolution (Goldrick and Bishop, 2007). The DS model was applied to 34 streams (Table 4.4; Appendix E). In the DS notation the value of λ is equivalent to θ but its dimensions are slightly different because there is a different proportional change of the distance downstream and the stream discharge . When $\lambda = 1$ a condition of equilibrium is likely but a more realistic value has been found to be $\lambda < 1$ (Goldrick and Bishop, 2007).

Observing the results of both values of k and λ (see equation 2.8) it can be noted the wide variation for all the streams analysed. The mean value of λ is 0.25 ± 0.07 and for k is 1.30 ± 0.73 at a 95% of confidence. The variation of λ among rivers makes difficult to set a mean regional value as in the case of θ and the t-test obtained for the 34 rivers give a $t = -7.10$. The null hypothesis is thus rejected, which means that it is not possible to assign a regional value of λ. Those rivers where the DS regression is not significant (p$>$ 0.05) and with a week correlation ($R^2 < 0.2$) were not considered for the analysis presented here. Analysing streams where $\lambda > 0$ a mean value of 0.43 ± 0.05 was obtained and 2.52 ± 1.48 for k. The Shapiro-Wilk normality test indicates that the values of λ have a normal distribution ($p > 0.05$) but this is not the case for k. Finding a regional mean of λ could not be achieved since the t-test yield a value of $t = 3.65$ and the null hypothesis is rejected. Although their values of λ were normally distributed, their still have a wide dispersion ($\sigma = 0.13$) (Figure 4.8).

Table 4.4: Exponent and coefficient of the power law function of the distance and channel slope for the rivers of Jura.

Stream ID	Equation	R^2	RSE	P-value
1	$2.3 \times 10^{-01} L^{-0.13}$	0.01	0.7977	1.0×10^{-01}
2	$1.5 \times 10^{-01} L^{-0.06}$	0.00	0.7775	3.2×10^{-01}
3	$1.2 \times 10^{-01} L^{-0.07}$	0.00	0.9671	3.9×10^{-01}
4	$1.1 \times 10^{-01} L^{0.04}$	0.00	0.6659	4.0×10^{-01}
5	$3.5 \times 10^{-01} L^{-0.18}$	0.07	0.7359	5.6×10^{-08}
8	$1.7 \times 10^{-01} L^{-0.10}$	0.02	0.7657	8.5×10^{-03}
10	$3.3 \times 10^{+00} L^{-0.49}$	0.37	0.7847	1.0×10^{-35}
11	$1.4 \times 10^{+00} L^{-0.38}$	0.22	0.7996	8.5×10^{-15}
12	$7.1 \times 10^{-02} L^{0.01}$	-0.01	0.6606	8.4×10^{-01}
13	$2.8 \times 10^{-01} L^{-0.12}$	0.01	0.8480	9.6×10^{-02}
14	$9.7 \times 10^{-01} L^{-0.42}$	0.25	0.8183	3.3×10^{-11}
15	$6.7 \times 10^{-01} L^{-0.29}$	0.19	0.7441	5.6×10^{-16}
16	$5.9 \times 10^{-01} L^{-0.32}$	0.25	0.8126	2.4×10^{-13}
17	$1.3 \times 10^{+00} L^{-0.33}$	0.32	0.6172	5.8×10^{-31}
18	$8.0 \times 10^{-01} L^{-0.28}$	0.11	0.7457	9.6×10^{-13}
19	$2.9 \times 10^{-01} L^{-0.16}$	0.05	0.7536	1.1×10^{-05}
20	$2.8 \times 10^{+00} L^{-0.46}$	0.46	0.6163	1.1×10^{-50}
21	$1.6 \times 10^{-01} L^{-0.06}$	0.00	0.6410	1.8×10^{-01}
22	$5.1 \times 10^{-01} L^{-0.29}$	0.10	0.9956	1.8×10^{-07}
23	$8.3 \times 10^{-01} L^{-0.25}$	0.20	0.5463	1.3×10^{-22}
24	$7.4 \times 10^{-01} L^{-0.26}$	0.09	0.7457	2.5×10^{-10}
25	$2.0 \times 10^{+00} L^{-0.42}$	0.44	0.5569	8.0×10^{-55}
26	$1.0 \times 10^{+00} L^{-0.38}$	0.25	0.8369	3.6×10^{-16}
27	$4.3 \times 10^{-02} L^{0.09}$	0.01	0.6669	1.2×10^{-01}
28	$1.4 \times 10^{-01} L^{-0.04}$	0.00	0.7589	4.0×10^{-01}
29	$1.2 \times 10^{+00} L^{-0.38}$	0.30	0.7348	1.7×10^{-21}
30	$1.5 \times 10^{+00} L^{-0.35}$	0.21	0.8354	3.8×10^{-19}
32	$7.4 \times 10^{-03} L^{0.32}$	0.12	0.7830	4.3×10^{-07}
33	$1.4 \times 10^{+00} L^{-0.36}$	0.22	0.8143	3.0×10^{-21}
34	$4.6 \times 10^{-01} L^{-0.31}$	0.15	0.9663	1.1×10^{-07}
35	$4.4 \times 10^{+00} L^{-0.55}$	0.31	0.8423	1.4×10^{-28}
36	$1.2 \times 10^{+01} L^{-0.66}$	0.62	0.7106	4.4×10^{-76}
37	$2.5 \times 10^{+00} L^{-0.50}$	0.30	1.0138	6.2×10^{-23}
38	$2.1 \times 10^{+00} L^{-0.46}$	0.41	0.7836	3.4×10^{-40}

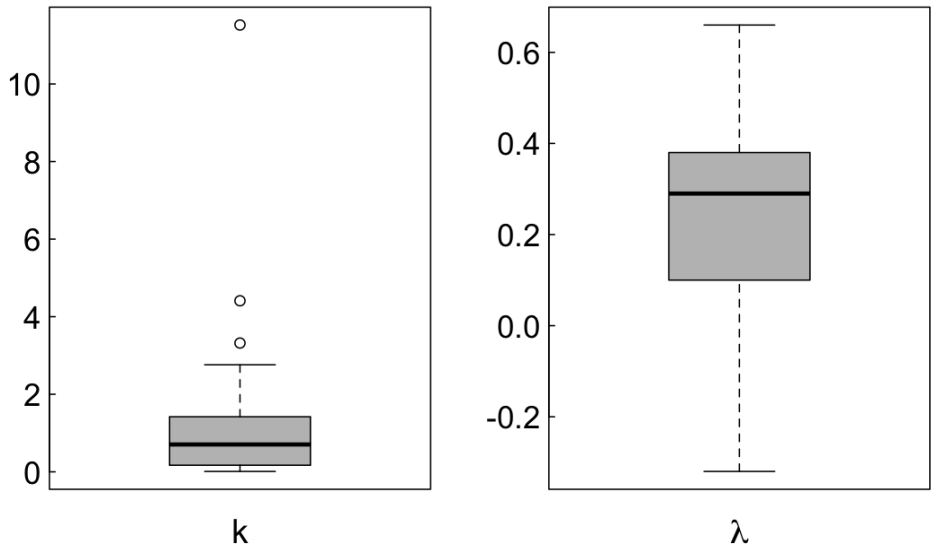

Figure 4.8: Boxplot of λ and k values for 34 streams of Jura. It is notable the wide range for both constant and exponents of the power law function which also denotes the variability of the rivers of Jura.

As for the SA model, the glacial and fluvial reaches were analysed using DS model. The equations and related statistics of the DS regression performed on glacial and fluvial reaches are given in Table 4.5 and the plots are given in appendices F and G.

For the glaciated reaches λ has a mean value of 0.22 ± 0.08. The mean value of k is 1.07 but a wide dispersion was observed ($\sigma = 0.59$). The analysis of the fluvial reaches also give a poor correlation (Table 4.5). However, it was observed that in general, the fluvial reaches are less concave than the glacial ones. The mean value of λ for the fluvial reaches where $p < 0.05$ and $R^2 > 0.2$ is -3.33 this value denotes a high convexity, condition which is difficult to be accepted since this values have not been reported for any bedrock river studied by Goldrick and Bishop (2007). On the glacial reaches where $p < 0.05$ and $R^2 > 0.2$ λ has a mean value of 0.44 ± 0.06 but the weak correlation in most of the reaches prevail ($n = 23$) (Table 4.5). Those

Table 4.5: Exponent and coefficient of the power law function of distance from the divide and channel slope for glaciated and non-glaciated reaches of Jura.

	Glaciated				Fluvial			
Stream ID	**Equation**	**R^2**	**RSE**	**P-value**	**Equation**	**R^2**	**RSE**	**P-value**
1	$0.04L^{0.15}$	0.01	0.7653	0.153	$5.8E-11L^{2.66}$	0.11	0.7282	0.021
2	$0.15L^{-0.04}$	0.00	0.6695	0.481	$1.0E+02L^{-0.91}$	0.00	0.7985	0.372
3	$0.02L^{0.19}$	0.02	0.8460	0.019	$2.2E-04L^{0.50}$	-0.07	0.4916	0.737
4	$0.09L^{0.08}$	0.01	0.4658	0.088	$6.9E-01L^{-0.20}$	0.00	0.7589	0.430
5	$0.28L^{-0.14}$	0.05	0.6632	0.000	$1.4E+11L^{-3.32}$	0.15	0.7186	0.000
8	$0.27L^{-0.17}$	0.08	0.6756	0.000	$4.0E+04L^{-1.52}$	0.01	0.8242	0.204
10	$3.20L^{-0.48}$	0.40	0.7073	0.000	$7.0E+42L^{-11.76}$	0.13	0.9589	0.043
11	$0.53L^{-0.22}$	0.08	0.6315	0.000	$5.0E+03L^{-1.34}$	0.02	0.5375	0.133
12	$0.08L^{0.00}$	-0.01	0.6893	0.974	$5.0E+02L^{-1.17}$	0.04	0.6306	0.100
13	$0.09L^{0.08}$	0.00	0.7572	0.239	$3.1E-05L^{0.95}$	-0.03	0.8069	0.633
14	$0.77L^{-0.38}$	0.20	0.7590	0.000	$1.6E+13L^{-4.10}$	0.18	0.7371	0.014
15	$0.46L^{-0.23}$	0.14	0.6581	0.000	$2.8E-05L^{0.88}$	0.00	0.9879	0.353
16	$0.84L^{-0.37}$	0.43	0.5671	0.000	$1.0E-21L^{5.38}$	0.55	0.5720	0.000
17	$2.30L^{-0.44}$	0.57	0.4578	0.000	$5.9E-01L^{-0.23}$	0.00	0.6279	0.402
18	$0.08L^{0.07}$	0.01	0.5275	0.042	$2.4E+07L^{-2.42}$	0.41	0.6834	0.000
19	$0.41L^{-0.21}$	0.12	0.6602	0.000	$4.8E+01L^{-0.76}$	0.00	0.8009	0.241
20	$3.90L^{-0.52}$	0.56	0.5536	0.000	$4.4E-37L^{9.65}$	0.10	0.8088	0.041
21	$0.13L^{-0.03}$	0.00	0.6172	0.589	$7.5E-11L^{2.60}$	0.11	0.6638	0.001
22	$0.15L^{-0.10}$	0.01	0.9117	0.090	$2.3E+04L^{-1.54}$	0.06	0.7312	0.035
23	$0.95L^{-0.28}$	0.22	0.5201	0.000	$9.4E-07L^{1.44}$	0.06	0.5909	0.005
24	$0.27L^{-0.10}$	0.01	0.7413	0.039	$5.7E+06L^{-2.20}$	0.17	0.5564	0.000
25	$2.10L^{-0.43}$	0.46	0.5268	0.000	$5.2E+10L^{-3.20}$	0.03	0.7331	0.137
26	$1.90L^{-0.48}$	0.38	0.7652	0.000	$2.1E-06L^{1.19}$	-0.01	0.9154	0.569
27	$0.17L^{-0.14}$	0.03	0.6329	0.030	$3.3E-01L^{-0.12}$	-0.02	0.4501	0.940
28	$0.31L^{-0.20}$	0.09	0.6942	0.005	$8.5E-17L^{4.72}$	0.58	0.5081	0.000
29	$1.40L^{-0.40}$	0.32	0.7139	0.000	$4.7E-28L^{7.15}$	0.12	0.7864	0.034
30	$1.30L^{-0.33}$	0.18	0.8106	0.000	$8.4E-35L^{8.88}$	0.21	0.5755	0.002
32	$0.07L^{-0.06}$	-0.01	0.7411	0.478	$1.5E-14L^{3.72}$	0.36	0.5485	0.000
33	$0.76L^{-0.26}$	0.15	0.6657	0.000	$3.2E-02L^{0.07}$	-0.01	1.0349	0.872
34	$1.50L^{-0.50}$	0.38	0.7526	0.000	$3.2E-29L^{7.16}$	0.21	0.8629	0.001
35	$0.55L^{-0.23}$	0.07	0.7136	0.000	$2.9E+01L^{-0.84}$	0.05	0.8575	0.035
36	$9.20L^{-0.63}$	0.57	0.6999	0.000	$9.7E+13L^{-4.12}$	0.58	0.4766	0.000
37	$0.67L^{-0.28}$	0.12	0.8535	0.000	$9.5E-05L^{0.62}$	0.03	0.9026	0.091
38	$1.50L^{-0.40}$	0.35	0.7564	0.000	$4.2E+03L^{-1.36}$	0.07	0.7242	0.014

glacial reaches where there is a weak correlation, are likely to be perturbed by glacial knickpoints. The values of k in the fluvial reaches also yield exceptionally high values as in the SA model and are related to high values of λ (Table 4.5 and Figure 4.9).

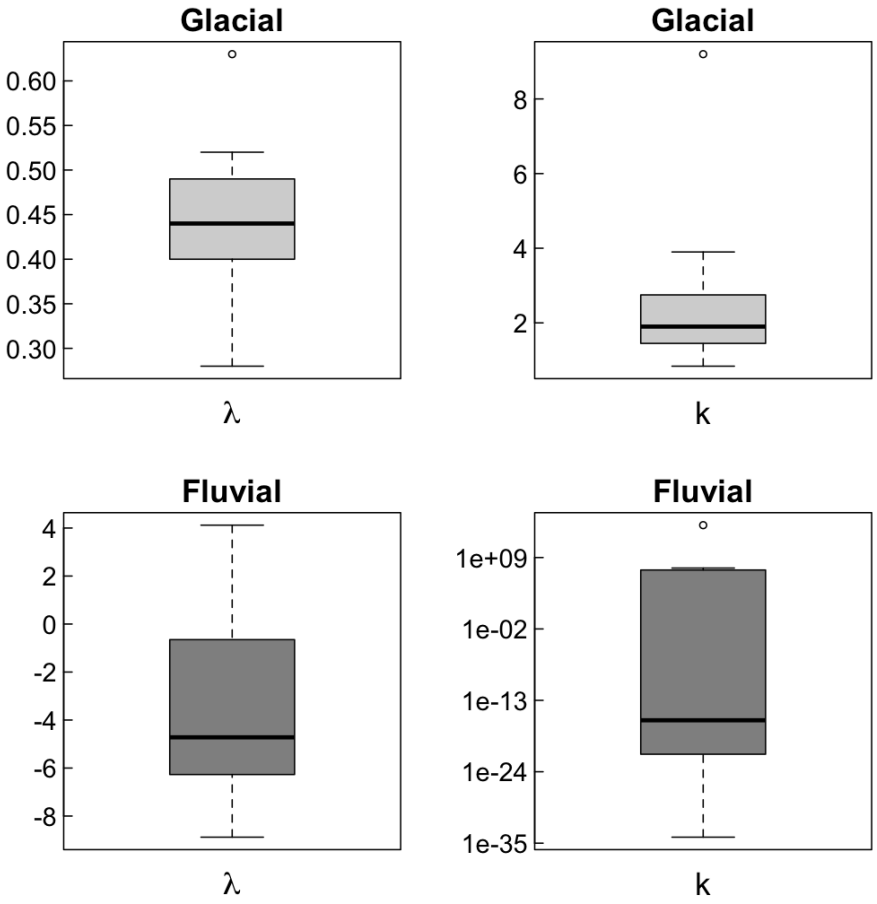

Figure 4.9: Boxplot of k and λ for the glacial and fluvial reaches. Note the positive values of θ for the glacial reaches and the negative values for the fluvial reaches. The values of k in the fluvial reaches denotes a high channel steepness as has also been confirmed with the SA model shown in Figure 4.7.

The analysis of channel slope using both SA and DS models demonstrates that the streams of Jura are highly perturbed by non-fluvial processes (i.e., glacial pro-

cesses) which impedes the direct estimation of fluvial incision as has been done for non-glaciated landscapes with large catchment areas (e.g., Seidl et al., 1994; Stock and Montgomery, 1999; Goldrick and Bishop, 2007). The perturbation of channels is evident in the DS plots because the change in channel slope is analysed continuously. Abrupt changes in channel slope appear as spikes in the DS plot and these can be interpreted as disequilibrium signals on channels (Goldrick, 1999). In the case of the SA plots, the detection of channel disturbances is obscured because the data are smoothed and the changes in channel slope can only be detected when there are important changes in drainage area (Figure 4.10). This does not mean that one method is better than the other; both approaches are well-based on empirical and physical formulas (e.g., Goldrick, 1999; Whipple and Tucker, 1999; Goldrick and Bishop, 2007).

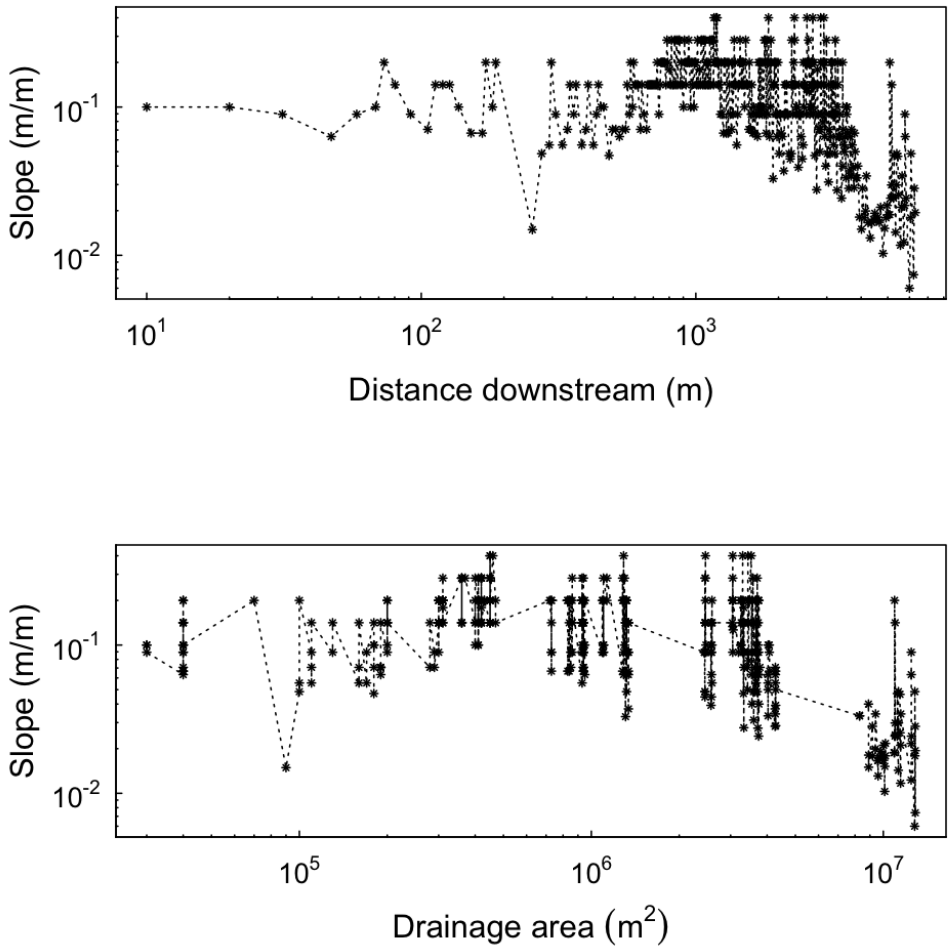

Figure 4.10: Distance-slope plot and slope-area plot of the Glenbatrick River (stream 18). The DS plot allows to record continuously the changes in channel slope, in contrast, the SA plot stacks up the values of channel slope when there are not major changes in drainage area.

The DS and SA approaches both allow to estimate quantitatively, the channel steepness and channel concavity. Nevertheless, both models have not been compared. Here the DS and SA models are compared by plotting the coefficients and exponents of the DS and SA regressions (Figure 4.11). A good correlation is ob-

served between θ and λ (Figure 4.11), this response indicates that both models capture the channel concavity. However, the dimensional coefficients related to incision expressed by k_s in the SA plot and k in the DS do not seem to be correlated. This is interpreted as the main difference in both models (Figure 4.11), that suggests a different estimation of channel steepness by each model which in turn result in a different estimation of channel incision. A fair correlation has been reported for the normalised channel steepness k_{sn} with the basin erosion rate in the Bolivian Andes (Safran et al., 2005), but for the case of the distance-slope model, the k and erosion rate correlation has not been reported.

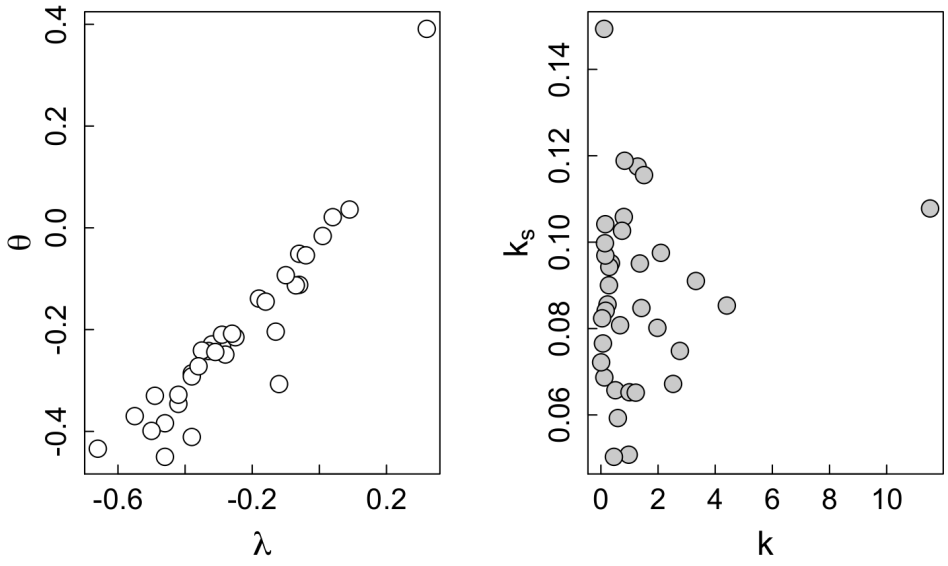

Figure 4.11: Plot of the constant and exponent of the power law equation for the DS and SA correlations of the streams of Jura ($n = 34$). Correlation of λ and θ yields $R^2 = 0.87$.

The variation of θ and k_s has been found to be sensitive to the DEM resolution (Finlayson and Montgomery, 2003); the same result would also apply if several

DEMs are used to obtain λ and k from the DS equation. Nevertheless, for the rivers of Jura, the effect of the DEM resolution is irrelevant as the DS and SA exponents and coefficients were extracted from the same DEM and were determined using the same data from the same reaches. The lack of correlation of between k_s and k is probably related to the way in which are calculated the DS and SA constant and exponents. As was mentioned above, the SA regression generates a smoothing of data and this is reflected by lower values in k_s compared to k obtained from the DS plot (compare figures 4.6 and 4.8). Although there are differences in between k and k_s both approaches (i.e., DS and SA regressions) produced similar results as can be confirmed by the correlation of the residual standard error (RSE) of the regression model (Figure 4.12).

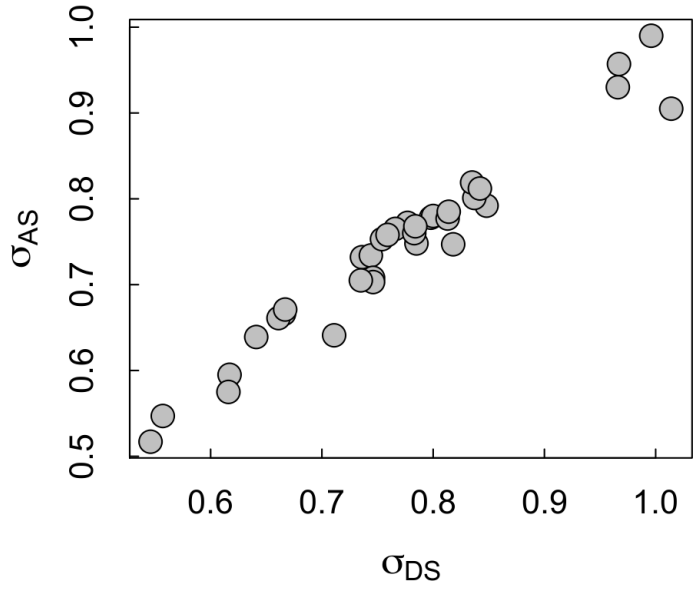

Figure 4.12: Plot of the RSE (σ) of the DS and SA regression models. The correlation coefficient is $R^2 = 0.95$.

The lack of correlation between k and k_s is somewhat unexpected since the SA

and DS models are believed to produced similar results. To detect the source of the difference between the DS and SA models, the coefficients and exponents of each model were plotted (Figure 4.13; Tables 4.2 and 4.4) The relationship between k_s and θ has received little attention, but a correlation between these has been reported (e.g., Brocklehurst and Whipple, 2002). Goldrick (1999) explored the correlation between k and λ suggesting that this relationship reflects the linkage between hillslope and fluvial processes in the landscape.

The constant and exponent of the DS and SA regressions where plotted separately to observed if their correlation (Figure 4.13). The results obtained from correlating the k and λ figure 4.13 suggest that there is an interdependence between channel concavity and the channel steepness, as has previously noticed by Goldrick (1999). However, the lack of correlation between θ and k_s is unexpected because *a priori* a correlation between k_s and θ might also occur (Brocklehurst and Whipple, 2002; Wobus et al., 2006b). The non correlation of θ and k_s suggests that channel steepness is quite independent of channel concavity implying that incision is not directly linked to the basin morphology. It is unclear if the lack of correlation between θ and k_s is related to the perturbation signals on the long profile. The dichotomy detected on the constants and exponents of the power law functions of the DS and SA regressions is not trivial and requires further explorations which are beyond the goal of the present research.

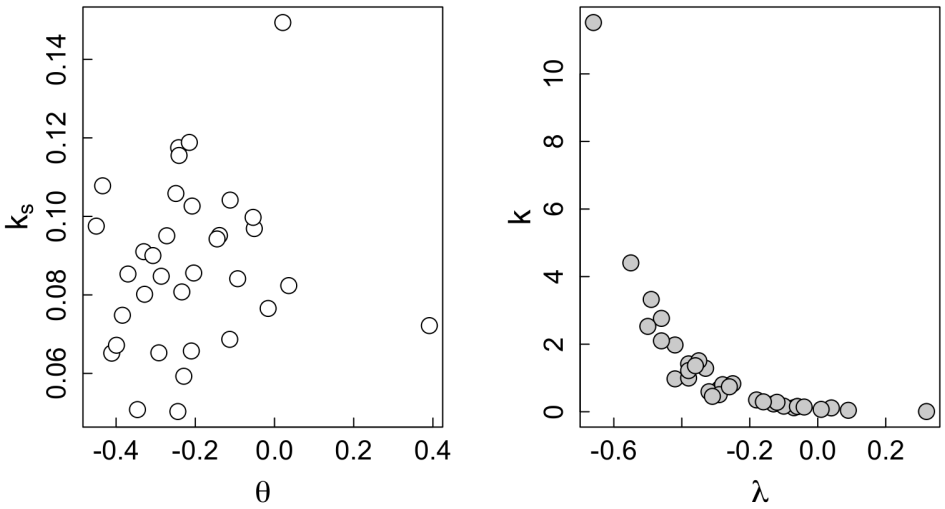

Figure 4.13: Plot of k_s and θ (SA regression) and k and λ (DS regression). The best fit was obtained for k_s and θ using an exponential function $k = 0.09e^{-7.0\lambda}$ and $R^2 = 0.95$.

Stream profile analysis using the DS and SA plots reveals that the rivers of Jura are quite variable in terms of their morphology. Also the wide variability of the values of θ and its non-normal distribution, difficult the use of a θ_{ref} as has been done by other authors for other settings (e.g., Snyder et al., 2000; Brocklehurst and Whipple, 2002; Duvall et al., 2004; Wobus et al., 2006b). The purpose of using θ_{ref} is useful on the conditions mentioned since it allows to detect deviations or anomalies given by tectonic or controls imposed to the lithology reflected on the k_s values. For the case of Jura, the finding of a θ_{ref}, or its alternative λ_{ref}, is not viable since most of the streams of Jura are perturbed on their long profile by other processes not related to the fluvial ones, as is the case of the glacial signals (i.e., glacial knickpoints). A regional pattern of channel concavity is unclear for the rivers analysed here since there is a wide variability in concavity. However, the results for θ and λ for the 34 long profiles indicate that the rivers of Jura have in general low concavity and for the case of the glacial reaches, the lower concavity found is con-

sistent with the pattern observed in other glaciated catchments (e.g., Brocklehurst and Whipple, 2002). The analysis of the channel slope indicates that the rivers of Jura are far from a condition of equilibrium and even though a differentiation was attempted between the glacial and fluvial domains, the results for the DS and SA regressions indicate that the rivers of Jura are highly perturbed and in some cases convexity prevails on the long profile.

4.3 Summary

The stream profile analysis presented in this chapter provide a quantitative characterisation of the bedrock rivers and basins of Jura. The stream profile analysis enables and evaluation of channel slope that, in turn, points to pervasive disequilibrium in the Jura streams. The results from stream profile analysis are also consistent with catchment morphometry exposed in chapter 3 and points to a strong inheritance in the landscape. The main outcomes of the analysis and its shortcomings are summarised below:

- The stream profile analysis is a powerful tool to test if a landscape has reached or is close to an state of equilibrium (steady-state). In this sense, the channel slopes are, as Gilbert (1877) and Hack (1957) noted, a key feature in understanding the erosion of rivers and landscape change.

- For the case of Jura, the poor fits for the SA and DS regressions indicate a highly perturbed landscape which confirms a landscape in disequilibrium characterized by the variation and range in the values of θ and λ. The landscape perturbation was confirmed by significant differences in both SA and DS model for the glacial and fluvial reaches.

- The glacial-inhterited landscapes poses several challenges to the use of the stream power model. Firstly, the domain of hillslope and debris flow processes and the fluvial domain may be disconnected by a wide valley that increases the area of operation of channel processes. Secondly, channel incision may operate at different basin reliefs on different basins size, making it difficult to use a θ_{ref} to normalize k_s and λ_{ref} to normalise K as has been proposed for non-glaciated landscapes (e.g., Sklar and Dietrich, 1998; Snyder et al., 2000; Wobus et al., 2006b; Goldrick and Bishop, 2007). The variability among streams in small and perturbed landscapes may make it impossible to extract a regional θ or λ value.

- The stream profile analysis and the morphometric analysis (chapter 3) demonstrate that the rivers and landscape of Jura are in transience. Both analyses indicate a departure from the theoretical expectations and highlight the importance of past processes that can control the landscape dynamics. In the study area, the glacial-processes and the effect of the base-level fall are responsible for the disequilibrium-state of Jura. The effect of the base-level fall is detailed in chapter 5.

Chapter 5

Base-level fall knickpoints and the morphology of transient reaches

5.1 Introduction

Gilbert (1877) observed that the irregularities formed in bedrock channels (i.e., knickpoints) enhance channel incision because channel declivity increases. He also suggested that the mechanism of formation of the channel irregularities is likely to occur at the contact of two lithological units (e.g., the contact between soft and hard rocks). This observation has been confirmed by others (e.g., Hack, 1973; McKeown et al., 1988; Goldrick and Bishop, 2007). Gilbert's observations in regard to knickpoints are summarised in his discussion of channel declivity and incision. He considered that "...where declivity of bed gives an increased velocity, the capacity for transportation will become greater than the load and there will be corrasion of the bed...where the rock is hard corrasion will be less rapid than where it is soft, and there will result inequalities of grade" (Gilbert, 1877; p. 106-107). Later, in 1924, Walter Penck used the term *knickpunkte* to name the convex irregularities observed on a stream profile. Penck proposed that the knickpoints are the result of continuous and uninterrupted tectonic uplift (Davis, 1932; von Engeln, 1940). Davis (1932) debated and refuted the hypothesis proposed by Penck and the term remained unused. von Engeln (1940) formally introduced the term 'knickpoint' into English to name the sharp breaks in slope between graded reaches on a longitudinal profile. The works of Penck and von Engeln were the basis for further studies aimed to understand the

role and genesis of knickpoints in the fluvial network. Since then, several studies based on observations in natural settings and flume experiments have been carried out to understand these so-called 'enigmatic' features of landscape (Crosby and Whipple, 2006). It must be noted, though, that the term knickpoint is still loose and poorly defined in geomorphology. A genetic classification of knickpoints is required because several processes may trigger them. Moreover, because knickpoints can occur in alluvial and bedrock rivers, as experiments and observation in cohesive and non cohesive materials have demonstrated (e.g., Holland and Pickup, 1976; Wolman, 1987; Gardner, 1983; Frankel et al., 2007), a morphogenetic classification of knickpoints is required.

The knickpoint understood as an expression of disequilibrium due to a drop in base-level was set once the plate tectonics and the equilibrium concept were firmly introduced into geomorphology (Bishop, 2007). As well, advances in the branch of fluvial geomorphology since the 1950s, particularly in alluvial rivers, have permitted the construction of a solid theoretical framework called the stream power model (Bagnold, 1960; 1977; Howard, 1994) which explains the principles of fluvial knickpoint propagation. According to the stream power model, rivers tend to adjust their channel slopes as stream discharge increases, the ideal morphological expression of an adjusted channel being smooth a concave profile (Mackin, 1948; Yatsu, 1955; Snow and Slingerland, 1987). Any disturbance or disequilibrium in a graded reach will then cause an abrupt step observed along in a longitudinal profile, which, according to the basic postulates of the stream power, propagates headwards as a result of an increase in quarrying and plucking on the knickpoint face (Gilbert, 1907; Gardner, 1983; Howard, 1994; Whipple and Tucker, 1999; Whipple et al., 2000a; Frankel et al., 2007).

Of particular interest for the landscape evolution is knickpoint formation and propagation due to changes in the rate of tectonic uplift and/or eustatic sea level. Base-level fall knickpoints are believed to be the main mechanism by which the

link between tectonics and climate is transmitted to the landscape (Kooi and Beaumont, 1996; Whipple and Tucker, 1999; Hasbargen and Paola, 2000; Bigi et al., 2006; Bishop, 2007). Base-level fall is more or less well understood, an abrupt fall of rivers base-level forms a scarp (i.e., knickpoint) located at the steam mouth that propagates headwards as a kinematic wave (Rosenbloom and Anderson, 1994; Whipple and Tucker, 1999). Nevertheless, rates of knickpoint retreat, the effect of structure and lithology on knickpoint recession and the secondary effects caused (e.g., landslide and hillslope instability) by the knickpoint retreat are not fully understood. Numerical models that reproduce channel incision under detachment-limited conditions have been able to reproduce knickpoint generation and propagation related to a base-level lowering event (e.g., Howard, 1998; Whipple and Tucker, 1999; Snyder et al., 2002). The empirical studies dealing with the knickpoint recession in bedrock rivers are less numerous (e.g., Hayakawa and Matsukura, 2003; Bishop et al., 2005; Anthony and Granger, 2007) nevertheless, these type of studies are highly required to fully understand the mechanics behind the knickpoint recession and its effect into landscape.

As mentioned above, understanding knickpoint propagation is key in to elucidating how landscapes evolve. These so-called 'bottom-up' processes (Bishop, 2007) have further implications in landscape dynamics and in the last instance into landscape morphology because the rate of incision during, and slightly after, the knickpoint propagates is likely to change the rates of incision in the landscape by propagating disequilibrium to hillslopes which result in a change in sediment supply to the rivers (Reinhardt et al., 2007a). Therefore, the empirical study of knickpoints is necessary to elucidate (1) the rate of knickpoint propagation, (2) what physical process controls the knickpoint propagation, (3) what is the role of lithology and structure and (4) how the reaches in transience respond to base-level fall. In this chapter I address some of these questions. As mentioned in previous chapters, knickpoint propagation is evaluated in a homogeneous lithology and the effect of structure is assessed. This chapter shows that the knickpoint propagation

caused by a change in the base-level is transmitted in small bedrock rivers catchments in a non-equilibrium setting. The role of structure is also evaluated to explore whether structural dip dampens or enhances knickpoint propagation. The final section presents an analysis of the transient reaches after a knickpoint migration.

5.2 Detection of base-level fall knickpoints on a stream longitudinal profile

The easiest way to the detect knickpoints on a longitudinal profile is by identifying those reaches that perturb the streams smooth, concave-up long profile (von Engeln, 1940). Nevertheless, this approach has several disadvantages. For example, at the simplest level the detection of steep reaches on a stream profile may result from errors in the cartography or DEM and these may not represent a true knickpoint. More importantly, because knickpoints can be formed by several processes not necessarily related to changes in the base-level or contrasts in lithology, their detection on the longitudinal profile requires detection of breaks in the hydraulic geometry of rivers. Hack (1973) proposed a more systematic approach to detecting gradient anomalies (i.e., steep reaches) observed on a longitudinal profile using the stream-gradient index. The stream-gradient index, SL, is easily obtained using the elevation and length of stream reaches thus:

$$SL = \frac{\Delta H \times L}{\Delta L} \tag{5.1}$$

where ΔH and ΔL are the difference in elevation and length of the reach respectively and L is from the full length of the stream. An alternative form of equation 5.1 is equation (Hack, 1973):

$$SL = \frac{\Delta H}{logL_2 - logL_1} \tag{5.2}$$

where the subscript of L correspond to the lower and upper limit of the reach respectively.

The stream-gradient index has been used in numerous studies, mostly to assess the presence of tectonic signals reflected in stream long profiles (e.g., McKeown et al., 1988; Hamdouni et al., 2008; Larue, 2008). Interestingly, this method has rarely been used to evaluate the propagation of disequilibrium (Goldrick and Bishop, 2007) and only in a few cases the detection of knickpoint and knickzones has been done (Larue, 2008). Goldrick and Bishop (2007) discussed Hack's SL and stream-

gradient index, arguing that such analysis does not necessarily allow the detection of disequilibrium on a stream long profile. These authors indicated that even when the stream-gradient index has high values, these not necessarily mean a condition of disequilibrium, instead, these values may reflect a change in the incision rates related to changes in lithology. Goldrick and Bishop (2007) proposed the use of DS model to analyse the stream long profiles. Using the DS analysis, the signals related to the base-level of rivers (i.e., knickpoints) can be detected as outliers on the DS regression. The DS model can also be evaluated in a more complex scenario where a river cuts into two different rock types where a knickpoint has migrated as result of a base-level lowering. In such a case, the DS plot shows a shifting of the scaling of channels against the length (Goldrick and Bishop, 2007; Fig. 6) (Figure 5.1). The DS model to evaluate the knickpoint recession can be obtained from the following equation:

$$DS_n = \frac{(H_{n-1} - H_n)(1-\lambda)}{L_n^{1-\lambda} - L_{n-1}^{1-\lambda}} \tag{5.3}$$

simplifying equation 5.3 yields:

$$DS_n = \frac{\Delta H(1-\lambda)}{\Delta L^{1-\lambda}} \tag{5.4}$$

where λ is the channel concavity, H is elevation and L the distance downstream (Goldrick and Bishop, 2007). The DS form of analysis requires, however, a reasonable scaling of channel slope with the channel length and avoiding perturbed reaches along the long profile is recommendable (Goldrick and Bishop, 2007), but the knickpoint can still be identified (Figure 5.2). The DS form equals the SA in the detection of the knickpoints. In the SA, case the segmentation several reaches an estimating the normalised steepness k_{sn} allows the detection of those zones where the incision rates are higher or where the channel slopes increase suddenly, in this case a knickpoint can be detected (e.g., Snyder et al., 2003; Wobus et al., 2006b; Harkins et al., 2007)(Figure 5.1).

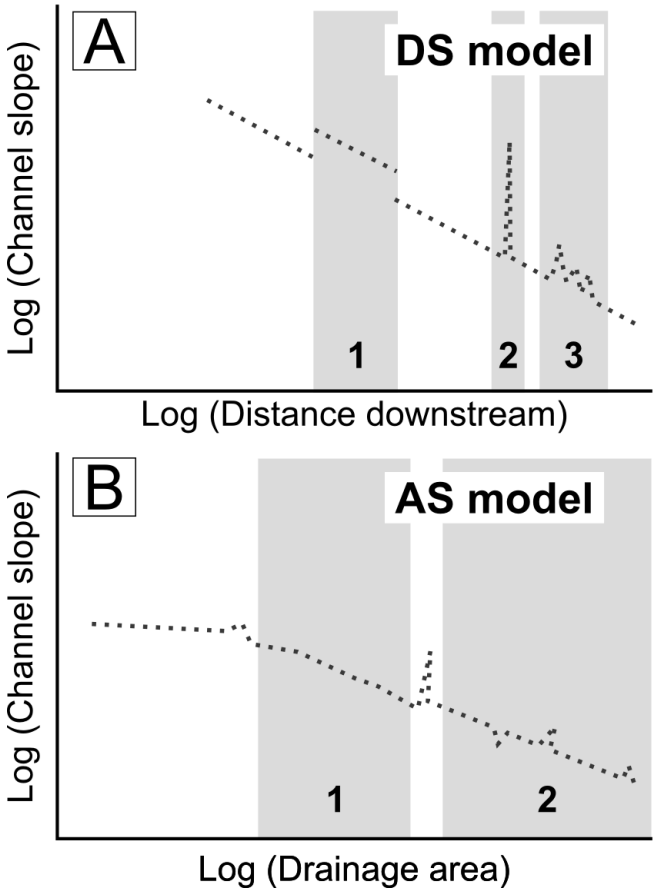

Figure 5.1: Hypothetical scenarios of changes in DS scaling. A1 shows the parallel shifting due to a change in lithology; A2 shows a knickpoint and A3 the knickzone (Modified from: Goldrick and Bishop, 2007). B. Scenarios of two reaches and the presence of a knickpoint using the SA model. B1 shows the unperturbed reach and B2 the reach affected by the knickpoint migration (Modified from: Harkins et al., 2007)

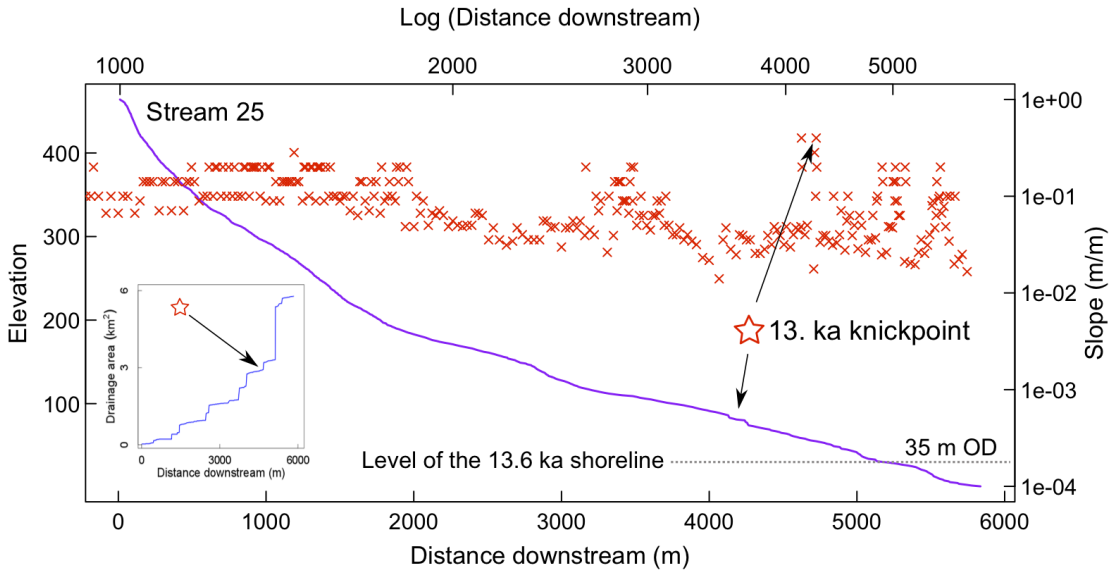

Figure 5.2: Example of the knickpoint detection using the DS plot approach on a perturbed reach (stream 25). The knickpoint appears as a peak in the DS plot (upper and right axis for reference in the plot), but because the channel is perturbed (note the spikes upstream of the 13.6 ka knickpoint) other geomorphic markers (see discussion below) are required to confirm if the knickpoints resulted from a base-level lowering

The DS and SA models are powerful tools that allow the detection of disequilibrium signals on a longitudinal profile. The advantage of using both approaches resides in the fact that both models incorporate information concerning channel incision and the stream long profile morphology (concavity and steepness). Nevertheless, the presence of several knickpoints on a longitudinal profiles makes it difficult to distinguish those knickpoints generated for example, by a base-level fall. In this case the selection of knickpoints requires the detection of geomorphic markers that are clearly related to base-level knickpoints along the stream profile. For the case of Jura the presence of strath-terraces (Figure 5.3) and the uplifted shingle beaches of the west coast, were key in locating the relevant base-level fall knickpoints.

Figure 5.3: Sequence of strath-terraces located downstream of the 13.6 ka knickpoint on the stream 38 (west coast of Jura). Such geomorphic markers have been used to detect and confirm the location of the base-level fall knickpoints.

The propagation of knickpoints in bedrock rivers has been evaluated using three different approaches: empirical (e.g., Hayakawa and Matsukura, 2003; Bishop et al., 2005; Anthony and Granger, 2007); numerical (e.g., Howard, 1998; Whipple and Tucker, 1999; Snyder et al., 2002) and experimental (e.g., Holland and Pickup, 1976; Gardner, 1983; Frankel et al., 2007). Each approach has its own strengths and weaknesses, and limitations. The results of flume experiments have provided useful information in regard to the knickpoint initiation, propagation and evolution (e.g., Brush and Wolman, 1960; Holland and Pickup, 1976; Gardner, 1983; Frankel et al., 2007; Lamb and Dietrich, 2009) and its relation to landscape dynamics and hillslope processes (e.g., Hasbargen and Paola, 2000; Bigi et al., 2006). Even though knickpoint propagation has been successfully reproduced, such experimental studies are limited by a proper calibration of time and the lithology used for every experiments and the rates of knickpoint propagation when compared to the real setting

require to be constrained.

Numerical modelling has been useful to explore knickpoint migration resulting from a drop of the base-level (e.g., Howard, 1998; Snyder et al., 2002) and the evolution of the knickpoint lip and its contiguous reaches (e.g., Haviv et al., 2006; Wyrick and Pasternack, 2008; Berlin and Anderson, 2009). Neverthless, the results of this approach require verification in natural settings. Oversimplifications can occur if unknown physical processes are omitted from the numerical models. Empirical studies have provided valuable information of the knickpoint retreat rates in different settings, climates and lithologies (e.g., Hayakawa and Matsukura, 2003; Bishop et al., 2005; Crosby and Whipple, 2006; Anthony and Granger, 2007; Loget and van den Driesseche, 2009). The major limitations of using the empirical approach are the accessibility to the sites and the detection of the knickpoints in the field.

Even though the approaches to study knickpoints are varied, results obtained are well explained by the stream power model. An interesting finding related to the evolution of knickpoints in bedrock rivers is provided by the experiments run by Gardner (1983) who tested the knickpoint evolution in cohesive materials with different resistances and in one case stratified (Gardner, 1983, his Figure 13). He found that the evolution of the knickpoint depends on the relationship between the shear stress at the bottom of the channel and a critical shear stress that must be overcome to initiate the erosion. The headwards migration of a knickpoint occurs when there is an excess of shear stress and there is a resistant layer overlaid by a non-resistant layer. For the case of a homogenous resistant material the knickpoint face rotates and fades away. This process, termed replacement by Gardner (1983), suggests that the propagation does not actually occur and the knickpoint vanishes *in situ*. The findings of Gardner (1983) are partially supported by more recent flume experiments done by Frankel et al. (2007). These authors found that replacement occurs simultaneously with the knickpoint migration on alternating bedding of weak

and hard substrates. Unfortunately, the flume experiments are crude representations of the natural settings and the replacement has not been documented for a natural settings. However, knickpoint replacement and parallel retreat seems to be consistent with some variations of the stream power (Howard, 1998).

The numerical and empirical approaches used to evaluate the knickpoint propagation are based on the stream power model. In both approaches, it is assumed that channel incision is dominated by detachment-limited conditions (Howard, 1994; Whipple and Tucker, 2002) and a knickpoint is likely to trigger and propagate when there is a sudden lowering of rivers base-level (Seidl and Dietrich, 1992; Howard, 1998; Whipple and Tucker, 1999). The use of the stream power model in the numerical and empirical approach is corroborated by current knickpoint retreat models (Table 5.1).

From Table 5.1 it can be noted that drainage area is always included in the models. This is sensible because drainage area is a surrogate of stream discharge and sediment flux (Sklar and Dietrich, 1998; Whipple and Tucker, 2002) that provides the tools to initiate incision once a critical shear stress is overcome (Howard and Kerby, 1983; Sklar and Dietrich, 1998; Attal et al., 2011). The results from empirical studies indicate that stream discharge controls the rate of the knickpoint propagation (Hayakawa and Matsukura, 2003; Bishop et al., 2005; Whittaker et al., 2008; Loget and van den Driesseche, 2009). The role of channel slope in the celerity of the knickpoint migration has not been clarified for the empirical models but it has been argued that because stream discharge is related to channel width and the local channel slope which captures incision, the stream discharge is a first-order control in the knickpoint propagation (Bishop et al., 2005).

The numerical simulations by Howard et al. (1994) using two variations of the stream power model (i.e., the stream power per unit length and the shear stress model) (Seidl and Dietrich, 1992; Howard et al., 1994; Whipple and Tucker, 1999;

Table 5.1: Models of knickpoint retreat in bedrock rivers.

Model	Approach	Reference
$E = KA^{0.3}S^{0.7}$	Modelling	Howard et al. (1994)
$V = \alpha A$	Modelling	Rosenbloom and Anderson (1994)
$C_e = -Kk_a^m x^{hm} S^{n-1}$	Theoretical	Whipple and Tucker (1999)
$D/T = \frac{AP}{WH}\sqrt{\frac{\rho}{S_c}}$	Empirical	Hayakawa and Matsukura (2003)
$D = cA^n$	Empirical	Bishop et al. (2005); Crosby and Whipple (2006)

In the first model E is the erosion rate, K is a dimensional coefficient of erosion, A is the drainage area and S is the channel slope.
In the second model, V is the velocity of retreat, α is a constant and A is the drainage area.
In the third model the knickpoint celerelity (C_e) of a wave speed given by the terms $Kk_a^m x^{hm} S^{n-1}$, where S is the channel slope and the first two terms capture the rock erodability and the stream discharge scaling on a given profile.
The fourth model D/T is the waterfall recession, A is the drainage area upstream of the waterfall, P is the mean annual precipitation, W is the width of the waterfall and H its height, ρ is the water density and S_c is a compressive strength value.
In the fifth model the distance of the knickpoint recession (D) is a function of the drainage area (A) where c and n are the constant and exponent of a power law function.

Bishop et al., 2005) give interesting results that are somewhat consistent with two models of the knickpoint evolution proposed by Gardner (1983) and Frankel et al. (2007). Modelling a base-level fall using stream profile rule with $m = 1$ and $n = 1$ (Seidl and Dietrich, 1992; Howard et al., 1994) shown here in equation 2.4 generates a knickpoint that migrates headwards as a discrete step (Figure 5.4). In contrast using the the stream power rule where $m = 0.3$ and $n = 0.7$, the knickpoint rotates and fades away while it is migrating upstream (Figure 5.4) (Bishop et al., 2005). Empirical studies of knickpoints have not fully confirmed that there is a knickpoint rotation during headwards propagation but some recent studies indicate that there is an increase in the channel slope in the area located upstream of knickpoint lip (Haviv et al., 2006; Berlin and Anderson, 2009) which suggests that there is a slight increase on incision upstream of a knickpoint (Berlin and Anderson, 2009).

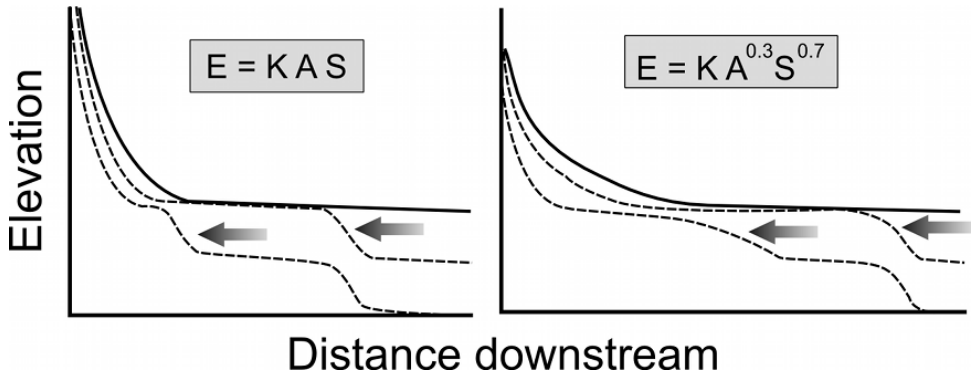

Figure 5.4: Modelling of knickpoint retreat using the stream power model (left) and the shear stress model (right). In the stream power case the knickpoint migrates as a discrete step. Using the shear stress model the knickpoint rotates and fades away as it moves upstream. Modified from Howard et al. (1994)

Empirically assessing rotation of a knickpoint as it migrates headward is challenging because field measurements on a knickpoint face is limited by accessibility and safety considerations. The longitudinal profile can be used to evaluate the knickpoint evolution by projecting a theoretical long profile (e.g., Berlin and Anderson, 2009) but this analysis is limited by the cartographic scale of the longitudinal profile

or the DEM resolution. Also, the reaches upstream of the knickpoint should lack any perturbation signals in order to reduce the uncertainty in the projection of the stream profile.

Although the propagation of knickpoints has been evaluated using different approaches, the results obtained throw light onto the mechanics of knickpoint propagation. The stream power model stills offers a solid framework to explain knickpoint propagation as long as plucking seems to control the knickpoint recession but more empirical data is still needed. Here the empirical approach is used to evaluate whether the knickpoint propagation in small basins behaves as in the case of large rivers, to which we now turn.

5.2.1 Main trunk knickpoints

The identification of base-level fall knickpoints on Jura was primarily based on the interpretation of DS plots. A second stage involved checking the locations of the knickpoints on air photographs and, when possible field verification. As it was mentioned above, the rivers of Jura are highly perturbed and several knickpoints that are not necessarily related to base-level lowering occur in the longitudinal profile. To find out which knickpoints were triggered by base-level fall, the DS analysis was constrained to the 13.6 ka shoreline by excluding any value <35 m OD.

The cosmogenic ages ($\sim$ 13.6ka) obtained by Bishop and co-workers (pers. comm.) on the raised beaches of the west coast of Jura $\sim$ 35 m OD and their consistency with the Perth Shoreline ($\sim$ 35 m OD, $\sim$ 13ka) located on the east of Scotland (Jardine, 1982) strongly indicate that the shingles of the west coast of Jura were abandoned $\sim$ 13.6 ka (Chapter 3). The abrupt decline in elevation of the beach deposits and the gap found $\sim$ 12 ka to $\sim$ 4 ka indicate that base-level lowering was very rapid after 13.6 ka as the exposure ages of shingles of Bishop and co-workers indicate. Such rapid base-levell fall is also consistent with the main pattern of the

glacio-isostatic rebound observed in Scotland (Shennan et al., 2006; Smith et al., 2007). The presence of the shingles on the west coast of Jura is a good indicator of the former deglaciation sea-level that can confidently be used to constrain the surface where the base-levell fall knickpoints were initiated. Thus, the first large spike found upstream of 35 m OD on a DS plot was interpreted as a base-level knickpoint.

Interpreting the DS plots for the 34 streams introduces some uncertainties in that some peaks on the DS plot were quite distant from the 13.6 ka shoreline. The glacial processes that modified Jura's landscape during the LGM are likely to have left glacial steps in the landscape that are still present on longitudinal profiles. Thus, the distinction between glacial and base-level fall knickpoints requires a further geomorphic marker.

To discard the non base-level fall knickpoints a second interpretation was necessary. Using air photographs, those knickpoints located upstream of the strath-terraces surfaces, and those where the channel walls were entrenched downstream of the knickpoint were interpreted as base-level fall knickpoints (Figure 5.5). The strath-terraces are a good indicator of a new pulse of incision in channels as has been observed from tectonic settings (e.g., Merrits et al., 1994; Rosenbloom and Anderson, 1994; Burbank, 2002). This has also been confirmed in settings where enhanced incision results from a sudden change in rivers base-level (e.g., Born and Ritter, 1970; Leland et al., 1998; Haviv et al., 2006).

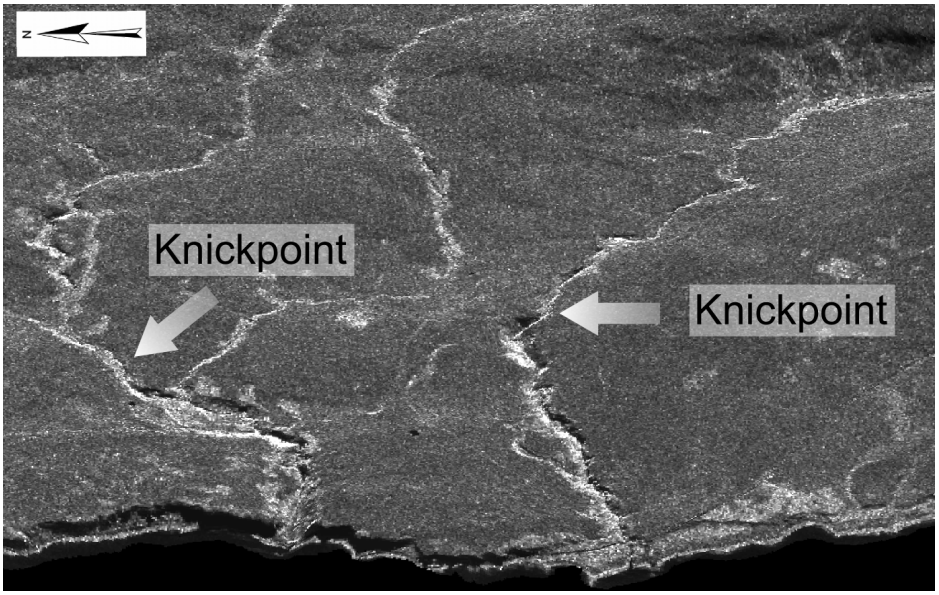

Figure 5.5: 3D snapshot (from SAR image overlaid on a 5m resolution DEM) where the approximate location of two base-level fall knickpoints of the west coast of Jura is shown. Note the narrowing and steepening of the valley walls downstream of the knickpoints and the wide open valley upstream.

The formation of the strath-terrace is related to the knickpoint propagation because the migration headwards of a knickpoint enhances channel incision (Wolman, 1987; Seidl and Dietrich, 1992). The approximate amount of the base-level lowering can be obtained by extracting the difference in elevation between the strath-terrace and riverbed (Seidl and Dietrich, 1992; Goldrick and Bishop, 1995; Schoenbohm et al., 2004; Berlin and Anderson, 2007) (Figure 5.6). In a condition close to equilibrium where the channel slopes are graded the estimation of the base-level fall can be achieved by projecting the longitudinal profile using the exponent and coefficients of the DS or SA regressions (e.g., Clark et al., 2005; Goldrick and Bishop, 2007). This approach could not be followed on Jura because the former fluvial stream profile is not sufficiently graded for values of k and λ to be assigned.

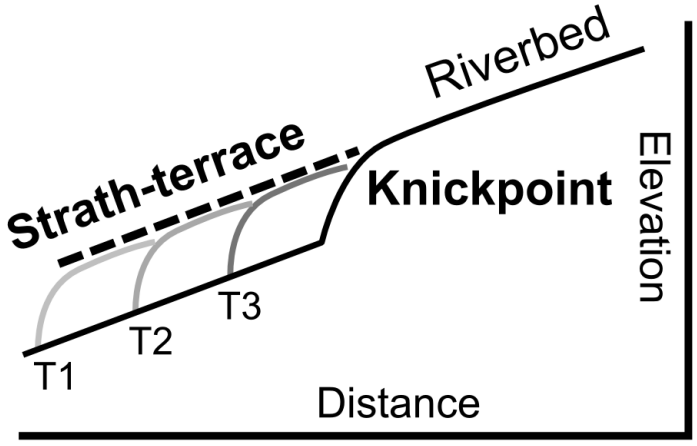

Figure 5.6: Schematic representation of the knickpoint retreat. The strath-terrace (dashed line) height may indicate the amount of base-level lowering as the knickpoint propagates upstream.

Although the rivers of Jura do not clearly exhibit any graded reaches upstream of the base-level fall knickpoints, the presence of the strath-terraces unequivocally demonstrate that a new pulse of incision by knickpoint retreat has occurred in the small bedrock rivers of Jura. In some rivers, the strath-terraces are well preserved and these can easily be detected on air photographs as well as in the field.

Constraining the DS analysis to the 35 m OD shoreline and selecting those knickpoints that are close to a sequence of strath-terraces or an entrenched valley, a total of 20 base-level fall knickpoints were obtained. Such knickpoints are interpreted as having been initiated $\sim$ 13.6 ka when the glacio-isostatic uplift started for this part of the west coast of Scotland. The knickpoints identified and their relationships to the 13.6 ka shoreline are shown in Table 5.2 and their location in Figure 5.7.

The tributary base-level fall knickpoints of Jura were obtained following the same criteria as the main trunk knickpoints. A reduced number of knickpoint on tributaries could be identified because few streams joining the main trunk in the

Table 5.2: Data of the base-level fall knickpoints and the 13.6 ka shoreline

Stream ID	**Grid reference for knickpoint**	**Elevation (m OD)**	**Drainage area at 13.6 ka shoreline (km^2)**	**Distance of retreat from 13.6 ka shoreline (m)**
1	168578, 699508	43	2.3	251
2	166673, 697928	51	2.1	145
5	157048, 690438	86	6.3	748
8	154368, 688943	77	4.4	431
12	151068, 684098	42	0.7	60
15	154798, 679278	51	7.1	748
17	147973, 677803	97	6.6	708
18	151733, 677158	108	9.9	1675
19	146378, 675233	86	6.4	949
21	153373, 671228	69	3.2	397
22	145788, 672138	55	11.1	710
23	153133, 670123	55	2.8	209
24	152058, 669263	84	4.4	768
25	144908, 668478	47	3.3	172
26	145198, 667543	51	5.7	416
27	147063, 664058	46	1.1	77
35	160983, 687438	68	7.3	1739
36	153808, 673338	77	11.9	977
37	162903, 691648	59	13.9	2834
38	145914, 670629	69	7.9	1062

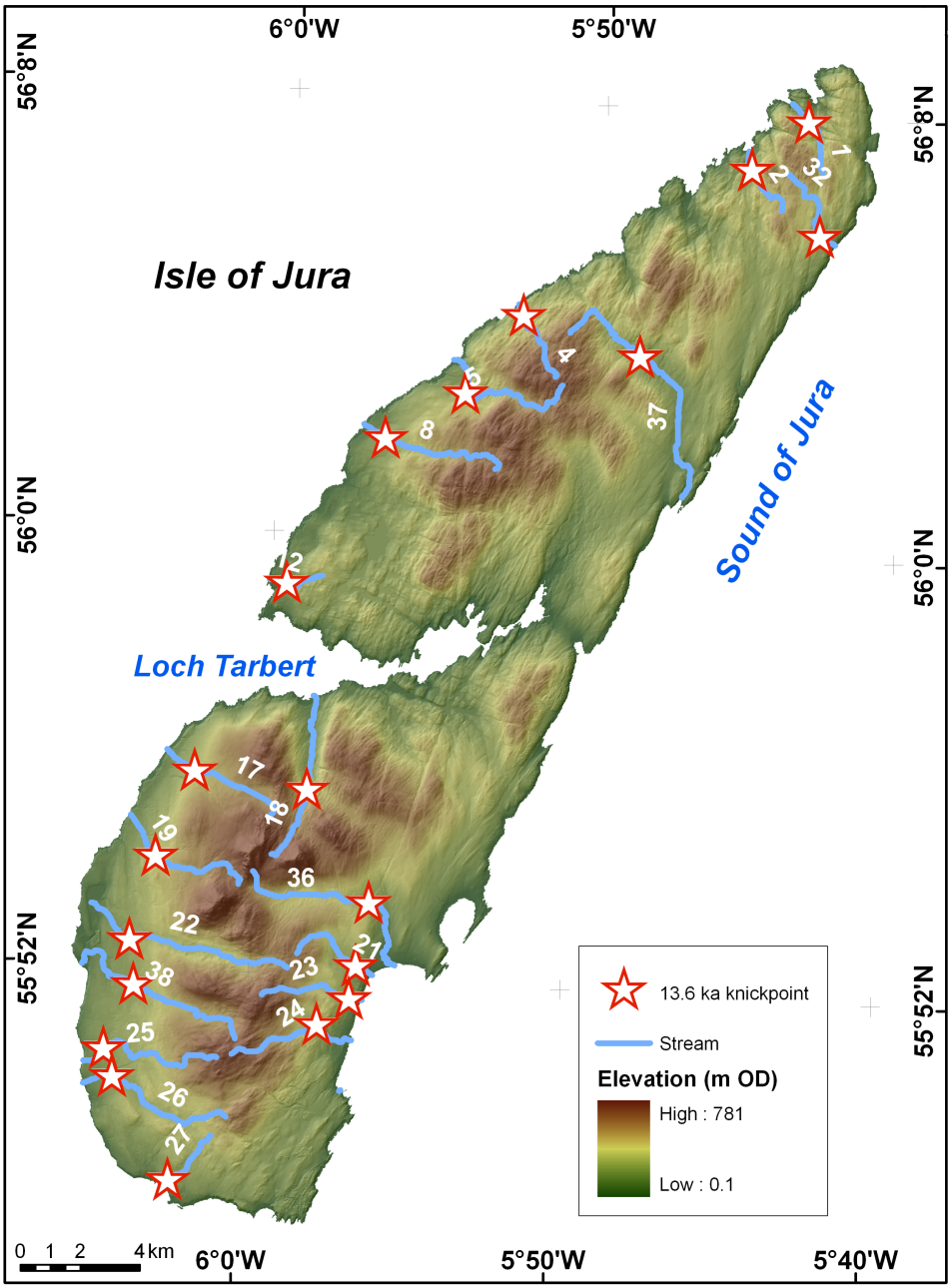

Figure 5.7: Location map of the 13.6 ka base-level fall knickpoints identified for Jura. Note that the knickpoints are found in small and large rivers of the isle. The numbers on the map refer to the knickpoint id (Table 5.2)

section comprised between the 13.6 ka shoreline (35 m OD) and the main trunk knickpoint 5.8. The data extracted from the tributary knickpoints identified are presented in Table 5.3.

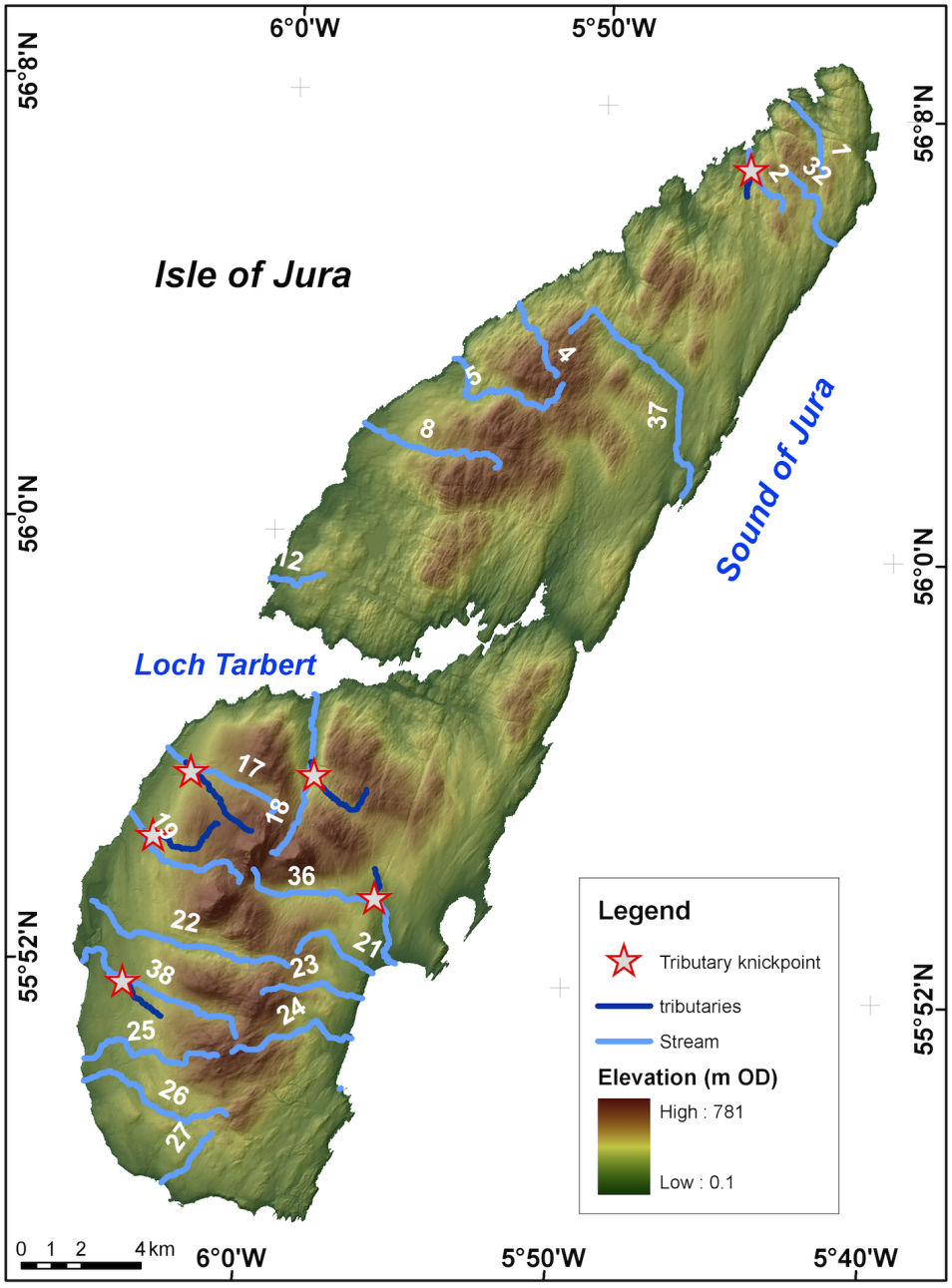

Figure 5.8: Location map of the tributary knickpoints related to the 13.6 base-leve fall event.

Table 5.3: Data of the tributary knickpoints related to the 13.6 base-level fall.

Stream ID	**Grid reference for knickpoint**	**Elevation (m OD)**	**Drainage area at 13.6 ka shoreline (km^2)**	**Distance of retreat from 13.6 ka shoreline (m)**
$2'$	166647, 697943	46	0.49	15
$18'$	151957, 677567	86	3.87	493
$17'$	147828, 677686	101	2.36	368
$19'$	146557, 675552	93	2.02	380
$38'$	145532, 670652	66	1.81	185
$36'$	154112, 673322	65	1.04	39

5.3 Knickpoint retreat on trunk and tributary streams of Jura

The retreat distance of the trunk stream knickpoints from the 13.6 ka shoreline was evaluated using the data shown in Table 5.2 and using the empirical model of Bishop et al. (2005) and Crosby and Whipple (2006) who expressed in a power law function:

$$D = cA^n \tag{5.5}$$

where D is distance of the knickpoint retreat and A is the drainage area at the point where the knickpoint was triggered and c is an constant an n the exponent of a power law function.

Because this approach uses drainage as a surrogate of stream discharge, this proportionality needs to be corroborated. There are no gauging stations on Jura and the only data available are from the basins of the west coast of Scotland, close to Jura. The scaling between drainage area and stream discharge was evaluated for small catchments ($\leq$ 100 km^2) of the west coast of Scotland (Table 5.4) assuming that the basins in Jura behave similarly the small basins of the west coast. This assumption is also consistent with by the pattern of rainfall widely distributed along the west coast of Scotland (MetOffice, 2010).

The regression plots using the values of mean, median and the 90th percentile of stream discharge are presented in Figure 5.9 and the regression summary in Table 5.5. The results confirm that the drainage area exhibits a good scaling with the different values of stream discharge. The exponents of the drainage area (Table 5.5) are in the range reported for humid temperate regions (Leopold et al., 1964). The best fit of discharge and drainage area is through the Q_{median}, which is reported to be the discharge prevailing during most of the floods (Marsh and Hannaford, 2008). The drainage area is, therefore a reliable surrogate for stream discharge.

Table 5.4: Hydrometric data for 11 streams in the west coast of Scotland, from the register of Marsh and Hannaford (2008).

Station	**River**	**Drainage area** ($\mathbf{km^2}$)	Q_{mean} ($\mathbf{m^3/s}$)	Q_{10}† ($\mathbf{m^3/s}$)	Q_{median} ($\mathbf{m^3/s}$)
80004	Green Burn	2.6	0.2	0.6	4
89008	Eas Daimh	4.5	0.44	1.1	7.7
80003	White Laggan Burn	5.7	2.33	5.7	13.5
89009	Eas a' Ghail	9.7	0.74	2	18.6
84035	Kittoch Water	16.8	0.55	1.3	19.1
89007	Abhainn a' Bhealaich	24.1	1.69	4.2	40.2
85004	Luss Water	35.3	2.65	6.8	55.2
89004	River Strae	36.2	2.93	7.7	57.6
89002	Linne nam Beathach	50.5	4.68	12.1	102.1
90003	River Nevis	62.5	6.56	16.0	124.8
85003	River Falloch	80.3	6.02	16.5	183.9

† The subscript indicates the 10 percentile flow. Further details on the periods for determine Q can be found in Marsh and Hannaford (2008)

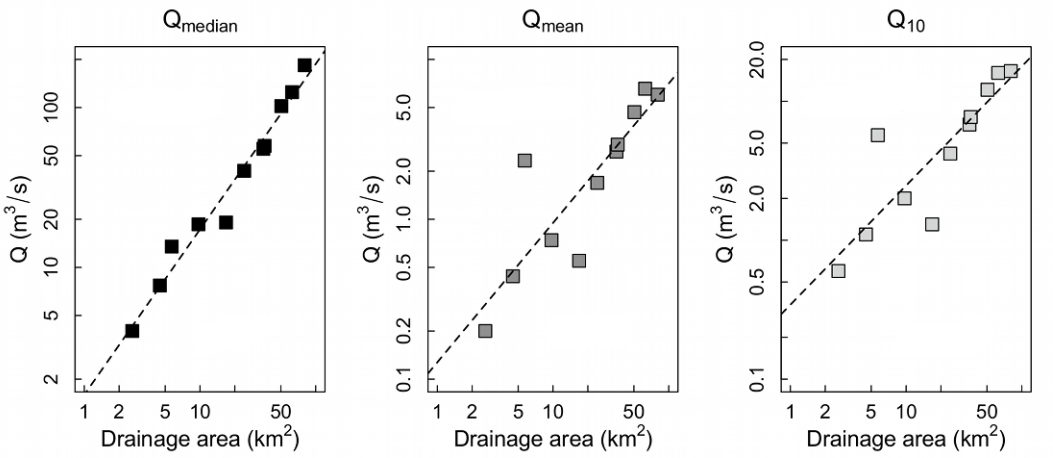

Figure 5.9: Plots of power law relationship of stream discharge against drainage area for small catchments of the west coast of Scotland. The equation and correlations coefficients are given in Table 5.5

Table 5.5: Equation and regression statistics of stream drainage area and stream discharge proportionality

Equation	$\mathbf{R^2}$	**RSE**	**P-value**
$Q_{median} = 1.6A^{1.0}$	0.97	0.2162	3.0×10^{-08}
$Q_{mean} = 0.1A^{0.8}$	0.75	0.6067	$5.4 \times 10^{-0.4}$
$Q_{10} = 0.3A^{0.8}$	0.75	0.5993	$5.6 \times 10^{-0.4}$

Plotting the distance of base-level fall knickpoints from the post-glacial shoreline against drainage area in a logarithmic scale gives a correlation (Figure 5.10). The tight relationship indicates stream discharge (and its associated sediment flux) is a first-order control the propagation of knickpoints. The empirical model of knickpoint retreat expressed in equation 5.5 and the results in Figure 5.10 indicate that the knickpoint propagation occurs in even low drainage areas where stream profiles do not exhibit any sign of graded reaches. Although equation 5.5 is still a crude explanatory model of knickpoint retreat, it seems to capture the processes involved in

the recession of knickpoints on Jura, including plucking, sediment flux and abrasion.

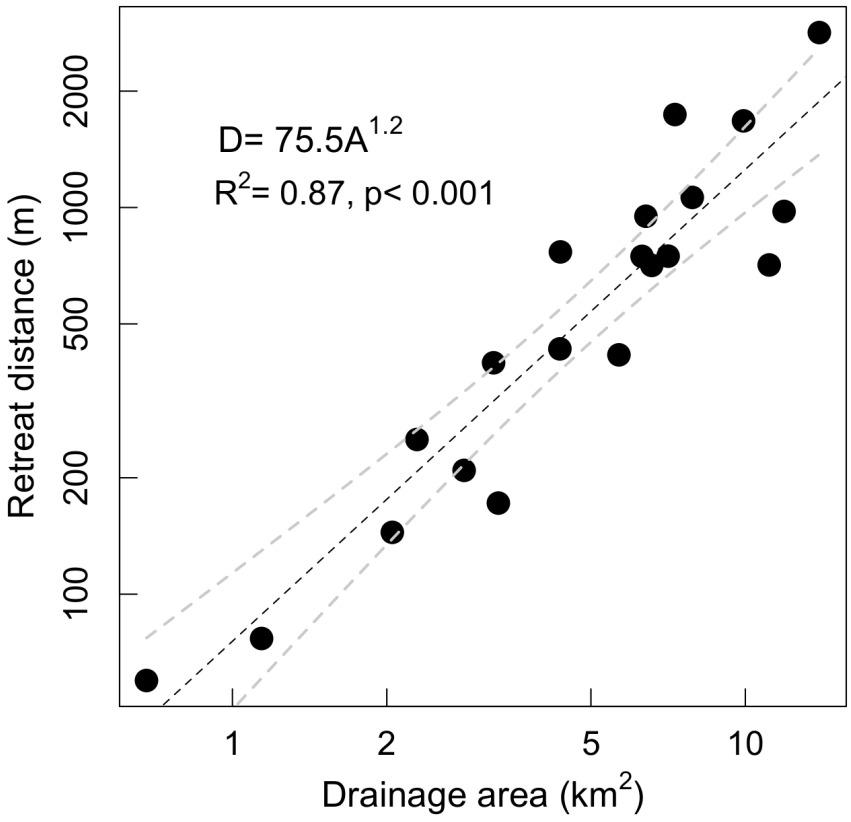

Figure 5.10: Scaling of the knickpoint retreat against drainage area for the small bedrock catchments of Jura. The axis on the plot are in logarithmic scale and the grey dashed lines correspond to the 95% confidence bounds.

In some models, the local channel slope is an important factor in the celerity of the knickpoint propagation (Table 5.1) (e.g., Howard et al., 1994; Whipple and Tucker, 1999). The role of channel slope cannot be inferred from equation 5.5 but this can be obtained using the shear stress model (Howard and Kerby, 1983; Howard

et al., 1994). An appropriate estimation of local channel slope on which a knickpoint propagates is important in this case because the exponent n captures the erosion process, the hydraulic geometry and the catchment hydrology (Whipple and Tucker, 1999) which is also related to knickpoint diffussion (Howard et al., 1994; Stock and Montgomery, 1999; Bishop et al., 2005).

The shear stress model was used here to assess the knickpoint propagation. The estimation of the local channel slope could not be obtained using the reaches located upstream of knickpoints as has been done in previous studies (e.g Bishop et al., 2005) because of the lack of graded slopes upstream, instead the slope of the knickpoint to the 13.6 ka shoreline was estimated assuming that this is the average slope on which the knickpoint has migrated upstream.

The shear stress model was evaluated by performing a regression between the logarithm of distance of knickpoint retreat against the logarithms of drainage area and the channel slope. The regression coefficients are presented in Table 5.6, the consolidated equation being:

$$D_r = 43.9A^{1.0}S^{-0.3} \tag{5.6}$$

Table 5.6: Regression coefficient and exponents of the regression of the knickpoint retreat distance againts local channel slope and drainage area.

Coefficients	**Estimate**	σ	**t value**	$Pr(>\|t\|)$
Intercept	43.9	0.9280	4.08	8.8×10^{-04}
Log(Drainage area)	1.06	0.4617	2.31	3.4×10^{-02}
Log(Channel slope)	-0.27	0.3894	-0.67	5.0×10^{-01}

The shear stress model predicts well the propagation of knickpoints ($R^2 = 0.88$, $p<0.01$) however, the exponent n deviates from the range of values observed for

other settings ($n \approx 0.7$ to 1) (Howard et al., 1994; Whipple and Tucker, 1999; Stock and Montgomery, 1999). The p-values of the regression model (Table 5.6) reveal that drainage area is the best predictor of the shear stress regression, which is also confirmed by the value of $m \approx 1$. Drainage area is then, a first-order control in knickpoint propagation according to the shear stress model. The role of channel slope is not minimised here but it is likely that the retreat of knickpoints is driven by the stream discharge during high stages as the exponent of equation 5.6 indicates. The uncertainty surrounding the estimation of the channel slope for the shear stress model and the strong influence exerted by stream discharge, makes the model of equation 5.5 the best candidate to evaluate the knickpoint retreat.

Knickpoint retreat in tributaries was evaluated using the model of equation 5.5. The results confirm that drainage area is the main factor driving knickpoint recession (Figure 5.11). The exponent of the power law function for the tributaries is higher than that observed for the main trunk knickpoints (Figure 5.10). The high exponent in the drainage area shown in Figure 5.11 implies a more rapid response of tributaries in terms of knickpoint propagation but, condition which requires a high stream discharge in tributaries in order to initiate channel incision and promote the knickpoint propagation upstream.

Comparing the retreat distances in both main trunk and tributaries from the confluence reveals a greater knickpoint migration distance upstream for the main trunk knickpoints (Table 5.7, Figure 5.12). This is explained by the large contributing areas located upstream of the main trunk knickpoints that increase the river capability to incise. Surprisingly, the regression of distance against drainage area scaled at the confluence on the main trunk knickpoint gives a weak correlation ($R^2 = 0.40$, $p < 0.5$). The weak correlation probably indicates a transient state of deceleration in the knickpoint retreat after the knickpoint has passed the tributary as long as there is a reduction of stream discharge (i.e. lost in drainage area) but more data is required to test this hypothesis.

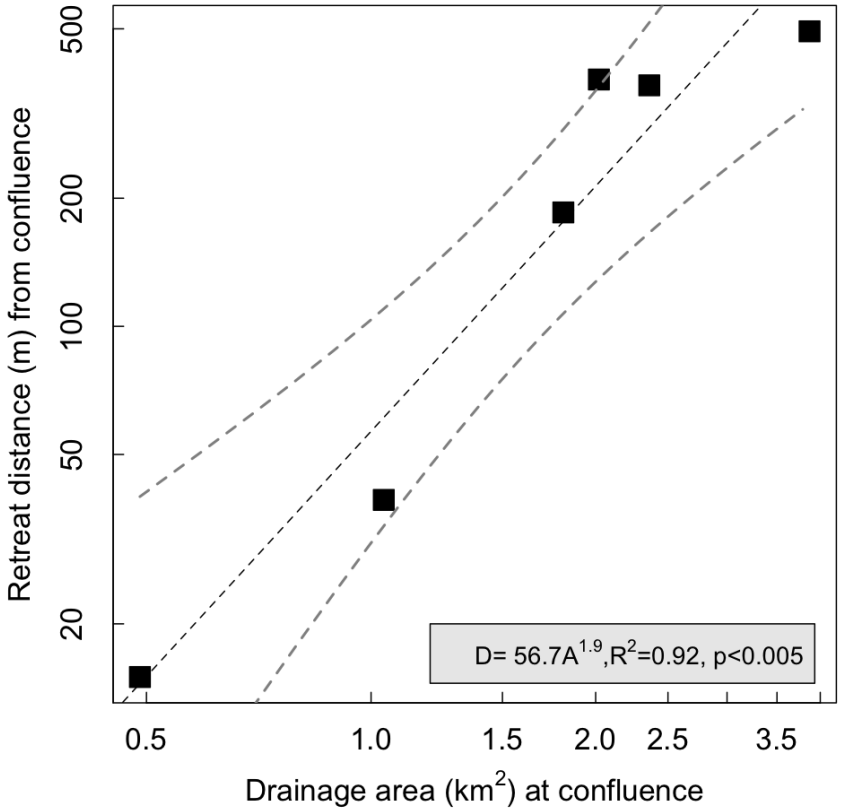

Figure 5.11: Plot of the distance of knickpoint retreat plot of the tributary streams

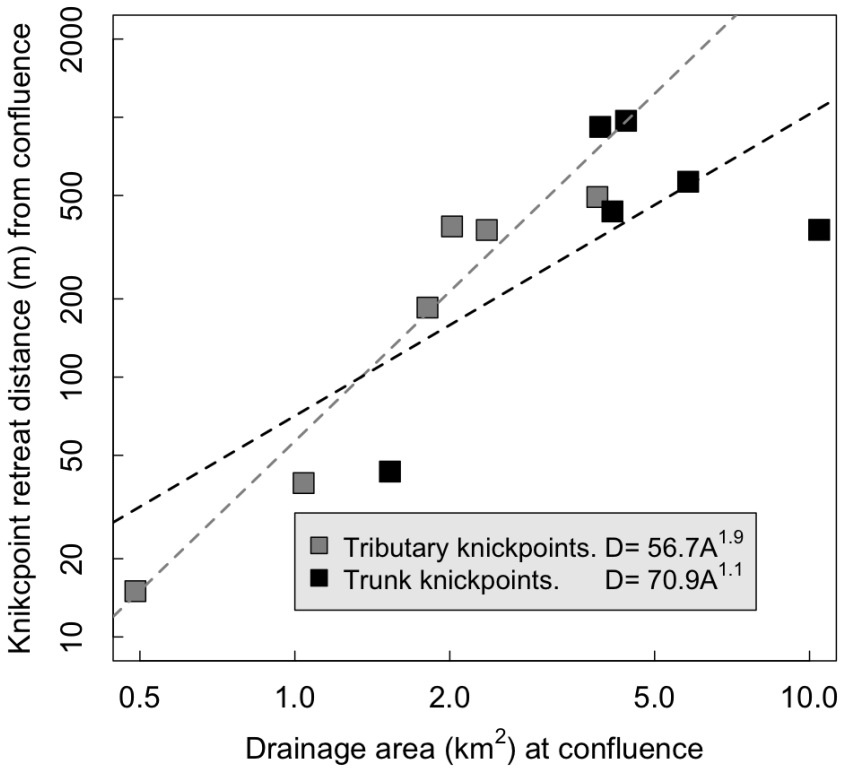

Figure 5.12: Plot of knickpoint retreat for trunk and tributaries knickpoints from their confluence. The trunk knickpoints have migrated farther than tributary knickpoints.

The ratio of drainage area and channel slope was also computed (Table 5.7) for the tributary and the main trunk knickpoints (A_p/A_t and S_t/S_p, where subscritpt p is for the main trunk and t for the tributary) to assess if stream incision can approximated by the stream power (Seidl and Dietrich, 1992). The results indicate that A_p/A_t and S_t/S_p are not correlated. The shear stress model was also tested for knickpoint propagation of the tributaries (Table 5.8) and for this case yielded

the equation:

$$D_t = 788A^{2.8}S^{1.1} \tag{5.7}$$

The exponent of area of equation 5.7 confirms the primary control by drainage area whereas the exponent of the channel slope suggests that the knickpoint may propagates as discrete step has been reported for the case when $n \approx 1$ (Howard et al., 1994). This model cannot be confirmed since the regression give a p-value of 0.06 even though it is highly correlated ($R^2 = 0.96$).

Table 5.8: Coefficients and exponents of the regression between the tributary knickpoint retreat distance against local channel slope and drainage area.

Coefficients	**Estimate**	σ	**t value**	$Pr(>\|t\|)$
Intercept	6.7	3.064	2.18	1.6×10^{-1}
Log(Drainage area)	2.8	3.627	0.78	5.1×10^{-1}
Log(Slope)	1.1	1.352	0.85	4.8×10^{-1}

5.3.1 The effect of structure on knickpoint retreat

Much of the incision in transient landscapes is controlled by knickpoint propagation (Bigi et al., 2006; Harkins et al., 2007; Reinhardt et al., 2007a) because knickpoint propagation transmits tectonic and/or climate changes by shifts in river base-level (Whipple and Tucker, 1999; Snyder et al., 2002). The control exerted by lithology and structure on knickpoint propagation is not fully understood (Miller, 1991). Flume experiments have confirmed that the propagation of knickpoints occurs in cohesive and non cohesive material (e.g., Brush and Wolman, 1960; Holland and Pickup, 1976; Gardner, 1983; Hasbargen and Paola, 2000; Bigi et al., 2006; Frankel et al., 2007). However, the rates of knickpoint propagation related to fractures, structure and lithology have not been addressed. The model of knickpoint replacement proposed by Gardner (1983) is likely to be confined to a homogeneous surface not affected by fractures or with not a particular structural arrangement. The ex-

Table 5.7: Hydrologic and distance data of the knickpoints found tributaries and main trunk streams in relation to tributary-trunk confluence

	Main trunk knickpoint			**Tributary knickpoint**				
ID	**Drainage area (km^2)**	**Slope (m/m)**	**Distance (m)**	**Drainage area (km^2)**	**Slope (m/m)**	**Distance (m)**	A_p/A_t	S_t/S_p
2	1.5	0.1826	43	0.5	0.1175	15	3.1	0.6
18	4.4	0.0694	969	3.8	0.0818	493	1.1	1.1
17	4.1	0.1089	434	2.4	0.1296	368	1.7	1.2
19	3.9	0.0797	918	2.0	0.0973	380	1.9	1.2
38	5.8	0.0401	565	1.8	0.0978	185	3.2	2.4
36	10.4	0.0477	369	1.0	0.0787	39	10.0	1.6

periments of Frankel et al. (2007) using a vertical stratification seem to explain the knickpoint rotation during its propagation upstream but this behaviour was not confirmed for the case of an homogeneous material with no stratification.

The flume experiments seem to partially capture the process involved in the knickpoint propagation because these experiments do not incorporate the role of fracture which is an important control in the bedrock channel incision and in the knickpoint formation (Miller, 1991; Whipple et al., 2000a; Phillips et al., 2010). The empirical studies have not explicitly evaluated the control of lithology in knickpoint retreat. However, the numerous empirical studies suggest that the recession rate of knickpoints triggered by a lowering of base-level is a function of drainage area (Bishop et al., 2005; Crosby and Whipple, 2006; Harkins et al., 2007; Berlin and Anderson, 2009; Loget and van den Driesseche, 2009) indicating a first-order control imposed by stream discharge. Some empirical studies report the knickpoint formation attributed to local lithological controls (i.e., stratigraphy) (Wohl and Ikeda, 1998; Phillips et al., 2010; Haviv et al., 2010) but how stratigraphy controls the rate of the knickpoint retreat has not been clarified.

The evaluation of the effects of lithology are not the primary goal of this research. Nevertheless, the data available for knickpoint retreat in Kincardineshire and Berwickshire (east coast of Scotland, Bishop et al., 2005) can be used to explore if lithology exerts any control on knickpoint propagation. The streams of the east coast of Scotland incise on sandstones (Bishop et al., 2005). In laboratory tests, Sklar and Dietrich (2001) reported that the erosion rates tested on different lithologies vary as a power function of the tensile strength. The tensile strength reported by these authors for quartzite is ~ 20 MPa and and ~ 3 MPa for the hardest sandstone (Sklar and Dietrich, 2001, their Figure 2); the corresponding estimated erosion rates (g/h) are 1.9×10^{-3} and 8.5×10^{-2} respectively. The difference in tensile strength and the erosion rate for quartzite and sandstone suggests, *a priori*, that differences in the knickpoint propagation rates might be found among the streams of Jura,

Berwickshire and Kincardineshire. Because the knickpoints were triggered more or less simultaneously in the east coast and west coast of Scotland as a consequence of the glacio-isostatic rebound (Bishop et al., 2005), both sets of knickpoints can be used to test the hypothesis of a lithological control on knickpoint recession.

The retreat distance of the knickpoints of Jura and the east coast and their corresponding catchment areas are plotted in Figure 5.13. The knickpoints of the east and west coasts lie on the same trend and the exponent of drainage area for both power laws indicates an equal rate of knickpoint migration for a given stream discharge (Figure 5.13). An ANCOVA on the east and west knickpoints data indicates that the two regression lines are not significantly different (Table 5.9). Thus, Figure 5.13 suggests that lithology may not be a first-order control of knickpoint propagation but an effect related to differences in climate are not discarded since the west coast has more rainfall ($\sim$ 3000 mm) than the east coast ($\sim$ 700 mm) (MetOffice, 2010). A sharp change in the total rainfall may result in a change in discharge which in turn affects the rate of the knickpoint propagation. Interestingly, the base-level fall knickpoints have propagated for both east and west coast, simultaneously as the strong correlation of Figure 5.13 indicates.

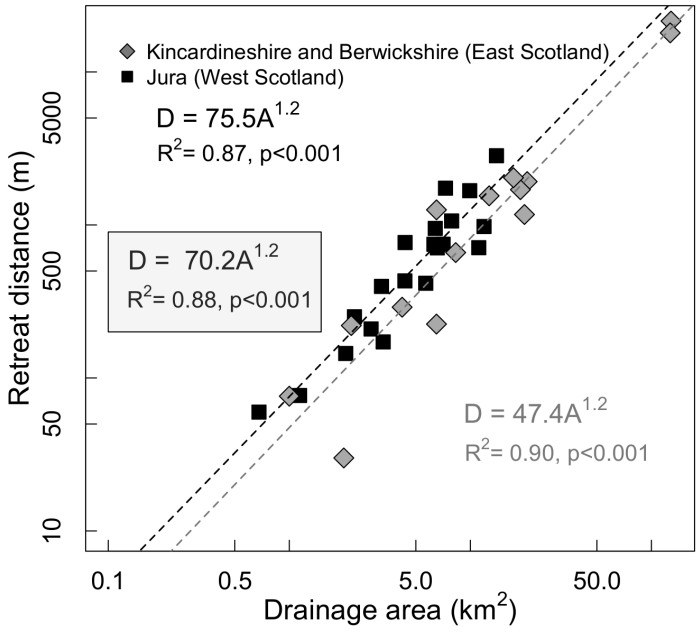

Figure 5.13: Knickpoint retreat plot for Kircardineshire, Berwickhshire and Jura. The exponent of the drainage area power law function suggests that lithology may not be a first-order control on knickpoint retreat but an effect related to changes in rainfall and discharge between the east and west coast is not discarded. The power law and coefficients for all the knickpoints is shown in the box. The data for the east of Scotland were obtained from Bishop et al. (2005)

Table 5.9: ANCOVA results for the retreat distance model of the Jura (quartzite) and east Scotland (sandstone).

Coefficient	**Estimate**	σ	**t value**	$Pr(>\|t\|)$
Intercept	4.3	0.2402	18.0	2.0×10^{-16}
Log(Drainage area)	1.2	0.1397	8.74	9.5×10^{-10}
Lithology (Sandstone)	-0.5	0.3501	-1.3	1.9×10^{-1}

The apparent lack of control imposed by lithology on knickpoint propagation in Scotland is intriguing because it would be expected that a variation in lithology may promote or dampen the rivers response to incision. The similar rates of knickpoint propagation suggest a response to base-level lowering that is strongly controlled by stream discharge and/or sediment flux.

The role of structure in the knickpoint propagation has received less attention than the knickpoint migration on cohesive and non-cohesive materials but there are notable exceptions (e.g., Gilbert, 1907; Miller, 1991; Frankel et al., 2007). Miller (1991) observed that lithology and jointing are factors that control the height of the knickpoint face and proposed a conceptual model for channel incision controlled by the dip of strata (Miller, 1991, his figure 7). However, the knickpoints studied by Miller (1991) are restricted to a lithology of carbonates and sandstones. Thus, comparison to other types of lithology and structure is needed.

Whether the dip of strata promotes or dampens knickpoint propagation is not fully understood. The results shown in Figure 5.14 suggest that neither lithology nor structure may be a first-order control on knickpoint recession. To evaluate if there is any control related to structure, an ANCOVA was performed on rivers flowing on the dip and scarp slopes on Jura. The rivers flowing along the strike were omitted from the analysis because there are only three of these cases. The results of the dip-slope and scarp-slope propagating knickpoints are shown in Figure 5.14 and the ANCOVA results in Table 5.10.

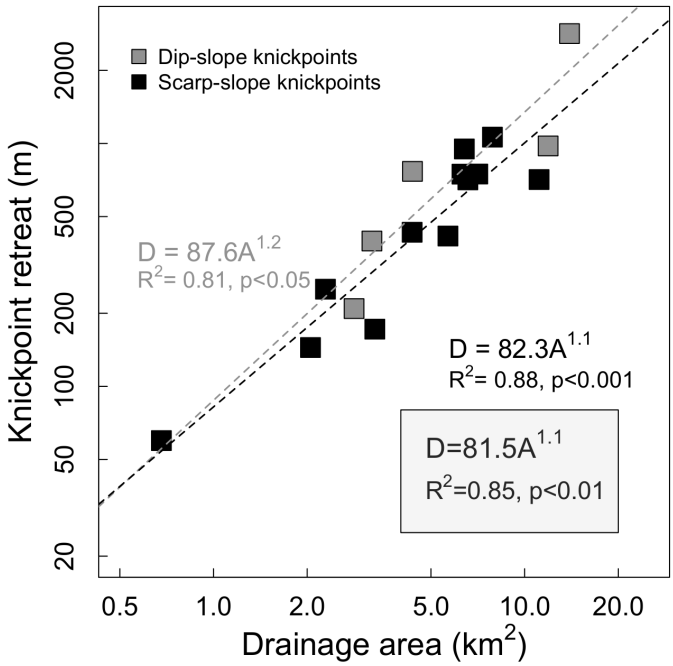

Figure 5.14: Plot of the knickpoint retreat differentiated by structure (dip-slope and stream-slope rivers). The exponents of the power law functions indicate similar knickpoint propagation rates implying that structure is not a first-order control of knickpoint retreat. In grey is shown the equation for dip-slope rivers and in black the equation fro scarp-slope rivers. The equation for the east and west coast data is shown in the shaded box.

Table 5.10: ANCOVA results for the knickpoint retreat differentiated by structure (i.e., dip-slope and scarp-slope streams).

Coefficient	**Estimate**	σ	**t value**	$Pr(>\|t\|)$
Intercept	4.5	0.4663	9.6	2.9×10^{-7}
Log(Drainage area)	1.2	0.2478	4.8	3.5×10^{-4}
Structure(Scarp)	-0.0	0.5233	-0.1	9.0×10^{-1}

The ANCOVA results (Table 5.10) indicate that there is no significant difference in knickpoint propagation rates between the dip-slope and scarp-slope stream. Thus, the Jura data confirm that structure is not first-order control on knickpoint propagation or at least, in the headward migration due to a drop of the base-level. The results in Figures 5.13 and 5.14 points towards a propagation of disequilibrium regardless of the lithology and the structural settings. This behaviour is likely to be controlled by a river capacity to transport sediments during high discharge events that are associated with incision into bedrock and knickpoint migration. In other words, equation 5.5 in this setting captures the essence of the knickpoint propagation revealed by empirical studies (e.g., Bishop et al., 2005; Crosby and Whipple, 2006; Berlin and Anderson, 2007; Loget and van den Driesseche, 2009). It should be recognised, though, that there are less obvious processes in this model which need to be treated in more detail. The rate of plucking and its relationship to fractures and rock jointing require observation in different settings to determine whether this can be integrated into equation 5.5 as has been discussed by Whipple et al. (2000a). Plucking and rock fracture seem to play an important role in the knickpoint propagation headwards. However, this processes depends on how much sediment is transported by rivers. Sediment flux is crucial for the channel incision but incorporating such flux into a model brings complications because how much of the sediment flux contributes to plucking and how much do abrasion is not known.

Another important issue for knickpoint retreat that needs to be tackled is the effect caused by drainage area as the knickpoint propagates headwards. The loss of drainage area as the knickpoint migrates headwards and in particular once a knickpoints passes a tributary, need the be assessed as has been recently stressed out and proposed (e.g. Whittaker et al., 2008; Attal et al., 2011). Finding a critical area where knickpoints can no longer migrate headwards is also needed. The results obtained in this research indicate that any such critical area must be less than 0.7 km^2, the smallest catchment area studied here (Figures 5.10 and 5.11; Tables 5.2 and 5.7). Likewise, the effect of the tributaries was limited by the small trunk

streams below knickpoints in this study. Further observations in other settings are required to test these issues, but the findings in Jura point to lower critical areas than others have suggested (e.g., Crosby and Whipple, 2006). In this sense, the empirical studies in medium to large catchments (> 100 km^2) where the base-level record is well constrained are optimal sites to test the propagation of knickpoints, especially for understanding the role of tributaries.

5.3.2 The vertical distribution of knickpoints

Niemann et al. (2001) evaluated analytically the vertical propagation of knickpoints by using the stream power model formulation and evaluating the case of graded rivers that join the main trunk according to Plairfair's law. These authors conclude that if rivers are in equilibrium, knickpoints in tributaries should lie at approximately the same contour line of elevation (Niemann et al., 2001; Wobus et al., 2006a). The vertical celerity of knickpoints in rivers in equilibrium due to a differential rock uplift is and considered that incision rates follows the steam power rule, the vertical migration rate of knickpoints is expressed as follows (Niemann et al., 2001; Wobus et al., 2006a):

$$C_{ev} = \frac{U_1 - U_2}{U_1^{1/n} - U_2^{1/n}} U_2^{1/n} \tag{5.8}$$

where U_1 and U_2 correspond to the initial and final uplift rate respectively and exponent n is derived from the steam power rule. Equation 5.8 provides a solid theoretical framework to asses the vertical distribution of knickpoints however, this model has not been tested enough with empirical data and it requires certain conditions of landscape which might be difficult to meet.

The model of equation 5.8 requires: (1) an homogeneous lithology, (2) a system where tributaries in equilibrium joining the main trunk incise at the same rate more or less at the same point and (3) equal drainage areas for the tributaries. These conditions are difficult to observe in natural settings due to changes in lithology,

climate and the geomorphic history of sites. Berlin and Anderson (2007) evaluating the knickpoint retreat in rivers of the Roan Plateau in Colorado (USA), found that the vertical distribution predicted by equation 5.8, does not apply for the rivers they studied because the lithology and stratigraphy seem to control the vertical propagation of knickpoints. Tributaries joining the main trunk are expected to have different incision rates even though these might join the main trunk at the same elevation (Seidl and Dietrich, 1992).

Here the vertical distribution of main trunk and tributaries knickpoints was assessed using two models. In the first one, the knickpoint elevation-drainage area regression was tested, and in the second one, a regression of elevation and a simplified stream power (drainage area multiplied by channel slope) was tested (Figure 5.15). The elevation and channel slope of main trunk knickpoints was estimated from the 13.6 ka shoreline to the knickpoint lip. The elevation and channel slope for tributaries was measured from the knickpoint lip to their confluence with trunks. The channel slope of the main trunk and tributary knickpoints (named local channel slope) is assumed to capture the average slope where the knickpoint has propagated. The results indicate that a poor correlation is observed between the knickpoint elevation and drainage area for trunk knickpoints (Figure 5.15). Such a poor fit indicates that other unknown factors besides stream discharge are exerting a control on the vertical distribution of knickpoints.

The regression of knickpoint elevation on stream power gives a better correlation in tributary and trunk knickpoints (Figure 5.15). The second model (i.e., stream power regression) points to a geometric effect caused that is related wit the vertical distribution of knickpoints. In order to evaluate any potential effect imposed by structure an ANCOVA on the dip-slope and scarp-slope streams was performed. The results obtained indicate the rate in the vertical distribution of the knickpoints is more or less the same for the dip-slope and scarp-slope rivers (Table 5.11) thus, stream discharge and the local channel slope are equally effective irrespective of the

structure.

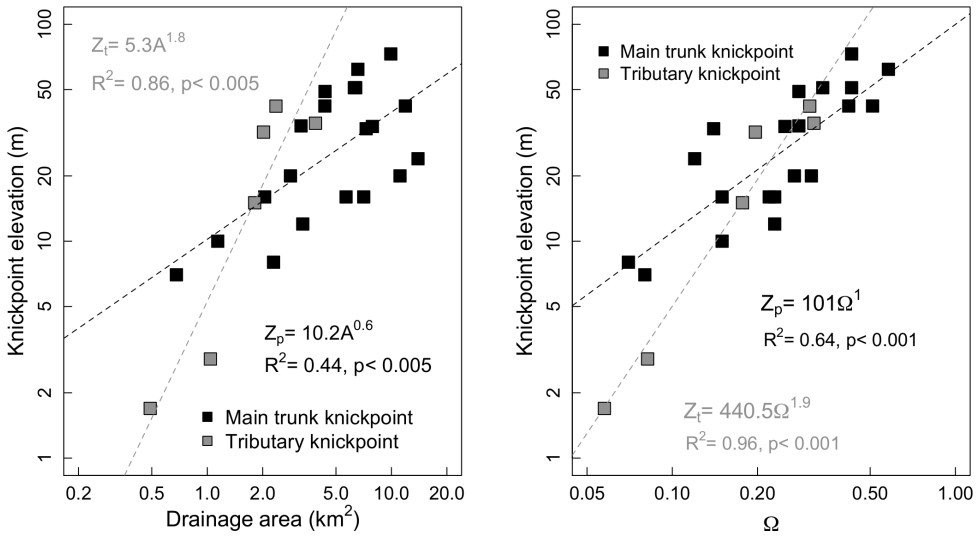

Figure 5.15: Models of knickpoint elevation for the main trunk and tributaries. The plot on the left shows that stream discharge does not fully controls the vertical distribution of trunk knickpoints. The plot on the right indicates that vertical distribution of knickpoints is controlled by stream power (Ω) which has been simplified in this plot by the product of the drainage area and the channel slope. The equation and statistics summary for trunk knickpoints are shown in the black text and in grey for tributary knickpoint.

Table 5.11: Ancova table for the regression of the vertical distribution of knickpoints (i.e., dip-slope and scarp-slope) against the stream power.

Coefficient	**Estimate**	σ	**t value**	$Pr(>\|t\|)$
Intercept	4.0	0.5730	6.9	9.5×10^{-6}
Log(Stream power)	0.4	0.4190	0.9	3.4×10^{-1}
Structure(Scarp)	0.5	0.6321	0.8	4.0×10^{-1}
Log(Stream power):Structure(Scarp)	0.6	0.4516	1.3	2.0×10^{-1}

The plot shown in Figure 5.15 confirms that there is a geometric effect in the vertical distribution of knickpoints caused by change in both local channel slope and the drainage area. It is thus hypothesised that streams with low drainage area are likely to have steeper channel slopes than larger drainage areas because of the stream power is not enough to flatten the channel slopes and knickpoints are concentrated at low elevation. In contrast, streams with large drainage areas have enough stream power to promote the knickpoint recession at higher elevation than the small ones.

Because the geometric effect on the reach in which a knickpoint propagates may result in a different vertical propagation of knickpoints, it is necessary to examine the relation between the slope on which a knickpoint propagates and the drainage area. Plotting the local channel slope estimated from the knickpoint to the 13.6 ka shoreline against the drainage area at the 13.6 ka shoreline in Figure 5.16 strongly suggests that the drainage area and the local channel slope are related. Interestingly, Figure 5.16 reveals a threshold located at $\sim$ 2 km^2 where the trend in the local channel slope against drainage area changes. Streams with $<$ 2km^2 of drainage area have more or less the same channel slope ($\sim$ 0.1 m/m) and this condition is extended to tributaries. Streams with drainage areas $>$ 2 km^2 seem to respond to drainage area as the stream power model predicts (Sklar and Dietrich, 1998; Whipple and Tucker, 1999).

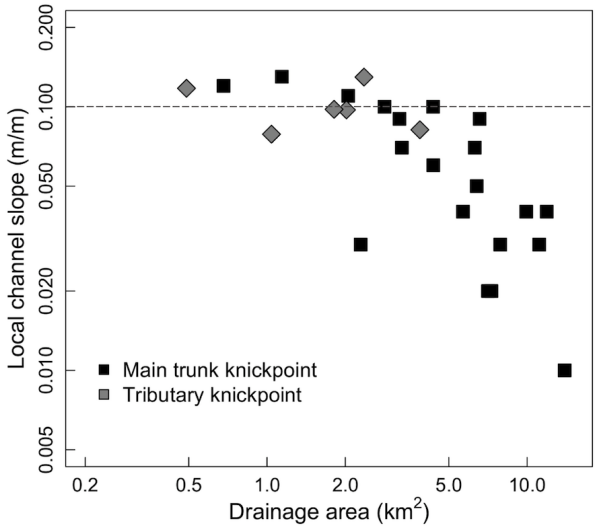

Figure 5.16: Plot of the local channel slope estimated from the base-level fall knickpoint to the 13.6 ka shoreline against the drainage area. At ~ 2 km^2 the local channel slopes becomes gentler as the drainage area increases. Axis are plotted in a logarithmic scale. The grey dashed line indicates the approximate limit of the debris flow zone in channels suggested by Sklar and Dietrich (1998).

Because the local channel slope shown in Figure 5.16 equals the elevation-distance ratio of knickpoint retreat from the 13.6 ka shoreline, the threshold found at ~ 2 km^2 has further implications for knickpoint propagation. It will be recalled that in the knickpoint retreat model for trunks (Figure 5.11) the drainage area exponent is ≈ 1 whereas, the exponent in tributaries is ≈ 2 (Figure 5.11). Figure 5.16 indicates that those knickpoints retreating on steep slopes do not scale with low drainage areas (< 2 km^2). Such a break in the scaling indicates that higher steam discharge is required to promote the knickpoint recession (Figure 5.11) and suggest that gravitational processes may be involved in the knickpoint recession as has been hypothesised for steep knickpoints (Haviv et al., 2010) with low drainage area (Crosby and Whipple, 2006).

5.4 Stream profile of reaches in transience

The stream power model (e.g., Whipple and Tucker, 1999; Snyder et al., 2002) or the shear stress model (e.g., Howard et al., 1994) both predict that as a base-level fall knickpoint propagates headwards, channel slopes in the reaches downstream of the knickpoint are re-established at their former values only if there is not a change in the rate of rock uplift. Such a condition implies that incision rates after knickpoint passage are re-established at their pre-knckpoint values and the final result is a shift downward of river bed elevation (Howard et al., 1994; Kooi and Beaumont, 1996; Whipple and Tucker, 1999). The morphology downstream of knickpoints has not been examined in detail but SA plots from active tectonic different settings indicate that channel slopes are scaled downstream of knickpoints which is commonly assessed by normalising the channel steepness (e.g., Snyder et al., 2000; Wobus et al., 2006b; Cyr et al., 2010). An increase in the channel steepness (ks_n) downstream of a knickpoint is interpreted as an effect of tectonic forcing or an adjustment of the river profile to channel incision (Snyder et al., 2000).

The Jura data on knickpoint propagation and vertical distribution strongly suggest that rivers respond to rock uplift according to catchment size. Such behaviour is well explained by a power law rule but further analysis is required to clearly elucidate the role of sediment. The next section analyses the morphology of transient rivers that have been affected by a knickpoint propagation (i.e., the reaches downstream of the knickpoint related to the 13.6 ka shoreline) in order to assess if channel response to base-level fall is expected from theory.

5.4.1 The concavity index

An assessment of the morphological response of rivers to base-level fall is necessary in order to elucidate if rivers can indeed accommodate the effects of tectonism (that is, in the particular case of Jura, glacio-isostatic uplift). The simplest approach

to extracting information on channel morphology is by referencing the long profile morphology to a straight line (Phillips and Lutz, 2008). Goldrick and Bishop (2007) used an geometric index to extract the channel morphology in a set of small reaches using the following formula:

$$R_g = \frac{((X_b - X_a)(Y_b + Y_a) + ... - (X_d - X_a)(Y_d + Y_a))}{2(X_d - X_a)(Y_a - Y_d)} \tag{5.9}$$

where X is the length of the reach and Y the elevation and subscripts differentiate the reach (Figure 5.17). Note that equation 5.9 gives a normalised index of the channel geometry that can equally be obtained by using the trapezoid rule. The geometry of a reach (R_g) can be calculated by integrating a normalised elevation with a normalised distance and compared with a straight line profile in the form:

$$\theta_i = 1 - [\int_0^1 f(y)\,dy \;\approx\; (1-0)\frac{f(0) + f(1)}{2}] \tag{5.10}$$

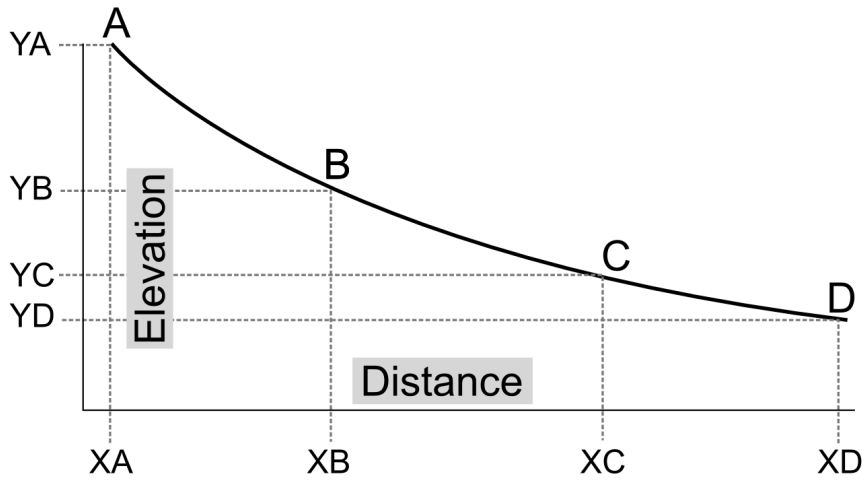

Figure 5.17: Scheme showing the reaches used for the geometric calculation of equation 5.9 to estimate the channel geometric index. Modified from Goldrick and Bishop, 2007

Using the formula 5.10 the concavity index (θ_i) is determined by subtracting the

integral to the first term of equation 5.10 which correspond to a straight long profile. A negative value denotes concavity and a positive value convexity (Figure 5.18).

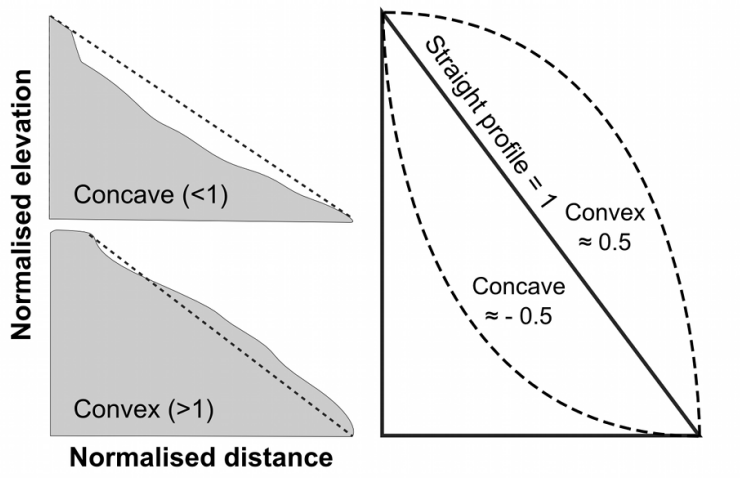

Figure 5.18: Schematic cartoon of the concavity index. The geometry of the concave and convex reaches is compared to a straight line profile. Because areas are subtracted from the straight profile the maximum concavity and convexity is -1 to 1 respectively but a value of ~ -0.5 would represent a full concave-up profile.

The morphology of the transient reaches on Jura were assessed by obtaining the concavity index from equation 5.10 for the reaches from the knickpoint tip to the 13.6 ka shoreline. The geometric response of the transient reach was analysed by comparing it to drainage area (Figure 5.19). In general most of the transient reaches tend to have a concave profile, however a clustering of reaches with low drainage area (< 5 km^2) can have a start to form a convex profile. One advantage of using the concavity index is that is based on a morphological basis in which no assumptions on the scaling of channel slope and stream discharge are needed as occurs for the stream power model.

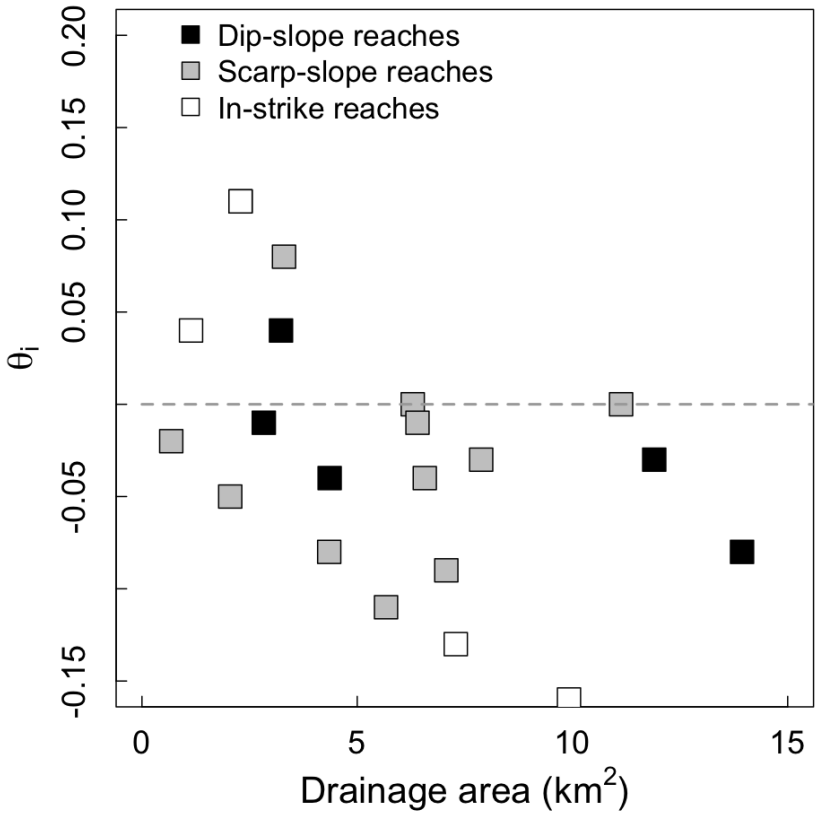

Figure 5.19: Concavity index for the transient reaches of Jura. Note the clustering of convex reaches for those reaches with a drainage area $< 5\text{km}^2$. The dashed grey line indicates the zone of a straight line profile.

Figure 5.19 reveals that streams with low drainage areas have a slow morphological response to the base-level fall. Even though the concavity index is not strongly correlated to the hypsometric integral, the clustering for the low drainage area streams implies that these streams are capable of transmitting the base-level fall through a knickpoint propagation of the knickpoint tip but unable to absorb the full effect of the base-level fall by complete adjustment of the long profile.

It may be recalled here that the base-level lowering in Jura has not been steady. The first event that occurred $\sim$ 13.6 ka is likely to have triggered the base-level fall knickpoint of Jura, but the subsequent drop of sea level at $\sim$ 7 ka years (Shennan et al., 2006) is likely to have been transmitted into the fluvial system by the propagation of younger knickpoints. Large drainage area streams (Figure 5.19) are likely to absorb the base-level fall by adjusting the channel slope. Such a response is expected because due to the rivers ability to mobilise sediments and incise into bedrock in contrast, small streams are unable to modify the channel slope due to their low stream power and a convex profile is likely to prevail in the small rivers.

The non-grading of channels slopes downstream of the base-level fall knickpoints demonstrated by extracting the hypsometric integral and the concavity index, strongly indicates that small bedrock rivers do not completely adjust their former profile once a knickpoint has migrated headwards. It is likely that several steps downstream of the 13.6 ka knickpoints may have also propagated more recently (11 ka) generating a delay in the response time of rivers to absorb the base-level fall. The decline over time of the glacio-isostatic rebound due to the visco-elastic recovery in the mantle does also imply, however, a decline in the intensity of the base-level lowering, which is likely to be transmitted as minor steps or knickpoints on the stream profile. Such a condition seems to explain why the small rivers are unable to absorb the base-level fall since they do not have enough stream power to absorb the full amount of the base-level fall to induce changes on its morphology. It is interesting though, that the horizontal propagation of knickpoints has been effectively transmitted in a wide range of rivers with variable drainage areas (Figure 5.6).

5.5 Summary

The results obtained here indicate that drainage area is a first-order control on knickpoint recession in small bedrock rivers. The role of plucking and abrasion in the knickpoint propagation has not fully tested but the results obtained empirically and through modelling suggest that plucking might promote the knickpoint migration headwards by the detach or blocks (Howard et al., 1994; Whipple and Tucker, 1999), but the knickpoint propagation though, a the presence of joint in which the sediment fills in forming a wedge that later can generate the detach of rocks (Whipple et al., 2000a, Figure 4). The role of jointing has further implications for channel degradation. A relation between the jointing spacing and the formation of strath-terraces has recently been stressed (e.g., Wohl, 2008). In this sense the detachment-limited model (Howard, 1994; Whipple and Tucker, 1999) seems to capture the main processes involved in the knickpoint propagation as the modelling results also indicate (Howard et al., 1994). Channel incision by abrasion is also an important process in bedrock channel degradation (Foley, 1980; Sklar and Dietrich, 1998) but this processes is likely to be limited to certain surfaces where bedrock can be polished or carved forming potholes and grooves (Whipple et al., 2000a; Wohl and Merritt, 2001). The knickpoint propagation in massive unjointed surfaces is not fully documented but such case, bedrock incision is more likely to be related to abrasion and possibly cavitation thus, (Whipple et al., 2000a) the knickpoint replacement model Gardner (1983) may take place.

The analysis performed on the main trunk rivers and its tributaries confirms that the 13.6 ka base-level fall event has been transmitted to the landscape by knickpoint propagation. The knickpoint retreat model shown in Figure 5.10 also demonstrates that even for the case of small bedrock rivers, the disequilibrium is transmitted regardless of the lithology and structure (Figures 5.13 and 5.14) and even in highly perturbed channels. The results presented in this chapter are summarised below:

- Drainage area (surrogate of stream discharge) and presumably the sediment

flux, drive the knickpoint propagation in small bedrock rivers catchments. The comparative analysis of knickpoint retreat in dip-slope and scarp-slope streams indicates that structure is not a first-order control on knickpoint recession. Likewise, lithology does not seem to influence the knickpoint recession, as the comparative analysis on the east coast of Scotland (Bishop et al., 2005) and the present study indicates.

- Knickpoint propagation has been transmitted to tributary streams as it is expected from the theory (Bishop et al., 2005; Wobus et al., 2006a; Goode and Burbank, 2009). In these low drainage area streams, the scaling in the exponent with drainage area increases, suggesting that other processes (e.g., gravitational toppling) might operate in knickpoint recession. This trend seem also to explain the steep reaches clustering at ~ 5 km^2 of drainage area (see Figure 5.16).

- The vertical distribution of knickpoints in non steady-state landscapes and where streams have different gradients is controlled by the geometry of the channel on which the knickpoint propagates. The geometric effect is also consistent with the horizontal knickpoint propagation shown in Figure 5.10, because low drainage area streams are steeper and the horizontal and vertical propagation is less than in the large rivers.

- The concavity index was useful to evaluate the morphological response of rivers to the base-level fall. Here it was observed that low drainage area streams (< 5km^2) have a slow response to the base-level fall (Figure 5.19) due to a reduced stream power. The slow response rivers keep a convex profile downstream of the knickpoint.

- The several analyses performed on the base-level fall knickpoints of Jura confirm that knickpoint propagation does operate in small bedrock rivers on a hard lithology. The model of the knickpoint retreat and as a function of drainage area also suggests that incision is mostly dominated by detachment-limited

conditions where is fractures may play an important role as has been stressed for other settings by some authors (e.g., Whipple et al., 2000a; Molnar et al., 2007; Wohl, 2008). The case of a knickpoint replacement suggested by Gardner (1983) is unlikely to occur in Jura because the quartzite is fractured but the possibility of a knickpoint rotation during headwards migration remain possible (Howard et al., 1994; Frankel et al., 2007).

- The lack of scaling between slope and drainage area downstream of knickpoints and the results interpreted from the concavity index on the transient reaches, suggest that rivers do not necessarily adjust the channel slopes once a knickpoint has migrated upstream. In some cases, particularly for the low drainage area streams, the slow response of rivers to the base-level fall is likely to maintain a higher erosion rates for larger times than the large stream rivers. Such a condition may result in an asynchronous response in landscape to the base-level fall which is dependent on river stream power. The next chapter quantifies the rates of channel lowering using cosmogenic nuclides.

Chapter 6

Bedrock river incision in transient landscapes

6.1 Introduction

Estimating the channel incision rate into bedrock is fundamental to understand how mountainous landscapes evolve in response to changes in tectonics and climate. The processes involved in channel bedrock incision (i.e., plucking, abrasion and cavitation) are well known and the governing equations have in some cases been settled. Nevertheless, a general incision law that combines all the processes involved in bedrock degradation has not yet been achieved (Whipple et al., 2000a).

The stream power model has proved to be a useful tool to assess channel incision into bedrock (e.g., Howard et al., 1994; Lavé and Avouac, 2001; Tucker and Whipple, 2002; Stolar et al., 2007; Attal et al., 2011). An advantage of the stream power based approach is that few measurements are required to assess channel incision (Whipple and Tucker, 1999). Nevertheless, some processes are not explicitly known, including the role of sediment flux in bedrock incision. This last is somewhat implicit in the stream power model but whether sediment plays an important role in channel incision remains a matter of future investigation (Sklar and Dietrich, 1998).

The importance of sediment flux in channel incision in mountainous settings has been stressed in several studies (e.g., Sklar and Dietrich, 1998; Hovius et al., 2000;

Hartshorn et al., 2002; Cowie et al., 2008; Stark et al., 2009). Some bedrock abrasion models different from the stream power rule, have been proposed to estimate the effect of sediment on channel incision by accounting for abrasion and the impact of particles on a bedrock surface (e.g., Foley, 1980; Sklar and Dietrich, 2004; Turowski et al., 2007). These can be integrated into the stream power approach to provide a more explicit model of the evolution of a stream profiles (Whipple and Tucker, 2002; Sklar and Dietrich, 2006). The importance of sediment in bedrock channel incision and its implication in evolution of the landscape have been considered in more recent studies (e.g., Crosby et al., 2007; Finnegan et al., 2007; Johnson et al., 2009) and in attempts to integrate all bedrock channel incision processes into a single model (e.g., Chatanantavet and Parker, 2009).

The relatively recent facility to quantify *in situ* produced Terrestrial Cosmogenic Nuclides (TCNs), via measurements in an Accelerator Mass Spectrometer (AMS), and the wide potential of TCNs to quantify geomorphologic processes (Cerling and Craig, 1994; Cockburn and Summerfield, 2004; Bishop, 2007) has enlivened landscape evolution studies by providing novel quantitative techniques to obtain ages and incision rates in the landscape (Bishop, 2007). For the particular case of rivers, the estimation of channel incision rates in bedrock has primarily been done dating geomorphic markers and using an exposure age to estimate the rate of incision in a given period of time (e.g., Seidl et al., 1997; Leland et al., 1998; Reusser et al., 2004; Schaller et al., 2005). Another approach consists in measuring the TCN concentrations in sediments to obtain a catchment-averaged denudation rates (e.g., Bierman and Steig, 1996; Reinhardt et al., 2007b; Codilean et al., 2008; Cyr et al., 2010). Use of this latter approach must be conscious of processes (i.e., hillslope processes) besides the fluvial ones. The possibility also of estimating erosion rates directly from a bedrock outcrop in the river bed using *in situ* produced TCNs is promising for the case of bedrock rivers. This approach is exploited in this research to obtain bedrock incision rates from an actively eroding surface.

The possibility of using TCNs to estimate bedrock channel incision rates is attractive to test the several existing models of bedrock channel incision. Because (1) sediment plays an important role in the bedrock channel degradation and (2) quantifying the incision rates is necessary to understand landscape response to tectonics and/or climate, in this chapter the effect of sediment and estimation of bedrock channel incision are presented together. The first part of this chapter analyses the in-channel sediment size distribution in order to clarify if plucking or abrasion or both control channel incision into bedrock. In the second part, rationale of using the *in situ* produced TCNs is presented as well as the sample strategy. Finally, the erosion rates obtained are compared with the stream power model and a variation of the saltation-abrasion model.

6.2 The role of sediment in bedrock channel incision

Gilbert was the first to emphasise the necessity to quantify the sediment flux to understand bedrock channel incision (Sklar and Dietrich, 2001). Gilbert (1877) suggested that sediment controls bedrock incision by causing two effects: (1) the cover of larger particles reduces the rates of bedrock incision rates because coarse fragments are difficult to mobilise and they shield the bed (the 'cover' effect) and (2) the potential work of medium size particles in providing tools for bedrock incision (the 'tools' effect)(Sklar and Dietrich, 1998; 2001). Gilbert's observations and hypothesis have been tested quantitatively in a model known as the saltation-abrasion model (Sklar and Dietrich, 2004).

The stream power model in its two forms (i.e., unit stream power and shear stress), does not explicitly include the effect of sediment, which is implicit in the term K (equation 2.4). The K term also accounts for other processes such as climate, lithology and sediment load (Howard, 1994; Howard et al., 1994; Whipple and Tucker, 1999). Sklar and Dietrich (2001) argued that the influence of sediment supply on streams might not be fully captured in the detachment-limited model where plucking is the main mechanism driving incision. These authors subsequently formulated their mechanistic-based saltation-abrasion model in which is stressed the non-linearity of bedrock incision by the effect of the sediment transport and sediment supply and the abrasion caused by the impact of grains on a bedrock surface (Sklar and Dietrich, 2004; 2006). In this approach the bedrock incision erosion (E_s) can be evaluated as the product of three terms (Sklar and Dietrich, 2006):

$$E_a = \frac{0.08 R_b g Y}{k_v \sigma_t^2} Qs \left(\frac{\tau^*}{\tau_c^*} - 1\right)^{-0.5} \left(1 - \frac{Q_s}{Q_c}\right) \times \left(1 - \left(\frac{u^*}{w_f}\right)^2\right)^{1.5} \tag{6.1}$$

where R_b is a non-dimensional buoyant density, g the gravitational acceleration, Y is Young's modulus of rock elasticity, k_v is a dimensionless rock resistant parameter, σ_t is the tensile rock strength, Q_s is the sediment supply rate, τ^* is the dimensionless

shear stress, τ_c^* is the threshold shear stress for sediment motion, Q_c is the bedload sediment transport capacity, u^* is the shear velocity and w_f is the grain fall velocity in still water. Interestingly the first term of equation 6.1 is somewhat similar to K in the stream power model as long as this term mainly reflects lithology, but for the case of the equation 6.1 this term is insensitive to variations in climate and tectonics. Sklar and Dietrich (2004) used equation 6.1 to test and obtain bedrock erosion rates of the Fork Eel River, in California (USA). They found that bedrock incision suddenly increases where there is an excess of sediment transport capacity, and in reaches where bedrock exposure is frequent on the riverbed (Sklar and Dietrich, 2004, their Fig. 12). Another key finding is that the higher erosion rates coincide with the transport of medium size particles ($D \approx 40\ mm$) (Sklar and Dietrich, 2004, their Figure 14).

The terms forming equation 6.1 allow to distinguish different processes affecting the channel incision. In the first term, the rock erodability is estimated assuming that the bedrock surface is mechanically eroded (Sklar and Dietrich, 2004), thus changes in the first term may result only from a change in lithology. In the second and third term the effect of saltation particles impacting on the bed and sediment flux are integrated. In the third term, the dimensionless ratio (τ^*/τ_c^*) the transport stage which accounts for the relative intensity of sediment transport. A high value of transport stage means that the saltation of a particle impacting the bed increases (Sklar and Dietrich, 2004). In the fourth term the tools and cover effects are considered (Sklar and Dietrich, 2004; Crosby et al., 2007) using the sediment transport (Q_s) and sediment capacity ratio (Q_c), in this case a low value (< 0.5) denotes a condition where sediment is abrading the bed because the sediment transport capacity is larger than the sediment supply, when the sediment supply is increases, the sediment transport capacity is reduced (> 0.5) and when $1 - Q_s/Q_c = 0$ the bed is armoured with sediments and abrasion is mitigated or nullified. In the fifth term the velocity of the particles impacting the bed are considered by the evaluating the ratio between the shear velocity and the particle settling velocity (u^*/w_f) which are

correlated with the transport stage included in the third term (Sklar and Dietrich, 2004). The model expressed in equation 6.1 allows to estimate the instantaneous bedrock incision caused by abrasion in which the impact of grains on the bedrock surface is the mechanism driving abrasion, such model also estimate the effects of sediment (tools and cover effects) on channel incision (Sklar and Dietrich, 2004).

The saltation-abrasion model seems to confirm the hypothesis originally posed by Gilbert (1877) on the role of sediment size and transport capacity as factors controlling bedrock abrasion. Other bedrock abrasion models have also been proposed (e.g., Foley, 1980; Gasparini et al., 2006; Turowski et al., 2007; Chatanantavet and Parker, 2009) but the saltation-abrasion model seems to capture the effects of tools and cover, which in some cases have not been fully considered (e.g., Foley, 1980). Here the model of Sklar and Dietrich (2004) is used as to evaluate bedrock abrasion and the role of sediment in bedrock channel degradation.

Bedrock incision by abrasion depends on two factors: (1) the stream's capacity to mobilise the sediment load, for which sediment transport must overcome the sediment supply, otherwise the channel is covered by sediment and incision is inhibited; and (2) the sediment size which may increase or reduce abrasion depending on the size and number of particles that impact on the bedrock surface. Large clasts of rocks ($>>$ 40 mm) are difficult to mobilise and if these predominate, transport capacity drops ($Q_s > Q_c$) generating a buffering in the channel against abrasion (Stark et al., 2009). In contrast, fine particles ($<<$ 40 mm) are more easily transported but their impact and abrasion on the bedrock will be reduced in terms of the impact area, so high sediment fluxes are required to initiate channel incision. Noting that sediment size and the channel bedrock exposure are related to the tools and cover effect, the key point in the field is to quantify both to assess the role played by sediment.

The role of sediment transport in bedrock incision is not limited to abrasion but

is also related to the detachment of rock fragments on fractured bedrock surfaces (Whipple et al., 2000a; Whipple and Tucker, 2002), in the process known as macroabrasion (Whipple, 2004; Chatanantavet and Parker, 2009). The detachment of blocks in the bedrock channel results from a wedging of medium to fine particles that fill the cracks generated at high pressures during flooding and detachment due to drag forces (Whipple et al., 2000a). The effect caused by sediment in the plucking of rocks is implicit in the steam power model.

6.2.1 Sediment size distribution in small bedrock rivers

The grain size distribution and fining of sediment with the increase of stream discharge in bedrock rivers is not a new topic but it remains less well known in comparison to alluvial and gravel bed rivers (Knighton, 1980; Brierley and Hickin, 1985; Fahnestock, 1963). In his pioneering study, Hack (1957) observed two different trends in the sediment size distribution: (1) the downstream fining as occurs for the alluvial rivers and which were observed in most of the rivers analysed by Hack and (2) and inverse relation observed in the Gillis Falls River where sediment size increased downstream. Hack (1957) established a power law function for channel slope using the ratio between sediment size particle and stream length (as proxy of stream discharge) in the form:

$$S = 25\frac{M^{0.6}}{L} \tag{6.2}$$

where S is the channel slope, M the median size of the sediment and L is the distance downstream. This functional relation was interpreted as response of channel slope to the ratio of sediment size and stream discharge which was summarised by Hack (1957, his Fig. 21) in a family of curves. The case of sediment size increasing with downstream length results in a reduction in the exponent of equation 6.2. Hack established a functional relation between grain size stream discharge and channel slope that is related to the stream profile morphology and attempted to integrate these into the stream profile equation (Hack, 1957, his Equations 14, and 15), while

suggesting that the SL form is preferable (but see Goldrick and Bishop, 2007).

Other studies in mountain and bedrock streams indicate that sediment size tends to decrease with distance downstream (e.g., Fahnestock, 1963; Bradley et al., 1972; McPherson, 1971; Brierley and Hickin, 1985; Jansen, 2006), a trend that is consistent with some laboratory experiments (Schumm and Stevens, 1973). If it is assumed that the channel slope and the sediment size are related and both decrease as drainage area increases, then it would be expected that the sediment size distribution will vary with different fluvial domains (Figure 6.1).

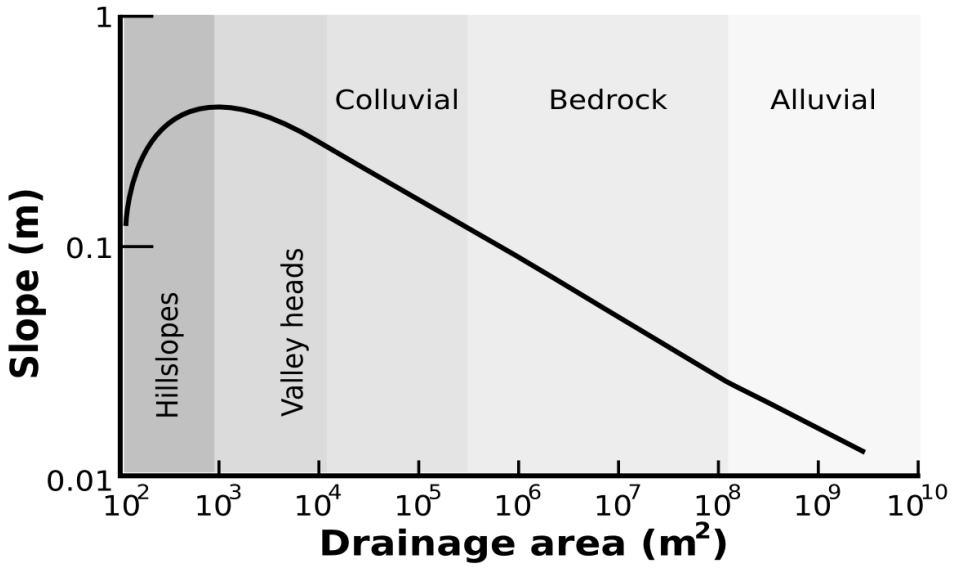

Figure 6.1: Fluvial domains of a river characteristic of a steady state landscape (Modified from: Montgomery, 2001).

Figure 6.1 indicates that channel slopes varies with drainage area. Coarse sediment would be expected to prevail in the colluvial domain where debris flow and hillslope processes dominate (Montgomery and Dietrich, 1989; Tarboton et al., 1991; Montgomery and Foufoula-Georgiou, 1993). Less coarse sediment is expected to be

found in the bedrock domain and the finest sediment and suspended load are likely to characterise the alluvial zone. This model is, however, a generalisation and field studies indicate that boundaries between the various zones are difficult to establish and mixed reaches have been proposed to exist (Montgomery and Gran, 2001; Turowski et al., 2008).

Whether the sediment size decreases with increasing drainage area, has not been fully documented for bedrock rivers. Studies on rivers affected by tectonic forcing indicate that bedrock is more frequently exposed in the channel (Snyder et al., 2003) and faulting and subsequent landscape steepening may also be related to an increase in the sediment size by the increase of sediment supply due to landslides activity (Whittaker et al., 2007). Another important factor in changes in sediment delivery to the channel is related to the propagation of knickpoints as has been observed in flume experiments (Hasbargen and Paola, 2000; Bigi et al., 2006). Even in the case of steady-state landscapes, variations in the sediment supply are likely to occur. Taiwanese rivers, for example, indicate that sediment production is partially controlled by earthquakes, landslides and typhoon activity (Hovius et al., 2000; Hartshorn et al., 2002; Dadson et al., 2003). These conditions are translated into sediment delivery from tributary basins that is likely to be reflected in changes in sediment grain size deposited along the main trunk. Other studies have also stressed on the increase of sediment size or a delay in sediment finning due to the supply of glacial sediment from the upper basins (Heller et al., 2001; Attal and Lavé, 2006), the transport of sediments due to landslides (Hovius et al., 2000; Attal and Lavé, 2006), and the coarsening of sediment in landscapes responding to a tectonic forcing (Whittaker et al., 2010).

Sediment size in the present study was examined by sampling five streams, four on the west coast and one in the east, all located at the south end of Jura (Figure 6.2). Sampling was aimed at assessing if there was any change in sediment size as the distance from the divide increases and if there were any sharp contrasts in

sediment size in the reaches located upstream and downstream of the base-level fall knickpoint. For this purpose, sediment patches and bars were examined upstream and downstream of the knickpoint towards the stream outlet. The surface of the sediment patches and bars were sampled based on the approach suggested by Wolman (1954) and the sediment was sampled in those reaches where the sediment patches or bars were of more than 20 m in length. When possible the sampling sites of sediment was every 10 m distance where 10 particles were measured at every meter. In some sites the measurement every 10 m was not possible because the sediment is under the water, in this case the sampling of sediment was done every large step inside the rivers where 10 particles were measured. In any case the grains were randomly selected. A metallic template with fixed squares of different size (11 mm to 128 mm) was used to measure the B axis of sediment (Figure 6.3). Boulders A and B axis were measured using a metallic metric tape.

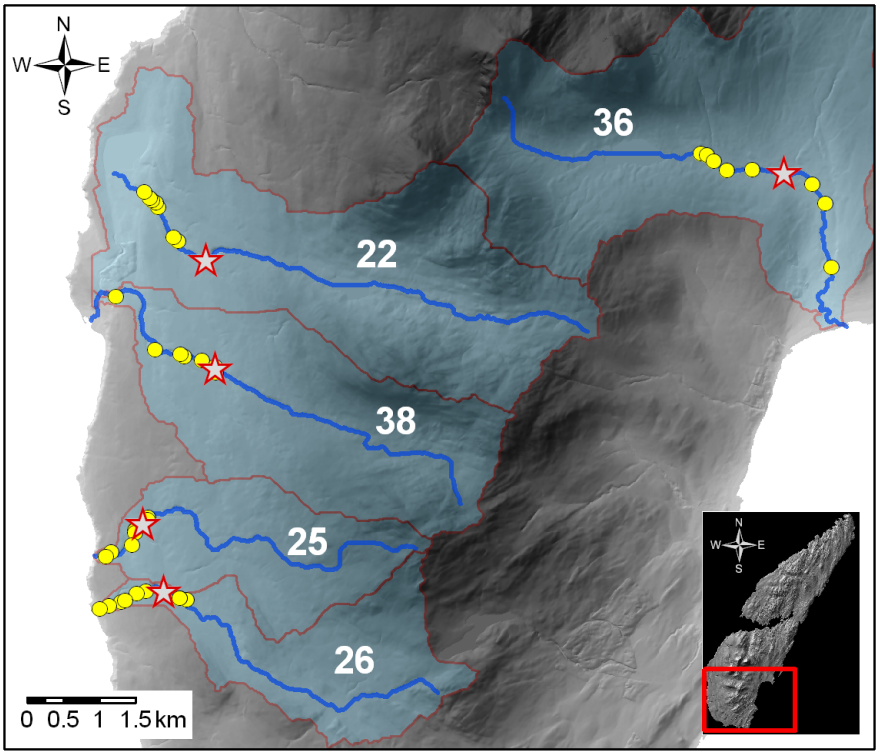

Figure 6.2: Grain size sampling sites (yellow circles) on the Isle of Jura. A total of 100 measurements were made at each site. The stars indicate the location of the 13.6 ka knickpoints.

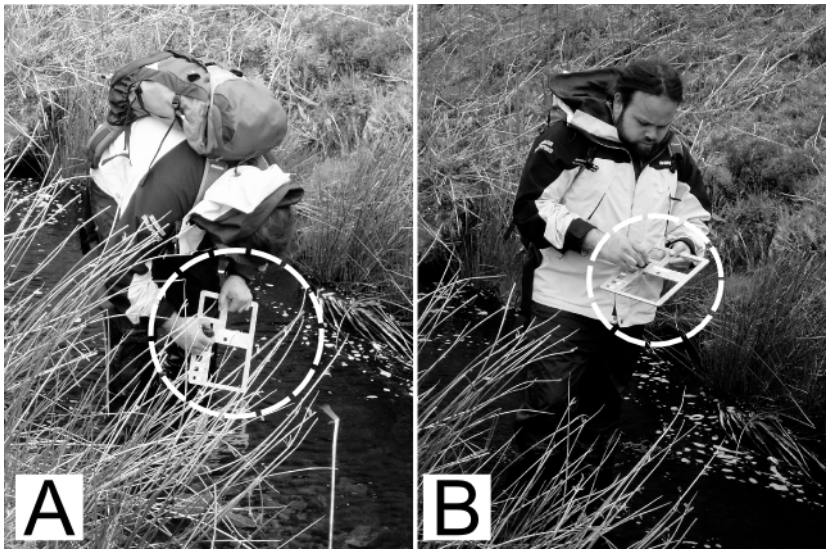

Figure 6.3: Metallic template (white dashed line in A and B pictures) used in fieldwork to measure the sediment size. In both photographs sediment measured was under the water.

Coverage by boulders is not ubiquitous and in some sites they are absent. Due the scarcity of boulders on sediment patches and bars, the largest boulder observed was measured whenever this was present. The coarsest fraction, recognised here as those particles larger than 128 mm and these were treated separately from the 11 to 128 mm fraction due to the reduced number of coarse particles ($>$ 128 mm) found on sediment patches and bars. For the coarse fraction, grains were measured using the metallic metric tape. The percentage of boulders in the sediment patch was estimated visually at each sampling site. The locations of sample sites, the boulder size and the different D fractions of the sediment patches are presented in Table 6.1, in Figure 6.4 is illustrated the nature of the reaches sampled.

Table 6.1: Sediment sampling sites for different fraction sizes (D_{10}, D_{50}, D_{90}) and the coarsest fractionD_b.

Stream ID	**Site**	**Coordinate (x,y)**	D_{10} **(mm)**	D_{50} **(mm)**	D_{90} **(mm)**	D_b[†] **(mm)**	**Cover**[†] **(%)**
22	1	145396, 672387	22	45	128	500	-
22	2	145333, 672437	16	45	90	500	-
22	3	145109, 672853	11	32	54	1000	10
22	4	145078, 672912	16	32	90	1500	50
22	5	145029, 672952	16	45	90	1500	30
22	6	145002, 672982	22	45	90	1000	10
22	7	144914, 673064	22	45	90	1000	10
25	1	144963, 668548	32	45	54	600	10
25	2	144953, 668517	32	45	90	700	10
25	3	144794, 668397	22	45	72	700	15
25	4	144788, 668369	32	45	90	1600	-
25	5	144784, 668336	16	32	54	500	5
25	6	144718, 668171	27	45	90	1500	40
25	7	144469, 668031	32	45	90	900	15
25	8	144392, 668020	19	32	90	900	40
26	1	145503, 667407	45	54	128	-	-
26	2	145422, 667438	32	45	90	2000	-
26	3	144948, 667542	32	45	90	1700	-
26	4	144812, 667517	32	45	90	500	-
26	5	144602, 667412	32	54	90	-	-
26	6	144651, 667422	32	54	90	-	-
26	7	144438, 667347	22	45	90	400	-
26	8	144305, 667297	11	45	90	-	-
36	1	152649, 673601	32	45	90	500	15
36	2	152747, 673577	22	45	128	650	15
36	3	152838, 673498	22	45	54	-	-
36	4	153006, 673367	32	54	90	400	-
36	5	153358, 673387	45	54	90	-	-
36	6	154192, 673170	45	54	90	-	-
36	7	154373, 672911	54	90	128	-	-
36	8	154460, 672026	32	45	90	1000	-
38	1	145918, 670561	22	32	90	500	-
38	2	145905, 670647	22	45	128	1300	-
38	3	145718, 670721	22	45	90	-	-
38	4	145484, 670796	22	45	90	-	-
38	5	145423, 670802	22	32	54	400	-
38	6	145082, 670880	22	38	72	400	30
38	7	144517, 671620	22	45	90	500	-

[†] The hyphen indicates no data.

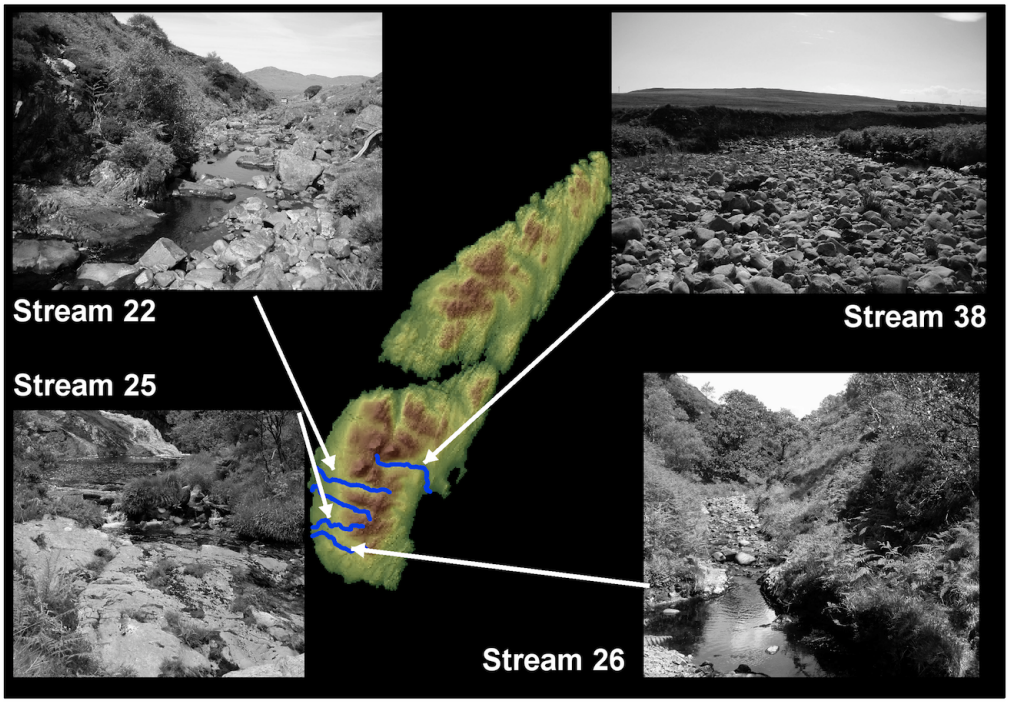

Figure 6.4: Photographs of different reaches where sediment has been sampled. Only in few cases (e.g. stream 22) coarse material has been observed on the channel

In Figure 6.5 the cumulative graphic of the sediment size reveals that the dominant fraction size in most of the sites sampled ranges between 20 mm and 50 mm (Figure 6.5). This size covers $\sim$ 80% of the sediment size of the patches and bars sampled. The homogeneity of the grain size distribution (Figure 6.5) and the scarcity of boulders armouring the riverbed (Table 6.1) suggest that drainage area is unlikely to be related with the sediment grain size distribution because a the 20 mm to 50 mm tends to prevail in the sites sampled.

To assess whether there is a downstream change in grain size, the D_{10}, D_{50} and D_{90} fractions are plotted against a normalised distance downstream (Figure 6.7). Figure 6.7, indicates that grain size does not change sharply as the distance downstream increases, in either D_{10} and D_{50} fractions. The largest fraction (D_{90}) slightly

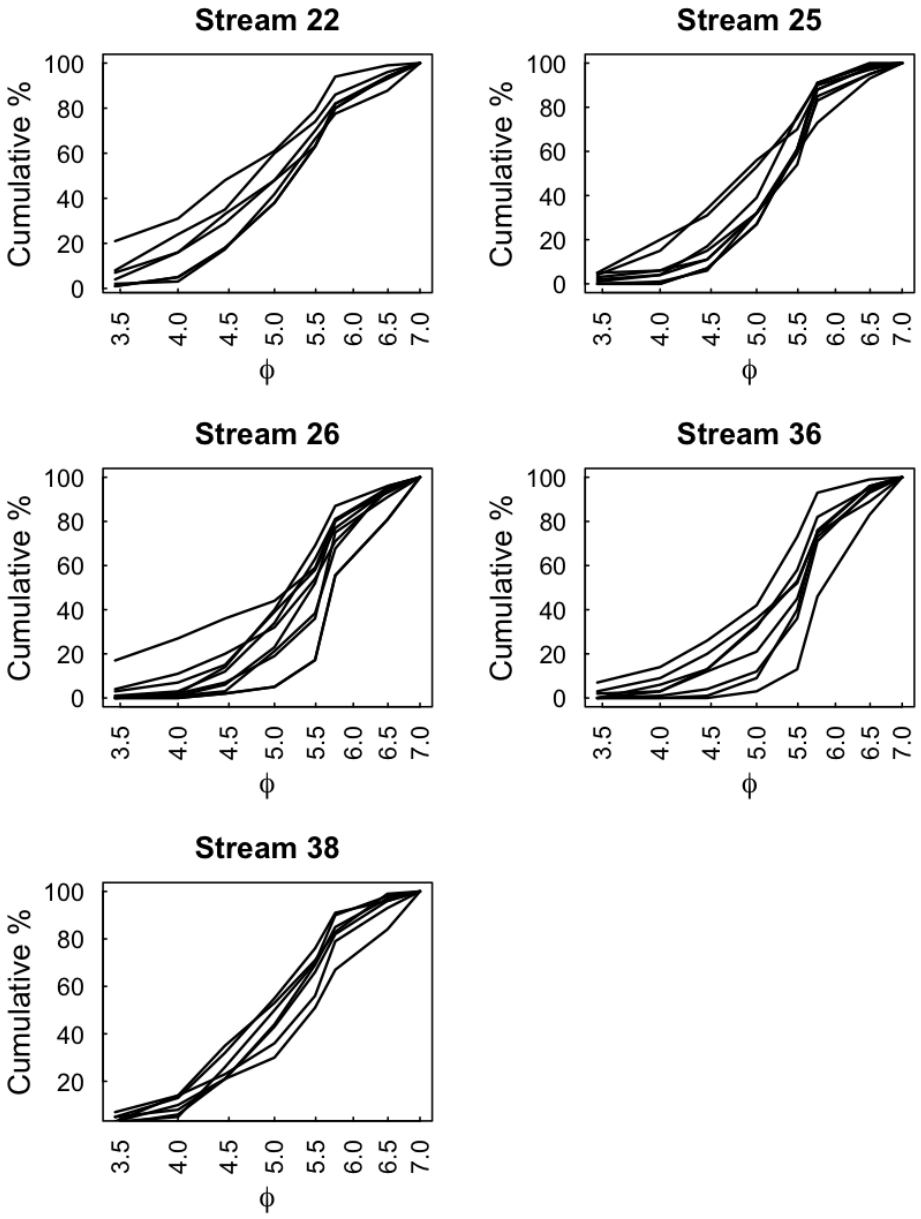

Figure 6.5: Cumulative graphs of the sediment size measured on 5 streams of Jura. Note the homogeneous distribution of sediment size given by the shape among the curves sketched.

increases downstream but D_{90} particles only represent $\sim 10\%$ at each site (Figure 6.5). The relative stability in the D_{50} and D_{10} fractions in all streams indicate that the sediment transport and the sediment supply in the rivers are more or less equal among all streams. During fieldwork it was observed that in the narrow valleys located downstream of the 13.6 ka knickpoints, the landslides are common, which is interpreted as a source of sediment supply. Also the erosion of glacial material (mainly till) on the upper catchments are deposited into the river by landslides (Figure 6.6).

Figure 6.6: The photograph on the right correspond to stream 38 where glacial material is being supplied to the rivers from unstable slopes, the scar of the landslide is marked with the white dashed line. On the left, a small talus cone (right bank of the picture, white dashed line) located downstream of the 13.6 ka knickpoint of stream 25. Note the steep valley walls of the picture of the left.

The possible effect of sediment contribution to the main trunk fed by tributaries is not evident because the lateral supply of sediment by tributaries is limited. The homogeneity in the sediment size distribution also suggests that the channel slope is not related to the sediment size. The lack of impact of the knickpoints on sediment size seems to confirm that there is no relationship between the sediment fraction and the channel slope (Figure 6.8).

The boulders measured in fieldwork were plotted against the normalised distance

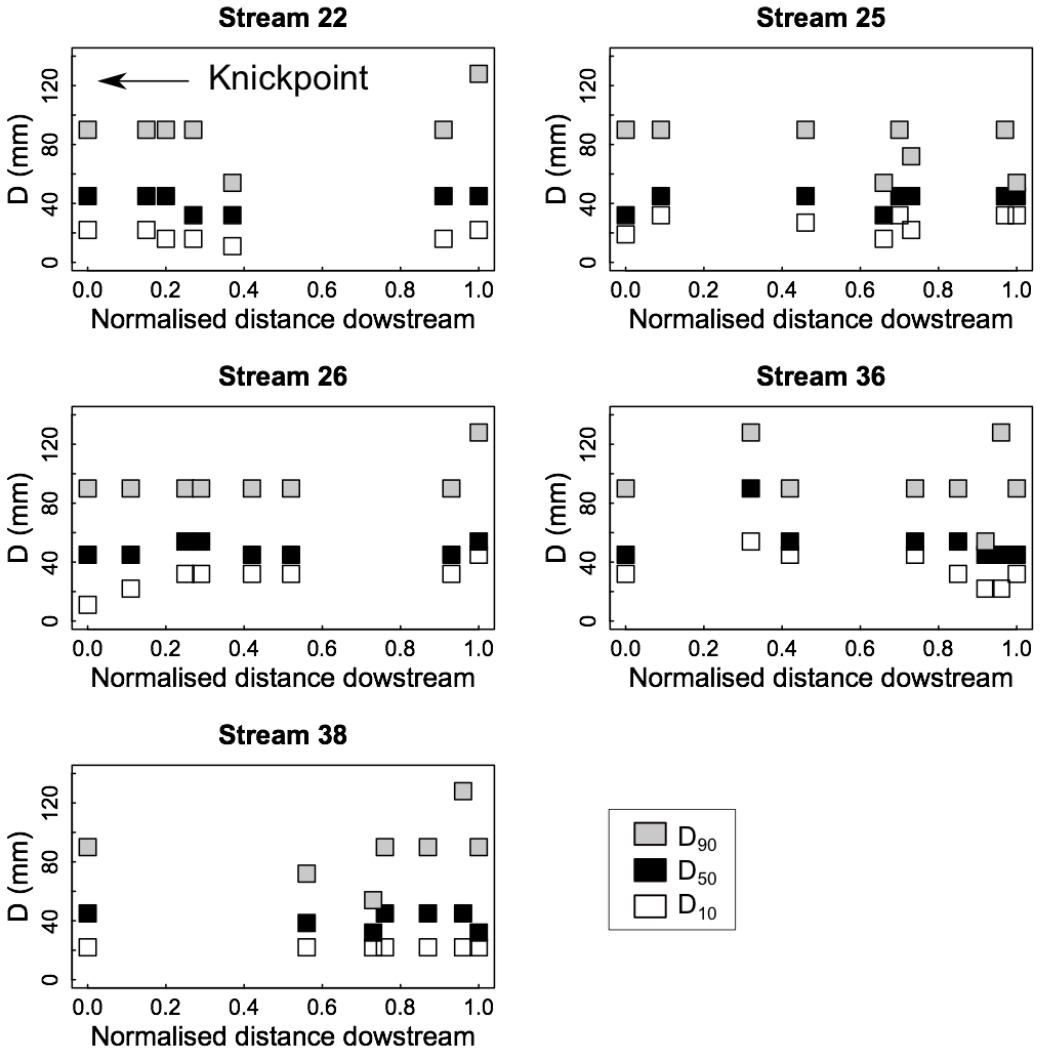

Figure 6.7: Variation of different sediment size fractions with increasing distance downstream. The trend observed for the median (D_{50}) is to remain almost constant as the distance downstream increases. No sharp changes on size are observed on the reaches sampled and the effect caused by knickpoints. The distance is normalised from the site sampled upstream of the 13.6 ka knickpoint towards the stream mouth.

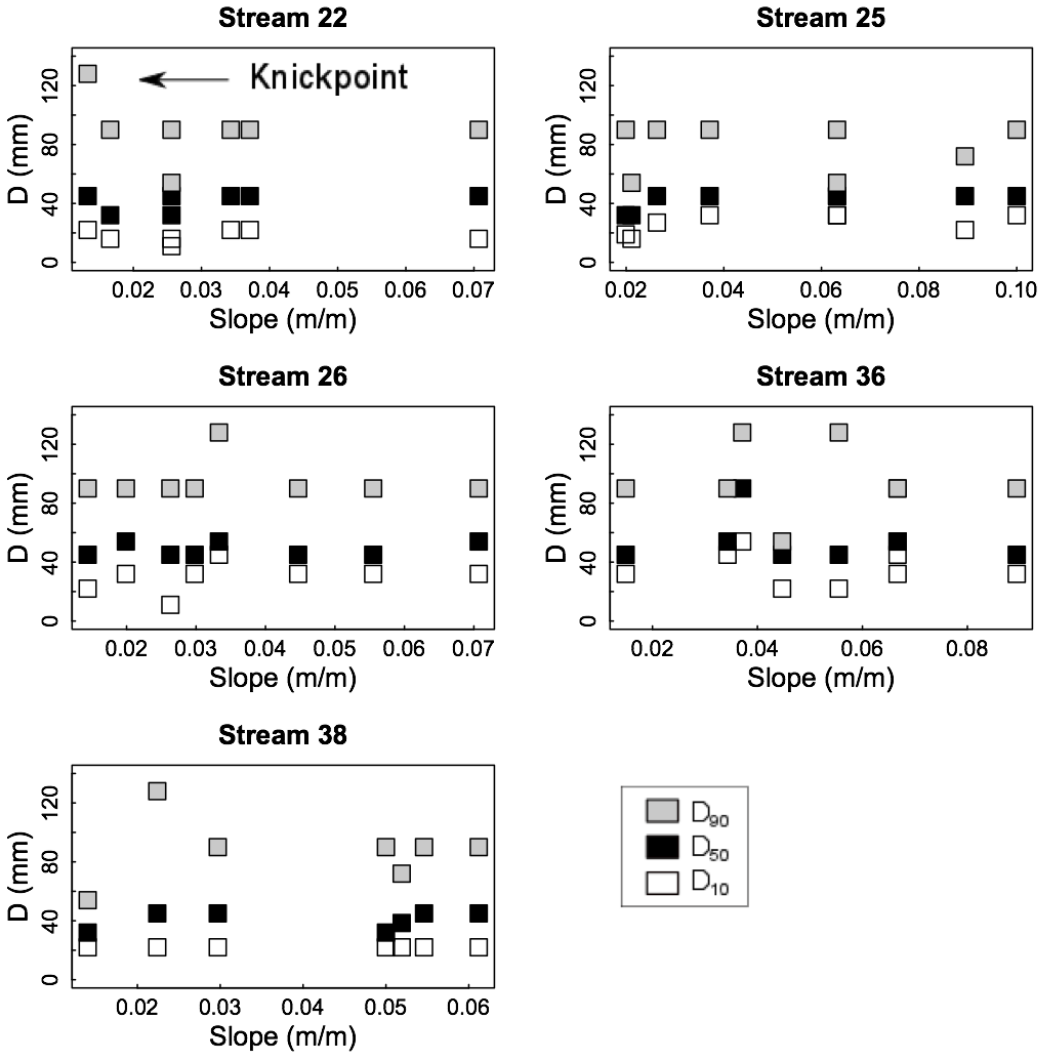

Figure 6.8: Variation of different sediment size fraction in relation to channel slope in a downstream direction.

(Figure 6.9). The plots indicate that large particles exhibit more variability but in any case no systematic increase or decrease in size is observed with distance downstream and sediment size is randomly distributed (Figure 6.9). The random distribution of boulders size is also observed when size is plotted against the local channel slope (Figure 6.10).

The sediment size distributions for both coarse and medium size particles shows no clear trends in fining or coarsening with distance downstream or slope. To confirm this quantitatively, equation 6.2 of Hack (1957) was applied to both coarse and medium fractions (Table 6.2). The results of the regressions indicate that there is no relation in the ratio of sediment size and stream discharge in respect to channel slope (Table 6.2). This lack of relationship contrasts with the findings of Hack (1957) where the scaling of equation 6.2 is reported.

Table 6.2: Regression coefficients of equation 6.2 for the medium and coarse fraction.

Medium size fraction (D_{50})				
Coefficients	**Estimate**	σ	**T value**	$Pr(>\|t\|)$
Intercept	-3.34541	0.3490	-9.584	1.91×10^{-11}
Log(D_{50}/Distance)	-0.01337	0.0943	-0.142	0.888
R^2= 0.0, p-value: 0.88				
Boulders ($> 120\ mm$)				
Coefficients	**Estimate**	σ	**T value**	$Pr(>\|t\|)$
Intercept	-2.9813	0.4752	-6.274	1.22×10^{-06}
Log(Bouler/Distance)	0.1737	0.2371	0.732	0.471
R^2= 0.0, p-value: 0.47				

The lack of scaling predicted by equation 6.2 indicates a condition where the channel slope and the bed sediment do not scale with stream discharge. This lack

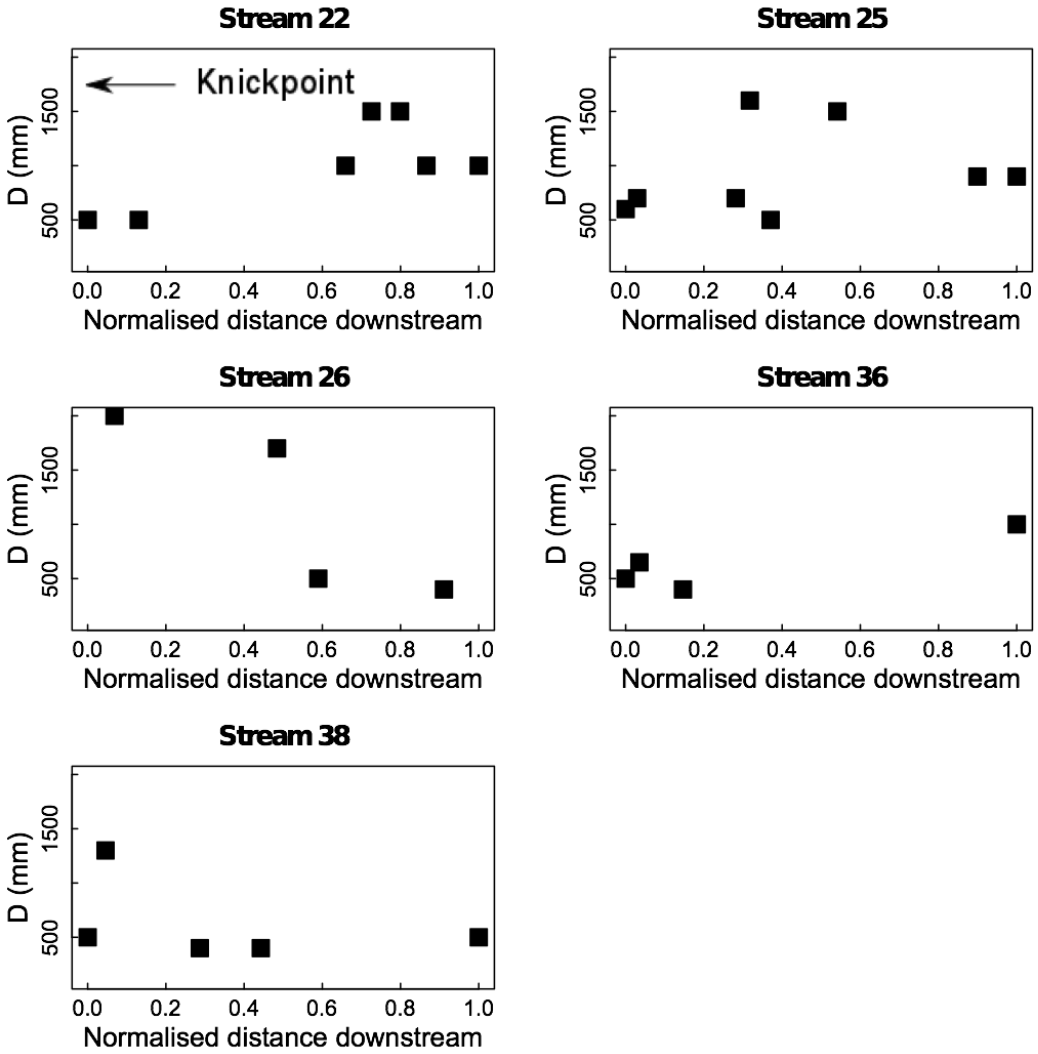

Figure 6.9: Variation of the largest boulders with the increase of the distance downstream. A random distribution of particles of size predominates with not clear signs of increase or decrease with the distance downstream.

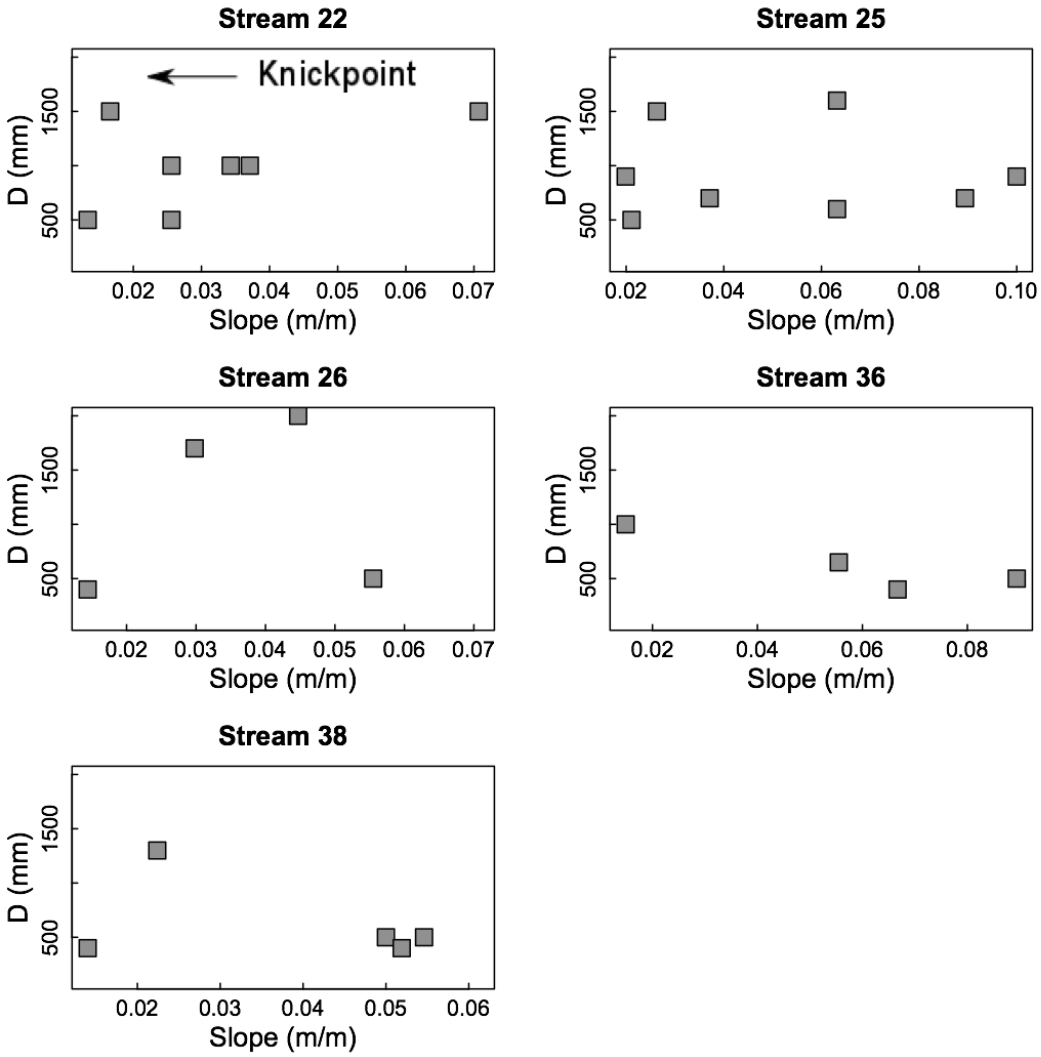

Figure 6.10: Distribution of boulders size with the local channel slope in a downstream direction. As in the case of Figure 6.9, not systematic behaviour of size and slope is observed.

or relationship reflects: (1) the transient nature on the streams of Jura, in which the channel slope is not adjusted on the upper parts of the rivers and even at the stream outlets and (2) the continuous supply of sediments from hillslopes, which are likely to be related to unstable slopes as has also been observed in other transient settings (e.g., Whittaker et al., 2010). The lack of adjustment in channel slope is also supported by the DS regressions already shown here.

6.2.2 Channel bedrock exposure

The amount of bedrock exposure on channel is believed to be indicative of active bedrock incision on streams in which detachment-limited conditions prevail (Sklar and Dietrich, 1998; Turowski et al., 2008) or zones in the channel where there is an influence of a tectonic forcing (Snyder et al., 2003; Cowie et al., 2008). No field methods have been proposed to estimate the area of exposed bedrock in rivers but the approach followed, generally consists in visual estimation of the percentage of the amount of of bedrock exposure in a given reach (Snyder et al., 2003; Johnson et al., 2009). Although this is a purely field-based semi-quantitative approach, estimating bedrock exposure is useful for assessing if stream incision is likely to be influenced by the effect of sediment transport (Johnson et al., 2009). The percentage of bedrock exposure was recorded at the same sites for which the grain-size analyses were undertaken (Figure 6.2). The bedrock exposure was obtained by estimating the percentage of bedrock exposed on the active channel along a distance of 20 m. The percentage of the bedrock exposed in the active channel was plotted against (1) non-dimensional downstream distance, and (2) local channel slope to detect if there is any systematic behaviour in the channel bedrock exposure (Figures 6.11 and 6.12).

Figures 6.11 and 6.12 indicate that bedrock exposure occurs regardless of local channel slope. Nevertheless, some rivers have a slight trend to have greater bedrock exposure where the slope increases in a downstream direction (Figure 6.12, streams

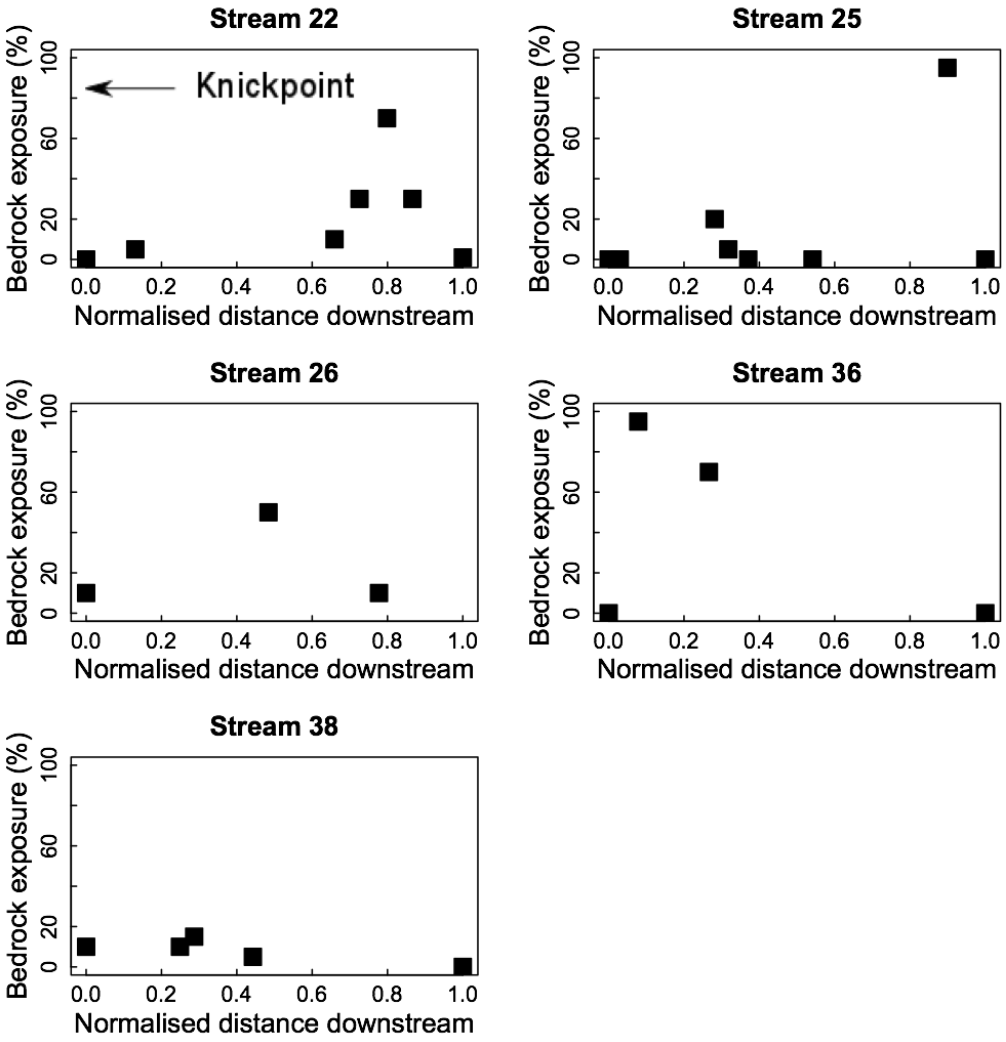

Figure 6.11: Plots of percentage of bedrock exposure in relation to the increase of distance downstream.

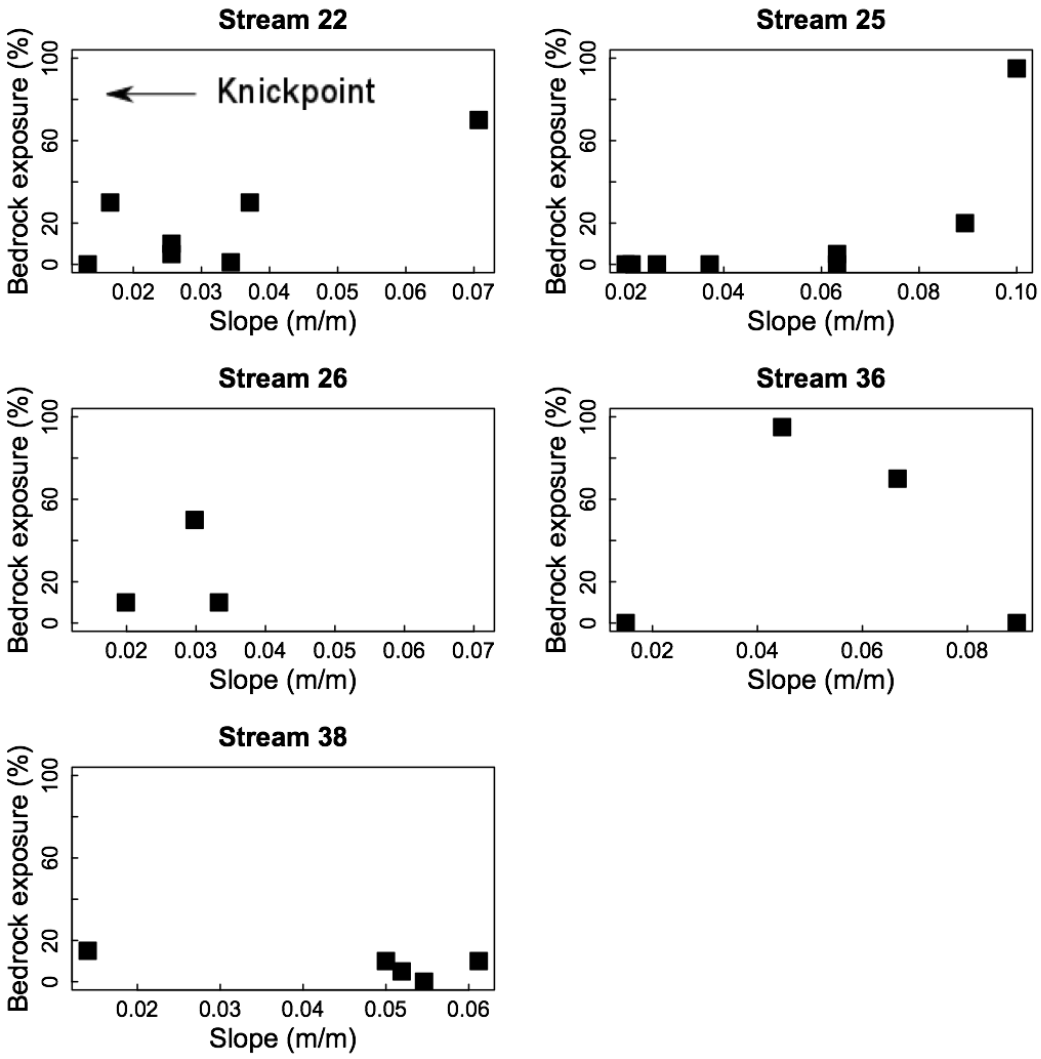

Figure 6.12: Plots of percentage of bedrock exposure against channel slope in a downstream direction.

22, 25 and 36).

The frequent bedrock exposure and overall pattern observed in the distribution of the sediment size for medium and coarse fraction clarify the nature of the bedrock streams of Jura and unequivocally confirming their bedrock river character following the criteria of Turowski et al. (2008). Bedrock exposure at streams outlet (Figure 6.13) indicate that these rivers are incising into an actively uplifting setting where channel slopes increase in downstream direction and where sediment does not cover the bed at stream outlets.

Figure 6.13: Photograph showing that bedrock is present at stream's mouth on stream 26. The bedrock exposure at the mouth of the stream confirms that Jura's landscape has been affected by rock uplift.

Although the sediment size distribution could be characterised here for the streams sampled and it is also confirmed that the median size fraction (i.e., D_{50} 45 mm) which according to the saltation-abrasion model is likely to contribute to channel incision by the impact of grains hitting the rock surface (Sklar and Dietrich, 2004), the lack of a complete armouring of the bed, the amount of bedrock expos-

ure, and lack of fining of sediment grain size with the increase of stream discharge, suggest that detachment-limited conditions are more likely to control the bedrock incision in the rivers of Jura.

6.3 Estimation of erosion rates using *in situ* produced terrestrial cosmogenic nuclides (TCNs)

Since the 1990s, an increasing number of papers dealing with obtaining exposure ages and incision rates by measuring the TCN concentrations have been published (Cockburn and Summerfield, 2004), revivifying quantitative techniques in the field (Laeter, 1998). The physical principles of the TCN production have been known since the middle of the 20th century (Lal, 1987; Cerling and Craig, 1994). However, the measurement of the long-lived cosmogenic isotopes was not possible until the development in the middle 1980s of the accelerator mass spectrometry (AMS) and the refinement of the noble-gas mass spectrometer (Lal, 1987; Gosse and Phillips, 2001). The AMS has resulted in a major advance because for the first time *in situ* TCNs could be measured in small grains due to the great sensitivity of the AMS for measuring isotopic ratios (Laeter, 1998; Granger and Riebe, 2007).

The half-lives of *in situ* produced TCNs used in geomorphological research range from thousand years to million of years (e.g., ^{14}C and ^{10}Be respectively) (Elmore and Phillips, 1987; Cockburn and Summerfield, 2004). This range makes TCNs very useful in geomorphology since the time span is wide when compared to the traditional dating of organic ^{14}C. Also, the possibility to date bedrock, grains and soils makes TCNs suitable for many physical settings. ^{26}Al and ^{10}Be have been widely used in geomorphology because their production rates are relatively well known (Nishiizumi et al., 1986; 1993; Lal, 1988; 1991) and are larger than for other isotopes (e.g ^{36}Cl and ^{14}C). Moreover, the ^{26}Al and ^{10}Be are produced in quartz by spallation and muon capture of atoms of O and Si (Nishiizumi et al., 1986; Lal, 1991) which are components of quartz, which is ubiquitous on the Earth's surface.

TCNs have been used to estimate incision rates in bedrock rivers by dating exposure ages on strath-terraces (e.g., Seidl et al., 1997; Leland et al., 1998; Schaller et al., 2005). Bedrock incision rates can also be quantified by measuring the concentration of *in situ* bedrock surfaces that are continuously eroding (Lal, 1991;

Nishiizumi et al., 1993). The Jura streams are ideal candidates to estimate the bedrock incision by measuring the concentration of ^{26}Al and ^{10}Be atoms because of the quartzite lithology and the constant bedrock exposure of channels, as well as the steep slopes free of sediment cover predominate in this setting.

In the following sections the general principles by which incision rates can be obtained by measuring the TCN concentrations are briefly explained focusing on ^{10}Be which was used here to estimate the incision rates in two rivers of Jura. The hypothesis and rationale of sampling are also presented as well as the procedures followed in the laboratory and the results obtained from the AMS measurements. In the last part of this chapter the incision rates and their implications for transient rivers are discussed.

6.3.1 Principles of *in situ* produced TCN

The literature on the use of *in situ* produced TCNs to estimate exposure ages or incision rates is extensive and several review papers have been published in the last twenty years (e.g., Lal, 1987; 1988; 1991; Nishiizumi et al., 1993; Cerling and Craig, 1994; Gosse and Phillips, 2001; Granger and Riebe, 2007). Also, improvements in scaling factors affecting nuclide production have appeared since then (e.g., Dunai, 2000; Desilets et al., 2006; Lifton et al., 2008), resulting in different models for the estimation of erosion and incision rates (Balco et al., 2008). In this study the papers of Lal (1991); Gosse and Phillips (2001) and Granger and Riebe (2007) are used for reference to describe the principles on the TCNs production. However, details on the formulations and the correction of scaling factors are not provided here and this can be found in the review of Gosse and Phillips (2001).

The ultimate mechanism by which *in situ* TCNs are produced in Earth's surface rocks is the cosmic radiation that enters the atmosphere, generating a secondary cosmic ray flux of high energy particles that hits Earth's surface and interacts with

the atoms of rocks (Lal, 1991; Granger and Riebe, 2007). The particle interaction at the surface is dominated by neutron, protons, nuclear fragments, pions and muons. Muons interact deeper ($\sim$ 2 to $\sim$ 3 m) but these only account for 2% of the total ^{10}Be production (Lal, 1991; Granger and Riebe, 2007).

The TCN production depends on the geomagnetic latitude and altitude. Lal (1991) scaled the production rates of ^{10}Be and ^{26}Al by spallation with a third degree polynomial (Lal, 1991, his equation 1). Later, Stone (2000) indicated that production rates depend on atmospheric pressure and proposed to include this for scaling of production rates (his equations 1 and 2 of Stone, 2000). The scaling factor proposed by Lal (1991) was contested by Dunai (2000) who proposed to include the contributions of the non-dipole field which accounts to 20% of Earth's magnetic field and significantly changes are expected in the cosmogenic nuclide production if this is not taken into account in the production rates at high altitude. Dunai (2000) proposed a scaling factor as an exponential function (Dunai, 2000, his equation 5). Other scaling factors have been published more recently. These include the effect of geomagnetic cutoff rigidity as a factor that determines the production of cosmogenic nuclides as long as these are energy-dependent (Desilets et al., 2006; Lifton et al., 2008). The variations in the production rates obtained from the different scaling factors for ^{10}Be and ^{26}Al can be calculated using the Cronus-Earth online calculator (Cronus-Earth Project, 2010); the details of this are explained by Balco et al. (2008).

Production rates of *in situ* ^{10}Be vary then, according to the scaling factor used. Balco et al. (2008) calibrated ^{10}Be cosmogenic production based on previous studies and obtained a rate of 4.96 ± 0.43 atoms g^{-1}yr^{-1} by spalleogenic production. The cosmogenic nuclides are produced in the near-surface and this decreases exponentially with depth (Lal, 1991) thus:

$$P(x) = P(0)e^{-\rho x/\Lambda} \tag{6.3}$$

where x is the rock depth (cm), P is the production rate of a given radio-nuclide

(atoms g^{-1} yr^{-1}), and $P(0)$ is the production at the surface, ρ is the density of the rock (g cm^{-3}) and Λ is the absorption mean free path (g cm $^{-2}$) for the nuclide interaction to depth. Because the production of TCN penetrates rocks at a depth of approximately 2 m, the exposure age or erosion rate can be obtained for a given surface that has been exposed to cosmogenic radiation. Also as long as the cosmogenic production depends on the spallation, negative muon capture and fast muons interaction (Figure 6.14) the total production of a cosmogenic production is expressed as Granger and Riebe (2007):

$$dN/dt = \sum P_i(t) - N/\tau \tag{6.4}$$

where $P_i(t)$ comprises all the production rates processes (i.e., spallation, negative muon capture and fast muons interactions), N is the cosmogenic nuclide concentration and τ is the radioactive mean-life. Solution of the exposure ages and erosion rates is based on equation 6.4 (Granger and Riebe, 2007).

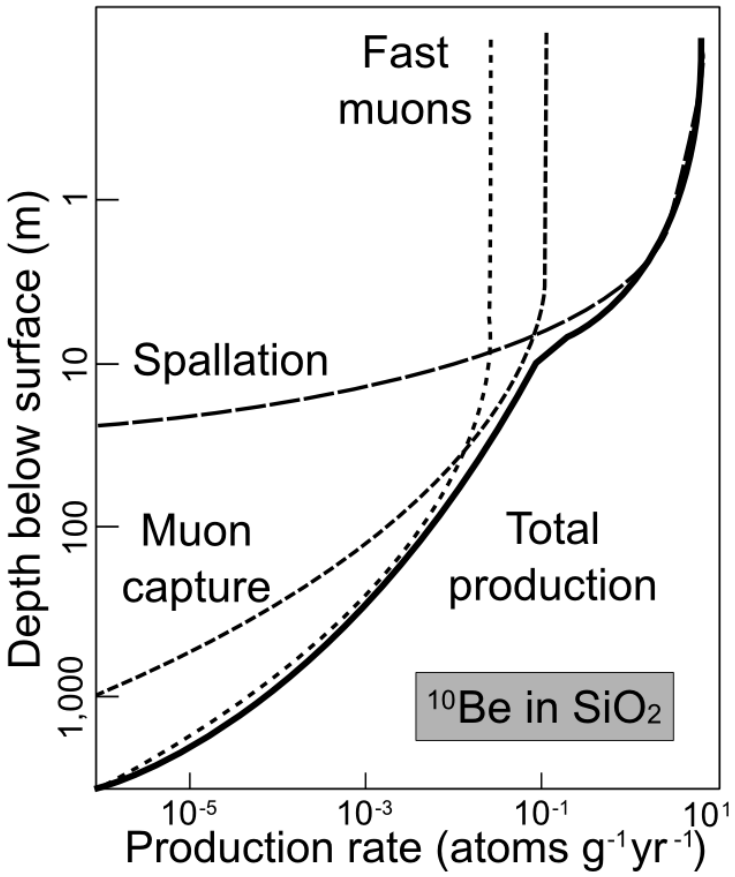

Figure 6.14: Cosmogenic production rates profiles for ^{10}Be nuclide as function of depth. The total production result from the three production rates shown (Modified from: Granger and Riebe, 2007)

Equation 6.4 predicts the production rate for a bedrock surface on a flat topography, free of obstacles and any cover. If the surrounding topography is steep or the sample is covered by snow, fine sediment or soils, a correction in the nuclide production must be made. Gosse and Phillips (2001) provide the equations to correct the production rates by the various types of shielding.

Lal (1991) described in the principles from which the erosion rates can be ex-

tracted from TCN concentrations. Lal (1991) indicated that if the surface has been under a steady state erosion[1] the nuclide production attains a secular equilibrium in its concentration (Nishiizumi et al., 1989; Lal, 1991). In such a case the nuclide production is expressed as:

$$N(x,t) = e^{-\mu x}\frac{P(0)}{\lambda} \tag{6.5}$$

where μ is the absorption coefficient (cm^{-1}), x is the depth into rock (m) $P(0)$ is the production rate at the surface (atom g^{-1} yr^{-1}), λ is the disintegration constant. If the condition above holds, the effective irradiation time at the surface can be obtained from (Lal, 1991):

$$T_{eff} = \frac{N(0)}{P(0)} \tag{6.6}$$

where $N(0)$ and $P(0)$ are the nuclide concentration and the production rate respectively. Then, the steady-state erosion model ϵ is given based on the following expression:

$$\epsilon = \frac{1}{\mu}\left[\frac{P}{N} - \lambda\right] \tag{6.7}$$

It must be noted that equation 6.5 can also be used to obtain exposure ages, and the difficulty in distinguishing between erosion rate and exposure age only using the TCN concentration has long been recognised. The exposure age and a erosion rate from a TCN concentration must be regarded as minimum and maximum, respectively (Gillespie and Bierman, 1995; Granger and Riebe, 2007).

The validity of the steady-state model has been questioned (Small et al., 1997) and other models assuming episodical erosion have been proposed (Small et al., 1997; Muzikar, 2008; 2009). However, the episodic erosion in the landscape is not fully understood for large time scales (i.e., geological time scales). In this sense the steady-state model is still useful but its limitations should not be overlooked (Small et al., 1997; Granger et al., 2001).

[1]The steady-state erosion is interpreted here according to Lal (1991), as a condition where the rocks surface has been eroded continuously at the granular scale without important losses of material due to episodic events.

The ^{10}Be and ^{26}Al cosmogenic calculator, available online (Cronus-Earth Project, 2010), enables the estimation of erosion rates from a single cosmogenic nuclide. The erosion rates are obtained by solving the following equation (Balco et al., 2008):

$$N = S_t S_G P_r \int_0^\infty S_x(t) exp(-\lambda t) exp\left(\frac{-\epsilon t}{\Lambda_{sp}}\right) dt + \int_0^\infty P_\mu(\epsilon t + z/2) exp(-\lambda t) dt \quad (6.8)$$

where S_t is the dimensionless correction for thickness, S_G the dimensionless correction for shielding, P_r is the production rate for spallation (atoms gr^{-1}yr^{-1}), $S_x(t)$ is the dimensionless scaling scheme for P_r, λ is the decay constant for the TCN (yr^{-1}), ϵ is the surface erosion rate (gr cm^{-2}yr^{-1}), Λ_{sp} is the effective attenuation length for spallogenic production (g cm^{-2}), P_μ is the surface production for muons (atoms g^{-1} yr^{-1}), and z correspond to the sample thickness. An advantage of using equation 6.8 to estimate the erosion rate is that the production of muons is included. This is important for the case of active eroding surfaces because if these are omitted, the erosion rates are underestimated by $\sim 25\%$ (Granger et al., 2001; Balco et al., 2008). In the present study, the erosion rates are based on the results of equation 6.8 processed in the Cronus-Earth Project (2010) calculator.

6.3.2 Hypothesis and field sampling strategy

Bearing in mind that the concentration of TCNs can be measured on an active eroding surface to estimate the maximum erosion rate, the bedrock beds of Jura channels were sampled to measure the concentration of cosmogenic ^{10}Be. The relatively constant bedrock exposure on the riverbed in most of the streams and their relative shallow valleys, and the slope steepness suit these river beds to the use of TCN, because samples are well exposed to cosmic radiation and the shielding caused by topography is minimum.

The sampling strategy was aimed at quantifying incision rates in those reaches affected by a base-level fall (i.e., where the knickpoint has propagated headwards)

and in unrejuvenated reaches above these 13.6 ka base-level fall knickpoints. The hypothesis tested was based on a model of knickpoint propagation generated by a sudden base-level drop (Whipple and Tucker, 1999) (Figure 6.15). In this model the rapid base-level lowering triggers a knickpoint that propagates upstream, lowering the elevation of the riverbed. The knickpoint carries the signal upstream of the amount of base-level fall to which the landscape must respond, such amount being given by the knickpoint relief (ΔZ). The model in Figure 6.15 indicates that once the knickpoint has migrated upstream, the former stream profile is re-established. Such condition and adjustment implies that incision rates below the knickpoint, once it has passed, return to their former values, reflecting the re-establisment of the pre-knickpoint channel gradient.

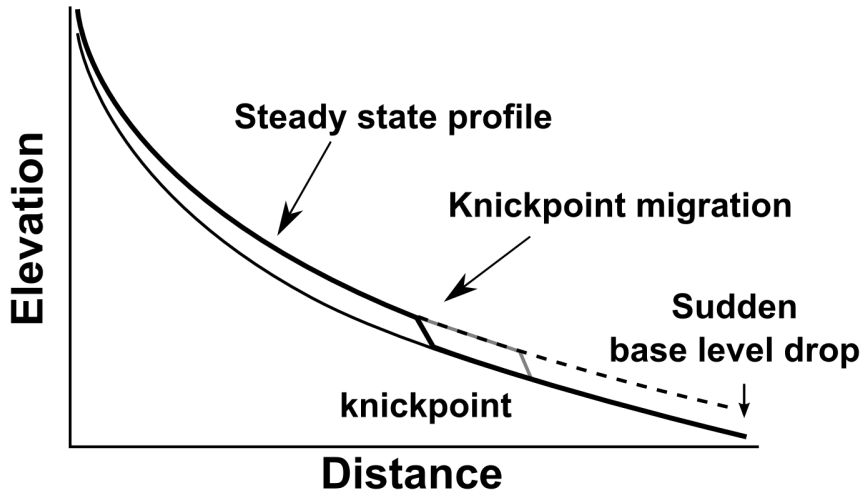

Figure 6.15: Knickpoint propagation after a sudden drop of base-level fall in steady-state long profile (Whipple and Tucker, 1999Modified from:). The base-level generates a shift on riverbed elevation resulting in the re-establishment of the former incision rates once the knickpoint has migrated upstream.

As has been demonstrated in the previous chapters, the channel slope of the

streams of Jura is not scaled to downstream distance, this condition strongly indicating a non steady-state on streams. However, the base-level lowering and subsequent knickpoint propagation has occurred as in the case of steady-state streams, with very orderly scaling of knickpoint retreat distance to catchment area. The response in the non-steady state streams to a base-level lowering pulse seems to confirm that the links between stream incision, climate and tectonics are related to the knickpoint propagation, but whether incision rates after the knickpoint propagation are reset in the reaches downstream of the knickpoint is not known.

The morphological response of rivers to the base-level fall assessed through the concavity index indicates that streams with low drainage area (< 5 km^2) are mainly convex from the 13.6 ka knickpoint to the 13.6 shoreline. Such convexity can be interpreted as a migrating knickzone as has been observed to in other active tectonic areas (e.g. Whittaker et al., 2008; Attal et al., 2011). Also the lack of scaling of channel slopes with the stream discharge downstream of the 13.6 ka knickpoints suggest that rivers have not fully absorbed the base-level fall. Moreover, for the case of large rivers, the propagation of younger knickpoints (i.e., younger than 13.6 ka and likely to be triggered after the Younger Dryas) are likely to be propagating upstream due to the high discharge prevailing in those streams. The slow response of the bedrock rivers of Jura to the base-level fall is likely to maintain high incision rates downstream of the 13.6 ka knickpoint. This can be demonstrated by (1) the lack of scaling of channel slope with the drainage area downstream of the 13.6 ka knickpoints and (2) the tendency observed in rivers in having steep slopes downstream of the 13.6 ka knickpoint, condition that points to an increase in the stream power towards the stream outlet that may result in high incision rates (Figure 6.16).

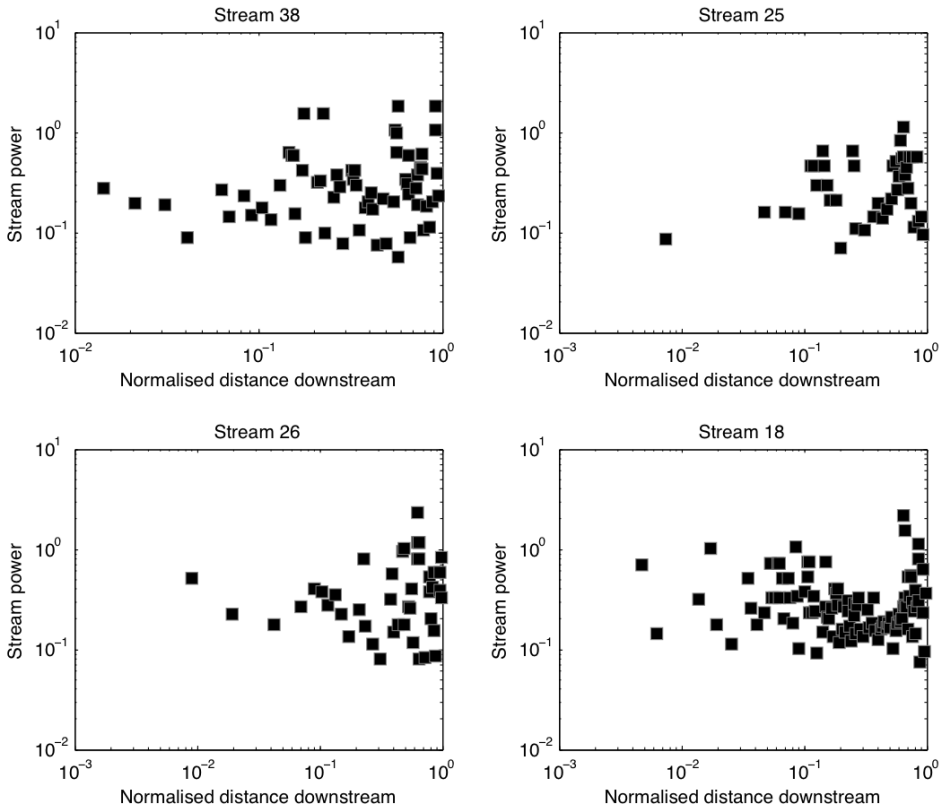

Figure 6.16: Plots of the stream power (simplified here by the product of drainage area and the channel slope) against the normalised distance from the 13.6 ka knickpoint to the stream mouth. In all cases it can be observed that the stream power increases at the mouth of streams, indicating that these zone is dominated by steep reaches (knickzones).

The main hypothesis tested here is that the incision rates on the reaches located upstream of the 13.6 ka knickpoint are equal to erosion rates on the reaches located downstream, as is expected from theory (Figure 6.15). The alternative hypothesis states that the erosion rates are not necessarily equal, therefore, incision rates can be higher on the reaches located downstream of the knickpoint. To test these hypotheses eight pilot testing sites on two streams were selected (Figure 6.18). The eight cosmogenic samples were extracted from the riverbed from smoothed and polished surfaces where abrasion has been the dominant mode of bedrock erosion. Those

surfaces where there is evidence of plucking were avoided (Figure 6.17). However, the possibility that the sampling sites have been plucked at some time in the past remains.

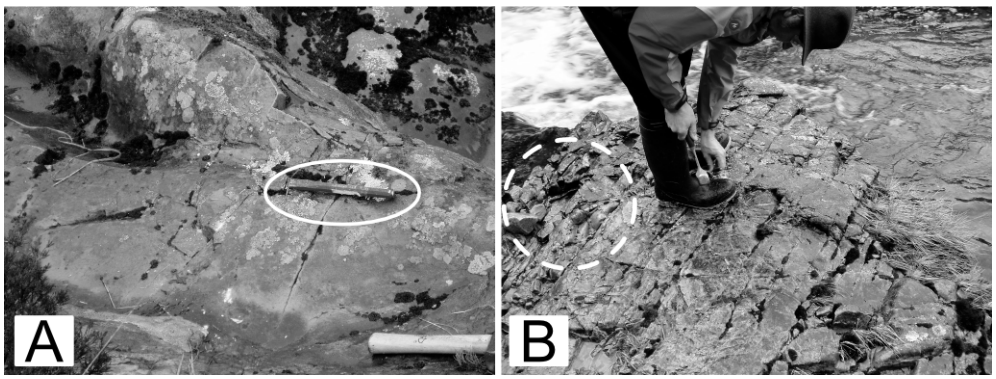

Figure 6.17: The photographs show the types of surfaces where the cosmogenic samples were extracted. In A a smoothened bedrock surface, the chisel circled is used for scale. In B is shown a fractured bedrock surface, the samples were extracted avoiding surfaces where plucking has taken place (white dashed circle).

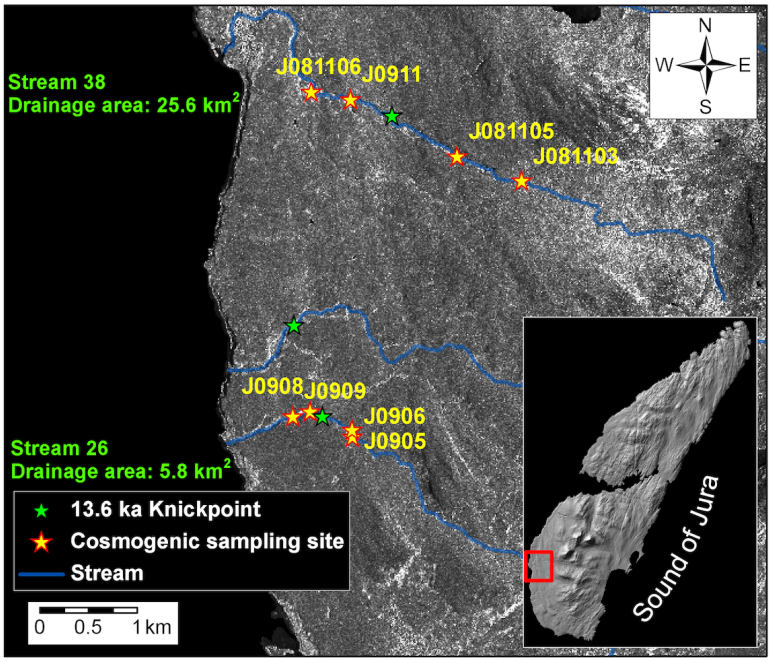

Figure 6.18: Cosmogenic sampling sites upstream and downstream of the 13.6 ka knickpoints of stream 38 and stream 28.

At each sampling site, the location was recorded using handheld GPS and ~ 1 to ~ 2 kg of rock ($\sim$2 cm of thickness from the surface) was collected. The shielding due to topographic obstacles was measured at each sampling site reading the inclination of the object referred from the sample with a portable inclinometer and registering the azimuths of that shielding with a compass. Using the 5 m resolution DEM the elevation was determined for each sampling site. The data for the cosmogenic samples is presented in Table 6.3.

Table 6.3: Sites coordinates and laboratory codes for the cosmogenic samples extracted on Jura

Sample code	Coordinate (Decimal degrees)	Elevation (m OD)	Shielding factor
J081103	55.8561, -6.0424	179	1.0
J081105	55.8583, -6.0514	122	0.9
J081106	55.8635, -6.0758	38	0.9
J0905	55.8322, -6.0656	72	1.0
J0906	55.8328, -6.0672	68	1.0
J0909	55.8321, -6.0792	36	0.9
J0911	55.8630, -6.0701	50	0.8
J0908	55.8330, -6.0772	38	0.8

6.3.3 Processing of cosmogenic samples in laboratory

The Jura cosmogenic samples (6.18, Table 6.3) were processed at the Centre for Geosciences Cosmogenic Nuclide Laboratory (CG-CNL) in the University of Glasgow and the Scottish Universities Environmental Research Centre (SUERC). The mineral separation and quartz cleaning were completed at the CG-CNL and the chemistry to obtain the ^{10}Be hydroxide is made at SUERC where the AMS measurements are also done. The processes described here are detailed in the procedure manual of the CG-CNL and the information provided here is to illustrate briefly how the samples were processed. The procedures follow at the CG-CNL to obtain ^{10}Be are similar to those reported elsewhere (Nishiizumi et al., 1993; Bierman, 1994; Gosse and Phillips, 2001). The process to obtain the cosmogenic ^{10}Be targets for the AMS is summarised in Figure 6.19 and in Appendix H.

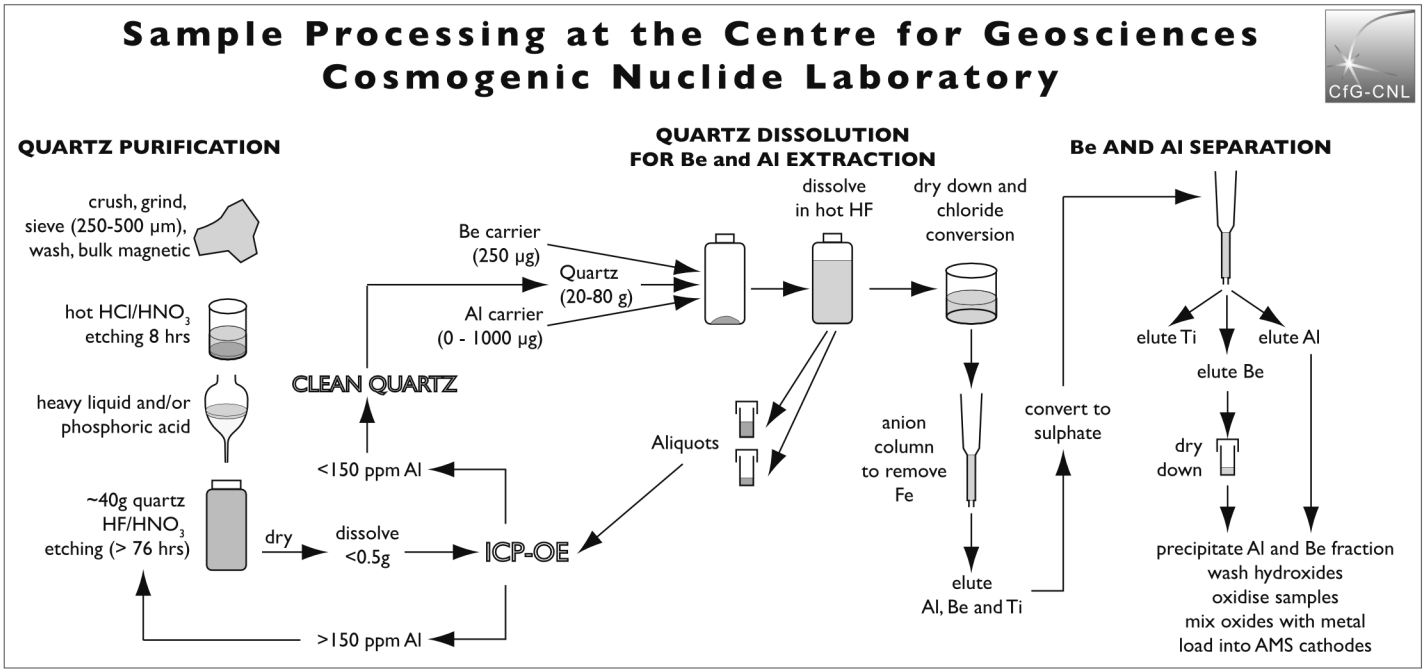

Figure 6.19: Processing of rock samples to obtain targets of to estimate the TCN ^{10}Be. Figure courtesy of Dr. Derek Fabel.

6.3.4 Bedrock incision incision rates using *in situ* produced ^{10}Be

The measurements performed in the AMS Laboratory at SUERC on the Jura samples are presented in Appendix I. The AMS results provide only the $^{10}Be/^{9}Be$ ratios. The concentration of cosmogenic ^{10}Be atoms has to be calculated along with the uncertainties, of nuclide concentration and in the blank. For this purpose the Cronus-Earth calculator (Cronus-Earth Project, 2010) was used (Appendix J).

The cosmogenic incision rates obtained are presented in Table 6.4 and the locations of the data on the stream profile is presented in Figure 6.20. Incision rates downstream of the 13.6 ka knickpoint are high, rates are lower downstream as it would be expected in theory (Figure 6.15). Thus, the initial hypothesis posed here is rejected and the hypothesis of high incision rates downstream of the knickpoints is accepted.

Table 6.4: Production and incision rates of the ^{10}Be samples extracted in Jura. The incision rates presented correspond to the model of Lal (1991) and Stone (2000).

Sample ID	**^{10}Be muons (atoms/g/yr)**	**Erosion rate (gr/cm^2/yr)**	**Erosion rate (m/Myr)**	**σ (m/Myr)**	**^{10}Be spallation (atoms/g/yr)**
J081103	0.193	0.03499	132.03	12.50	5.50
J081105	0.189	0.14247	537.64	131.59	4.92
J081106	0.184	0.10745	405.47	53.50	4.32
J0905	0.186	0.07950	299.99	38.69	4.90
J0906	0.185	0.04218	159.17	15.74	4.76
J0908	0.184	0.05504	207.69	25.73	4.04
J0909	0.183	0.06666	251.55	28.64	4.26
J0911	0.184	0.13430	506.80	92.57	4.00

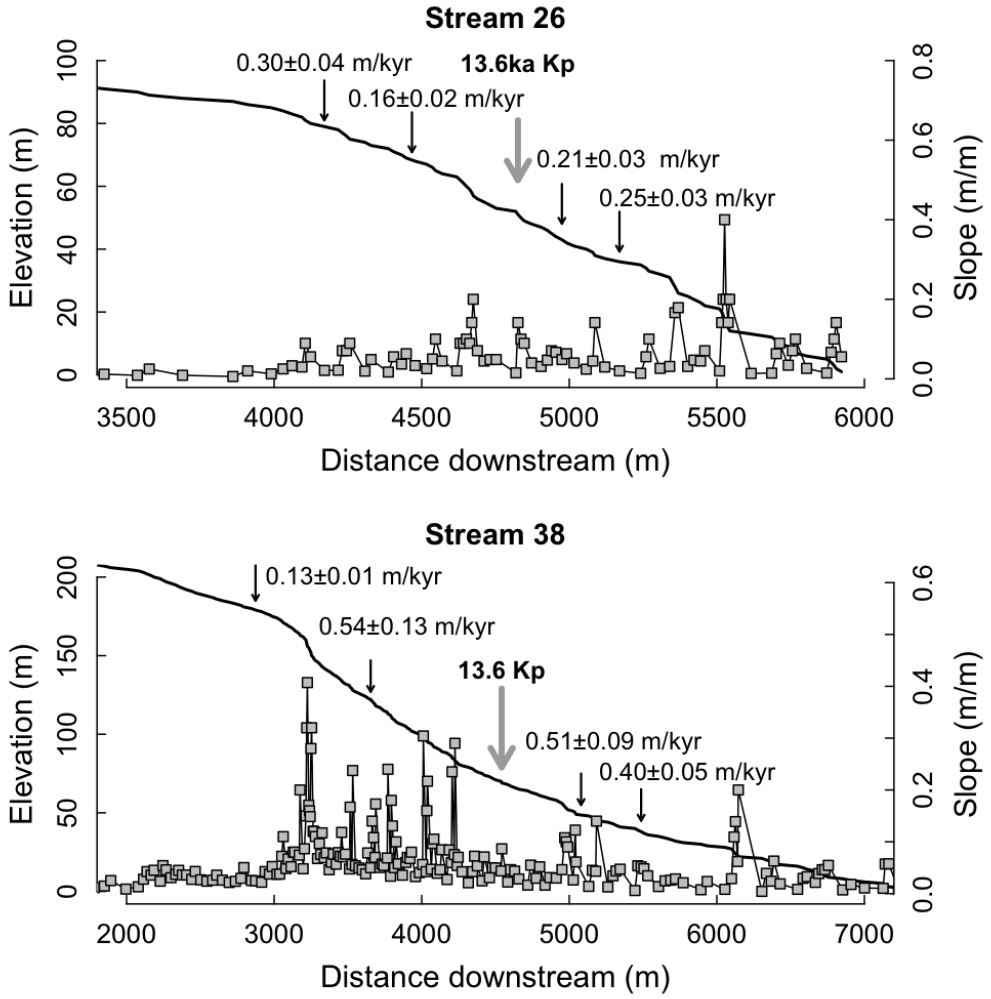

Figure 6.20: Incision rates estimated from cosmogenic ^{10}Be obtained from steams 26 and 38 of the isle of Jura. Note that the high incision rates are related to those reaches where there is the channel slope are steep.

The incision rates observed upstream of the 13.6 ka knickpoint do also exhibit at first glance, an unexpected behaviour as long as in two samples on streams 26 and 38 high incision rates have been recorded. Low values would be expected in the upper reaches (above the 13.6 ka knickpoint) assuming that these are not affected by the knickpoint or knickzone migration has occur in areas under tectonic

forcing (Snyder et al., 2000; Whittaker et al., 2007; Attal et al., 2011) (Figure 6.20). The high incision rates observed upstream of the 13.6 ka knickpoint indicates that non-base-level fall knickpoints are related to high bedrock incision rates. The high incision rate observed on stream 26 (i.e., 0.30 m/kyr located at $\sim$ 85 m OD) (Figure 6.20) is somewhat unexpected because downstream the rate is of $\sim$0.1 m/kyr. It should be noted though, that the reaches sampled upstream of the 13.6 ka knickpoint on stream 26 have step slopes and small knickpoints are likely to have an effect on the incision rates as can be confirmed by the lack of adjustment of channel slope with the increase of distance downstream. The rates of incision downstream of the 13.6 ka knickpoint on stream 26 suggest that these are likely to be controlled by steam discharge and the local channel slope.

The effect of non-base-level fall kncikpoint on incision rates is clearer for the case of stream 38 (Figure 6.20). The incision rate of 0.54 m/kyr found on the reach located upstream of the 13.6 ka knickpoint is located in a zone where channel slope steepens abruptly, such steepening in channel may be responsible of promoting an increase in the incision rate. The high incision rate recorded above the 13.6 ka knickpoint contrasts when it is compared to the incision rate estimated in the reach above, in this case the incision rate drops and the reach seems to be unaffected by a channel steepening. The incision rates downstream of the knickpoint seems to variate as a function of the change in the local channel slope as can be observed in the change in rates from 0.5 m/kyr to 0.40 m/kyr on the profile in Figure 6.20. The relationship between the incision rates and the channel slope is more evident when these value are plotted (Figure 6.21) and where it can be appreciated that the incision rates increase when the channel slope is steepens.

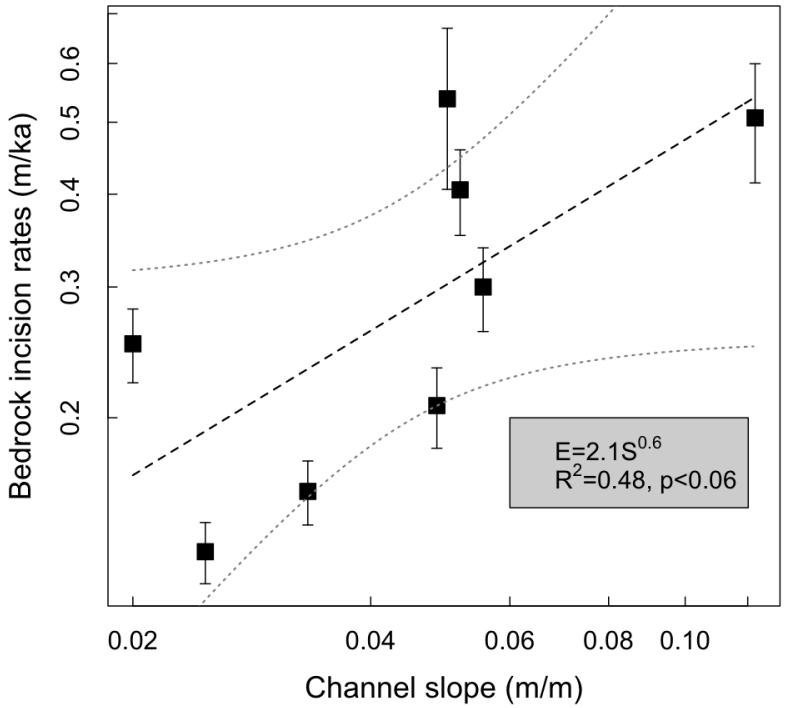

Figure 6.21: Regression between cosmogenic bedrock incision rates and the channel slope at the sampling site. Although the correlation is week, the plot reveals that channel slope controls partially, the bedrock incision rates of Jura streams.

Estimating the former incision rates previous to the base-level fall for the streams of Jura is challenging because the steams carry a strong imprint of glacial processes, meaning that the fluvial reaches upstream of the base-level fall knickpoint are also in transience. The sampling sites selected to obtain the pre-knickpoint incision rates were located close to the base-level fall knickpoint in order to avoid capturing the incision rates from the strongly glacial headwater reaches (Figure 6.18). However, the channel steps located above the 13.6 ka knickpoint indicate that the glacial signals are likewise present at lower elevation. This condition makes it difficult to test a knickpoint retreat model as show in Figure 6.15 but the drop of the incision

rates observed in upstream 13.6 ka knickpoint when there is not an abrupt changes in the steepening of channel slope suggest that a these incision rates may represents the pre-knickpoint incision rates when there is no effect of glacial steeps.

Accepting the alternative hypothesis that states that incision rates after a knickpoint propagation are higher than the former incision rates is supported by: (1) the results obtained from the DS model that show the non-scaling of channel slopes to stream discharge and the presence of steep slopes close to the stream outlet (Appendix B) (2) the relation between the incision rates and the channel slope (6.21) in which the presence of steep slopes downstream of the base-level fall knickpoint are common, (3) the low values in the concavity index of rivers which suggest a slow morphological response of rivers to the base-level fall and the predominance of in some cases, of a convex profile and finally, (4) the increase of stream power toward the stream's mouth (Figure 6.22) condition that can be also observed in rivers 26 and 38 in which high stream power can be interpreted as proxy of channel incision (Finlayson and Montgomery, 2003; Montgomery, 2003) (Figure 6.23).

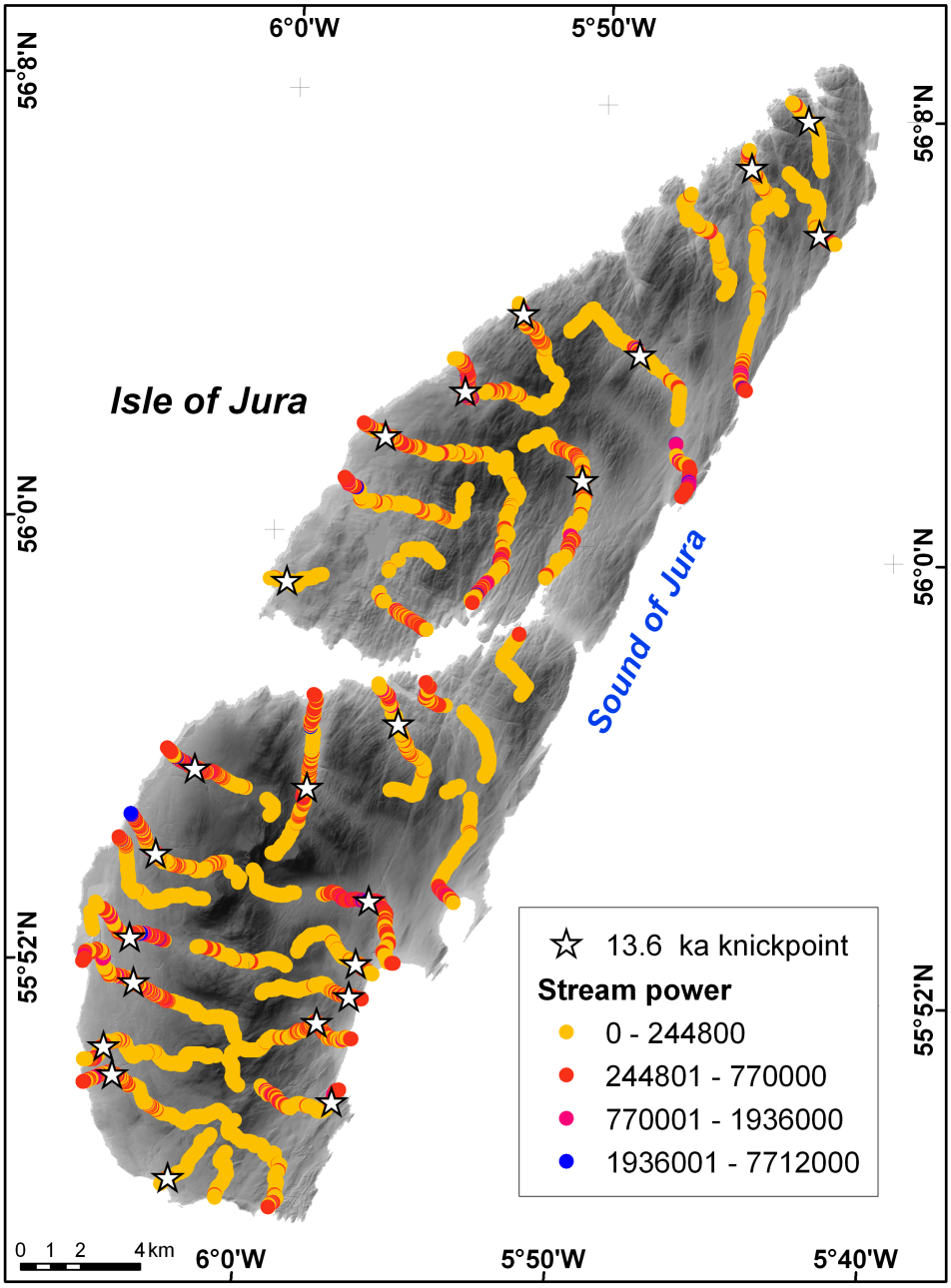

Figure 6.22: Map of the stream power of the rivers of Jura. High stream power values can be observed at the mouth of streams and persistent downstream of the base-level fall knickpoints. High stream power values at the mouth of streams suggest higher incision rates than in the upper reaches.

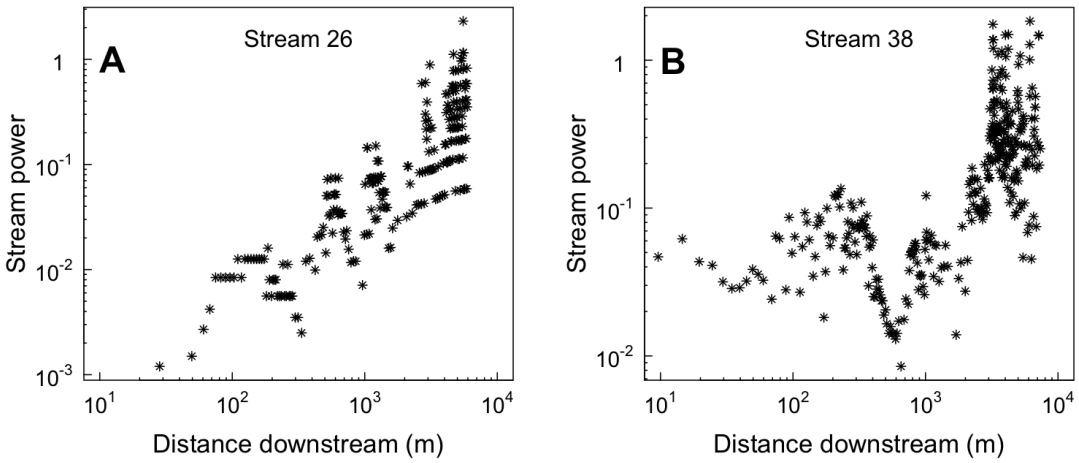

Figure 6.23: Plot of the stream power against the distance downstream for streams 26 and 38. In both cases, stream power increases toward the stream mouth, condition suggesting high incision rates due to the presence of steep reaches.

The theoretical response of incision after knickpoint propagation, as depicted in Figure 6.15, fails for the case of small bedrock rivers in active tectonic settings since younger knickpoints which are not necessarily associated with a strath-terrace, propagate headwards leaving small steps on channel that delay the resetting of the former incision rates (Figure 6.24). This condition seems to operate in Jura where also the concavity index indicates that the rivers response to the base-levell fall depends on streams capacity to incise channels which is dependent on the drainage size and the local channel slope. Small (low drainage area) rivers in active tectonic settings are likely to have steeper slopes than the large drainage area rivers because of the lower capacity of small rivers to transport sediment and incise into their bed (Whittaker et al., 2008; Cyr et al., 2010; Attal et al., 2011).

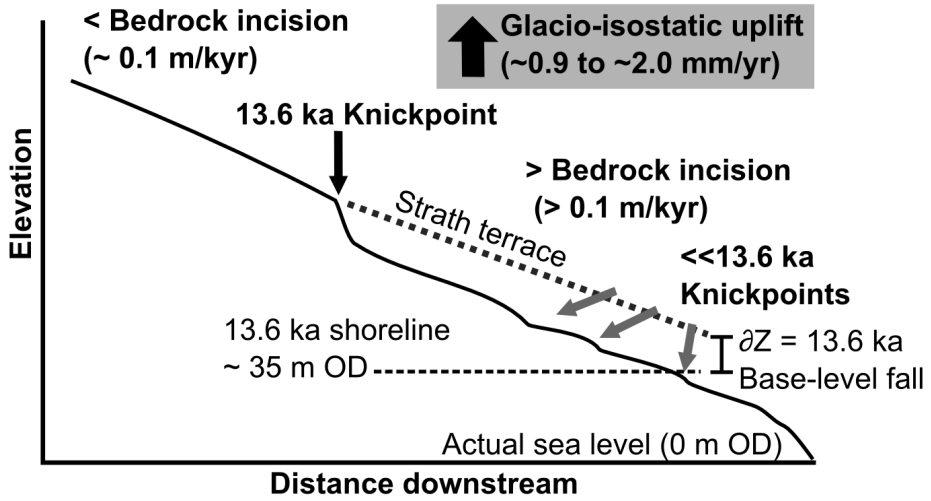

Figure 6.24: Conceptual model of the bedrock incision responding to a base-level fall event in Jura. Assuming that the reaches upstream of the 13.6 ka knickpoint are not strongly perturbed, the high incision rates downstream of the 13.6 ka knickpoint do not adjust to the former incision rates due to the propagation of younger knickpoints. The uplift rates shown in the grey box correspond to the estimations of Firth and Stewart (2000)

6.4 Testing TCN-derived erosion rates against fluvial erosion model predictions

Uncertainties surrounding the incision rates from TCNs concentration arise mainly from nuclide concentrations at depth as the bedrock surface is being eroded. The steady-state erosion model assumes a situation in which the bedrock lowering is occurring by constant and continuous erosion at the granular to small chip scales, a condition corresponding to bedrock abrasion. All the sites investigated here using TCNs are dominated by smooth, fluted bedrock surfaces, as would be expected under conditions of abrasion. In bedrock rivers, plucking is perhaps the main mechanism controlling bedrock incision, however (Howard et al., 1994; Whipple and Tucker, 1999). The removal of slabs in bedrock channels is likely to dominate even when abrasion also takes place. This process is problematic because the concentration of TCNs on a plucked surface is lower than for steadily abrading surface and therefore overestimates the incision rate (because large slabs of rocks have been removed). Assessing the effects of plucking on the TCNs is required to assess the accuracy of the incision rates. Numerical models introducing the episodic events of erosion on bedrock surfaces (e.g., Brown et al., 1995; Muzikar, 2008; 2009) are becoming useful in estimating more accurately the incision rates into bedrock but they require the record of the climatic events that have prevailed on the landscapes and are likely to produce the episodic removal of bedrock.

The consistency of the erosion rates obtained here from the measurement of TCN concentrations is now tested by comparing the incision rates on the two streams sampled with the formulation of the stream power model. The comparison with the model that incorporates the effect of sediment on bedrock incision is also undertaken. It is acknowledged here that a model that incorporates the effect of plucking on the concentration of TCN production is required but for the purpose of this research the consistency bedrock incision rates obtained from cosmogenic nuclides with those from the stream power model is adequate to answer the questions formulated for this study.

6.4.1 Cosmogenic incision rates vs the stream power model approach

The simplest approach to test the validity of bedrock incision rates using the cosmogenic approach (Table 6.4 and Figure 6.20) is by comparing the rates with the drainage area. In this case, incision is driven solely by stream discharge. A second variation of this approach is to use the stream power which can be approximated by simply multiplying the stream discharge and the local channel slope. For every site sampled, the stream discharge and the local channel slope were determined using the available information from the stream profiles already produced. The two models tested are presented in Figure 6.25.

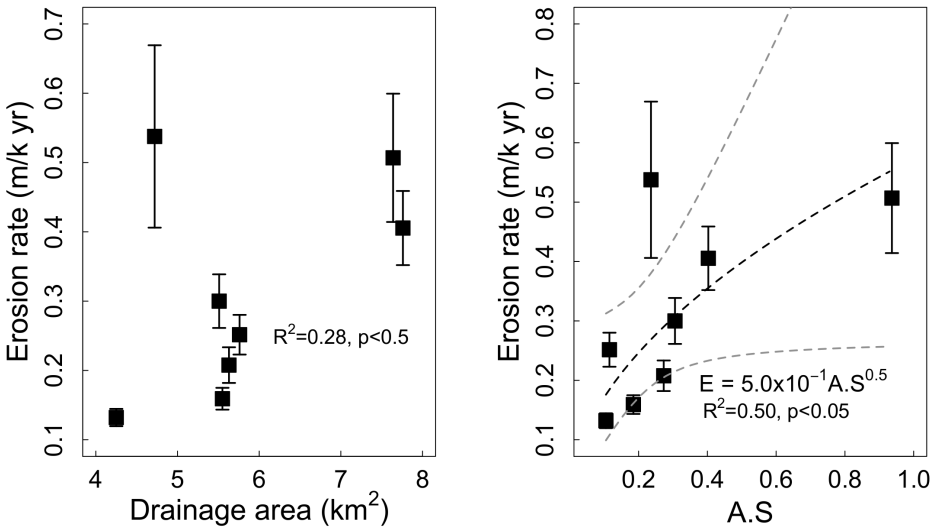

Figure 6.25: Relationship between the cosmogenic bedrock incision rates and the stream discharge (left) and unit length stream power model (right plot). Error bars correspond to the uncertainty of the incision rates (see table 6.4).

At first glance the TCN-derived incision rates do not scale at first glance with

drainage area (Figure 6.25). The incision value of 0.54 m/kyr seems to break the apparent trend that other incision rates follow. The incision rate of 0.54 m/kyr was obtained from a reach located on a glacial knickzone on stream 38 (Figure 6.20) and it is considered as an outlier because these reaches are extremely perturbed by abrupt glacial steps that increase the channel incision. A moderate correlation is observed when the erosion rates are a function of the local stream power (Figure 6.25). The 0.53 m/kyr point lies outside off of the 95% confidence limits, situation that confirming its condition as an outlier.

The moderate correlation observed on the right-hand plot of Figure 6.25 suggests that stream power controls the incision rates on bedrock channels. In order to confirm if this is the case the outlier value of 0.54 m/kyr was removed and the regressions were performed again (Figure 6.26). The correlation model improved significantly for the two models and confirms that the Jura incision rates depend on drainage area and local channel slope.

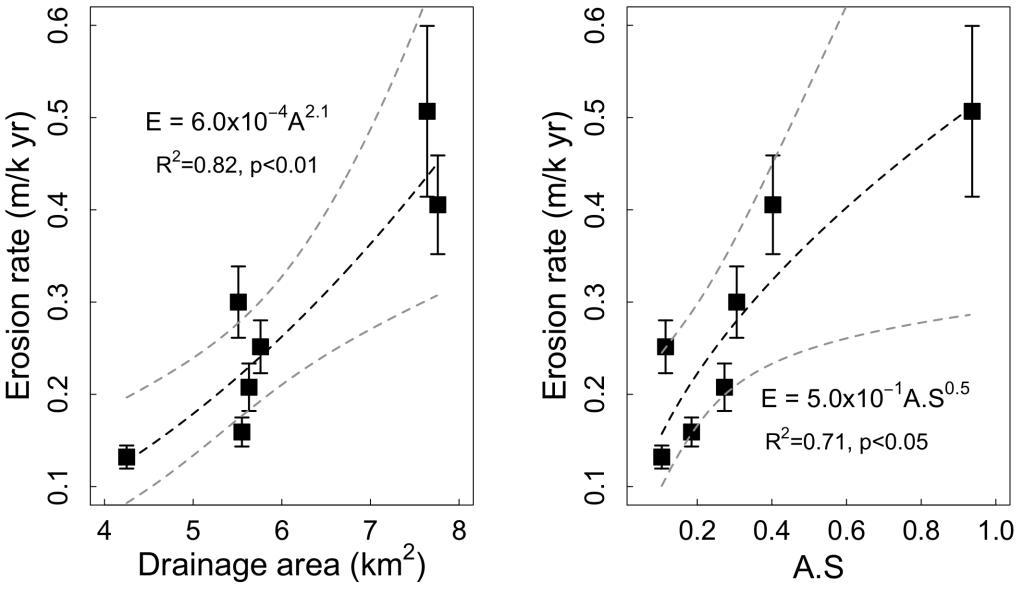

Figure 6.26: Model of the bedrock incision response as function of drainage area and stream power model by using seven sites.

The unit length stream power model is likely to be the best predictor as all the incision rate values fall in the 95% confidence limits. The results in Figure 6.26 demonstrate two things: (1) the validity of the stream power model to predict bedrock incision as the detachment-limited model indicates (Howard et al., 1994; Whipple and Tucker, 1999), and (2) the applicability of TCN analysis to estimate incision rates. Using the shear stress model (Howard and Kerby, 1983; Howard, 1994) a good correlation was observed but this model has been discarded due to the high p-value observed in the regression model (Table 6.5).

Table 6.5: Regression coefficients of the shear stress model to predict the bedrock incision rates. The equation is shown at the bottom of the table and the R^2 and p-values respectively.

Coefficients	**Estimate**	σ	**t-value**	$Pr(>\|t\|)$
Intercept	-4.63	7.0406	-0.656	5.5×10^{-2}
Log(Drainage)	2.16	3.6470	0.593	5.9×10^{-2}
log(Slope)	-0.06	2.0772	-0.030	9.8×10^{-2}
Equation: $E = 9.8 \times 10^{-3} A^{2.16} S^{-0.06}$				
$R^2 = 0.85, p - value : 9.0 \times 10^{-3}$				

The outlier of Figure 6.25 has interesting implications for considering fluvial incision into bedrock. The high rates obtained for the outlier located on the glacial knickzone indicate that channel incision largely depends on the stream discharge and the local channel slope. The incision rates above the 13.6 ka knickpoint would be expected to be low if channel were not perturbed by glacial steps in such a case, the stream power would be also low however, the abrupt steepening at even low drainage area suggests that bedrock incision might respond as a function of the local channel slope as was envisaged for bedrock rivers by Gilbert (1877) but also, a change in channel width given by a narrowing would be expected as occurs in rivers where channel width is affected by a tectonic forcing (Amos and Burbank, 2007; Finnegan et al., 2005; 2007; Attal et al., 2011). Although it is possible that the reach sampled might have experienced recent plucking that resulted in a low concentration of ^{10}Be, the plot of stream power as a predictor of bedrock incision rates indicates that if channel slope is high, the incision rates increase. The dependence of channel incision on channel slope at even low drainage areas has further implications for the propagation of knickpoints, which can migrate headwards even if these are located on low drainage areas.

Even though the stream power model has a simple form, it seems to capture the processes that control the rate of bedrock incision. Nevertheless, the effect of

sediment is not known when this approach is used. In the following section the possible effect due to sediment flux is evaluated.

6.4.2 Bedrock incision rates and the effect of sediment

The effect of sediment on bedrock channel incision has been discussed by, for example Beaumont et al. (1992); Sklar and Dietrich (1998; 2004; 2006) and Whipple and Tucker (2002). Here a simplification of the saltation-abrasion model of Sklar and Dietrich (2004; 2006) is used to asses the role of sediment in bedrock channel incision. The general generic equation used for channel incision (E_i) is (Sklar and Dietrich, 2006):

$$E_i = K_\gamma \gamma Q_s \left(1 - \frac{Q_s}{Q_t}\right) \left[1 - \left(\frac{u^*}{w_f}\right)^2\right] \tag{6.9}$$

where K_λ is a dimensional coefficient of erosion, γ is used to measure the stream power or flow intensity which vary according to the model tested, Q_s corresponds to the total sediment flux (kg/s), Q_t is the sediment transport capacity (kg/s) and the term in brackets estimate the impact of grains on the bedrock surface where u^* is the shear velocity and w_f is the grain fall velocity of still water. An advantage of using equation 6.9 is that several models of bedrock incision can be parameterized (Sklar and Dietrich, 2006, Table 2, Figure 4) to evaluate the different process involved in channel incision.

The equation 6.9 can be written in a dimensionless form to obtain dimensionless bedrock incision rates (E_*), this is written as (Sklar and Dietrich, 2004):

$$E^* = k3 q_s^* (1 - q_s) \left[\frac{\tau^*}{\tau_c^*} - 1\right] \left(1 - \left(\frac{u^*}{w_f}\right)^2\right)^{3/2} \tag{6.10}$$

where $k_3 = 0.46 R_b^{3/2} \tau_c^*$ and $q_s = Q_s/Q_t$. To estimate the bedrock channel incision using equation 6.10 several parameters must previously specified. The input vari-

ables required to solve E^* are shown in Table 6.6 and the results obtained as well as the hydraulic geometry of the sites analysed (i.e. cosmogenic sampling sites) are summarised in Table 6.7.

Table 6.6: Input variables used to estimate the bedrock channel incision and other hydraulic variables on cosmogenic sampling sites.

Inputs	**Value/unit**
Channel slope (S)	(m/m)†
Channel width (W)	(m)†
Flow depth(H_w)	(m)†
Sediment diameter (D_s)	0.045 m
Non-dimensional critical shear stress (τ_c^*)	0.030‡
Sediment density (ρ_s)	2650 kg/m^3
Sediment water density (ρ_w)	1000 kg/m^3
Gravity constant (g)	9.81 m/s
Sediment flux (Q_s)	kg/s§
Rougnhess (n)	0.035‡

† Value observed on the cosmogenic sampling site
‡ Assumed value
§Assumed values: 25, 50, 75 and 100 kg/s

For the case of the sediment size the fraction of 0.045 m which is representative for this setting (Table 6.1), has been used. The channel width has been estimated using the power law scaling of Jansen et al. (2010), who analysing the rivers of Scotland found that in a quartzite lithology, for drainage areas between 2.2 to 181 km^2, channel width (W) scales to drainage area with equation:

$$W = 0.13A^{0.26} \tag{6.11}$$

Because the streams of Jura are more or less in the same climate and lithology as the rivers evaluated by Jansen et al. (2010), equation 6.11 can be used to confidently estimate the channel width of the rivers of Jura. The flow depth (H_w) was estimated

Table 6.7: Data of discharge (Q), channel width(W), channel slope (S), flow depth (H_w), hydraulic radius (R_h), flow velocity (u), basal shear stress (τ_b), dimensionless shear stress (τ^*), transport stage ($\tau^*\tau_c^*$), shear flow velocity (u^*), sediment transport capacity (Q_c) and shear flow and particle setting velocity ratio (u^*/w_f) obtained for every cosmogenic sampling site to solve equation 6.10. See text for details for how the else eight variables were calculated

Site	Q_w	S	W	H_w	R_h	u	τ_b	τ^*	$\tau^*\tau_c^*$	u^*	Q_c	u^*/w_f
Decimal degrees	**(m^3/s)**	**(m/m)**	**(m)**	**(m)**	**(m)**	**(m/s)**	**(Pa)**			**(m/s)**	**(kg/s)**	
55.8561, -6.0424	6.8	0.0247	6.90	0.25	0.23	1.7	56	0.08	2.58	0.24	41	0.25
55.8583, -6.0514	7.6	0.0500	7.10	0.20	0.19	2.1	93	0.13	4.25	0.30	125	0.33
55.8635, -6.0758	12.4	0.0519	8.00	0.31	0.29	2.8	146	0.20	6.70	0.38	328	0.41
55.8322, -6.0656	8.8	0.0555	7.40	0.22	0.21	2.4	113	0.16	5.17	0.34	190	0.36
55.8328, -6.0672	8.9	0.0333	7.40	0.28	0.26	2.1	85	0.12	3.89	0.29	110	0.31
55.8321, -6.0792	9.2	0.0200	7.40	0.35	0.32	1.9	63	0.09	2.87	0.25	57	0.27
55.8630, -6.0701	12.2	0.1226	8.00	0.22	0.21	3.5	251	0.34	11.48	0.50	818	0.54
55.8330, -6.0772	9.0	0.0485	7.40	0.24	0.23	2.3	107	0.15	4.91	0.33	172	0.35

by solving iteratively the discharge on a trapezoidal channel, thus:

$$Q = \frac{1}{n}\frac{A^{2/3}}{P2/3}S^{1/2} \tag{6.12}$$

where Q is the discharge, n is the channel roughness, A is the cross sectional area, P the wetted perimeter and S is channel slope. For the channel roughness a value of $n = 0.035$ has been used as this represent the condition prevailing on natural channels (Knighton, 1998) and this value has also been used for evaluating the effect of sediment on abrasion (e.g., Sklar and Dietrich, 2004; Turowski et al., 2007). For the dimensionless critical shear stress a value of $\tau_c^* = 0.030$ has been selected because this value is in the range of the dimensionless critical shear stress of rough flows with high Reynold's number (> 500) (Buffington and Montgomery, 1997) and because given the steep channels in Jura, a low critical shear stress value is likely to be enough to start the grain motion. The values of sediment flux (Q_s) used to estimate the dimensionless erosion rate show in equation 6.10, have been assumed since no field-based data exists of the sediment supply of the rivers of the west of Scotland. The Qs values used here are close to the range of values estimated by Sklar and Dietrich (2004) for the South Fork Eel River in California (USA). The sediment supply rate for the Sourth Fork Eel River is of ~ 42.6 kg/s at a discharge of ~ 39.1 m^3/s. Higher sediment supply rates for bedrock abrasion have been used by Turowski et al. (2007) who estimated a sediment supply rate for the Lushui river of ~ 263 kg/s. The rivers of Jura receive less discharge than in the South Fork Eel River and the Lushui river and the complete armouring of bed in Jura streams suggest that the sediment supply is limited. For these reasons, a range of values from 25 kg/s to 100 kg/s are considered here optimum to evaluate the effect of sediment supply for the rivers of Jura since these fall in the range of values reported for larger rivers but these do not exceed the values for rivers with high sediment supply (e.g. Lushui river).

The parameters shown in Table 6.7 were mostly based on the same equations

used by Sklar and Dietrich (2004; 2006). The hydraulic radius (R_h) has been estimated using equation (Sklar and Dietrich, 2006; Turowski et al., 2007):

$$R_h = H_w W/(2H_w + W) \tag{6.13}$$

where H_w is the flow depth (m) and W is the channel width (m). The shear velocity (u) was estimated from the following equation:

$$u = R_h^{2/3} S^{1/2}/n \tag{6.14}$$

where R_h is the hydraulic radius, S the channel slope and n the channel roughness. The boundary shear stress (τ_b) was is estimated from:

$$\tau_b = \rho_w g R_h S \tag{6.15}$$

The dimensionless shear stress (τ^*) was obtained from equation:

$$\tau^* = \tau_b/(\rho_s - \rho w) g D_s \tag{6.16}$$

The transport stage is simply the ratio between the dimensionless shear stress and the non-dimensional critical shear stress (τ^*/τ_c^*). The flow shear velocity (u^*) is given by:

$$u^* = \tau_b/\rho_w \tag{6.17}$$

The sediment transport capacity (Q_c) was estimated from the equation 4 of Sklar and Dietrich (2006) which is a modification of Fernandez-Luque and van Beek (1976), the sediment transport capacity is obtained from:

$$Q_c = 5.7\rho_s (R_b g D_s^3)^{1/2} (\tau^* - \tau_c^*)^{3/2} \tag{6.18}$$

and finally, for the particle settling velocity (w_f) the equation of proposed by Ferguson and Churh (2006) has been used because its broad applicability in this case

the settling velocity is estimated from:

$$w = \frac{R_b g D^2}{C_1 \nu + (0.75 C_2 R_b g D^3)^{0.5}} \tag{6.19}$$

where R_b is the buoyant density, g the gravity constant, D the particle size, C_1 and C_2 are parameters that estimate the shape and smoothness of grains, for this case the values of 20 and 1.1 have been selected for C_1 and C_2 respectively since these relate to natural grains (Ferguson and Churh, 2006).

The role of sediment on bedrock abrasion was evaluated by plotting the dimensionless bedrock incision rates (equation 6.10) against the transport stage and by plotting the ratio between the sediment supply and the sediment transport capacity, both graphics are shown in Figure 6.27.

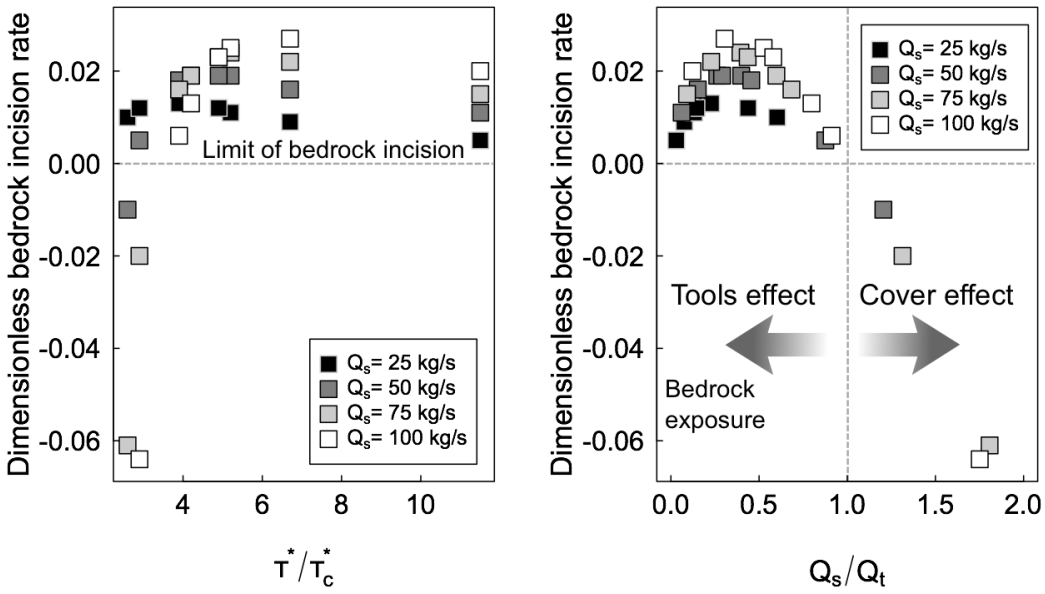

Figure 6.27: The plot on the left shows the response of bedrock incision (dimensionless) as a function of transport stage. Note that an increase in sediment supply prevents the bedrock incision during a low transport stage thus, bedrock incision can only take place for all the sites selected, when the sediment supply is low (Q_s = 25 kg/s). The plot on the right shows the response of bedrock incision (dimensionless) as a function of the tools and cover effect given by the ratio between the sediment supply and the sediment transport capacity (Q_s/Q_t). When $Q_s/Q_t \approx 0.5$ the high bedrock incision rates are likely to occur according to the saltation-abrasion model.

The trend observed for the dimensionless incision rates obtained by the saltation-abrasion model indicates that high bedrock incision rates occur at low transport stages ($\tau^*/\tau_c^* < 10$) (Figure 6.27). The incision rates slightly decline as the transport stage increases. The trend observed for the response of bedrock incision in Jura is consistent with the trend reported by Sklar and Dietrich (2004, their Figures 12 and 13). It must be noted the bedrock incision is possible in all the reaches analysed here when there is a low sediment supply ($Q_s = 25$ kg/s). An increase in sediment supply results in the nullify of bedrock incision at the low values of transport stages (negative values on Figure 6.27).

The tools and cover effect can be appreciated in the second plot of Figure 6.27. In this case the dimensionless bedrock incision rates are compared with the ratio between the sediment supply and the sediment transport capacity (Q_s/Q_t). When $Q_s/Q_t = 1$ the cover dominate and no bedrock incision is possible. The cover effect only takes place at large volumes of sediment flux and this is more important at low transport stages (Figure 6.27). The highest bedrock incision rates occur when $Q_s/Q_t \approx 0.5$ condition which suggest that sediment is used an effective tool for bedrock incision. As long as the sites used here for to test the saltation-abrasion model correspond to the cosmogenic sampling sites which are dominated by bedrock exposure, it is likely that the rivers of Jura have a low sediment supply ($Q_s \leq 25$ kg/s) as the saltation-abrasion model suggest. The low sediment supply in the rivers of Jura is also supported by the frequent bedrock exposure and the low frequency of large bars and sediment patches observed during fieldwork.

The scaling between the cosmogenic bedrock incision rates and the simplified stream power (channel slope times drainage area) (Figure 6.25), indicates that bedrock incision is proportional to the stream power, condition in which plucking is likely to predominate (Howard, 1994; Whipple and Tucker, 1999; Whipple et al., 2000a). The bedrock incision rates predicted by the saltation-abrasion model indicate, on the other hand, that bedrock incision response no-linearly on transport stage. As long as the transport stage increases for the sites selected with the stream power (Figure 6.28) its is unlikely that abrasion dominates the channel incision in the rivers of Jura.

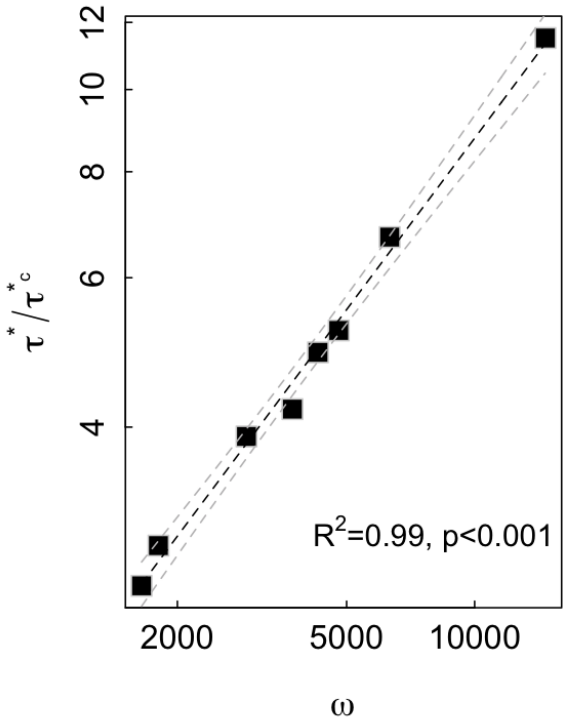

Figure 6.28: Scaling between the transport stage and the stream power (ω).

As long as the scaling between the cosmogenic bedrock incision rates and stream power suggest that the channel incision in Jura rivers respond to linearly to a shear stress as the power model predicts (Whipple and Tucker, 1999), four models were tested: (1) the transport stage model, (2) the parabolic stream power, (3) the modified-alluvial beload (Whipple and Tucker, 2002; Sklar and Dietrich, 2006) and (4) a simplified specific stream power (Snyder et al., 2003; Attal et al., 2011). The four models were tested on the eight cosmogenic sampling sites (Figure 6.18). The transport stage model is given by the dimensionless shear stress and dimensionless critical shear stress ratio. The transport stage model is similar as using the stream power model (Figure 6.28) but in this case the grain size and the hydraulic radius are implicit in the transport stage value (Sklar and Dietrich, 2006). The parabolic stream power was initially proposed by Whipple and Tucker (2002) based

on the early sediment model of Sklar and Dietrich (1998) to incorporate the effect of sediment (tools) to the stream power model. The parabolic stream power model was parameterized assuming that incision is mostly dominated by detachment limited conditions. That is, the model where $n = 2$ (Whipple and Tucker, 2002) was selected resulting in the following equation:

$$E_i = \omega \frac{Q_s}{W} \left(1 - \frac{Q_s}{Q_t}\right) \tag{6.20}$$

where ω correspond to the stream power per unit bed area ($\omega = \rho g Q S / W$). In equation 6.20, the effect of cover and tools is included. In the third model the effect of sediment supply and grain size are considered in the equation expressed as:

$$E_i = (\tau^* / \tau_c^* - 1)^{1.5} \left(1 - \frac{Q_s}{Q_t}\right) \tag{6.21}$$

In the first three models used, the value of γ is replaced by the generic abrasion equation 6.9, depending on the model used. In the cases where the equation uses the value of sediment flux, the lower values has been used (i.e. $Q_s = 25$ kg/s) as long as bedrock incision occurs for all reaches at that value. For the case of the specific stream power model, this has been simplified as:

$$E = \omega / W \tag{6.22}$$

The relationship between the cosmogenic incision rates for each model is shown in Figure 6.29.

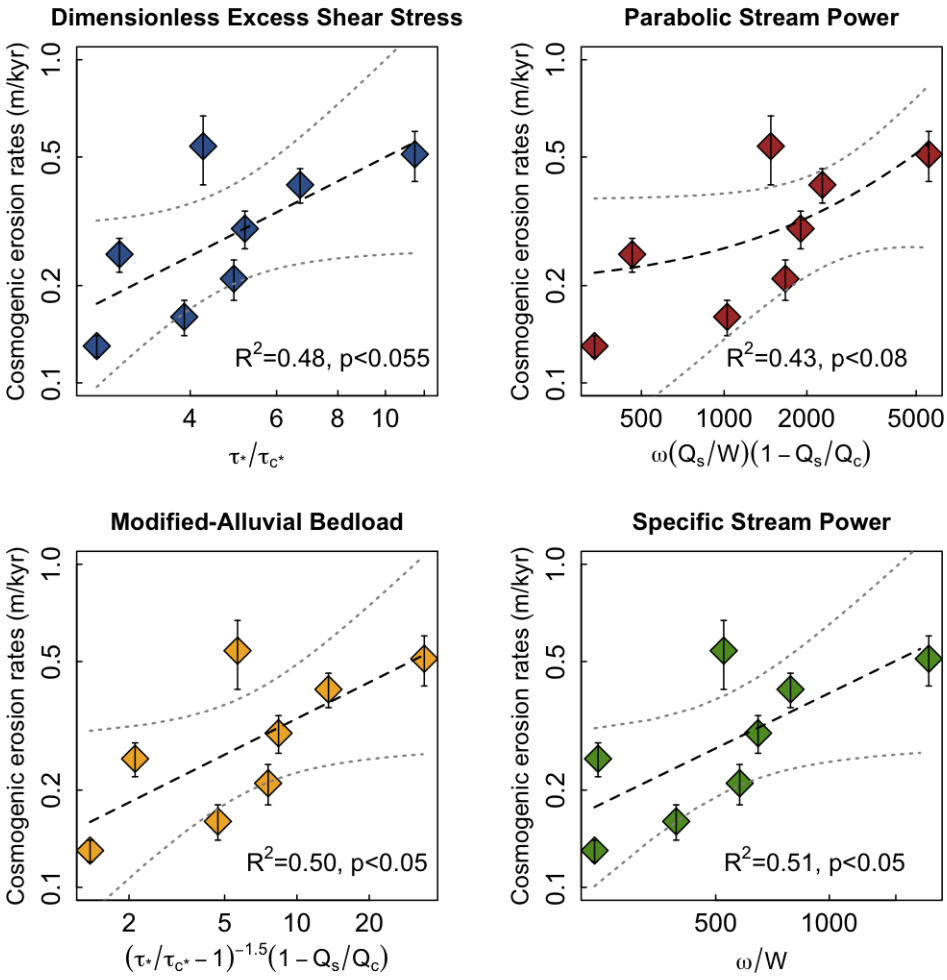

Figure 6.29: Response of the cosmogenic bedrock incision rates to different bedrock incision models (transport statge, parabolic stream power, modified-alluvial bedload and the specific stream power). Note the similar response of these models as predictors of bedrock incision.

The four abrasion models tested have a good correlation when regressed with the cosmogenic incision rates. The similarity of the various models of Figure 6.29 with the incision rates predicted by stream power in Figure 6.26 suggests that stream power is likely to be the main factor controlling bedrock incision. In order to confirm this hypothesis, the erosion rates predicted for each model (i.e., transport stage,

parabolic stream power, modified-alluvial bedload and specific stream power) were normalised by their results and plotted against the stream power (Figure 6.30). The four bedrock incision models are well correlated with stream power. Such strong correlation validates the model shown in Figure 6.26, where stream power is a predictor of bedrock incision rates.

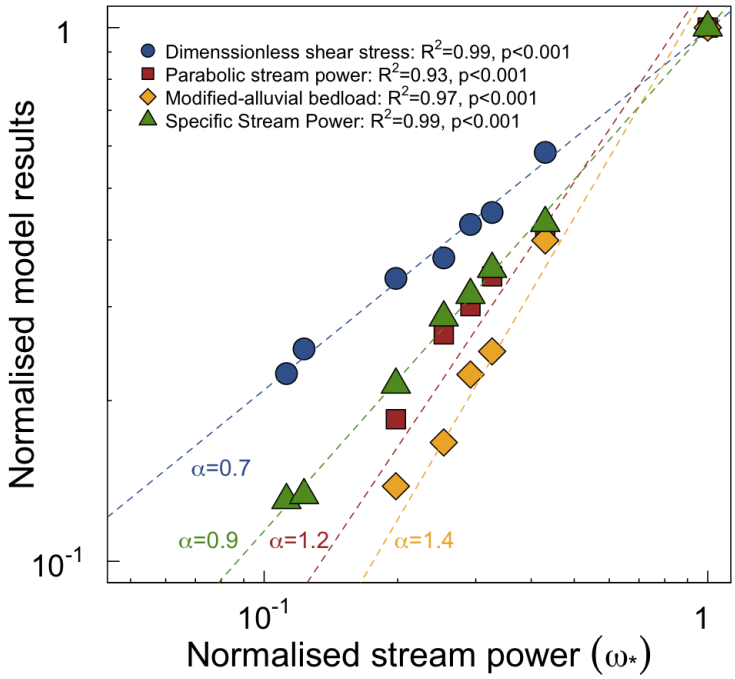

Figure 6.30: Response of the incision rates of four bedrock incision models as function of the stream power. The four models tested are highly correlated to stream power. The bedrock incision rates produced by each model were normalised according to every model. Note that only a change in the exponent of the regression (α) varies according to the model used.

The four bedrock abrasion models used here confirm that the bedrock incision in Jura is driven by detachment-limited conditions as the formulation of the stream

power model predicts. The frequent bedrock exposure and the homogeneous sediment fraction suggest that incision occurs at a $Q_s \approx 25$kg/s or less as the tools and cover effects indicated in Figure 6.27. The findings used here also validate the use of TCNs to obtain bedrock incision rates and the stream power model as a tool to estimate the incision into bedrock.

Although simple in its form, the stream power rule seems to be a reliable tools to bedrock incision, as the results presented here demonstrate. The validity of the saltation-abrasion model is not debated here but its applicability seems to be restricted in fluvial systems where the bedrock incision is combined between mixed alluvial and bedrock reaches. For the case of streams where bedrock is frequently exposed, the detachment-limited conditions incorporated into the stream power model seems to fully capture the processes controlling bedrock channel incision.

6.5 Summary

The analysis of sediment in Jura rivers and estimating channel incision rates using TCNs produced results consistent with the stream power model. Also high incision rates downstream of the 13.6 ka knickpoints seems to be predominating in Jura as the model of stream power and bedrock incision and the increase of stream power downstream of the river of Jura indicate. The main results of this chapter are:

- The grain size distribution in the streams of Jura does not scale with stream discharge and local channel slope. The lack of fining of bed sediment and the extent of bedrock exposure in the channel suggest that the base-level fall is having an effect on the sediment size, presumably by increasing the channel incision and generating unstable hillslopes which may supply more sediment to the rivers.

- The concentration of cosmogenic ^{10}Be atoms were used to estimate bedrock incision rates using the steady-state erosion model (Lal, 1991; Gosse and Phillips, 2001). Bedrock incision rates obtained here are well correlated with the stream power, validating both approaches for estimating bedrock incision. Here it is demonstrated that the re-establishment of the former incision rates after the propagation of a knickpoint does not necessarily occur in an active tectonic settings, as theory predicts. In contrast, incision rates can increase due either to (1) the propagation of younger knickpoints or (2) to a slow lowering of the channel because of low stream power. It is possible that small bedrock rivers require more time to absorb base-levell fall, generating an asynchronous response and delaying the resetting of the former bedrock channel incision rates.

- The effects of sediment are limited in the Jura rivers where the tools are apparently used for rock detachment. This process is likely to predominate as the stream power model predicts for stream incising into bedrock (Howard and Kerby, 1983; Howard et al., 1994; Whipple and Tucker, 1999). Based

on the sediment analysis and the frequent bedrock exposure, it is concluded here that low sediment flux (Q_s <100 kg/s) is required in order to avoid the effect of cover, as the results of the saltation-abrasion model indicate (Figure 6.27). This model does not capture bedrock incision in Jura where plucking is probably the main mechanism of bedrock channel incision, thus limiting the applicability of the saltation-abrasion model to mixed-alluvial bedrock rivers.

- Testing the cosmogenic bedrock incision rates with different bedrock erosion models (Figure 6.29) has been useful to demonstrate the usefulness of the stream power model to assess the bedrock channel incision of the landscape. The consistency observed between the TCN-based and the stream power model is a promising area which can be exploited to solve long-standing problems in obtaining rates of bedrock river incision.

Chapter 7

Final remarks, conclusions and future research work

Conclusions

The links between tectonics, climate and landscape are still not fully resolved, requiring field-based studies, flume experiments and numerical surface process models in rivers and hillslopes to elucidate landscape evolution. Research on bedrock rivers is thus relevant and necessary because these control the rate of incision in landscapes, particularly, in mountainous settings. Nevertheless, bedrock rivers are not well understood yet. However, several advances have been achieved in the last twenty years (Tinkler and Wohl, 1998). Rates of bedrock incision into different lithologies and climates, as well as hydraulic geometry and its limits are required in order to establish, if possible, a single bedrock incision law.

Research in landscape evolution has demonstrated that steady-state can be attained in the landscape but, such a condition is probably an exception rather than the rule. This is mainly because: (1) the response time of landscape to reach the steady-state is probably longer than the time over which climate changes (Whipple, 2001); and (2) as has been pointed out by Bishop (2007), landscapes where steady-state is likely are confined to active tectonic areas, thus, transience due to the rock uplift or surface uplift may delay or impede reaching a steady-state. The effects of landscape transience is, and probably will be for a while, a main goal leading

research in landscape evolution. Therefore, understanding the effects in rivers and landscape during and after knickpoint propagation is required.

In this research four main issues of transient bedrock rivers were treated: (1) knickpoint propagation after a sudden base-level lowering, (2) riverbed morphology after the propagation of a knickpoint, (3) bedrock incision rates in reaches affected by the passage of knickpoint and in those reaches not affected by knickpoint passage and (4) the effect of sediment on bedrock incision rates. Using a natural setting as a laboratory to assess processes introduces into the research the particularities given of geological controls (e.g., differences in the rate of rock or surface uplift, contrasts in lithology, structure, etc) and geomorphic history (e.g., glaciations, sediment production, etc). The homogeneous lithology, the well defined structure and the rapid base-level fall experienced 13.6 ka in Jura makes it special site to assess bedrock incision and knickpoint propagation. However, the glacial history in Jura is likely to have introduced local particularities. In any case, the results obtained here provide information on transience in already perturbed landscapes which have not been fully explored previously. The conclusion of this research are presented in the paragraphs below focusing in the case of Jura but having in mind that these are likely to be representative of small perturbed bedrock rivers.

- The melting of the BIIS ∼16 ka generated a glacio-isostatic rebound in most of Scotland that in Jura resulted in a base-level fall of ∼ 15 m, at ∼13.6 ka, as has been demonstrated here by analysing the ages and elevation of the shingle beaches along the west coast of Jura which correspond to the Perth shoreline (Jardine, 1982); and confirmed with the unpublished cosmogenic exposure ages (Bishop and co-workers). The cosmogenic exposure ages of the shingle beaches strongly indicate that the base-level fall in Jura was very rapid and triggered the 13.6 ka knickpoints. Knickpoint propagation is demonstrated by the presence of strath-terraces downstream of knickpoints, at least on the scarp-slope streams.

- Glacial inheritance is still imprinted on Jura's landscape, and so the streams

are highly perturbed in most reaches. Here the transient state unrelated to the base-level fall was assessed and confirmed through morphometric analysis on the stream long profile and using the SA and DS regressions in the full profiles as well as in the glaciated and fluvially dominated reaches. Using the DS plot, interpreting air-photographs and based on fieldwork observations, the base-level fall knickpoints on the streams of Jura were confirmed.

- The results here confirm that the distance of retreat of base-level fall knickpoints scales to the drainage area as suggested by other authors (e.g., Bishop et al., 2005; Crosby and Whipple, 2006; Harkins et al., 2007; Loget and van den Driesseche, 2009). Although simple in form, the power law relationship for knickpoint retreat seems to capture the main processes driving the knickpoint recession (i.e. stream discharge and possibly sediment flux). The analysis on the knickpoint retreat in Jura's structural settings and also comparing knickpoint retreat on Jura with synchronous knickpoints in the east of Scotland (Bishop et al., 2005), suggests that lithology and structure do not play a primary role in knickpoint propagation. The vertical distribution of knickpoints has also been evaluated and the results indicate that in perturbed streams, the vertical distribution of knickpoints is controlled by local geometry of rivers.

- The Jura rivers affected by the passage of the 13.6 ka base-level fall knickpoint were found to maintain a convex profile for drainage areas less than 5 km^2. This values is a threshold below which rivers cannot fully respond to the base-level fall. This slow response is also compounded by the headwards propagation of knickpoints younger that < 13.6 ka, which likewise delays the grading of channel slopes in large streams.

- Measuring the concentration of cosmogenic ^{10}Be in samples extracted from rivers bed allowed the estimation of bedrock incision rates. Here it has been demonstrated that the reaches downstream of the 13.6 ka knickpoint have higher incision rates than in the glacial reaches that are not affected by a

glacial steepening (~ 0.1 m/ka). The high incision rates (> 0.1 m/ka) observed in two reaches located upstream of the 13.6 ka knickpoint, reveal an effect due to steep slopes inherited from glacial processes.

- Here it has been confirmed the correlation of the cosmogenic incision rates with the stream power. The cosmogenic incision rates along with the trend observed in the rivers of Jura to increase their stream power towards the stream's mouth, strongly indicate that the incision rates downstream of the 13.6 ka knickpoint increase, condition that suggest that the base-level fall has not been fully absorbed by the rivers of Jura as the concavity index also suggest.

- The sediment analysis in five streams reveals that medium size particles ($D_{50} \approx$ 45 mm) characterise most of the material transported by the Jura rivers and no changes in sediment size were found as the stream discharge increases. In addition, bedrock exposure is frequent in these rivers path. The effect of cover and tools for abrasion in the Jura rivers is interpreted here as minimal as the interpretation of the saltation-abrasion model to predict bedrock incision rates indicates. In contrast, the best explanation for bedrock incision was obtained using the stream power model. Thus, bedrock channel incision on Jura is dominated by detachment-limited conditions where plucking dominates. Although simple in its form, the stream power model in either of its forms (shear stress or unit stream power) has been found here to explain bedrock channel incision.

- Using the TCNs to estimate bedrock incision rates from the active eroding surface was found to be valid here as long as the bedrock incision rates obtained from ^{10} Be samples are correlated with the local stream power where samples were extracted. Even though the Jura rivers have low drainage areas, the stream power is enough to promote bedrock incision and propagate the disequilibrium dictated by an increase in the rate of rock uplift.

Future research work

In this research I have demonstrated that knickpoint recession driven by a sudden lowering of rivers base-level occurs in small bedrock rivers catchments and this is regardless of the pre-existing condition in the landscape. The following issues, in my judgement, require further attention in the study of bedrock rivers and in the landscape evolution.

- The loss of drainage areas and subsequently the deceleration experienced by the knickpoint as it propagates headwards needs to be fully addressed. In this study this processes could not be evaluated because few tributaries join between the 13.6 ka shoreline and the base-level fall knickpoint. Because the knickpoint migrates upstream and retreat is a function of stream discharge, loss of areas implies a deceleration of knickpoints, a function that account such loss in drainage area is required to obtain a more accurate model for the knickpoint propagation.

- The secondary effects caused by the the knickpoint migration needs to be quantified for the bedrock channels. During fieldwork it was observed that downstream of the knickpoints the adjacent slopes of channels are unstable and prone to landslides. Landslides related to the propagation knickpoint have previously been reported in flume experiments (e.g., Hasbargen and Paola, 2000; Bigi et al., 2006) and in the field (Whittaker et al., 2008; 2010) but how these related to the knickpoints is unclear. The unstable slopes are likely to cause covering of bed to prevent channel incision or to provide tools to incise and abrade the bedrock.

- The stream power model requires further field-base studies with the estimation of bedrock incision in situ. TCNs are very useful for this purpose as long as incision rates can be estimated from the riverbed if bedrock is exposed and the shielding by topography and sediment is minimal. The approach followed here to estimate the bedrock incision rates can be accomplished by the dating

of exposure ages from geomorphic markers (e.g., strath terraces) to constrain incision rates. *In situ* bedrock incision rates are required to: (1) test if bedrock incision can be cast by the stream power model and if possible, (2) calibrate K as has been proposed by other authors.

- More field-studies are required to asses the role of sediment in bedrock incision. In this research it has been demonstrated that bedrock channel incision in Jura is driven by detachment-limited conditions; however, this may not always be the case in other small bedrock rivers catchments where sediment cover and bedrock abrasion may be more important. Thus, the rates of sediment production and how much sediment remains in channels are crucial in research on landscape evolution because rates of bedrock incision depend on it. Again, TCNs can be used to estimate the overall incision in a catchment to assess the rates of sediment production.

Appendix A

The stream long profiles of Jura

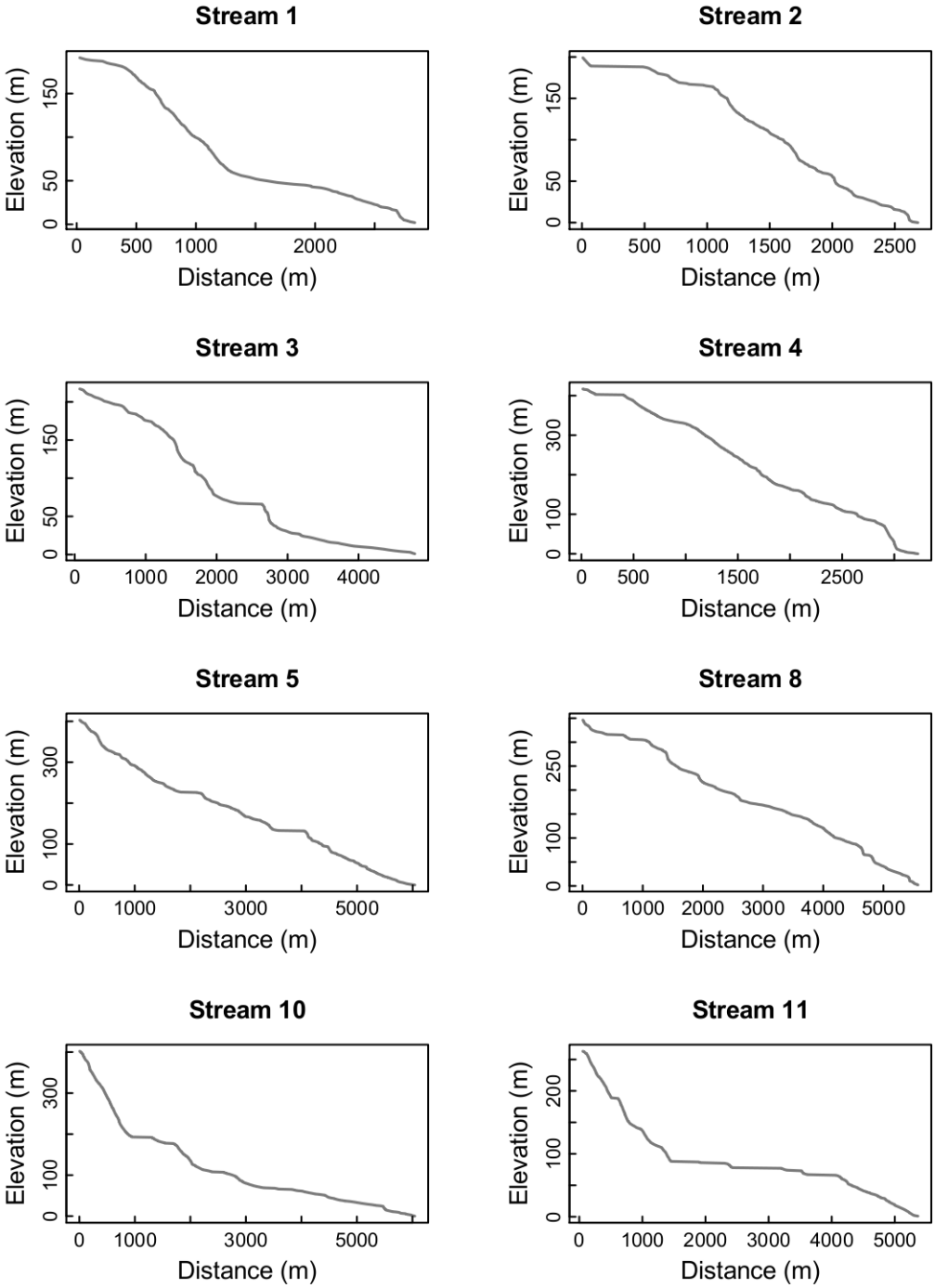

Figure A.1: Stream long profiles of Jura. All profiles were obtained from the 5 m resolution DEM and resampled at 1m (ΔZ)

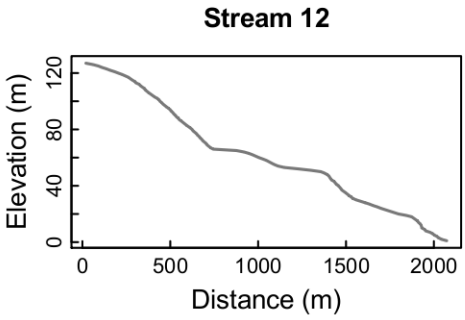
Stream 12
Elevation (m)
0
40
80
120
0
500
1000
1500
2000
Distance (m)

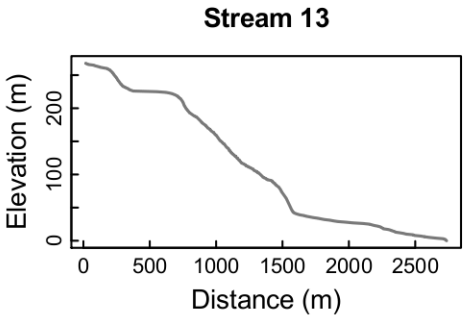
Stream 13
Elevation (m)
0
100
200
0
500
1000
1500
2000
2500
Distance (m)

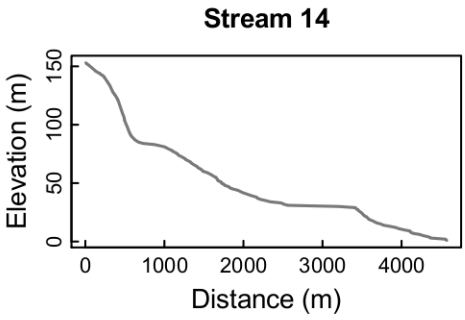
Stream 14
Elevation (m)
0
50
100
150
0
1000
2000
3000
4000
Distance (m)

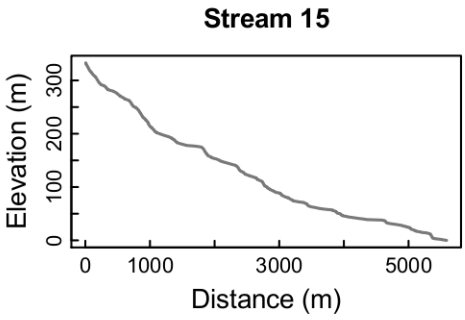
Stream 15
Elevation (m)
0
100
200
300
0
1000
3000
5000
Distance (m)

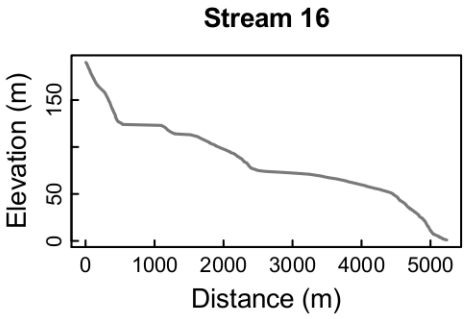
Stream 16
Elevation (m)
0
50
150
0
1000
2000
3000
4000
5000
Distance (m)

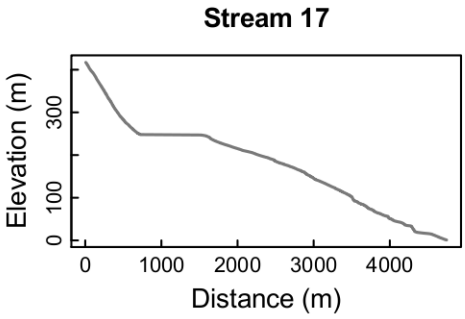
Stream 17
Elevation (m)
0
100
300
0
1000
2000
3000
4000
Distance (m)

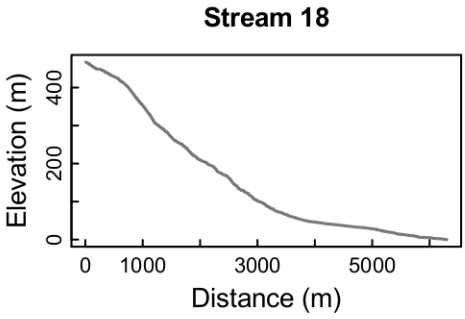
Stream 18
Elevation (m)
0
200
400
0
1000
3000
5000
Distance (m)

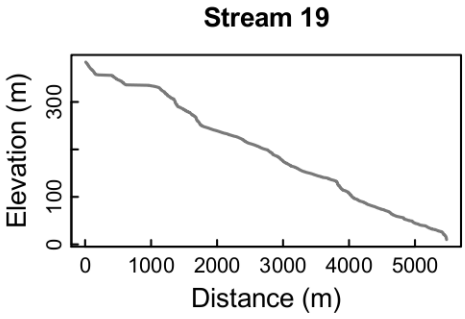
Stream 19
Elevation (m)
0
100
300
0
1000
2000
3000
4000
5000
Distance (m)

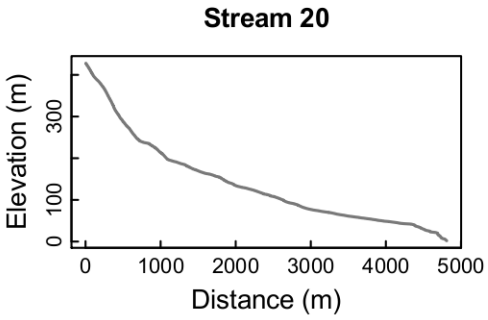
Stream 20
Elevation (m)
0
100
300
0
1000
2000
3000
4000
5000
Distance (m)

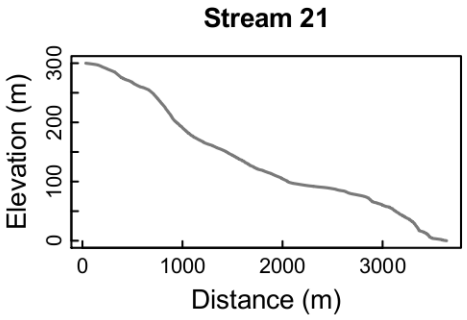
Stream 21
Elevation (m)
0
100
200
300
0
1000
2000
3000
Distance (m)

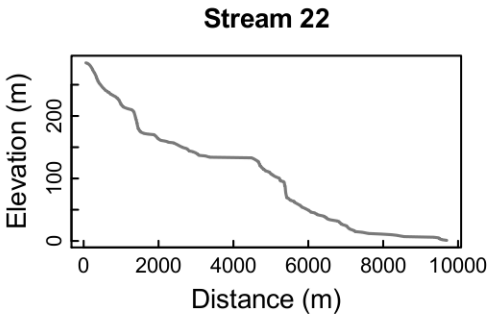
Stream 22
Elevation (m)
0
100
200
0
2000
4000
6000
8000
10000
Distance (m)

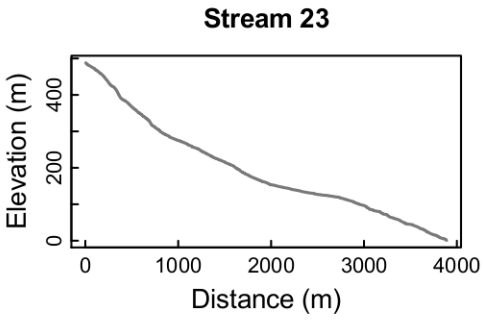
Stream 23
Elevation (m)
0
200
400
0
1000
2000
3000
4000
Distance (m)

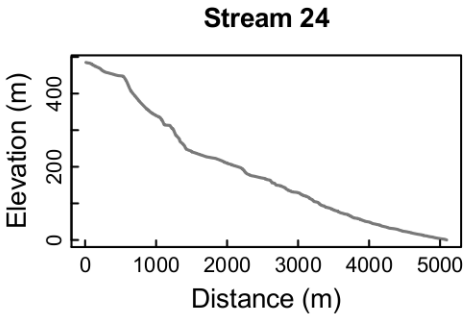
Stream 24
Elevation (m)
0
200
400
0
1000
2000
3000
4000
5000
Distance (m)

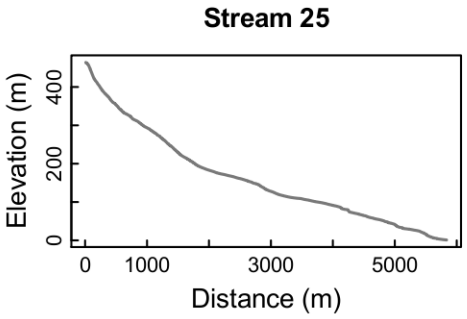
Stream 25
Elevation (m)
0
200
400
0
1000
3000
5000
Distance (m)

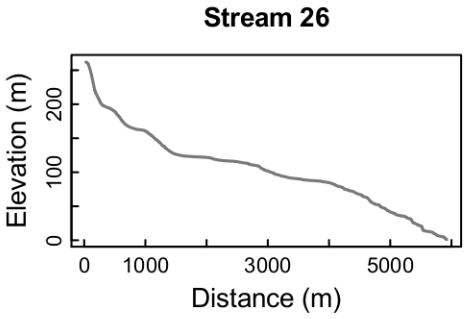
Stream 26
Elevation (m)
0
100
200
0
1000
3000
5000
Distance (m)

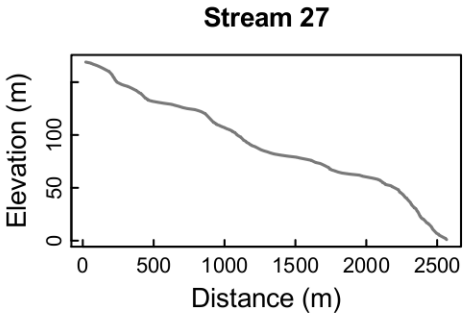
Stream 27
Elevation (m)
0
50
100
0
500
1000
1500
2000
2500
Distance (m)

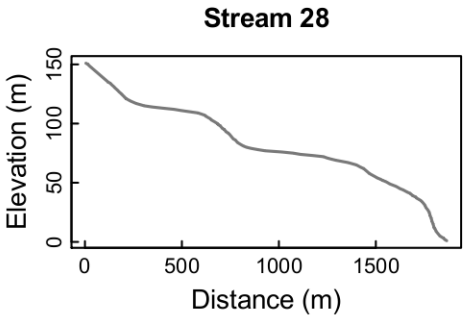
Stream 28
Elevation (m)
0
50
100
150
0
500
1000
1500
Distance (m)

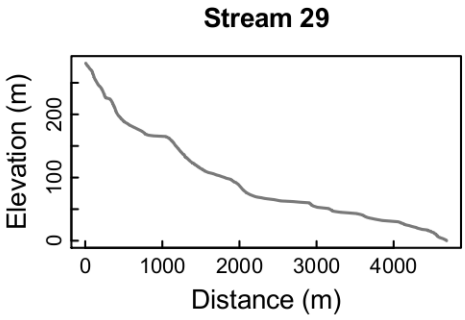
Stream 29
Elevation (m)
0
100
200
0
1000
2000
3000
4000
Distance (m)

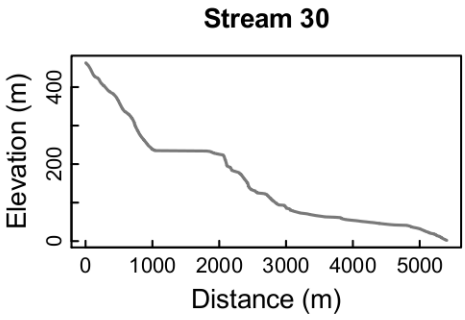
Stream 30
Elevation (m)
0
200
400
0
1000
2000
3000
4000
5000
Distance (m)

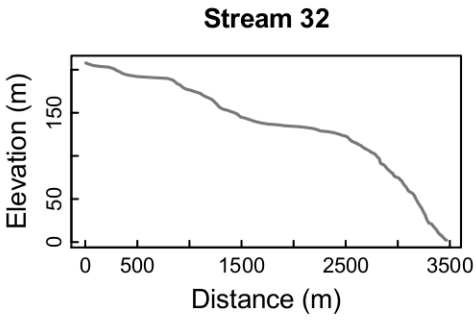
Stream 32
Elevation (m)
0
50
150
0
500
1500
2500
3500
Distance (m)

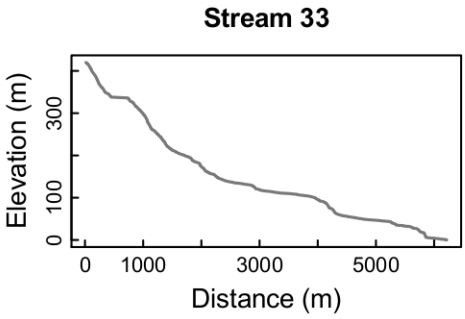
Stream 33
Elevation (m)
0
100
300
0
1000
3000
5000
Distance (m)

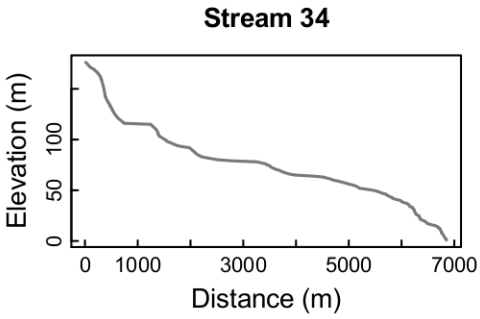
Stream 34
Elevation (m)
0
50
100
0
1000
3000
5000
7000
Distance (m)

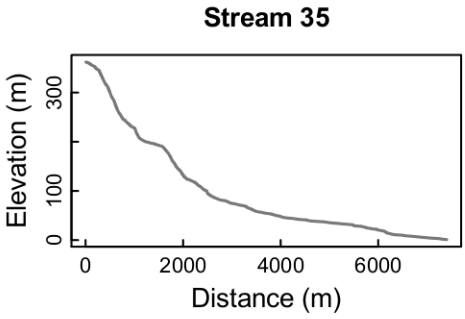
Stream 35
Elevation (m)
0
100
300
0
2000
4000
6000
Distance (m)

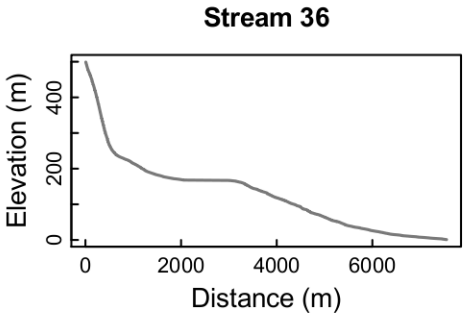
Stream 36
Elevation (m)
0
200
400
0
2000
4000
6000
Distance (m)

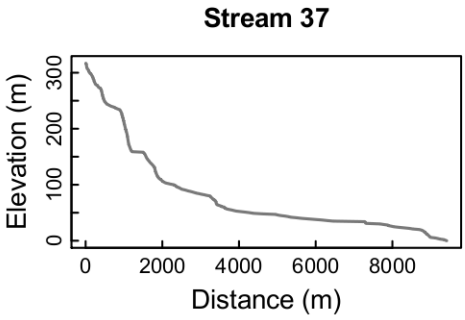
Stream 37
Elevation (m)
0
100
200
300
0
2000
4000
6000
8000
Distance (m)

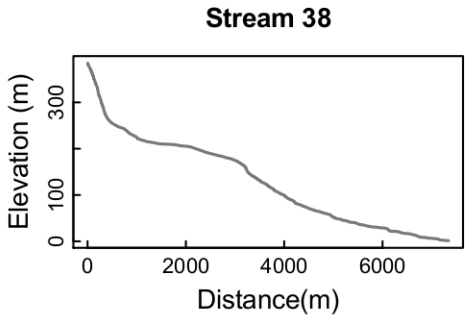
Stream 38
Elevation (m)
0
100
300
0
2000
4000
6000
Distance(m)

Appendix B

The slope-area plots

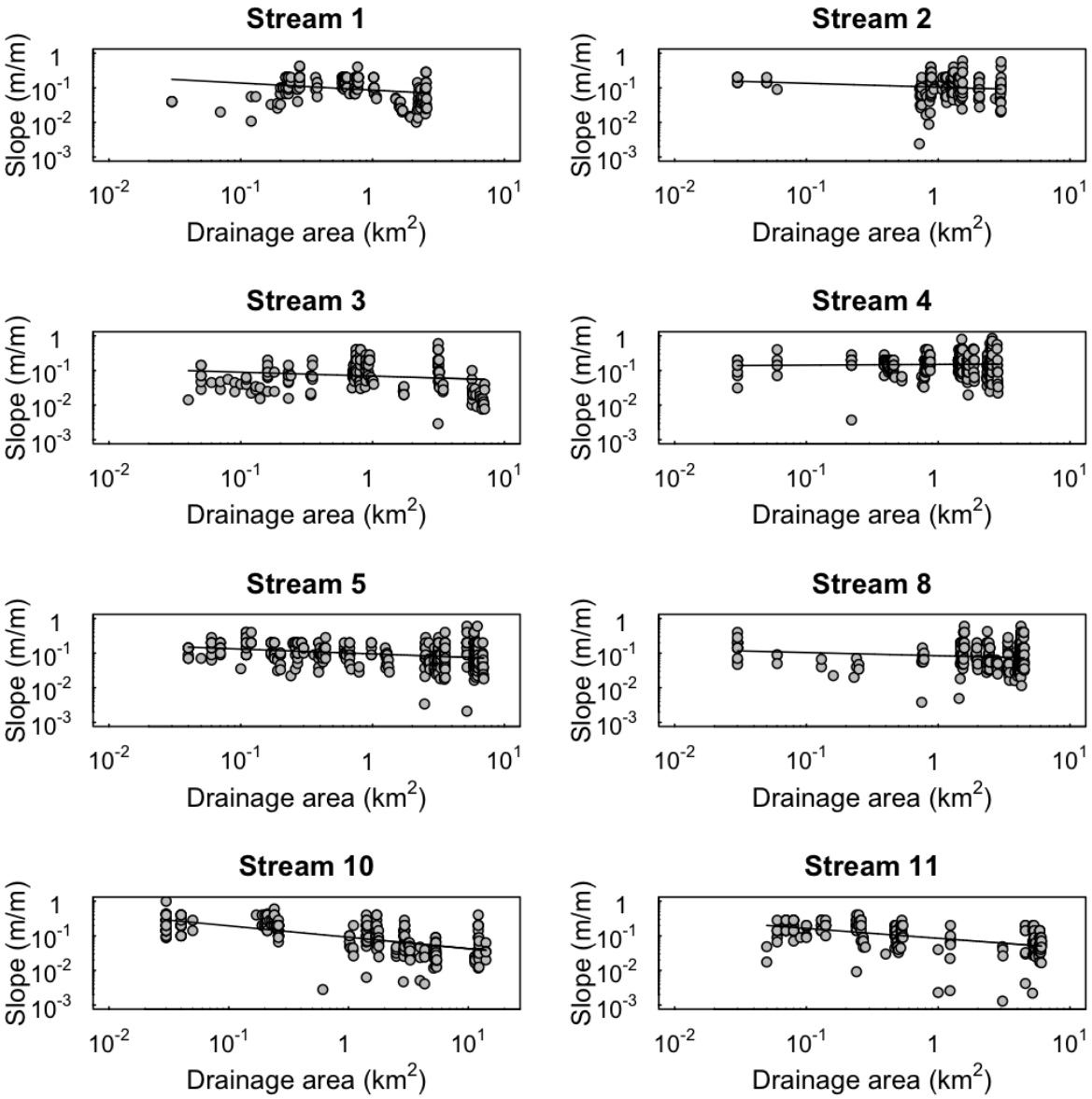

Figure B.1: Plots of channel slope against drainage area. The regression line is marked as a solid line.

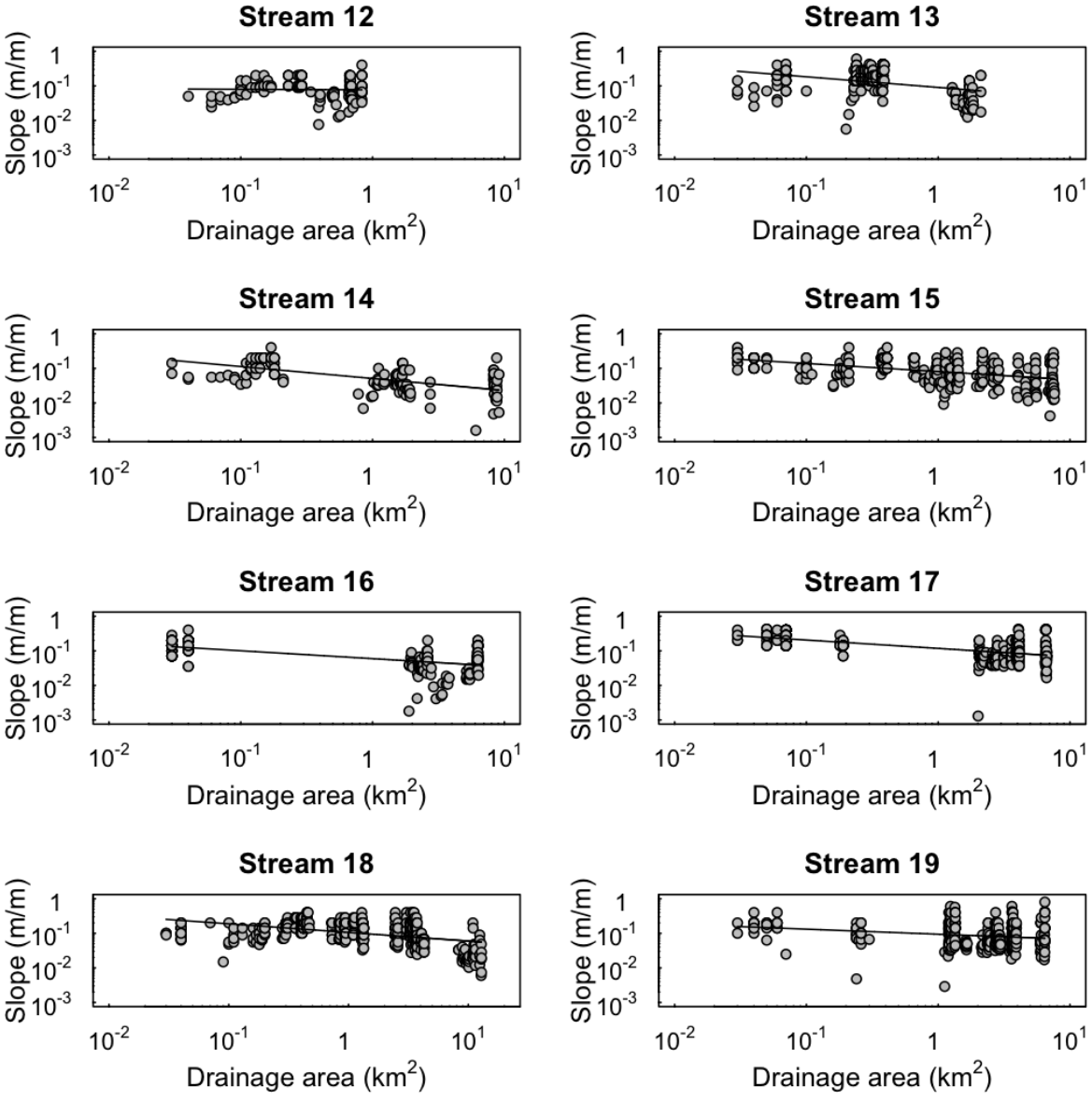
Stream 12
Stream 13
Stream 14
Stream 15
Stream 16
Stream 17
Stream 18
Stream 19
Slope (m/m)
Drainage area (km^2)
1
10^{-1}
10^{-2}
10^{-3}
10^{-2}
10^{-1}
1
10^{1}

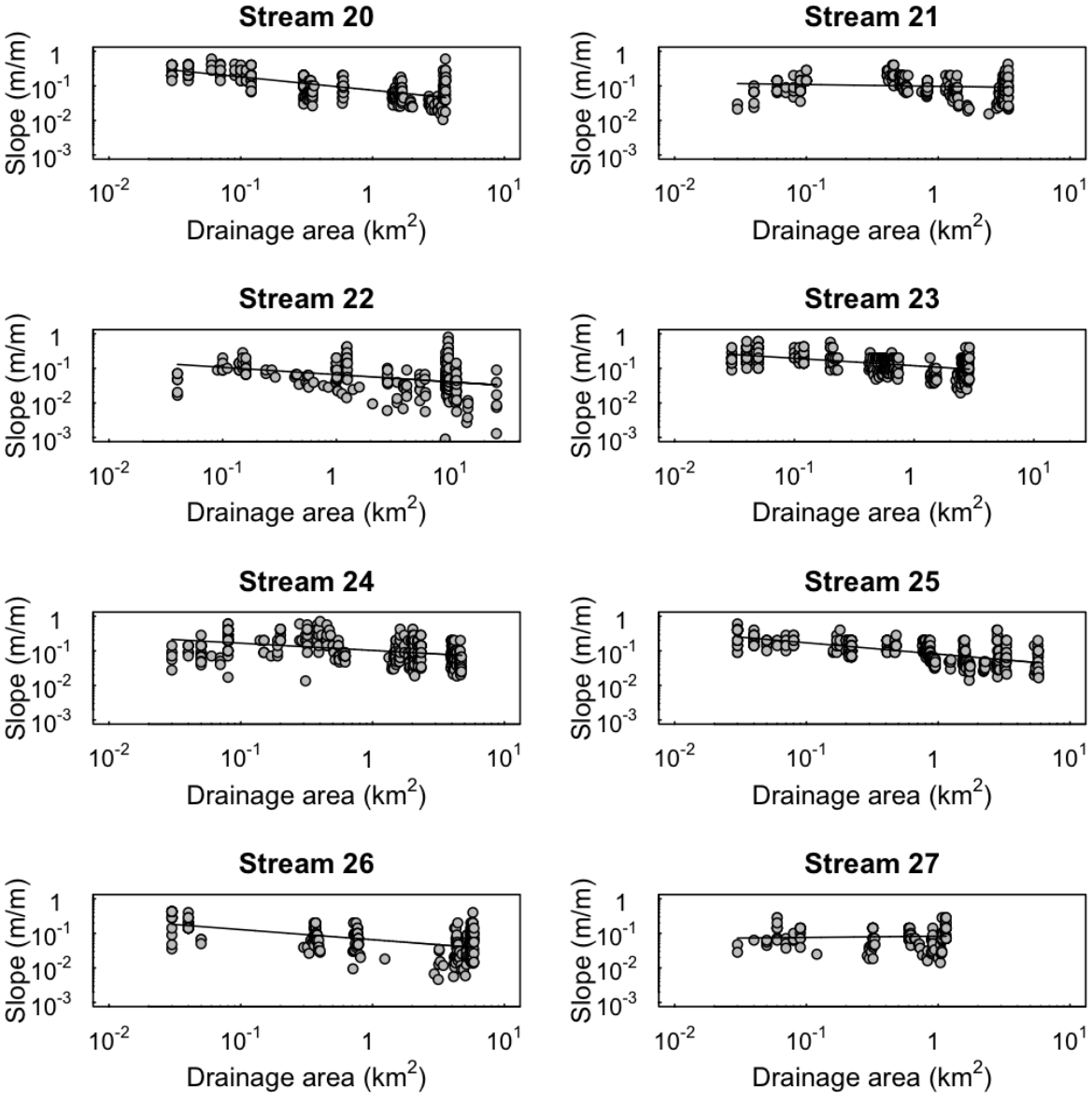
Stream 20
Stream 21
Stream 22
Stream 23
Stream 24
Stream 25
Stream 26
Stream 27
Slope (m/m)
Drainage area (km^2)
1
10^{-1}
10^{-2}
10^{-3}
10^{-2}
10^{-1}
1
10^{1}

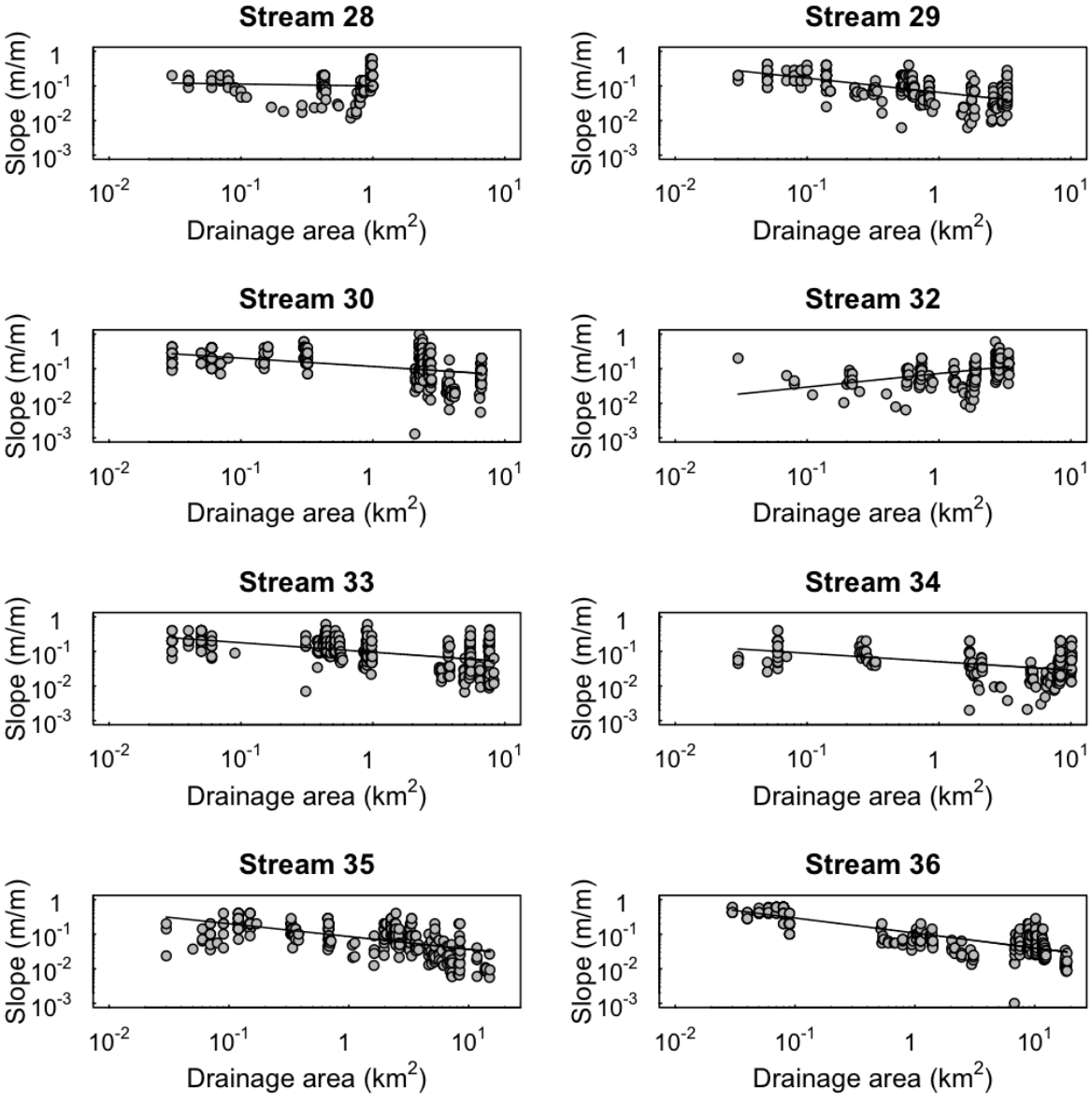
Stream 28
Stream 29
Stream 30
Stream 32
Stream 33
Stream 34
Stream 35
Stream 36
Slope (m/m)
Drainage area (km^2)

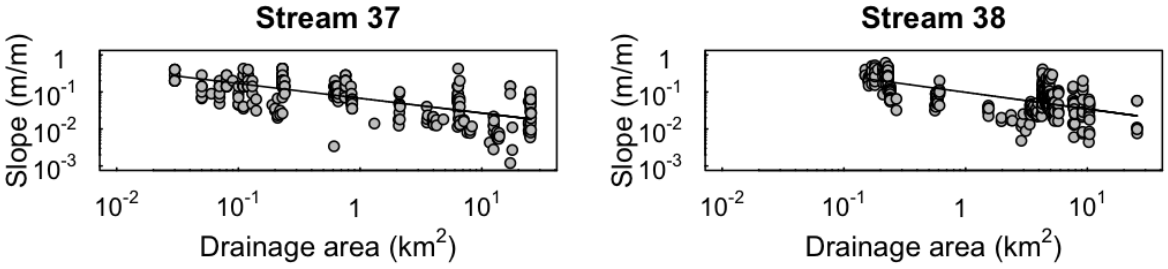
Stream 37
Slope (m/m)
1
10-1
10-2
10-3
10-2
10-1
1
101
Drainage area (km2)
Stream 38
Slope (m/m)
1
10-1
10-2
10-3
10-2
10-1
1
101
Drainage area (km2)

Appendix C

The slope-area plots of the glaciated reaches

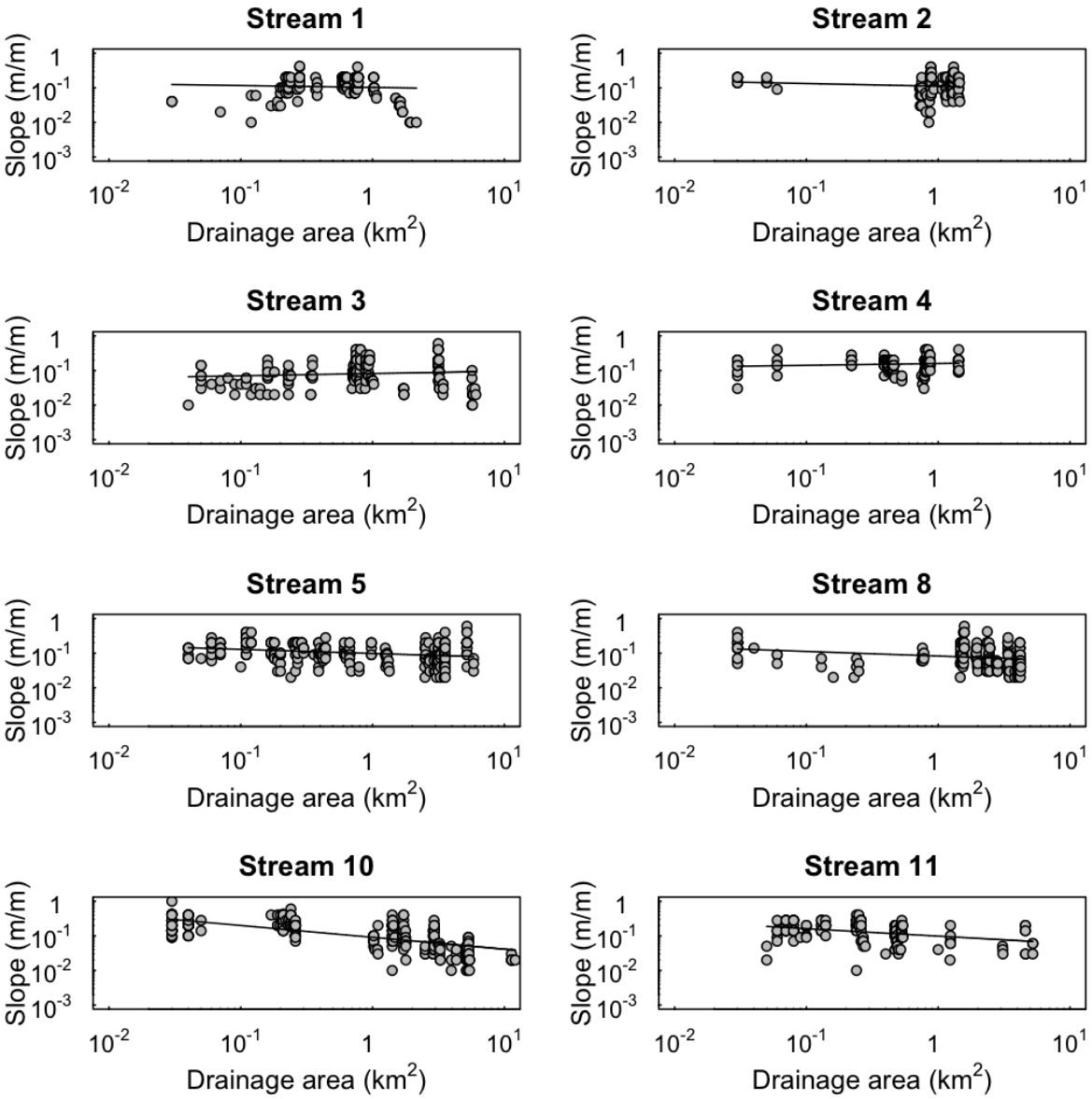

Figure C.1: Plots of channel slope against drainage area on glaciated reaches. The regression line is marked as a solid line.

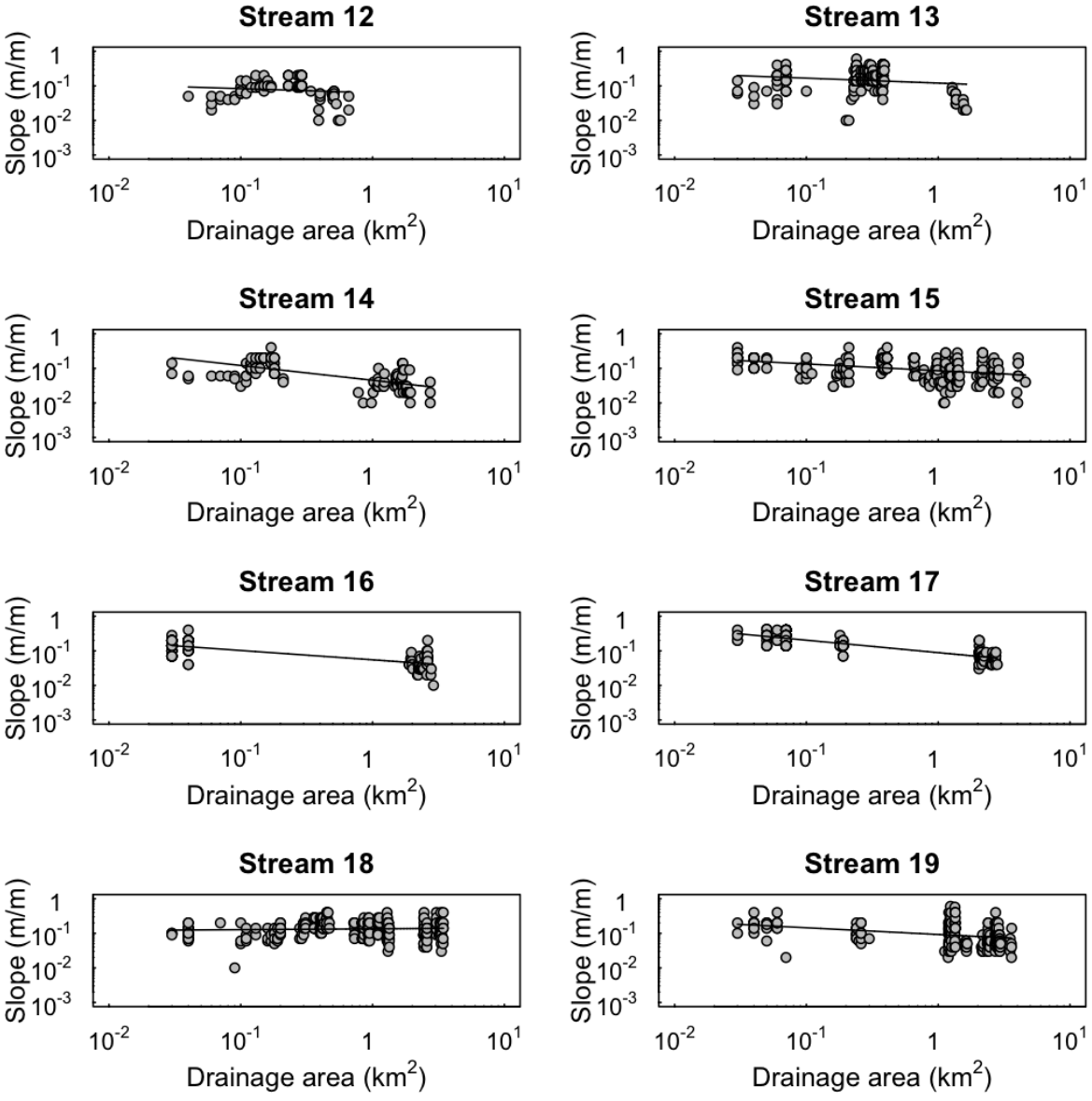
Stream 12
Stream 13
Stream 14
Stream 15
Stream 16
Stream 17
Stream 18
Stream 19
Slope (m/m)
Drainage area (km^2)
1
10^{-1}
10^{-2}
10^{-3}
10^{-2}
10^{-1}
1
10^{1}

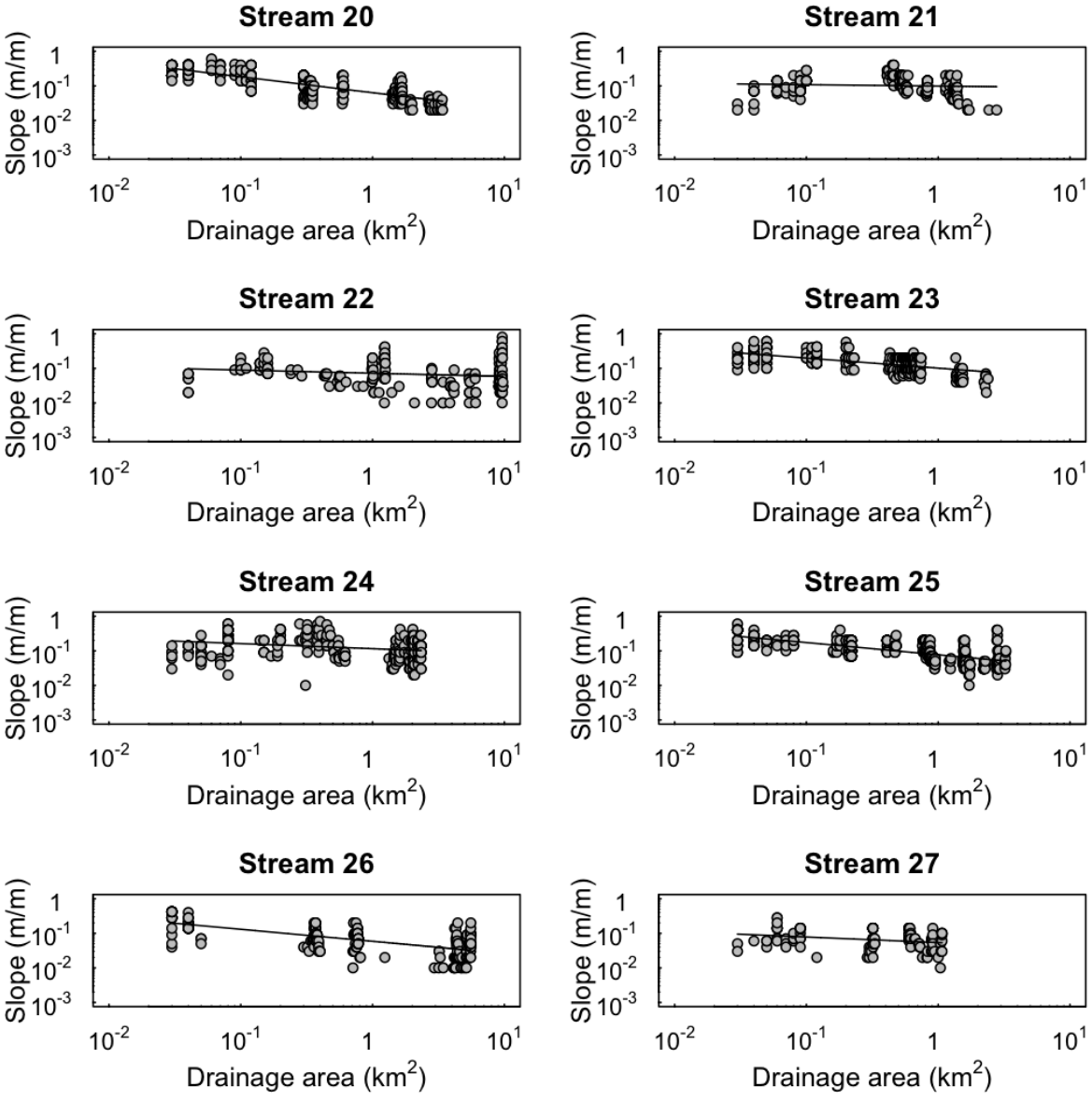
Stream 20
Stream 21
Stream 22
Stream 23
Stream 24
Stream 25
Stream 26
Stream 27
Slope (m/m)
Drainage area (km^2)
1
10^{-1}
10^{-2}
10^{-3}
10^{-2}
10^{-1}
1
10^{1}

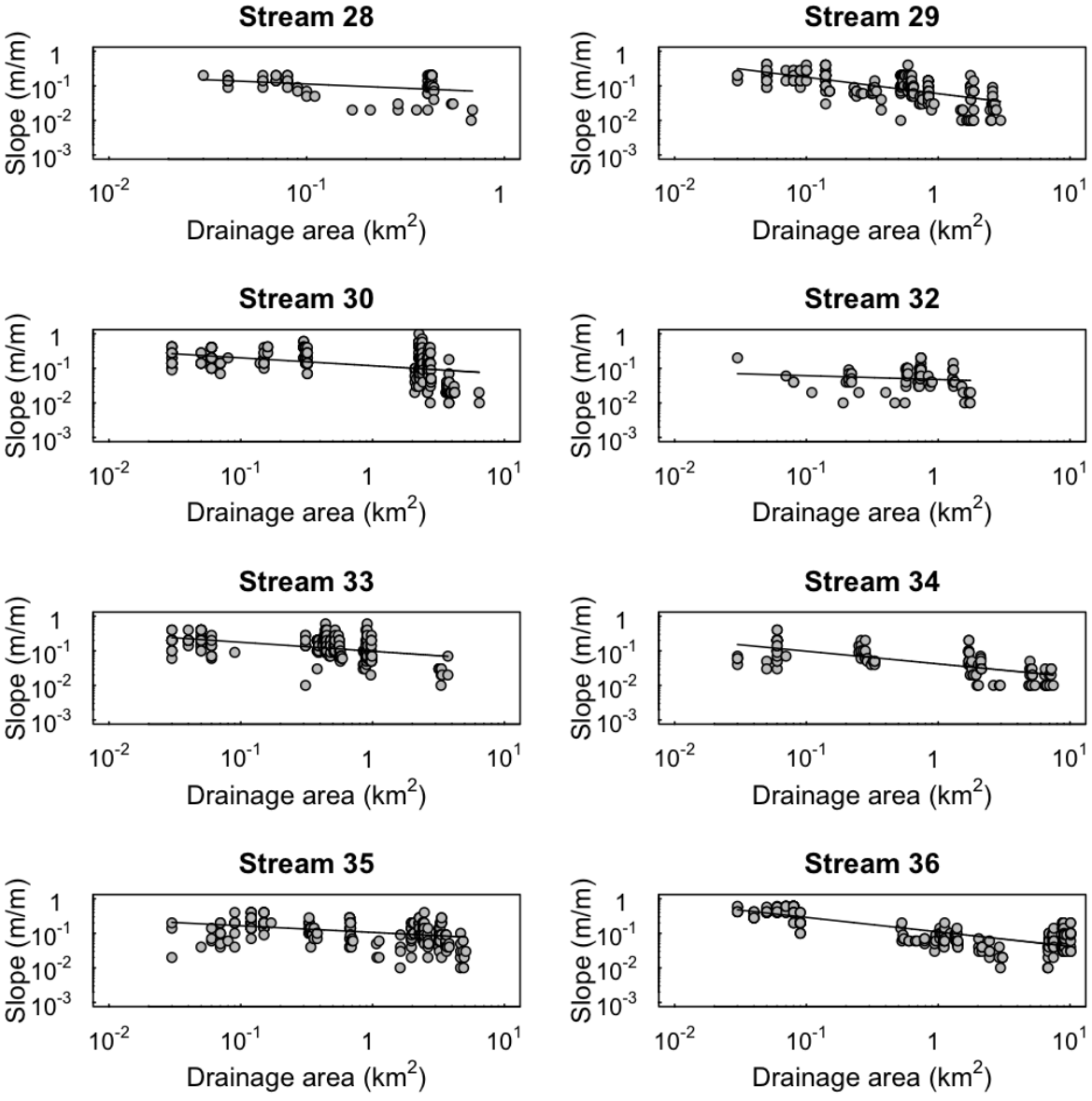
Stream 28
Stream 29
Stream 30
Stream 32
Stream 33
Stream 34
Stream 35
Stream 36
Slope (m/m)
Drainage area (km^2)

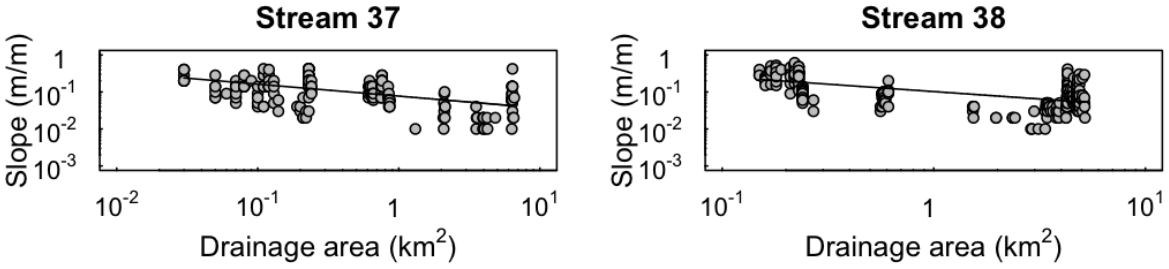
Stream 37
Slope (m/m)
1
10^{-1}
10^{-2}
10^{-3}
10^{-2}
10^{-1}
1
10^{1}
Drainage area (km^2)
Stream 38
Slope (m/m)
1
10^{-1}
10^{-2}
10^{-3}
10^{-1}
1
10^{1}
Drainage area (km^2)

Appendix D

The slope-area plots of the fluvial reaches

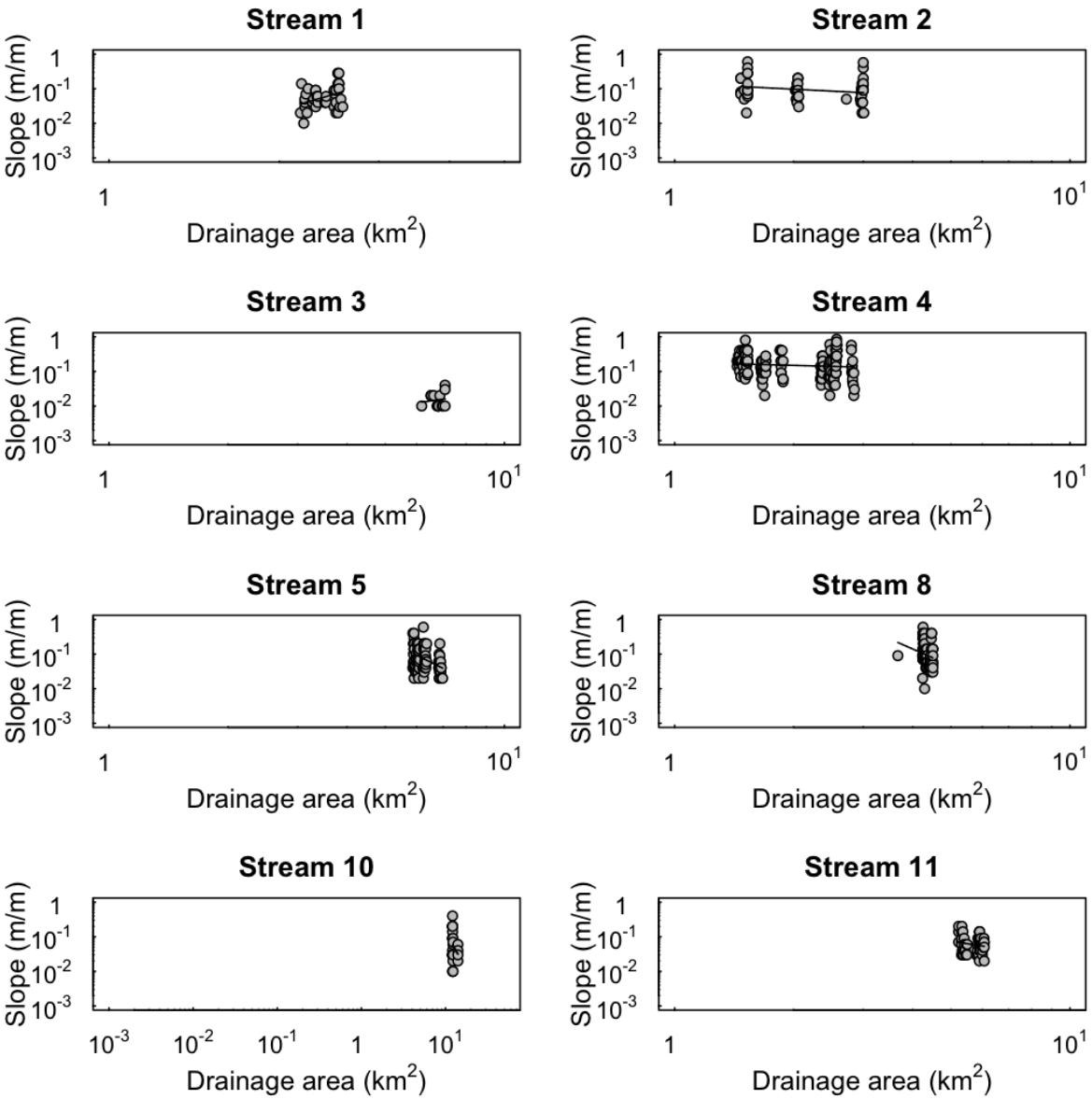

Figure D.1: Plots of drainage-area against channel slope of the fluvial reaches. The regression line is marked as a solid line and the dashed lines depict the 95% confidence limits

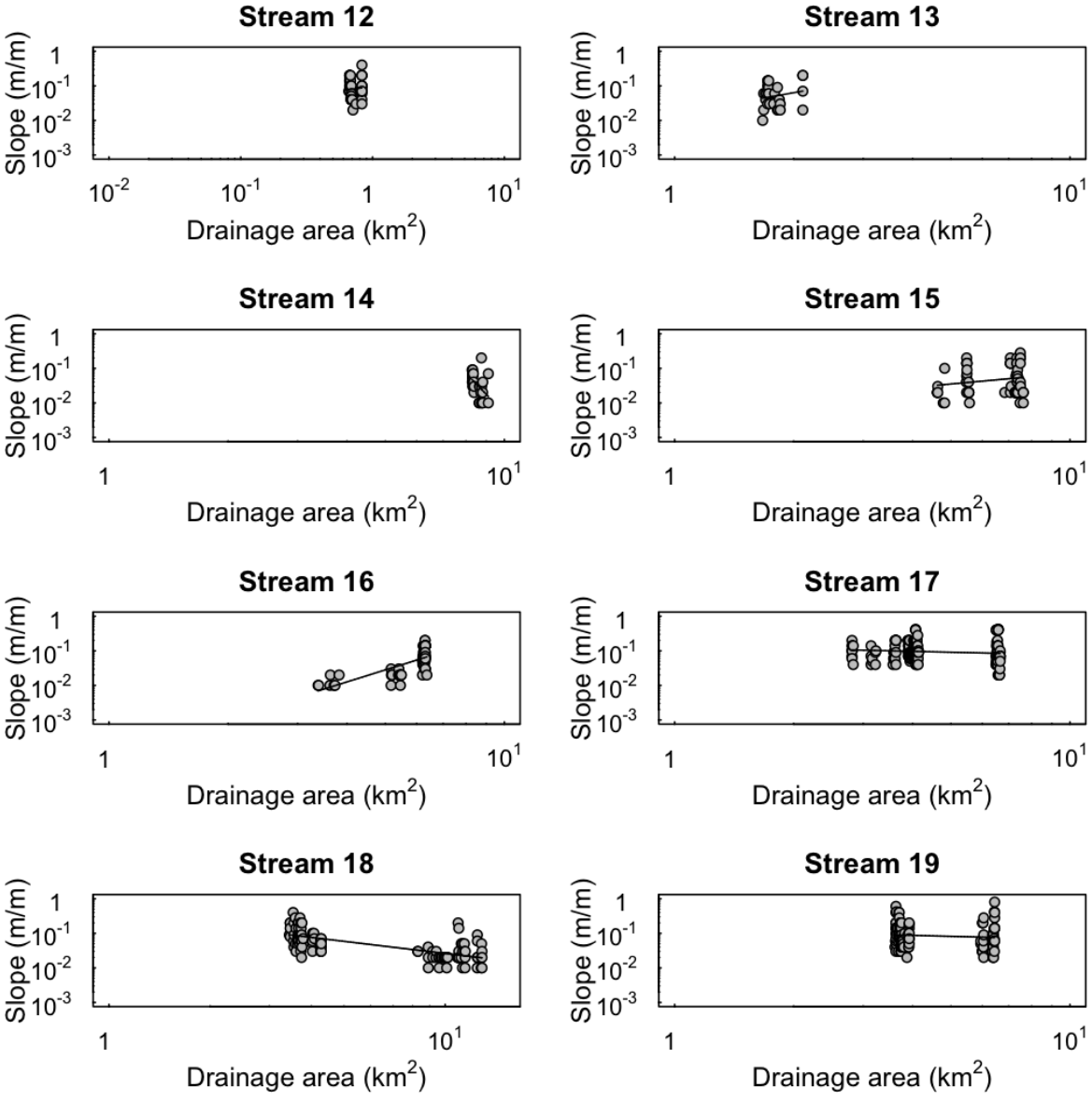
Stream 12
Stream 13
Stream 14
Stream 15
Stream 16
Stream 17
Stream 18
Stream 19
Slope (m/m)
Drainage area (km^2)

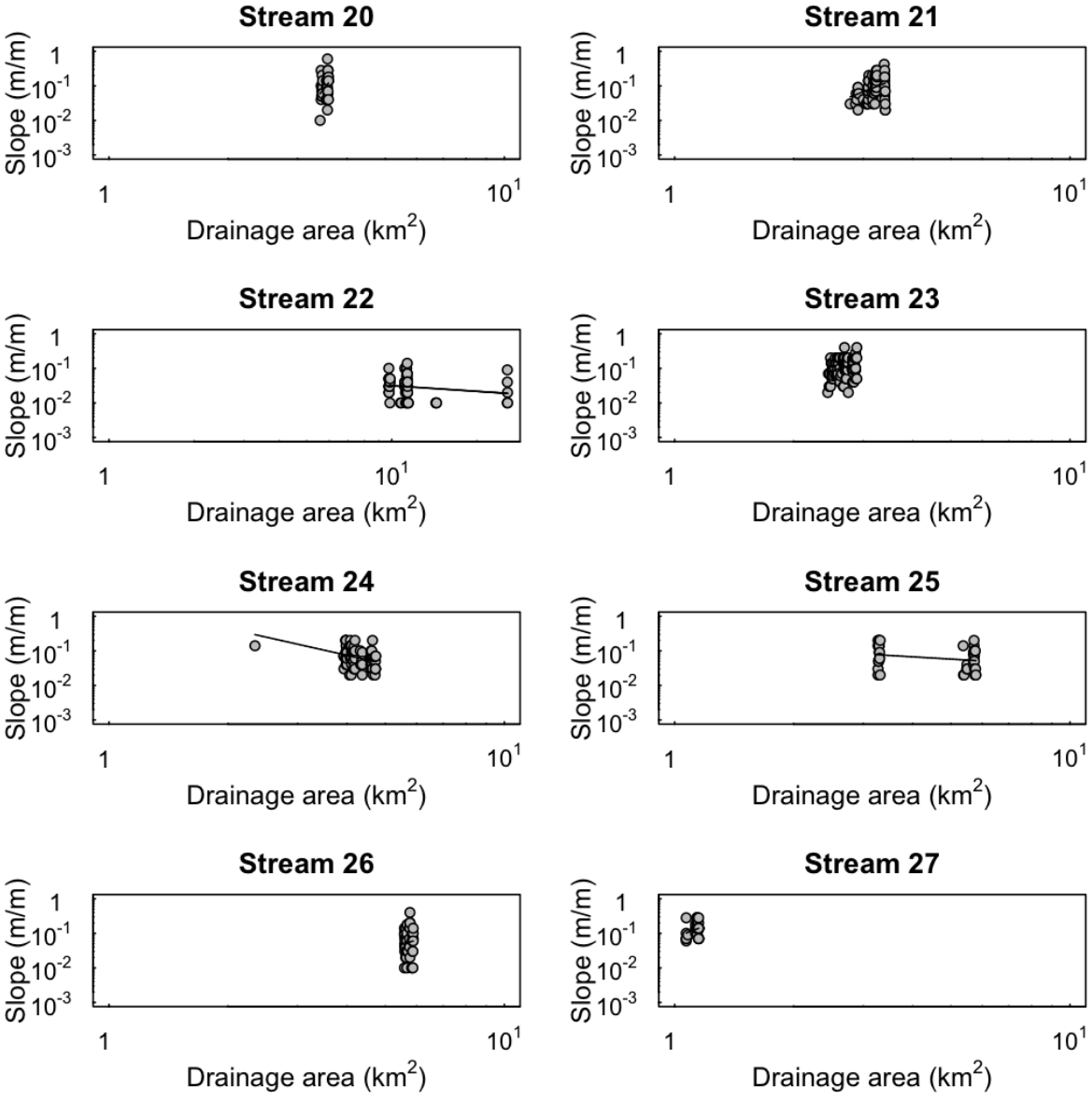
Stream 20
Stream 21
Stream 22
Stream 23
Stream 24
Stream 25
Stream 26
Stream 27
Slope (m/m)
1
10^{-1}
10^{-2}
10^{-3}
1
10^{1}
Drainage area (km^2)

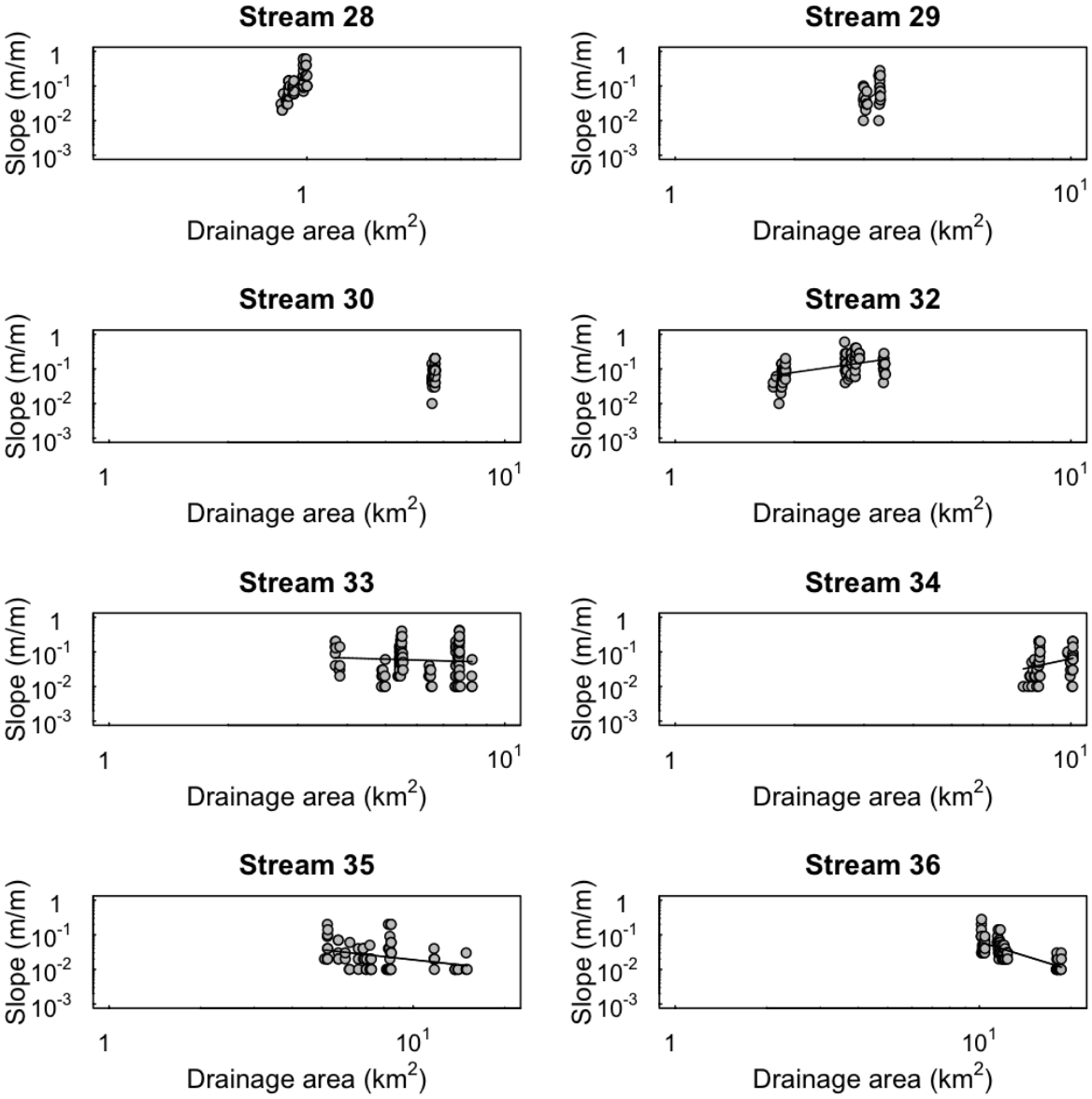
Stream 28
Stream 29
Stream 30
Stream 32
Stream 33
Stream 34
Stream 35
Stream 36
Slope (m/m)
1
10-1
10-2
10-3
1
101
Drainage area (km2)

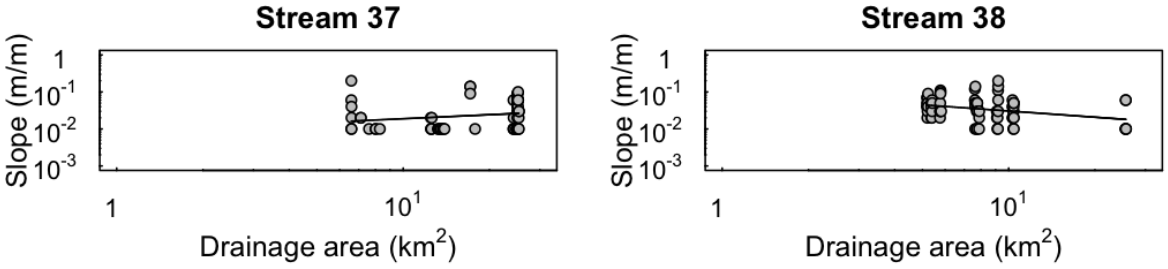
Stream 37
Slope (m/m)
1
10^{-1}
10^{-2}
10^{-3}
1
10^{1}
Drainage area (km^2)
Stream 38
Slope (m/m)
1
10^{-1}
10^{-2}
10^{-3}
1
10^{1}
Drainage area (km^2)

Appendix E

The distance-slope plots

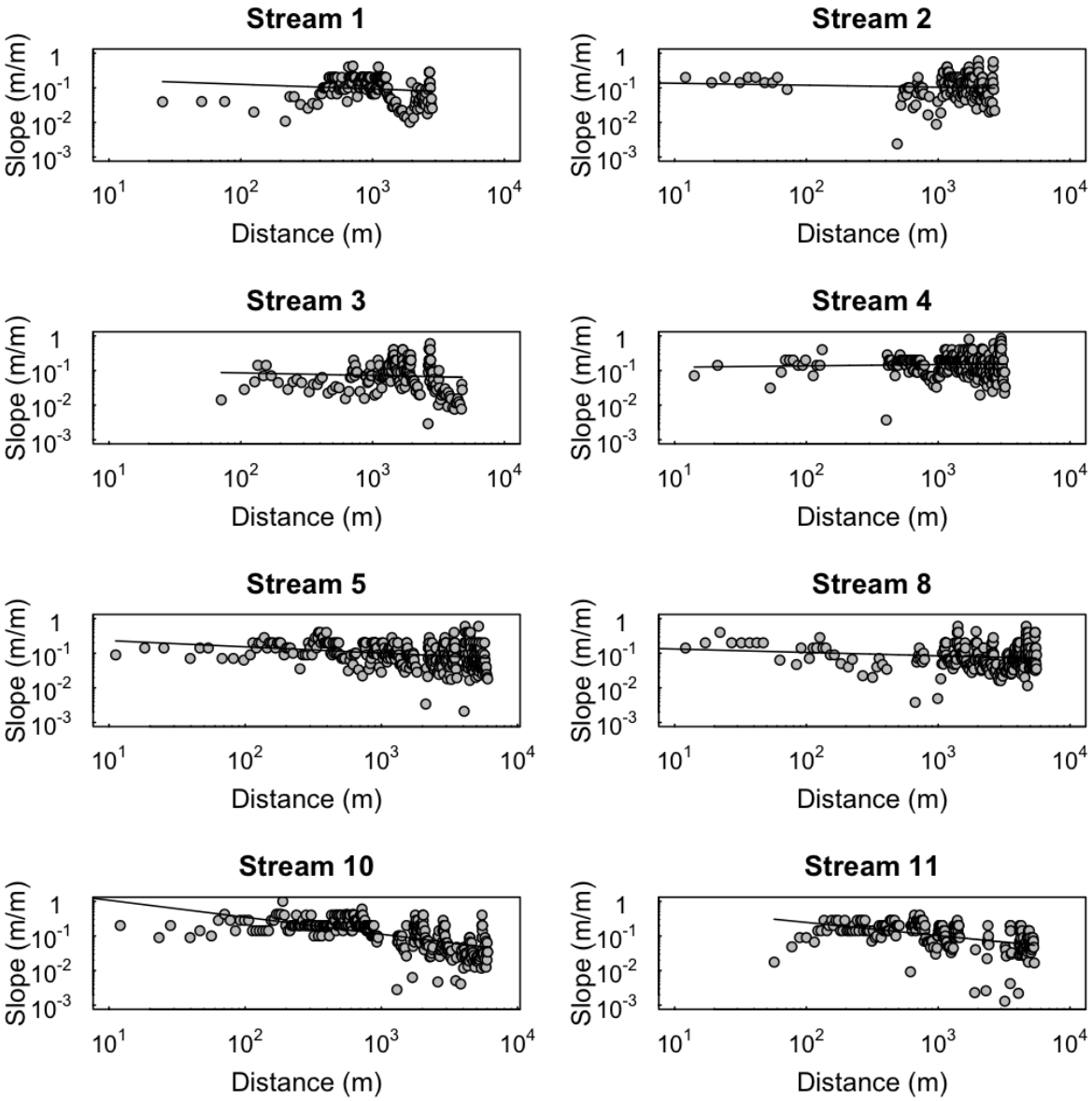

Figure E.1: Plots of channel slope against the distance downstream. The regression line is marked as a solid line.

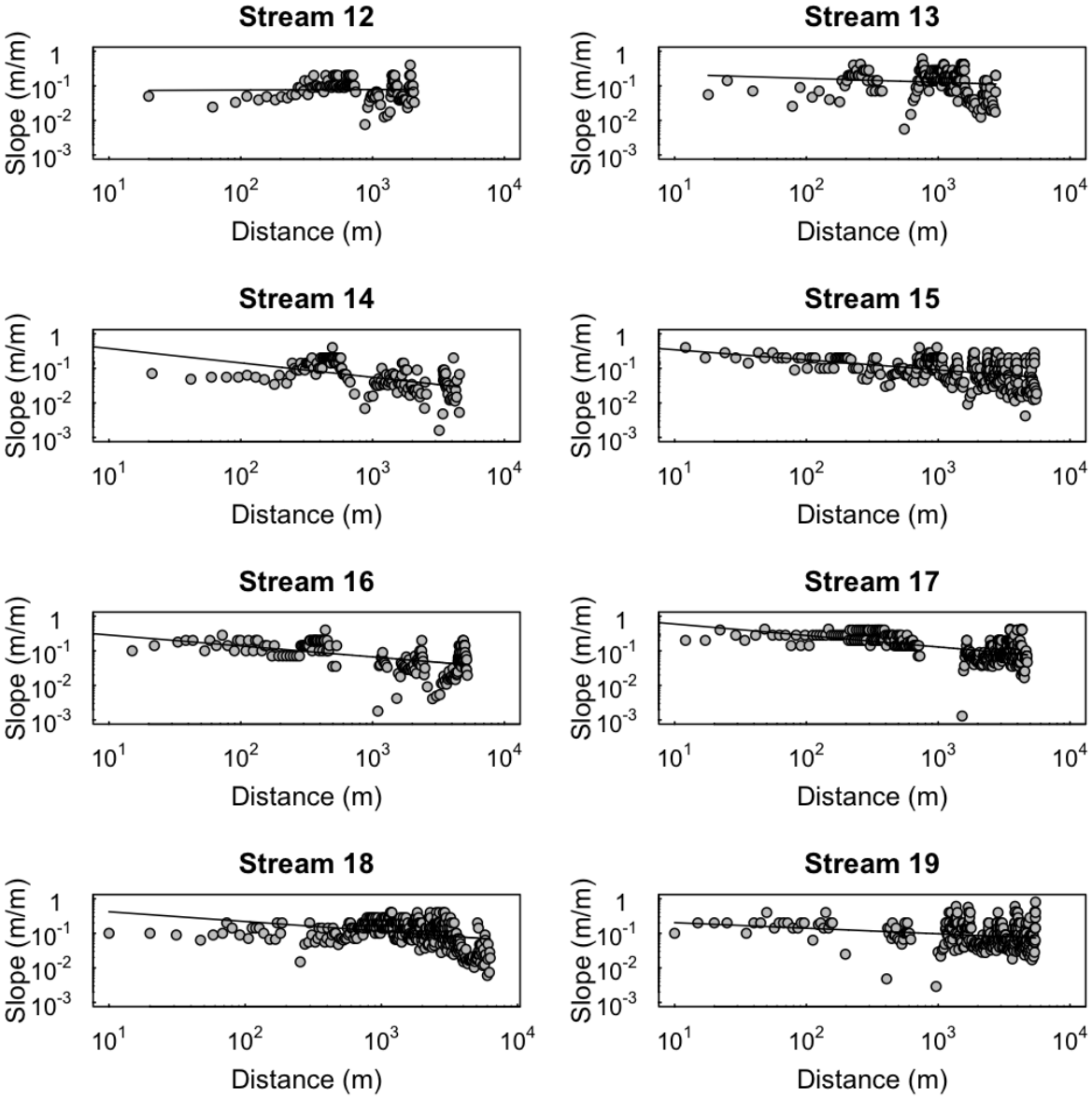
Stream 12
Stream 13
Stream 14
Stream 15
Stream 16
Stream 17
Stream 18
Stream 19
Slope (m/m)
1
10-1
10-2
10-3
10^1
10^2
10^3
10^4
Distance (m)

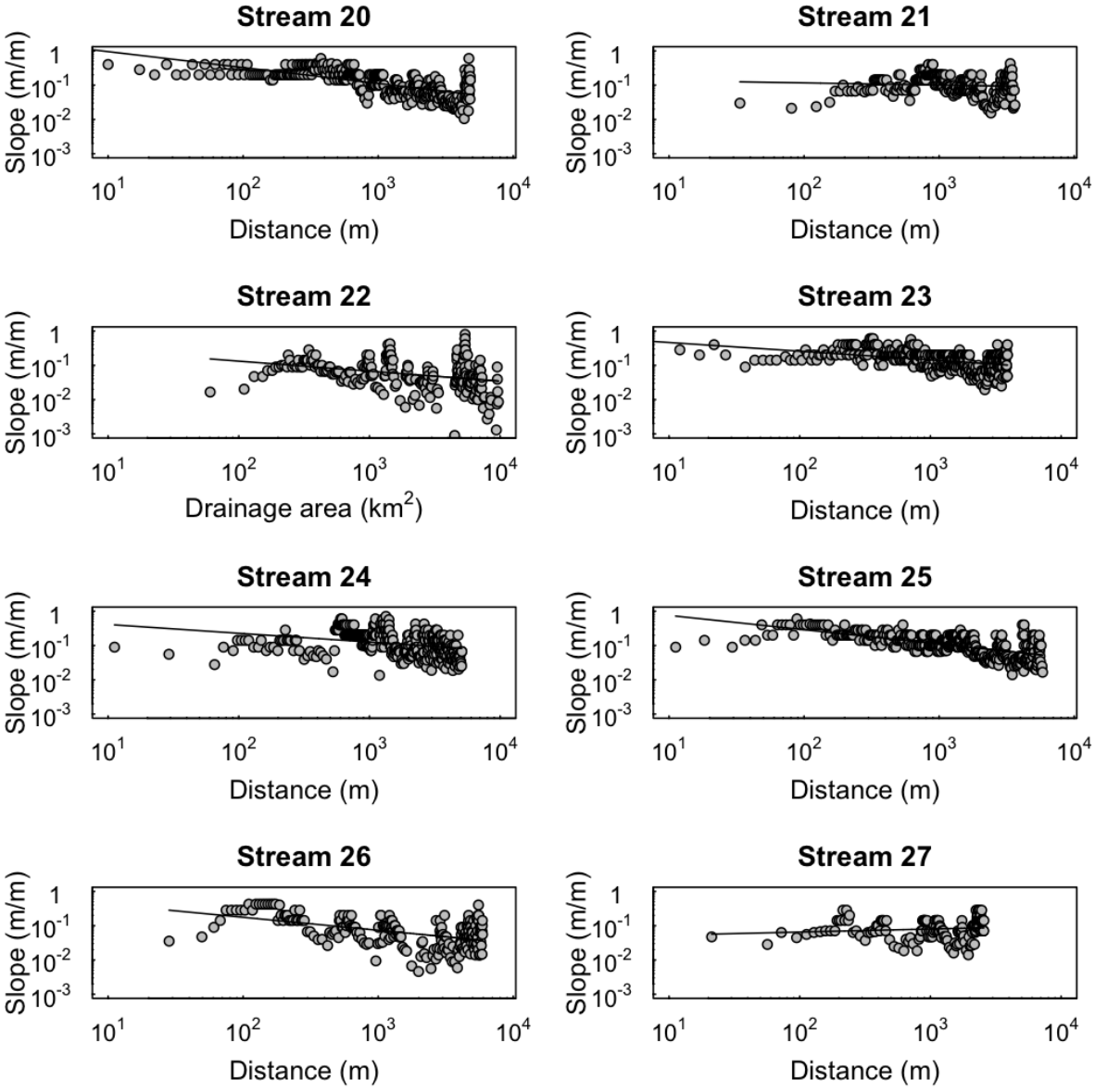
Stream 20
Slope (m/m)
1
10-1
10-2
10-3
10^1
10^2
10^3
10^4
Distance (m)
Stream 21
Slope (m/m)
Distance (m)
Stream 22
Slope (m/m)
Drainage area (km2)
Stream 23
Slope (m/m)
Distance (m)
Stream 24
Slope (m/m)
Distance (m)
Stream 25
Slope (m/m)
Distance (m)
Stream 26
Slope (m/m)
Distance (m)
Stream 27
Slope (m/m)
Distance (m)

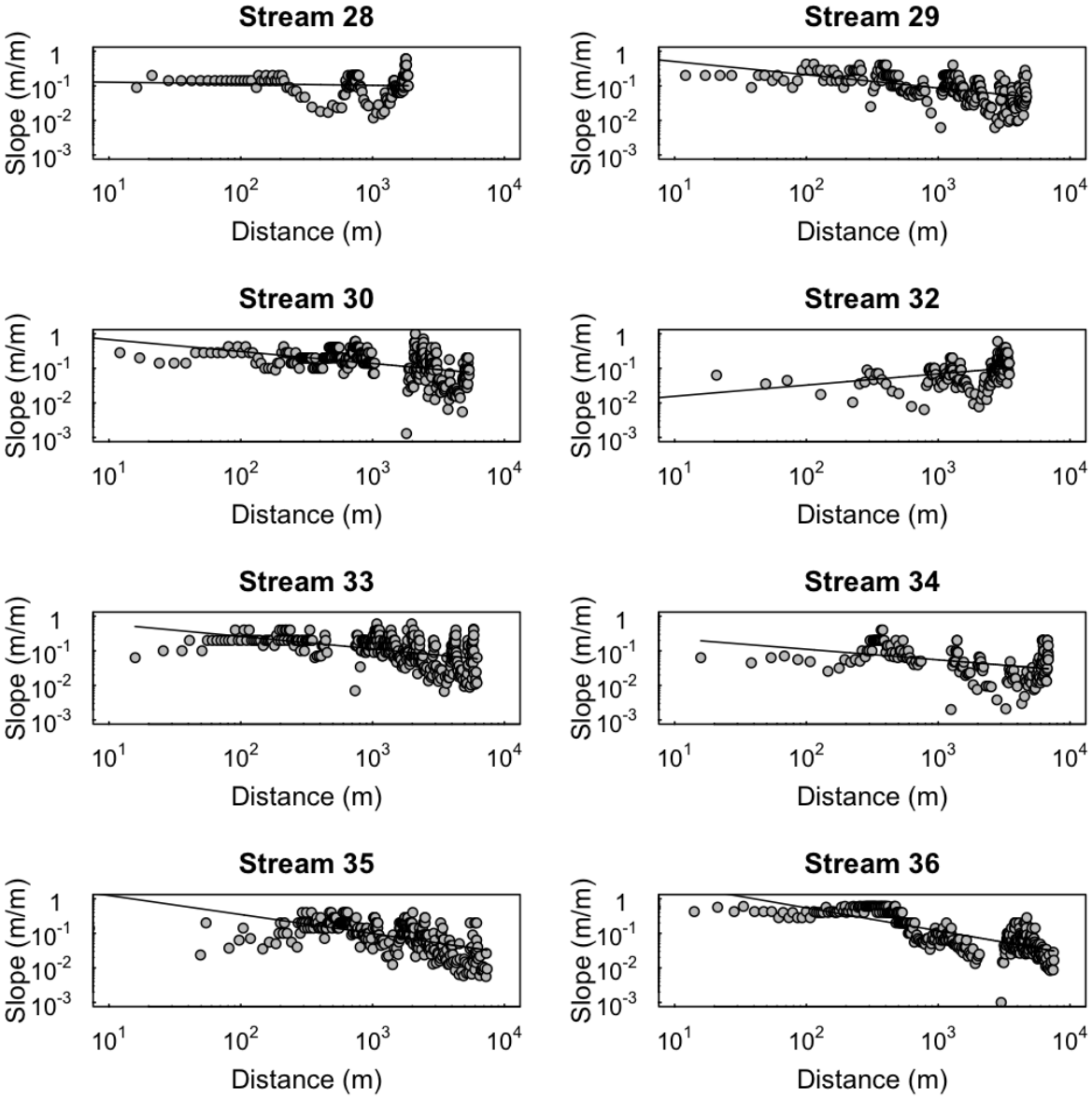
Stream 28
Stream 29
Stream 30
Stream 32
Stream 33
Stream 34
Stream 35
Stream 36
Slope (m/m)
1
10-1
10-2
10-3
10^1
10^2
10^3
10^4
Distance (m)

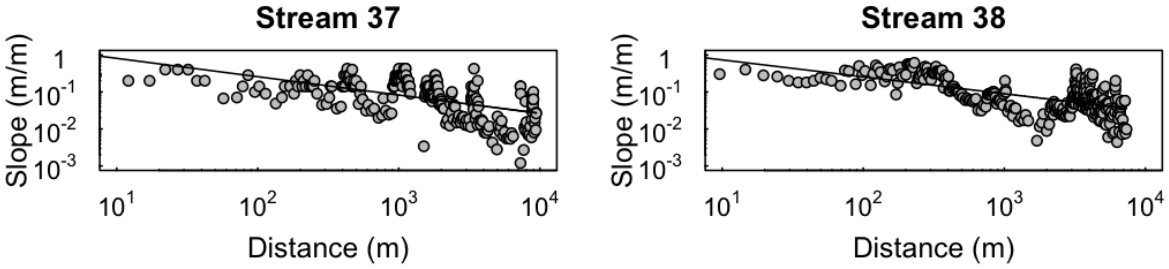
Stream 37
Slope (m/m)
1
10-1
10-2
10-3
101
102
103
104
Distance (m)
Stream 38
Slope (m/m)
1
10-1
10-2
10-3
101
102
103
104
Distance (m)

Appendix F

The distance-Slope plots of glaciated reaches

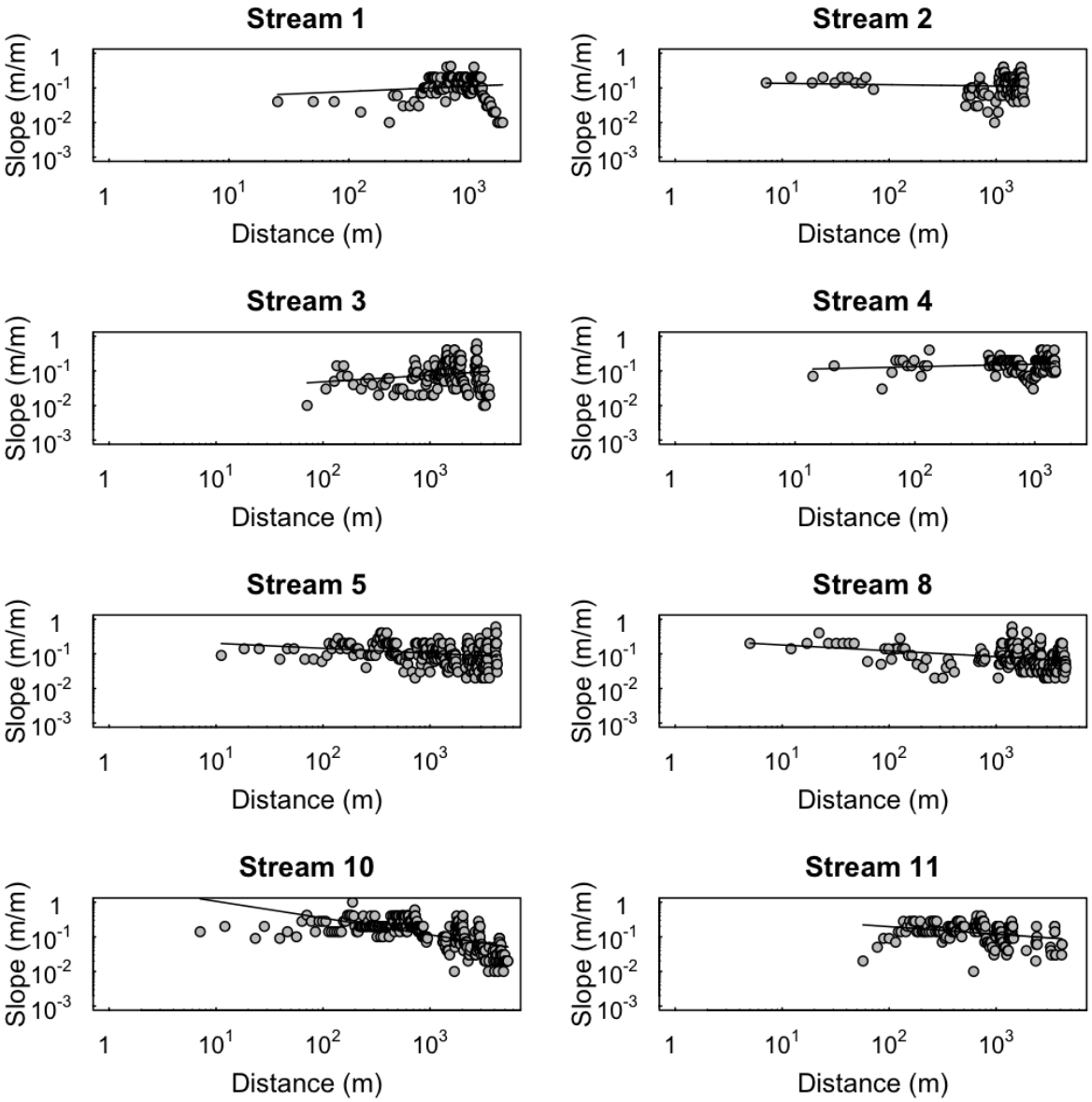

Figure F.1: Plots channel slope against drainage area of the glaciated reaches. The regression line is marked as a solid line.

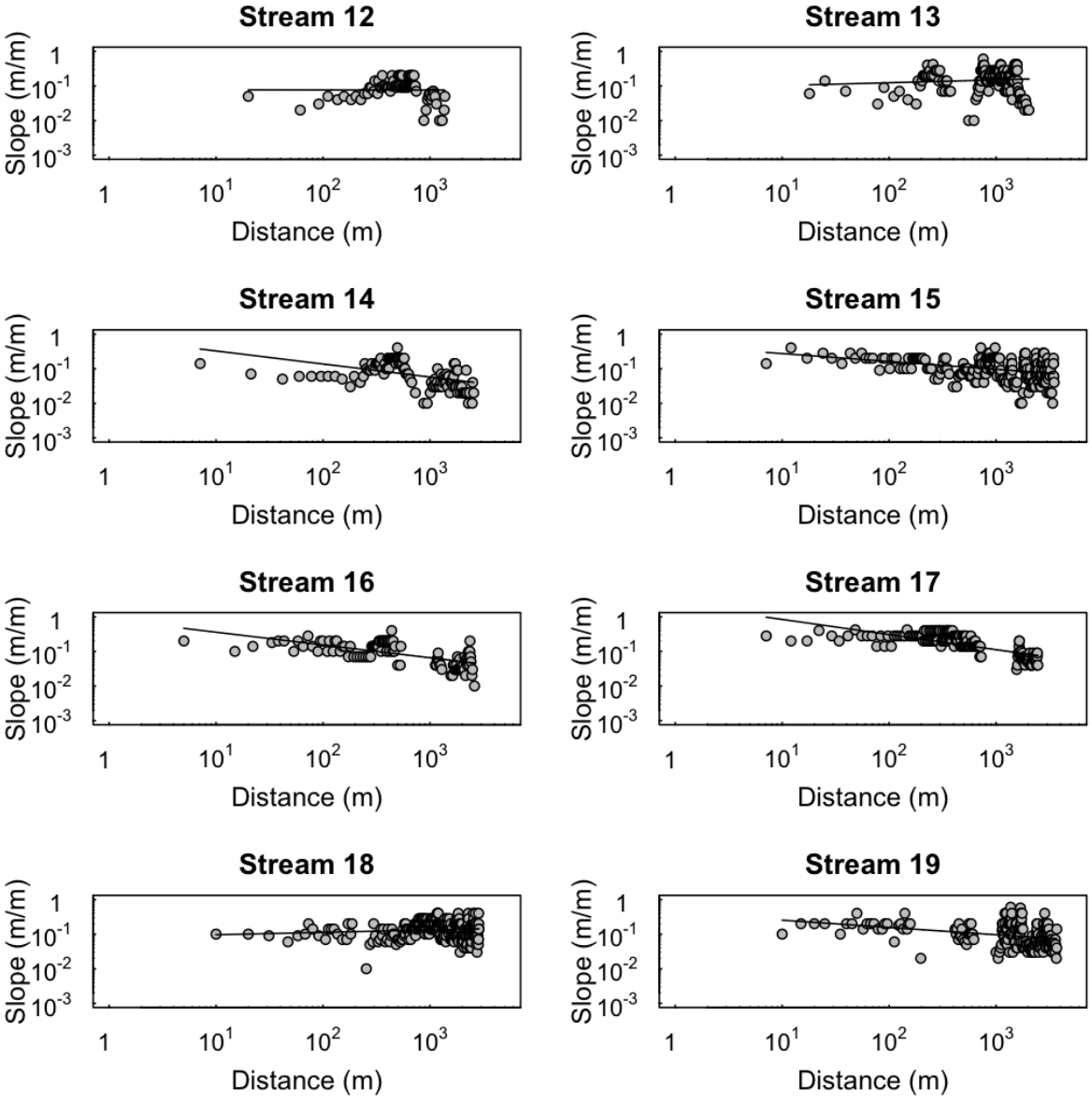
Stream 12
Stream 13
Stream 14
Stream 15
Stream 16
Stream 17
Stream 18
Stream 19
Slope (m/m)
1
10-1
10-2
10-3
1
101
102
103
Distance (m)

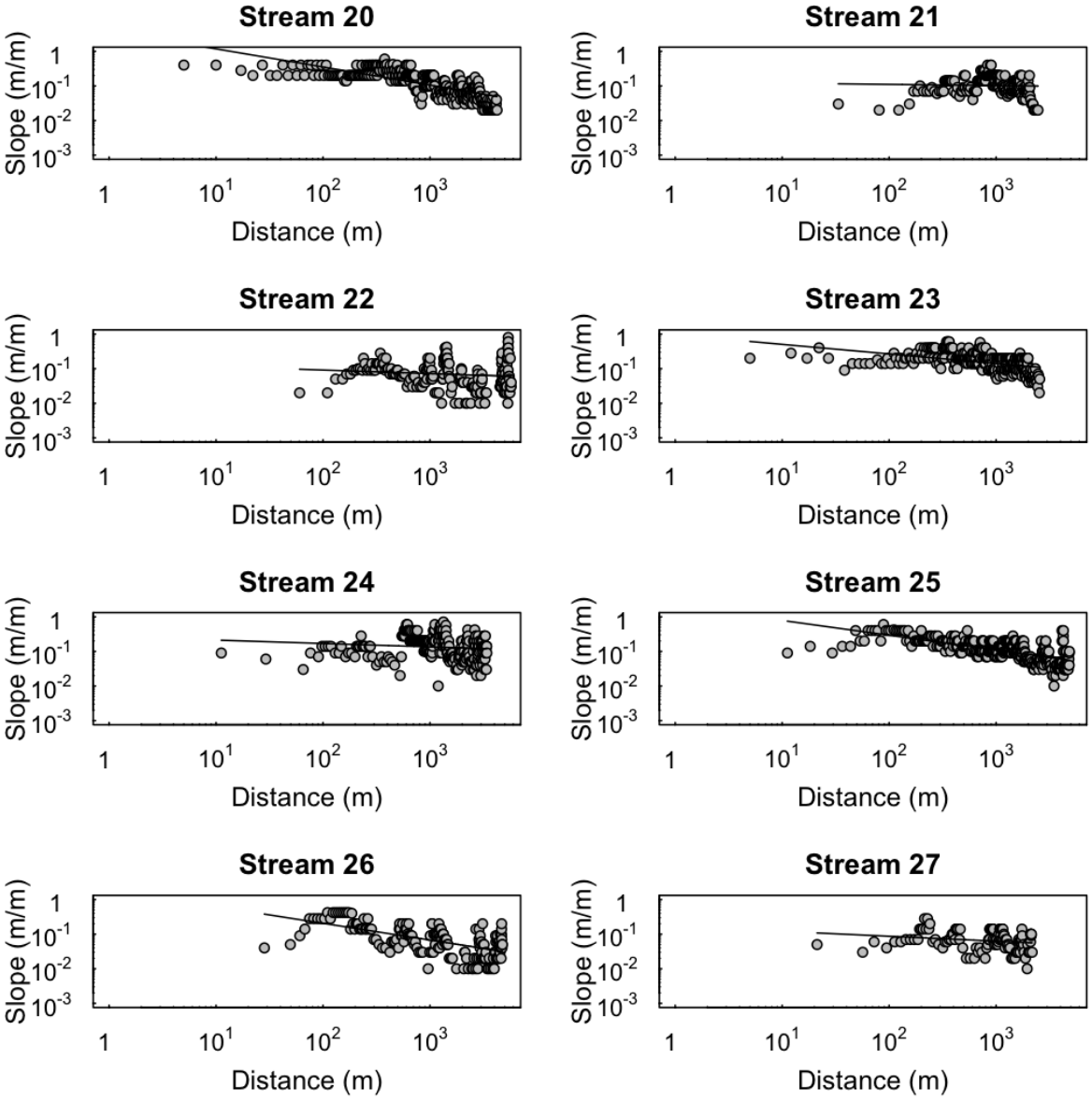
Stream 20
Stream 21
Stream 22
Stream 23
Stream 24
Stream 25
Stream 26
Stream 27
Slope (m/m)
Distance (m)
1
10^{-1}
10^{-2}
10^{-3}
10^{1}
10^{2}
10^{3}

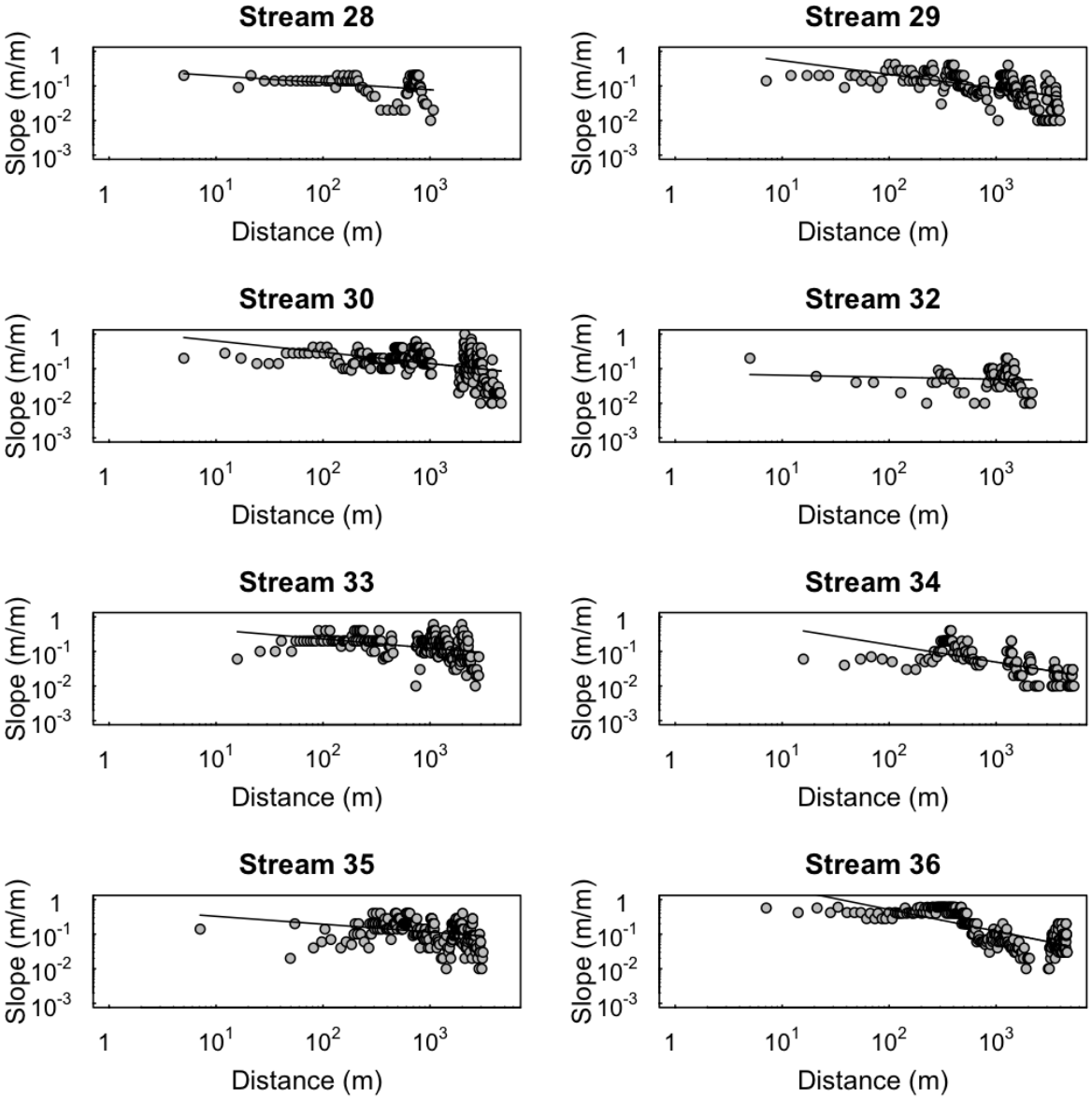
Stream 28
Stream 29
Stream 30
Stream 32
Stream 33
Stream 34
Stream 35
Stream 36
Slope (m/m)
Distance (m)
1
10^{-1}
10^{-2}
10^{-3}
10^{1}
10^{2}
10^{3}

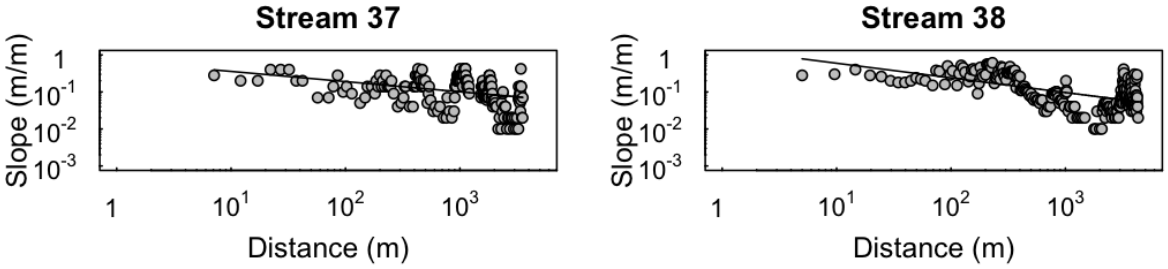
Stream 37
Slope (m/m)
1
10-1
10-2
10-3
1
101
102
103
Distance (m)
Stream 38
Slope (m/m)
1
10-1
10-2
10-3
1
101
102
103
Distance (m)

Appendix G

The distance-Slope plots of fluvial reaches

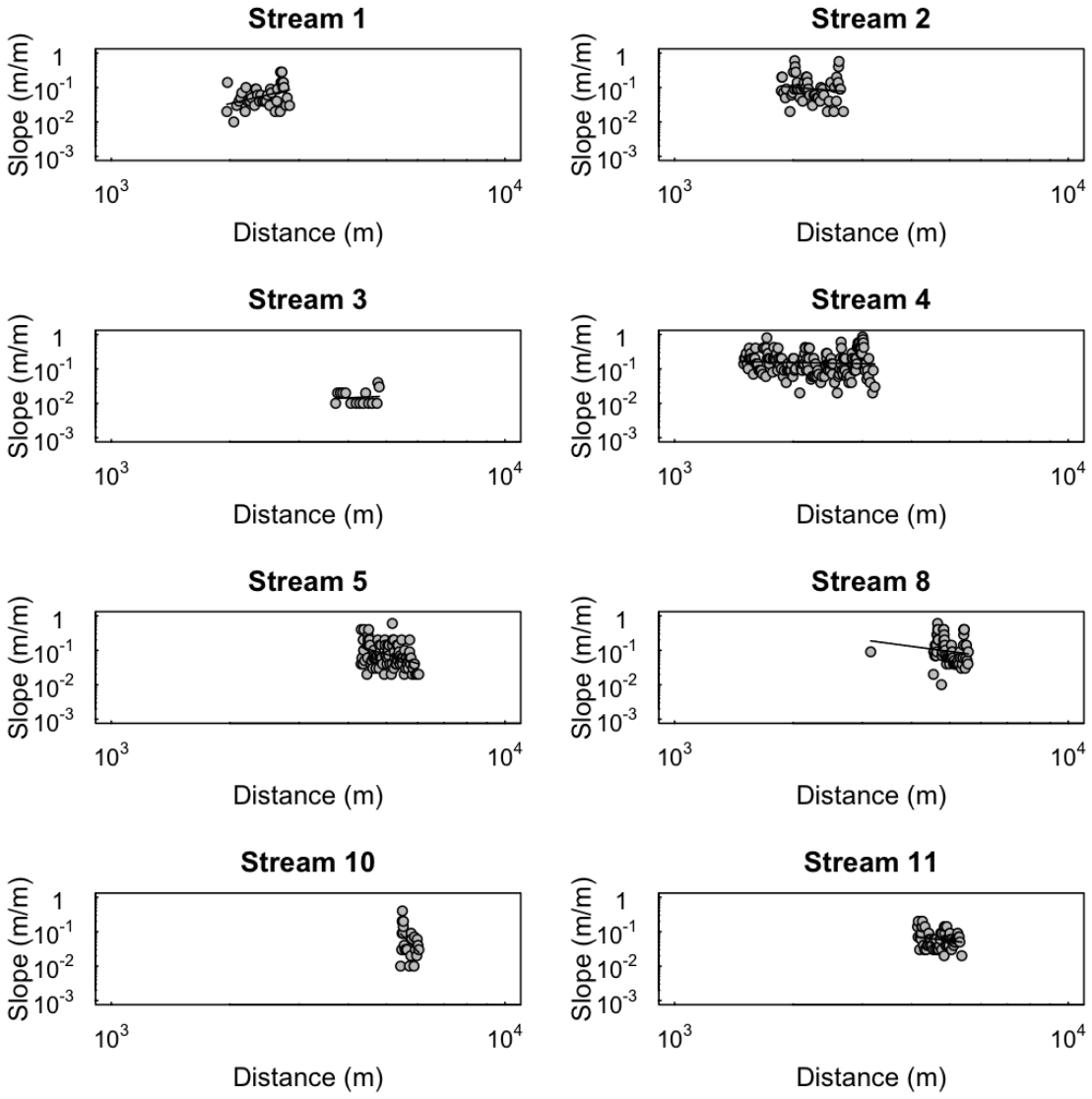

Figure G.1: Plots of drainage-area against channel slope of the fluvial reaches. The regression line is marked as a solid line and the dashed lines depict the 95% confidence limits

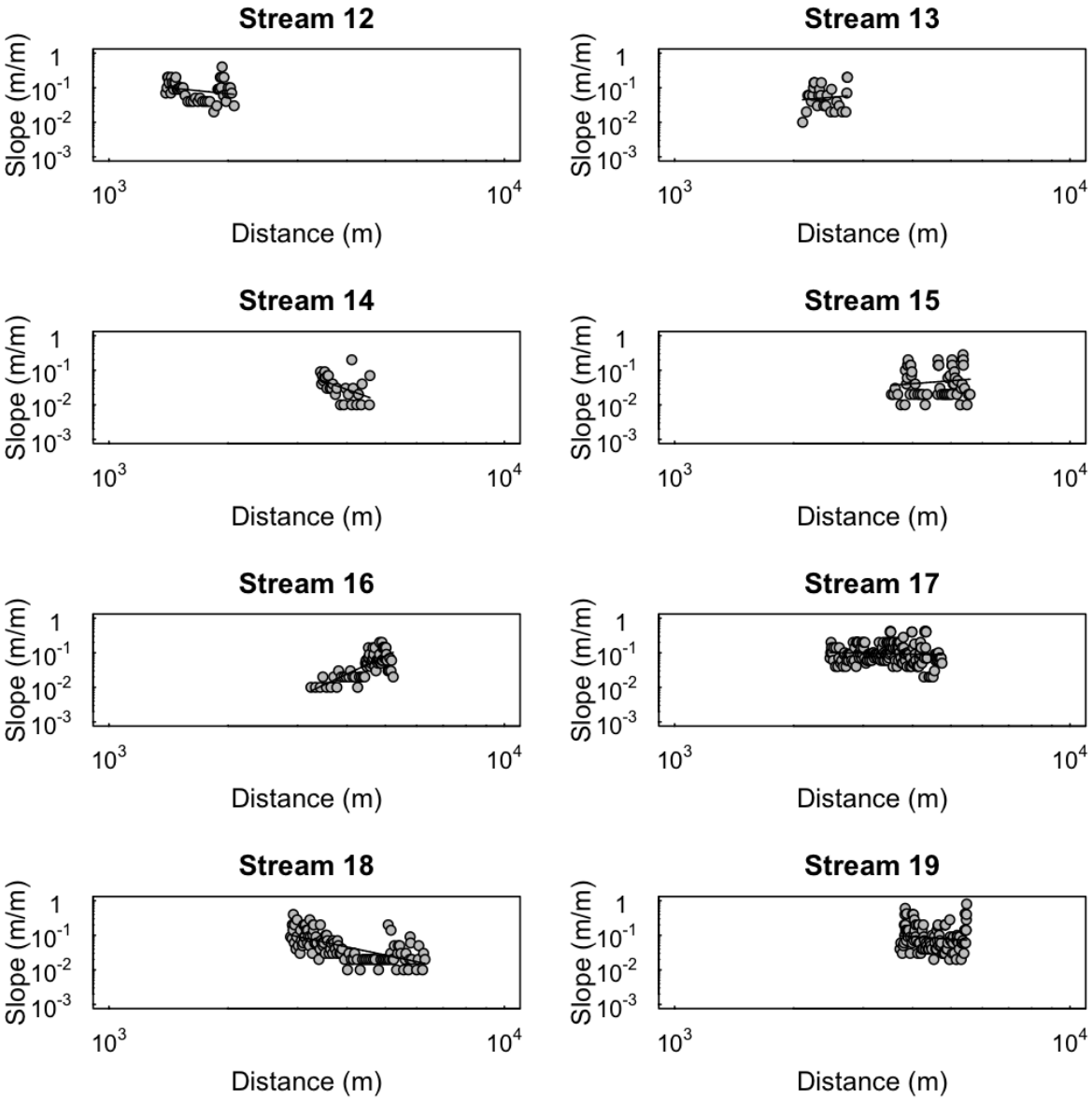
Stream 12
Stream 13
Stream 14
Stream 15
Stream 16
Stream 17
Stream 18
Stream 19
Slope (m/m)
1
10-1
10-2
10-3
10^3
10^4
Distance (m)

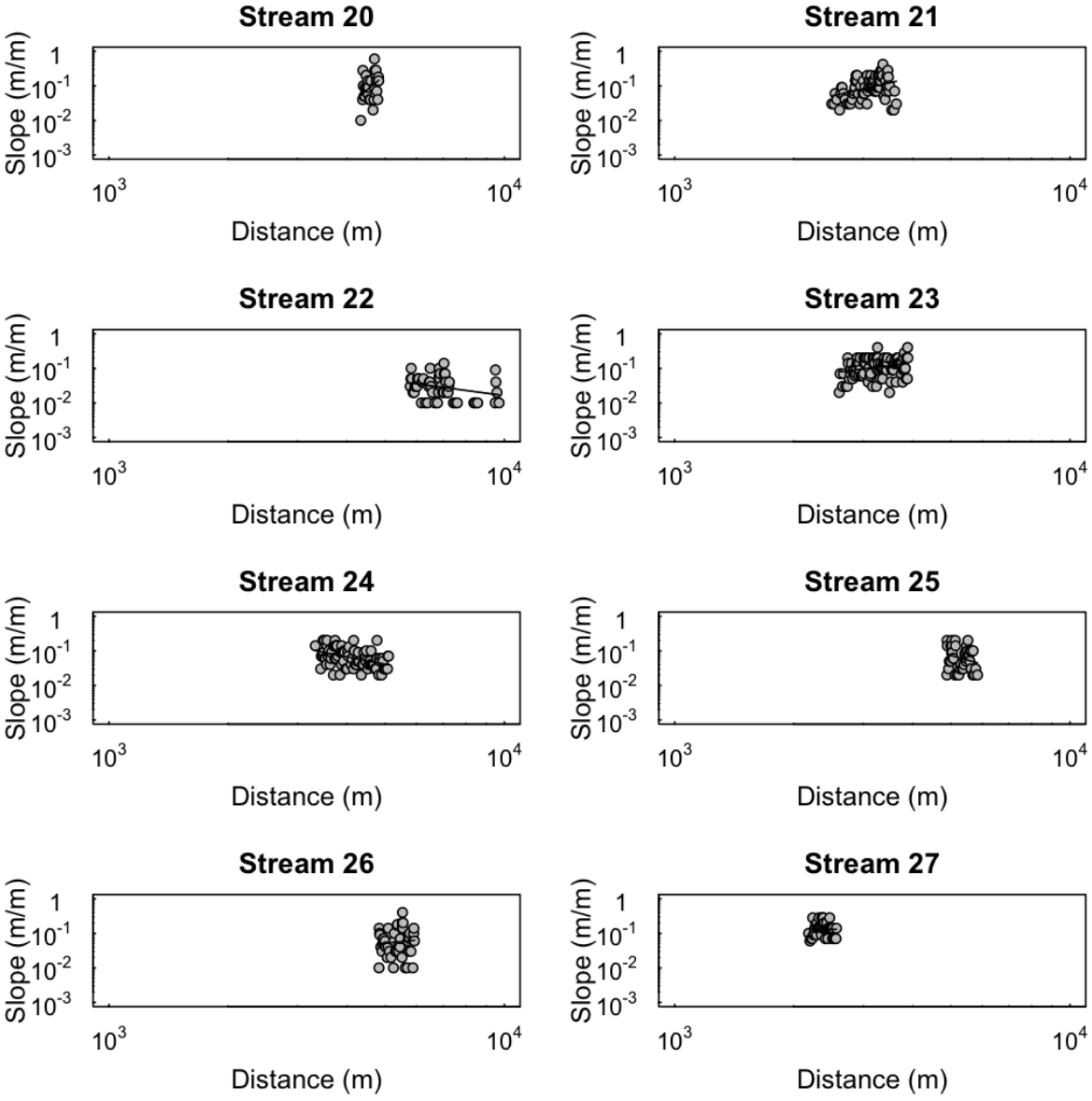
Stream 20
Stream 21
Stream 22
Stream 23
Stream 24
Stream 25
Stream 26
Stream 27
Slope (m/m)
1
10^{-1}
10^{-2}
10^{-3}
10^{3}
10^{4}
Distance (m)

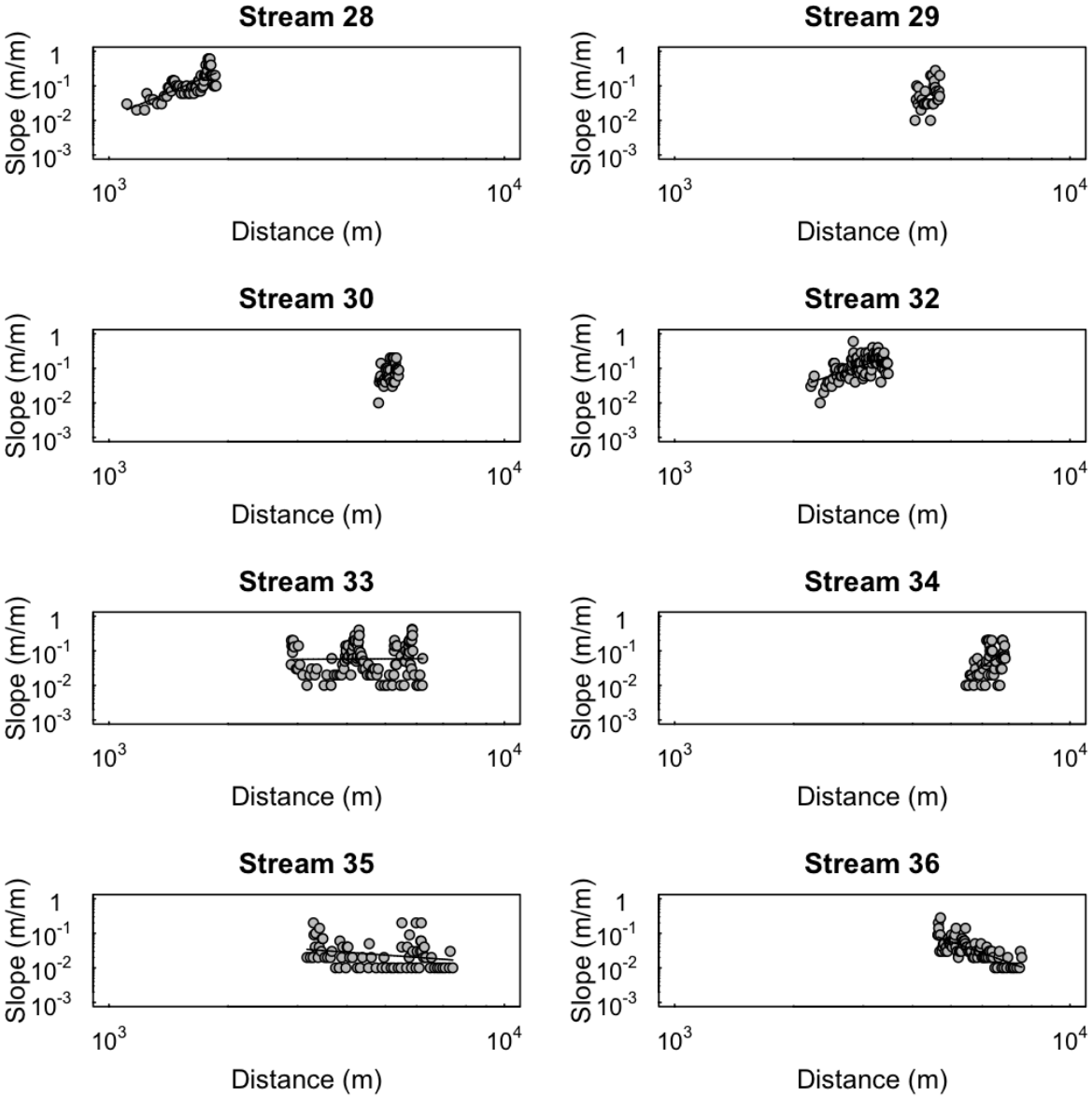
Stream 28
Stream 29
Stream 30
Stream 32
Stream 33
Stream 34
Stream 35
Stream 36
Slope (m/m)
1
10^{-1}
10^{-2}
10^{-3}
10^{3}
10^{4}
Distance (m)

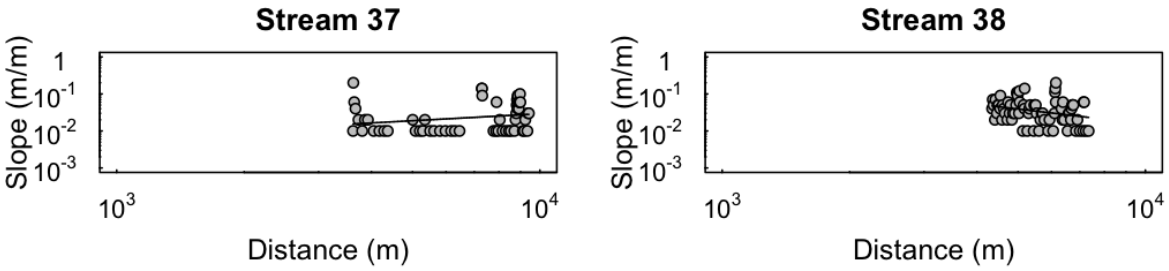
Stream 37
Slope (m/m)
1
10-1
10-2
10-3
10^3
10^4
Distance (m)
Stream 38
Slope (m/m)
1
10-1
10-2
10-3
10^3
10^4
Distance (m)

Appendix H

Lab procedures for the cosmogenic ^{10}Be samples

The samples were crushed and sieved in three fractions: $> 500\mu$, $250 - 500\mu$ and $< 250\mu$. The $250 - 500\mu$ fraction was washed three times and left to dry in the oven at 60°C for three days. Once dried, for each sample sin 100 g of sample was put in a glass beaker adding 10% of HCL/HNO_3 in order to remove carbonates and minerals. Beakers were placed on a hot plate and heated to 90°C and left there for one day. After cooling, samples were rinsed using distilled water and left to dry in an oven at $\sim$ 60°C for one night.

Once carbonates and other minerals were removed $\sim$ 60 g of sample was transferred to a 500 ml polyethylene bottle that was filled with distilled water and 100 ml of HF and 5 ml of HNO_3. Solution was added in other to remove the feldspar and remove the meteoric ^{10}Be. The samples were left in an ultrasonic bath for three days, the solution was homogenised three times per day. The samples were leached three times (washing the samples with distilled water and renewing the HF and HNO_3). Completed the three leaches, the samples were prepared to measure the aluminium concentration.

The samples to measure the aluminium concentration were prepared by collection $\sim$ 0.6 g of sample clean quartz sample and deposited in a teflon vial. Samples were weighted and diluted in 5 ml of HF and 5 drops of 1:1 H_2SO_4 were added. Vials were heated at 90°C and left to cool down. The remaining solution and solids on

the vial were diluted in 5 ml of 3% HNO_3 and the solution was homogenised. The concentration of aluminium was measured in the Thermo Scientific Atomic Absorption Spectrometry (AAS). Samples with a concentration of aluminium $> 120\mu$g/ g were leached again in HF until the Al concentration was reduced. The results for the aluminium concentrations are presented in Table H.1.

Table H.1: Concentration of aluminium measure in the AAS after the leaching of samples in HF

Sample code	**Sample weight (g)**	**Al (μg/g)**
J081103	0.6	118.3
J081105	0.4	86.4
J081106	0.4	55.3
J0905	0.5	103.0
J0908	0.5	97.3
J0906	0.6	65.5
J0909	0.5	87.1
J0911	0.4	101.3

Once the concentration of Al was below 120 ppm, the samples were transported to the CG-CNL at SUERC. There, the blank preparation and spiking of samples with a ^{9}Be carrier was used in order to determine the ^{10}Be/^{9}Be ratio in the AMS. The ultra pure clean quartz samples were transferred into a polyethylene bottle and weighted, 1000 μl of Be carrier was added to each samples and weighted again.

The samples were dissolved in concentrated HF and left in a hot plate at ~ 90°C degrees to dissolve them completely. The remaining solution after the HF evaporation was transferred to a beaker and the solution on the polyethylene bottle was rinsed with Milli-Q water, 3 ml of 6M HCL and 1 ml of 8M HNO_3 was added in order to remove the TiO_2. The samples were heated and fluoride salts precipitated, 2 ml of 6N HCL were added and the samples where heated again until they were

dissolved. The samples were transferred to a centrifuge tube and 1 ml of 6N HCL was added. The samples were centrifuged for 10 minutes at 3500 rpm and were by this way their were ready for the anion exchange chromatography.

For the anion exchange chromatography a resin AG-1 X8 200-400 was moisturised in 1.2N HCL. The resin was prepared with 10 ml 6N HCL and diluted in a column, the solution was placed in the column, the Al and Be was collected in a 20 ml Teflon vial and labelled. The Fe and Ti fraction was eluted into a tube and 1 drop of 2% H_2O_2 was added to facilitate dilution of Ti. To remove the AL bulk and Be, the Al and Be solution was heated at 90°C and left to dry. 10 ml of Milli-Q water and 2ml of HNO_3 were added, once the solution was dried. Samples were transferred to a centrifuge tube and spin. NH_4OH was added for the solution to reach a pH 8 and warmed in warm water for approximately 2 hours. Al was split by rising the pH to 11.5 with 0.2 ml of 50% of NaOH and drops of 6M NaOH. The Be was precipitated at the bottom of tubes and the solutions were centrifuged for 10 minute at 3500 rpm. The precipitate was collected by adding 20 ml of Milli-Q water and HN3, samples were centrifuged again and 5 ml 1.2 MHCL were added. The solutions were transferred to a Teflon vial and dried into a hot plate.

The dried samples were converted to sulphate by adding 5 drops of 2% H_2O_2, 2 ml of Milli-Q water and 0.5M H_2SO_4. The solution was heated at 90°C. After samples were dissolved, they were left for 12 hour in 2% H_2O_2 and transferred after that time into a centrifuge tube, adding 1 ml of 0.5M H_2SO_4. For the final split of Be a cation exchange chromatography was required. Cation exchange uses a resin AG 50W -X8 200-400 moisturised with HCL. For Ti, the columns were conditioned with 10 ml 0.2M H_2SO_4 and the solution was poured into the columns, 8 ml 0.5M H_2SO_4 were added. The Be was obtained by adding 10 ml 1.2N HCL and collected into a Teflon vial. Once eluted 5 drops of 8M HNO_3 were added an heated at 60° to the Be solution but avoiding the full dryness. The Al was obtained by adding 6 ml of 4M HCL in the column. The solution containing Al was collected and

stored. The Be was precipitated in hydroxides by transferring the samples into a centrifuge tube and adding 2 ml 1% of HNO_3. The Be was precipitated by reaching a pH 8 adding a solution of 25% NH_4OH and centrifuging the samples to collect the precipitates. The Be precipitates were dried by putting these into a oven at 70°C. After drying, a pellet of BeO were transferred into a crucible and prepared for mixing an pressing. The BeO pellets were mixed with Nb powder containing the NIST306000 to standardise the AMS measurements (Nishiizumi et al., 2007) and pressed in cathodes for their further measurements in the AMS.

Appendix I

Measurements of cosmogenic ^{10}Be

Table I.1: Measurements obtained for the cosmogenic ^{10}Be samples send at SUERC.

Sample ID†	^{10}**Be**/^{9}**Be**	$\sigma(^{10}$**Be**/^{9}**Be)**	σ%	**%of Standard**	**BeO^{-}current**
GCFG1004	5.6940E-15	1.3810E-15	24.25	0.019	0.005
GJ081103	5.6138E-14	2.7710E-15	4.94	0.183	0.009
GJ081105	71.9032E-14	2.3250E-15	12.22	0.062	0.008
GJ081106	2.8976E-14	1.8710E-15	6.46	0.095	0.006
GJ0905	3.6869E-14	2.8540E-15	7.74	0.120	0.009
GJ0906	6.7069E-14	4.0840E-15	6.09	0.219	0.013
GJ0909	3.3856E-14	1.8240E-15	5.39	0.111	0.006
GJ0911	2.0931E-14	1.7100E-15	8.17	0.068	0.006
GCFG1005	4.9918E-15	1.2890E-15	25.82	0.016	0.004
GJ0908	3.1275E-14	2.0630E-15	6.60	0.102	0.007

† Blanks are labelled as CFG1004 and CFG1005. Letter G in samples indicates that the sample was processed at the CG-CNL

Appendix J

Data submitted to the Cronus-Earth calculator

Table J.1: Data set submitted to Cronus-Earth Project (2010) calculator to obtain bedrock incision rates

Sample ID	**Coordinate (Lat. Long.)**	**Elevation (m OD)**	**Pressure†**	**Thickness (cm)**	**Density (g/cm^3)**	**S.f.†**	**^{10}Be (atoms)**	**σ^{10}Be (atoms)**	**Be AMS Std**
J081103	55.86, -6.04	179	Std	2	2.65	0.9969	41793	2907	NIST30600
J081105	55.86, -6.05	122	Std	2	2.65	0.9469	9838	2207	NIST30600
J081106	55.86, -6.08	38	Std	2	2.65	0.9086	11985	1384	NIST30600
J0905	55.83, -6.07	72	Std	2	2.65	0.9946	17399	1940	NIST30600
J0906	55.83, -6.07	68	Std	2	2.65	0.9686	31683	2413	NIST30600
J0909	55.83, -6.08	36	Std	2	2.65	0.8975	18976	1805	NIST30600
J0911	55.86, -6.07	50	Std	2	2.65	0.8293	9207	1540	NIST30600
J0908	55.83, -6.08	38	Std	2	2.65	0.8491	22189	2356	NIST30600

†Refers to the standard atmospheric pressure correction proposed by Stone (2000)

‡ Shielding factor, also presented in Table 6.3

References

Alley, R., Clark, P., Huybrechts, P., and Joughin, I. (2005). Ice-sheet and sea-level changes. *Science*, 310:456–460.

Amos, C. and Burbank, D. (2007). Channel width response to differential uplift. *Journal of Geophysical Research*, 112(F2010).

Anderton, R. (1971). Dalradian Palaeocurrents from the Jura Quartzite. *Scottish Journal of Geology*, 7(2):175–178.

Anderton, R. (1976). Tidal-shelf sedimentation: an example from the Scottish Dalradian. *Sedimentology*, 23:429–458.

Anderton, R. (1977). The Dalradian rocks of Jura. *Scottish Journal of Geology*, 13(2):135–142.

Anderton, R. (1985). Sedimentation and tectonics in the Scottish Dalradian. *Scottish Journal of Geology*, 21(4):407–436.

Anderton, R., Bridges, P., Leeder, M., and Sellwood, B. (1979). *A Dynamic Stratigraphy of the British Isles*. George Allen & Unwin, London.

Andrews, J. and Dugdale, R. (1970). Age prediction of glacio-isostatic strandlines based on their gradients. *Geological Society of America Bulletin*, 81:3769–3772.

Anthony, D. and Granger, D. (2007). An empirical stream power formulation for knickpoint retreat in Appalachian Plateau fluviokarst. *Journal of Hydrology*, 343:117–126.

Attal, M., Cowie, P., Whittaker, A., Hobley, D., Tucker, G., and Roberts, G. (2011). Testing fluvial erosion models using the transient response of bedrock rivers to tectonic forcing in the Apennines, Italy. *Journal of Geophysical Research*, 116:F02005.

Attal, M. and Lavé, J. (2006). Changes of bedload characteristics along the Marsyandi River (central Nepal): Implications for understanding hillslope denudation in active orogenic belts. In Willet, S., Hovious, N., Brandon, M., and Fisher, D., editors, *Tectonics from topography: Procedures, promise and pitfalls*, number 398 in Special Paper. Geological Society of America.

Attal, M., Tucker, G., Whittaker, A., Cowie, P., and Roberts, G. (2008). Modeling fluvial incision and transient landscape evolution: influence of dynamic channel adjustment. *Journal of Geophysical Research*, 113.

Bagnold, R. (1960). Sediment discharge and stream power. *Geological Survey Circular*, 421.

Bagnold, R. (1977). Bed load transport by natural rivers. *Water Resources Research*, 13(2).

Bailey, E. (1916). The Islay Anticline (Inner Hebrides). *Quarterly Journal of the Geological Society*, 72:132–164.

Balco, G., Stone, J., Lifton, N., and Dunai, T. (2008). A complete and easily accesible means of calculating surface exposure ages or erosion rates from ^{10}Be and ^{26}Al measurements. *Quaternary Geochronology*, 3:174–195.

Baldwin, J., Whipple, K., and Tucker, G. (2003). Implications of the shear stress river incision model for timescale of postorogenic decay of topography. *Journal of Geophysical Research*, 108(B3).

Ballantyne, C. (1999). Maximum altitude of Late Devensian glaciation on the Isle of Mull and Isle of Jura. *Scottish Journal of Geology*, 35(2):97–106.

Ballantyne, C. (2009). Extent and deglacial chronology of the last British-Irish Ice Sheet: implications of exposure dating using cosmogenic isotopes. *Journal of Quaternary Science*, 25(4):515–534.

Ballantyne, C., McCarroll, D., Nesje, A., Dahl, S., and Stone, J. (1998). The last ice sheet in north-west Scotland: Reconstruction and implications. *Quaternary Science Reviews*, 17:1149–1184.

Beaumont, C., Fullsack, P., and Hamilton, J. (1992). Erosional control of active compressional orogens. In McClay, K., editor, *Thrust Tectonics*. Chapman and Hall, United Kingdom.

Berlin, M. and Anderson, R. (2007). Modeling of knickpoint retreat on the Roan Plateau, western Colorado. *Journal of Geophysical Research*, 112(F03S06).

Berlin, M. and Anderson, R. (2009). Steepened channels upstream of knickpoints: Controls on relict landscape response. *Journal of Geophysical Research*, 114(F03018).

BGS (2010). *Geologic map of Great Britain*. British Geological Society and EDINA.

Bierman, P. (1994). Using in situ produced cosmoegenic isotopes to estimate rates of landscape evolution: A review from the geomorphic perspective. *Journal of Geophysical Research*, 99(B7):13885–13896.

Bierman, P. and Steig, E. (1996). Estimating rates of denudation using cosmogenic isotope abundances in sediment. *Earth Surface Processes and Landforms*, 21:125–139.

Bigi, A., Hasbargen, L., Montanary, A., and Paola, C. (2006). Knickpoint and hillslope failures: Interactions in a steady-state experimental landscape. In Willet, S., Hovious, N., Brandon, M., and Fisher, D., editors, *Tectonics, climate and landscape evolution*, number 398 in Special Paper, pages 101–126. Geological Society of America.

Bird, M., Austin, W., Wurster, C., Fifield, L., Mojtahid, M., and Sargeant, C. (2010). Punctuated eustatic sea-level rise in the early mid-Holocene. *Geology*, 38:803–806.

Bishop, P. (2007). Long-term landscape evolution: linking tectonics and surface processes. *Earth Surfaces Processes and Landforms*, 32:329–365.

Bishop, P. (2009). Landscape evolution. In Gomez, B., Baker, V., Goudie, A., and Roy, A., editors, *Handbook of Geomorphology*. SAGE Publications, London.

Bishop, P., Hoey, T., Jansen, J., and Lexartza, I. (2005). Knickpoint recession rate and catchment area: the case of uplifted rivers in Eastern Scotland. *Earth Surface Processes and Landforms*, 30:767–778.

Born, S. and Ritter, D. (1970). Modern terrace development near Pyramid Lake, Nevada, and its geologic implications. *Geological Society of America Bulletin*, 81:1,233–1,242.

Boulton, G. and Hagdorn, M. (2006). Glaciology of the British Isles Ice Sheet during the last glacial cycle: form, flow, streams and lobes. *Quaternary Science Reviews*, 25:3359–3390.

Boulton, G., Peacock, J., and Sutherland, D. (1991). Quaternary. In Craig, G., editor, *Geology of Scotland*, pages 503–557. The Geological Society, London, third edition.

Bowen, D. (1989). The Last Inter-Glacial cycle in the British Isles. *Quaternary International*, 3-4(41-47).

Bradley, W., Fahnestock, R., and Rowekamp, E. (1972). Coarse sediment transport by flood flows on Knik River, Alaska. *Geological Society of America Bulletin*, 83:1,261–1,284.

Bradwell, T., Stoker, M., Golledge, N., Wilson, K., Merritt, J., Long, D., Everest, J., Hestvik, O., Stevenson, A., Hubbard, A., Finlayson, A., and Mathers, H.

(2008a). The northern sector of the last British Ice Sheet: Maximum extent and demise. *Earth Science Reviews*, 88:207–226.

Bradwell, T., Stroker, M., and Krabbendam, M. (2008b). Megagrooves and streamlined bedrock in NW Scotland: The role of ice streams in landscape evolution. *Geomorphology*, 97:135–156.

Brierley, G. and Hickin, E. (1985). The downstream gradation of particles in the Squamish River, British Columbia. *Earth Surface Processes and Landforms*, 10(597-606).

Brocard, G. and van der Beek, P. (2006). Influence of incision rate, rock strength and bedload supply on bedrock river gradients and valley-flat width: Field-based evidence and calibrations from western Alpine rivers (southeast France). In Willet, S., Hovious, N., Brandon, M., and Fisher, D., editors, *Tectonics, climate and landscape evolution*, number 398 in Special Paper, pages 101–126. Geological Society of America.

Brocklehurst, S. and Whipple, K. (2002). Glacial erosion and relief production in the Eastern Sierra Nevada, California. *Geomorphology*, 42:1–24.

Brocklehurst, S. and Whipple, K. (2004). Hypsometry of glaciated landscapes. *Earth Surface Processes and Landforms*, 29:907–926.

Brown, E., Stallard, R., Larsen, M., Raisbeck, G., and Yiou, F. (1995). Denudation rates determined from the accumulation of in situ-produced ^{10}Be in the Luqillo Experimental Forest, Puerto Rico . *Earth and Planetary Science Letters*, 129:193–202.

Brush, L. and Wolman, G. (1960). Knickpoint behaviour in noncohesive material: a laboratory study. *Bulletin of the Geological Society of America*, 71:59–74.

Buffington, J. and Montgomery, D. (1997). A systematic analysis of eight decades of incipient motion studies, with special reference to gravel-bedded rivers. *Water Resources Research*, 33(8):1,993–2,029.

Burbank, D. (2002). Rates of erosion and their implications for exhumation. *Mineralogical Magazine*, 66:25–52.

Burbank, D. and Anderson, R. (2001). *Tectonic Geomorphology*. Blackwell Science, USA.

Cerling, T. and Craig, H. (1994). Geomorphology and in-situ cosmogenic isotopes. *Annual Review Earth Planetary Science*, 22:273–317.

Chatanantavet, P. and Parker, G. (2009). Physically based modeling of bedrock incision by abrasion, plucking, and macroabrasion. *Journal of Geophysical Research*, 114(F04018).

Chiverrell, R. and Thomas, G. (2010). Extent and timing of the Last Glacial Maximum (LGM) in Britain and Ireland: a review. *Journal of Quaternary Science*, 25(4):535–549.

Chorley, R., Schumm, S., and Sugden, D. (1984). *Geomorphology*. Methuen & Co., Great Britain.

Church, M. and Slaymaker, O. (1989). Disequilibrium of Holocene sediment yield in glaciated British Columbia. *Nature*, 337:452–454.

Clark, C., Evans, D., Khatwa, A., T., B., Jordan, C., Marsh, S., Mitchell, W., and Bateman, M. (2004a). Map and GIS database of glacial landforms and features related to the last British Ice Sheet. *Boreas*, 33:359–375.

Clark, M., Maheo, G., Salaeby, J., and Farley, K. (2005). The non-equilibrium landscape of the southern Sierra Nevada, California. *Geological Society of America Today*, 15(9):4–10.

Clark, M., Schoenbohm, L., Royden, L., Whipple, K., Burchfiel, B., Zhang, X., Tang, W., Wang, E., and Chen, L. (2004b). Surface uplift, tectonics, and erosion of eastern Tibet from large-scale drainage patterns. *Tectonics*, 23(TC1006).

Cockburn, H. and Summerfield, M. (2004). Geomorphological applications of cosmogenic isotope analysis. *Progress in Physical Geography*, 28(1):1–42.

Codilean, A., Bishop, P., and Hoey, T. (2006). Surface process models and the links between tectonics and topography. *Progress in Physical Geography*, 30:307–333.

Codilean, A., Bishop, P., Stuart, F., Hoey, T., Fabel, D., and Freeman, S. (2008). Single-grain cosmogenic ^{21}Ne concentrations in fluvial sediments reveal spatially variable erosion rates. *Geology*, 36:159–162.

Cowie, P., Attal, M., Roberts, G., and Ganas, A. (2008). New constrains on sediment-flux-dependent river incision: Implications for extracting tectonic signals from river profiles. *Geology*, 36(7):535–538.

Cronus-Earth Project (2010). Cronus-Earth Online Calculator. Technical report, Cosmogenic Nuclide Laboratory, University of Washington.

Crosby, B. and Whipple, K. (2006). Knickpoint initiation and distribution within fluvial networks: 236 waterfalls in the Waipaoa River, North Island, New Zealand. *Geomorphology*, 82:16–38.

Crosby, B., Whipple, K., Gasparini, N., and Wobus, C. (2007). Formation of fluvial hanging valleys: Theory and simulation. *Journal of Geophysical Research*, 112.

Cyr, A., Granger, D., Olivetti, V., and Molin, P. (2010). Quantifying rock uplift rates using channel steepness and cosmogenic nuclide-determined erosion rates: Examples from northern and southern Italy. *Lithosphere*, 2:188–198.

Dadson, S., Hovius, N., Chen, H., Dade, B., Hsieh, M., Willet, S., Hu, J., Horng, M., Chen, M., Stark, C., Lague, D., and Lin, J. (2003). Links between erosion, runoff variability and seismicity in the Taiwan orogen. *Nature*, 426:648–651.

Davis, W. (1889). The Geographical Cycle. *The Geographical Journal*, 14(5):481–504.

Davis, W. (1932). Piedmont benchlands and primärruümpfe. *Geological Society of America Bulletin*, 43:399–440.

Dawson, A. (1979). A Devensian Medial Moriane in Jura. *Scottish Journal of Geology*, 15(1):43–48.

Dawson, A. (1980). The low rock platform in western Scotland. *Proceedings of the Geological Association*, 91(4):339–344.

Dawson, A. (1982). Lateglacial sea-level changes and ice-limits in Islay, Jura and Scarba, Scottish Inner Hebrides. *Scottish Journal of Geology*, 18(4):253.

Dawson, A. (1984). Quaternary sea-level changes in western Scotland. *Quaternary Science Reviews*, 3:345–368.

Dawson, A. (1997). Introduction. In Dawson, A. and Dawson, S., editors, *Quaternary of Islay and Jura*. Quaternary Research Association, Great Britain.

Dawson, A., Smith, D., Dawson, S., Brooks, C., Foster, I., and Tooley, M. (1999). Lateglacial climate change and coastal evolution in western Jura, Scottish Inner Hebrides. *Geologie en Mijnbouw*, 77:225–232.

Desilets, D., Zreda, M., and Prabu, T. (2006). Extended scaling factor for in situ cosmogenic nuclides: New measurements at low altitude. *Earth and Planetary Science Letters*, 246:265–276.

DiBiase, R., Whipple, K., Heimsath, A., and Ouimet, W. (2010). Landscape form and millenial erosion rates in the San Gabriel Mountains, CA. *Earth and Planetary Science Letters*, 289:134–144.

Dietrich, R., Ivins, E., Casassa, G., Lange, H., Wendt, J., and Fritsche, M. (2010). Rapid crustal uplift in Patagonia due to enhance ice loss. *Earth and Planetary Science Letters*, 289:22–29.

Dunai, T. (2000). Scaling factors for production rates of in situ produced cosmogenic nuclides: a critical reevaluation. *Earth and Planetary Science Letters*, 176:157–169.

Duvall, A., Kirby, E., and Burbank, D. (2004). Tectonic and lithologic controls on bedrock channel profiles and processes in coastal California. *Journal of Geophysical Research*, 109.

Elmore, D. and Phillips, F. (1987). Accelerator Mass Spectrometry for measurement of long-lived radioisotopes. *Science*, 236:543–550.

Emery, K. and Aubrey, D. (1985). Glacial rebound and relative sea levels in Europe from tide-gauge records. *Tectonophysics*, 120:239–255.

England, P. and Molnar, P. (1990). Surface uplift, uplift of rocks and exhumation of rocks. *Geology*, 18:1173–1177.

Fahnestock, R. (1963). White River, Mount Rainier Washinton: A study of the hydraulic and morphologic processes by which a valley train is formed in a proglacial stream.

Fairbanks, R. (1989). A 17,000-year glacio-eustatic sea level record: influence of glacial melting rates on the Younger Dryas event and deep-ocean circulation. *Nature*, 342:637–642.

Ferguson, R. and Churh, M. (2006). A simple universal equation for grain settling velocity. *Journal of Sedimentary Research*, 74(6):933–937.

Fernandez-Luque, R. and van Beek, R. (1976). Erosion and transport of bed-load sediment. *Journal of Hydraulic Research*, 14:127–144.

Finlayson, D. and Montgomery, D. (2003). Modeling large-scale fluvial erosion in geographic information systems. *Geomorphology*, 53:147–164.

Finnegan, N., Roe, G., Montgomery, D., and Hallet, B. (2005). Controls on the channel width of rivers: Implications for modeling fluvial incision of bedrock. *Geology*, 33(3):229–232.

Finnegan, N., Sklar, L., and Fuller, T. (2007). Interplay of sediment supply, river incision and channel morphology revealed by the transient evolution of an experimental bedrock channel. *Journal of Geophysical Research*, 112(F03S11).

Firth, C. and Stewart, I. (2000). Postglacial tectonics of the Scottish glacio-isostatic uplift centre. *Quaternary Science Reviews*, 19:1469–1493.

Flint, J. (1974). Stream gradient as a function of order magnitude and discharge. *Water Resources Research*, 10(5):969–973.

Foley, M. (1980). Bed-rock incision by streams: Summary. *Geological Society of America Bulletin*, 91(10):577–578.

Frankel, K., Pazzaglia, F., and Vaughn, J. (2007). Knickpoint evolution in a vertically bedded surface, upstream-dipping terraces and Atlantic slope bedrock channels. *Geological Society of America Bulletin*, 119(3-4):476–486.

Fuller, T., Perg, L., Willenbring, J., and Lepper, K. (2009). Field evidence for climate-driven changes in sediment supply leading to strath terrace formation. *Geology*, 37:467–470.

Gardner, T. (1983). Experimental study of knickpoint and longitudinal profile evolution in cohesive, homogeneous material. *Geological Society of America Bulletin*, 94:664–672.

Gasparini, N., Bras, R., and Whipple, K. (2006). Numerical modeling of non-steady state river profile evolution using a sediment-flux-dependent incision model. In Willet, S., Hovious, N., Brandon, M., and Fisher, D., editors, *Tectonics, climate and landscape evolution*, number 398 in Special Paper. Geological Society of America.

Gilbert, G. (1877). *Geology of Henry Mountains*. Government Printing Office.

Gilbert, G. (1907). Rate of recession of Niagara Falls. *Descriptive Geology*, 109(306):5–67.

Gilchrist, A., Summerfield, M., and Cockburn, H. (1994). Landscape dissection, isostatic uplift and the morphologic development of orogens. *Geology*, 22:963–966.

Gillespie, A. and Bierman, P. (1995). Precision of terrestial exposure ages and erosion rates estimated from analysis of cosmogenic isotopes produced in situ. *Journal of Geophysical Research*, 100(B12):24,637–24,649.

Golden, L. and Springer, G. (2006). Channel geometry, median grain size and stream power in small mountain streams. *Geomorphology*, 78:64–76.

Goldrick, G. (1999). *Bedrock stream long profile form and evolution: a new framework with case studies from the Lachlan catchment, N.S.W.* Phd thesis, Department of Geography and Environmental Science, Monash University.

Goldrick, G. and Bishop, P. (1995). Differentiating the roles of lithology and uplift in the steepening of bedrock river long profiles: An example from southeastern Australia. *Journal of Geology*, 103:227–231.

Goldrick, G. and Bishop, P. (2007). Regional analysis of bedrock stream long profiles: evaluation of Hack's SL form and formulation and assessment of an alternative (the DS form). *Earth Surface Processes and Landforms*, 32:649–671.

Golledge, N. (2010). Glaciation of Scotland during the Younger Dryas stadial: a review. *Journal of Quaternary Science*, 25(4):550–566.

Golledge, N., Fabel, D., Everest, J., Freeman, S., and Binnie, S. (2007). First cosmogenic 10Be age constraint on the timing of the Younger Dryas glaciation and ice cap thickness, western Scottish Highlands. *Journal of Quaternary Science*, 22:785–791.

Goode, J. and Burbank, D. (2009). Numerical study of degradation of fluvial hanging valleys due to climate change. *Journal of Geophysical Research*.

Gordon, J. and Sutherland, D. (1993). Introduction. In Gordon, J. and Sutherland, D., editors, *Quaternary of Scotland*. Chapman & Hall, London.

Gosse, J. and Phillips, F. (2001). Terretrial in situ cosmogenic nuclides: theory and application. *Quaternary Science Reviews*, 20:1475–1560.

Graf, W. (1970). The geomorphology of the glacial valley cross section. *Artic and Alpine Research*, 2(4):303–312.

Graham, C. and Borradaile, G. (1984). The petrology and structure of Dalradian metabasaltic dykes of Jura: implications for early Dalradian evolution. *Scottish Journal of Geology*, 20(2):257–270.

Granger, D. and Riebe, C. (2007). Cosmogenic Nuclides in Weathering and Erosion. In Drever, J., editor, *Treatise on Geochemestry and Ground Water, Weathering, and Soils*. Elsevier.

Granger, D., Riebe, C., Kirchner, W. J., and Finkel, R. (2001). Modulation of erosion on steep granitic slopes by boulder armoring, as revelaed by cosmogenic ^{26}Al and ^{10}Be. *Earth and Planetary Science Letters*, 186(269-281).

Gray, M. (1975). The Loch Lomond Readvance and contemporaneous sea-levels in Loch Etive and neighbouring areas of western Scotland. *Proceedings of the Geological Association*, 2:227–238.

Gray, M. (1978). Low-level shore platforms in the south-west Scottish Highlands: Altitude, age and correlation. *Transactions of the Institute of British Geographers*, 3(2):151–164.

Gray, M. and Ivanovich, M. (1988). Age of the Main Rock Platforms, western Scotland. *Palaeogeography, Palaeoclimatology, Palaeoecology*, 68:337–345.

Hack, J. (1957). Studies of longitudinal stream profiles in Virginia and Maryland. *USGS Professional Paper*, 249(3):45–97.

Hack, J. (1960). Interpretation of erosional topography in humid temperate regions. *American Journal of Science*, 258-A:80–97.

Hack, J. (1973). Stream-profile analysis and stream gradient index. *Journal of Research*, 1(4):421–429.

Hack, J. (1975). Dynamic equilibrium and landscape evolution. In Melhorn, W. and Flemal, R., editors, *Theories of Landform Development*, pages 87–102. George Allen & Unwin.

Hamdouni, R., Irigaray, C., Fernandez, T., Chacon, J., and Keller, E. (2008). Assessment of relative tectonics, southwest border of the Sierra Nevada (southern Spain). *Geomorphology*, 96:150–173.

Hancock, G. and Anderson, R. (2002). Numerical modeling of fluvial strath-terrace formation in response to oscillating climate. *Geological Society of America Bulletin*, 114(9):1131–1142.

Hancock, G., Anderson, R., and Whipple, K. (1998). Beyond power: Bedrock river incision process and form. In Tinkler, K. and Wohl, E., editors, *Rivers Over Rock: Fluvial Processes in Bedrock Channels*, volume 107 of *Geophysical Monograph*, pages 35–60. American Geophysical Union.

Harkins, N., Kirby, E., Heimsath, A., Robinson, R., and Reiser, U. (2007). Transient fluvial incision in the headwaters of the Yellow River, northeastern Tibet, China. *Journal of Geophysical Research*, 112(F03S04).

Hartshorn, K., Hovius, N., Dade, W., and Slingerland, R. (2002). Climate-driven bedrock incision in an Active Mountain Belt. *Science*.

Hasbargen, L. and Paola, C. (2000). Landscape instaibility in an experimental drainage basin. *Geology*, 28:1,067–1,070.

Haviv, I., Enzel, Y., Whipple, K., Zilberman, E., Stone, J., Matmon, A., and Fifield, L. (2006). Amplified erosion above waterfalls and oversteepened bedrock reaches. *Journal of Geophysical Research*.

Haviv, I., Enzel, Y., Whipple, K., Zilberman, E., Stone, J., Matmon, A., and Fifield, L. (2010). Evolution of vertical knickpoint (waterfalls) with resistant caprock: Insights from numerical modeling. *Journal of Geophysical Research*, 115(F03028).

Hayakawa, Y. and Matsukura, Y. (2003). Recession rates of waterfalls in Boso Peninsula, Japna and a predictive equation. *Earth Surface Processes and Landforms*, 28:675–684.

Hayakawa, Y. and Matsukura, Y. (2009). Factors influencing the recession rate of Niagara Falls since the 19th century. *Geomorphology*, 110:212–216.

Heller, P., Beland, P., Humphrey, N., Konrad, S., Lynds, R., McMillan, M., Valentine, K., Widman, Y., and Furbish, D. (2001). Paradox of downstream fining and weathering-rind formation in the lower Hoh River, Olympic Peninsula, Washington. *Geology*, 29:971–974.

Holbrook, J. and Schumm, S. (1999). Geomorphic and sedimentary response of rivers to tectonic deformation: a brief review and critique of a tool for recognizing subtle epeirogenic deformation in modern and ancient setting. *Tectonophysics*, 305:287–306.

Holland, W. and Pickup, G. (1976). Flume study of knickpoint development in stratified sediment. *Geological Society of America Bulletin*, 87:76–82.

Horton, R. (1945). Erosional development of streams and their drainage basins: hydrophysical approach to quantitative morphology. *Geological Society of America Bulletin*, 56:275–370.

Hovius, N., Stark, C., and Allen, P. (1997). Sediment flux from a mountain belt derived by landslide mapping. *Geology*, 25:231–234.

Hovius, N., Stark, C., Hao-Tsu, C., and Jiun-Chuan, L. (2000). Supply and removal of sediment in a landslide-dominated mountian belt: Central Range, Taiwan. *Journal of Geology*.

Howard, A. (1994). A detachment-limited model of drainage basin evolution. *Water Resources Research*, 30(7):2261–2285.

Howard, A. (1998). Long profile development of bedrock channels: interactions of weathering, mass wasting, bed erosion and sediment transport. In Tinkler, K. and Wohl, E., editors, *Rivers Over Rock: Fluvial Processes in Bedrock Channels*, number 107 in Geophysical Monograph. American Geophysical Union, USA.

Howard, A., Dietrich, W., and Seidl, M. (1994). Modeling fluvial erosion on regional to continental scales. *Journal of Geophysical Research*, 99(B7):13971–13986.

Howard, A. and Kerby, G. (1983). Channels changes in badlands. *Geological Society of America Bulletin*, 94(6):739–752.

Hubbard, A., Bradwell, T., Golledge, N., Hall, A., Patton, H., Sugden, D., Cooper, R., and Stoker, M. (2009). Dynamic cycles, ice streams and their impact on the extent, chronology and deglaciation of the British-Irish ice sheet. *Quaternary Science Reviews*, 28:758–776.

Humphrey, N. and Konrad, S. (2000). River incision or diversion in response to bedrock uplift. *Geology*, 28(1):43–46.

ITC (2005). Integrated Land and Water Information System (Ilwis). Technical report, Faculty of Geo-Information Science and Earth Observation.

Jansen, J. (2006). Flood magnitude-frequency and lithology control on bedrock river incision in post-orogenic terrain. *Geomorphology*.

Jansen, J., Codilean, A., Bishop, P., and Hoey, T. (2010). Scale dependence of lithological control on topography: bedrock channel geometry and catchment morphometry in western Scotland. *Journal of Geology*, 118:223–246.

Jardine, W. (1982). Sea-level changes in Scotland during the last 18,000 years. *Proceedings of the Geological Association*, 93(1):25–41.

Jenson, S. and Domingue, J. (1988). Extracting topographic structure from Digital Elevation Data for Geographic Information System Analysis. *Photogrammetric Engineering and Remote Sensing*, 54:1593–1600.

Johnson, J., Whipple, K., Sklar, L., and Hanks, T. (2009). Transport slopes, sediment cover and bedrock channel incision in the Henry Mountains, Utah. *Journal of Geophysical Research*.

Johnson, M. (1991). Geology of Scotland. In Craig, G., editor, *Geology of Scotland*, chapter Dalradian. The Geological Society, London.

Kirby, E. and Whipple, K. (2001). Quantifying differential rock-uplift rates via stream profile analysis. *Geology*, 29(5):415–418.

Knighton, A. (1980). Longitudinal changes in size and sorting of stream-bed material in four English rivers. *Geological Society of America Bulletin*, 91:55–62.

Knighton, D. (1998). *Fluvial forms and processes*. Hodder Arnold, London and New York.

Kooi, H. and Beaumont, C. (1996). Large-scale geomorphology: Classical concepts reconciled and integrated with contemporary ideas via a surface process model. *Journal of Geophysical Research*, 101(B2):3361–3386.

Laeter, J. (1998). Mass spectrometry and geochronology. *Mass Spectrometry Reviews*, 17:97–125.

Lal, D. (1988). In situ-produced cosmogenic isotopes in terrestrial rocks. *Annual Review Earth Planetary Sciences*, 16:355–88.

Lal, D. (1991). Cosmic ray labeling of erosion surfaces: in situ nuclide production rates and erosion models. *Earth and Planetary Science Letters*, 104:424–439.

Lal, J. (1987). Cosmogenic nuclides produced in situ in terrestrial solids. *Nuclear Instruments and Methods in Physics Research*, B29:238–245.

Lamb, M. and Dietrich, W. (2009). The persistence of waterfalls in fractured rock. *Geological Society of America Bulletin*, 121:1,123–1,134.

Lambeck, K. (1991). Glacial rebound and sea-level change in the British Isles. *Terra Nova*, 3:379–389.

Lambeck, K. (1993a). Glacial rebound of the British Isles -II. A high-resolution, high precision model. *Geophysical Journal International*, 115:960–990.

Lambeck, K. (1993b). Glaciar rebound of the British Isles - I Preliminary model results. *Geophysical Journal International*, 115:941–959.

Lambeck, K. (1995). Late Devensian and Holocene shorelines of the British Isles and North Sea from models of glacio-hydro-isostatic rebound. *Journal of the Geological Society of London*, 152:437–448.

Lambeck, K., Yokoyama, Y., Johnston, P., and Purcell, A. (2000). Global ice volumes at the Last Glacial Maximum and early Lateglacial. *Earth and Planetary Science Letters*, 181:513–527.

Larue, J. (2008). Effects of tectonics and lithology on long profiles of 16 rivers of the southern Central Massif border between the Aude and the Orb (France). *Geomorphology*, 93:343–367.

Lavé, J. and Avouac, P. (2001). Fluvial incision and tectonic uplift across the Himalayas of central Nepal. *Journal of Geophysical Research*, 106(B11):26561–26591.

Leland, J., Reid, M., Burbank, D., Finkel, R., and Cafee, M. (1998). Incision and differential bedrock uplift along the Indus River near Nangat Parbat, Pakistan Himalaya, from ^{10}Be and ^{26}Al exposure age dating of bedrock straths. *Earth and Planetary Science Letters*, 194(93-107).

Leopold, L. and Bull, W. (1979). Base level, aggradation, and grade. *Proceeding of the American Philosophical Society*, 123:168–202.

Leopold, L., Wolman, G., and Miller, J. (1964). *Fluvial Processes in Geomorphology*. Dover Publications, USA.

Lifton, N., Smart, D., and Shea, M. (2008). Scaling time-integrated in situ cosmogenic nuclide production rates using continou geomagnetic model. *Earth and Planetary Science Letters*, 268:190–201.

Loget, N. and van den Driesseche, J. (2009). Wave train model for knickpoint migration. *Geomorphology*.

Lopez, A. (1995). Trends in the Pattern and Variability of Rainfall in the Loch Lomond Basin, Scotland. Master's thesis, University of Glasgow, Great Britain. M.Sc. Thesis.

MacGregor, K., Anderson, R., Anderson, S., and Waddington, E. (2000). Numerical simulations of glacial-valley longitudinal profile evolution. *Geology*, 28(11):1037–1034.

Mackin, J. (1948). Concept of graded river. *Bulletin of the Geological Society of America*, 59:463–512.

Mark, D. (1975). Geomorphic parameters: a review and evaluation. *Geografiska Annaler*, 57(3/4):165–167.

Marsh, T. and Hannaford, J. (2008). *UK Hydrometric Register. Hydrological data UK series*. Centre for Ecology and Hydrology, United Kingdom.

MathWorks, T. (2007). *MATLAB 2007a*. The MathWorks, http://www.mathworks.com.

McCann, S. (1964). The raised beaches of north-east Islay and western Jura, Argyll. *Transactions of the Institute of British Geographers*, 35:1–16.

McKeown, F., Jones-Cecil, M., Askew, B., and McGrath, M. (1988). Analysis of stream-profile data and inferred tectonic activity, eastern Ozark Mountains Region.

McPherson, H. (1971). Donwstream changes in sediment character in high energy mountain stream channel. *Artic and Alpine Research*, 31(1):65–79.

Merrits, D., Vincent, K., and Wohl, E. (1994). Long river profiles, tectonism and eustasy: A guide to interpreting fluvial terraces. *Journal of Geophysical Research*, 99(B7):14031–14050.

MetOffice (2010). The UK's National Weather Service. http://www.metoffice.gov.uk.

Miller, J. (1991). The influence of bedrock geology on knickpoint development and channel-bed degradation along downcutting streams in south-central Indiana. *Journal of Geology*, 99:591–605.

Milne, G., Shennan, I., Youngs, B., Waugh, A., Teferie, F., Bingley, R., Bassett, S., C., C.-B., and Bradley, S. (2006). Modelling the glacial isostatic adjusment of the UK region. *Philosophyical Transactions fot the Royas Society A*, 364:931–948.

Molin, P., Pazzaglia, F., and Dramis, F. (2004). Geomorphic expression of active tectonics in a rapidly-deforming forearc, Sila Massif, Calabria Southern Italy. *American Journal of Science*.

Molnar, P., Anderton, R., and Anderson, S. (2007). Tectonics, fracturing of rock, and erosion. *Journal of Geophysical Research*, 112(F03014).

Molnar, P. and England, P. (1990). Late Cenozoic uplift of mountain ranges and global climate change: chicken or egg. *Nature*, 346:29–34.

Montgomery, D. (1994). Valley incision and the uplift of mountain peaks. *Journal of Geophysical Research*, 99(B7):13913–13921.

Montgomery, D. (2001). Slope distributions, threshold hillslopes and steady-state topography. *American Journal of Science*, 301:432–454.

Montgomery, D. (2003). Predicting landscape-scale erosion rates using digital elevation models. *Comptes Rendus Geoscience*.

Montgomery, D. (2004). Observations on the role of lithology in strath terrace formation and bedrock channel width. *American Journal of Science*, 304:454–476.

Montgomery, D. and Dietrich, W. (1989). Source areas, drainage density, and channel initiation. *Water Resources Research*, 25:1907–1918.

Montgomery, D. and Foufoula-Georgiou, E. (1993). Channel network source respresentation using digital elevation models. *Water Resources Research*, 29(12):3925–3934.

Montgomery, D. and Gran, K. (2001). Downstream variations in the width of bedrock channels. *Water Resources Research*, 37(6):1841–1846.

Moran, J. and Bryson, R. (1969). The contribution of Laurentide Ice wastage to eustatic rise of sea level: 10,000 to 6,000 BP. *Artic and Alpine Research*, 1(2):97–104.

Muzikar, P. (2008). Cosmogenic nuclide concentrations in episodically eroding surfaces: Theoretical results. *Geomorphology*, 97:407–413.

Muzikar, P. (2009). General models for episodic surface denudation and its measurements by cosmogenic nuclides. *Quaternary Geochronology*, 4:50–55.

Niemann, J., Gasparini, N., Tucker, G., and Bras, R. (2001). A quantitative evaluation of Playfair's Law and its use in testing long-term erosion models. *Earth Surface Processes and Landforms*, 26:1317–1332.

Nishiizumi, K., Inamura, M., Caffe, M., Southon, J., Finkel, R., and McAninch, J. (2007). Absolute calibration of ^{10}Be AMS standards. *Nuclear Instruments and Methods in Physics Research B*, 258:403–413.

Nishiizumi, K., Kohl, C., Arnold, J., Dorn, R., Klein, J., Fink, D., Middleton, R., and Lal, D. (1993). Role of in situ cosmogenic nuclides ^{10}Be and ^{26}Al in the study of diverse geomorphic processes. *Earth Surface Processes and Landforms*, 18:407–425.

Nishiizumi, K., Lal, D., Klein, J., Middleton, R., and Arnold, J. (1986). Production of ^{10}Be and ^{26}Al by cosmic rays in terrestrial quartz in situ and implications for erosion rates. *Nature*, 319:134–136.

Nishiizumi, K., Winterer, E., Kohl, C., and Klein, J. (1989). Cosmic ray production rates of ^{10}Be and ^{26}Al in quartz from glacially polished rocks. *Journal of Geophysical Research*, 94(B12):17,907–17,915.

Ouimet, W., Whipple, K., and Granger, D. (2009). Beyond threshold hillslope: Channel adjustment to base-level fall in tectonically active mountain ranges. *Geology*.

Pan, D., Burbank, D., Wu, G., Li, J., and Guan, Q. (2003). A 900 k.y. record of strath terrace formation during glacial-interglacial transitions in northwest China. *Geology*, 31(11):957–960.

Peltier, W. (1996). Mantle viscosity and ice-age ice sheet topography. *Science*, 273:1359–1364.

Peltier, W. and Fairbanks, R. (2006). Global glacial ice volume and Last Glacial Maximum duration from an extended Barbados sea level record. *Quaternary Science Reviews*, 25:3322–3337.

Peltier, W., Shennan, I., Drummond, R., and Horton, B. (2002). On the postglacial isostatic adjusment of the British Isles and the shalow viscoelastic structure of the Earth. *Geophysical Journal International*, 148:443–475.

Philbrick, S. (1970). Horizontal configuration and the rate of erosion of Niagara Falls. *Geological Society of America Bulletin*, 81:3723–3732.

Phillips, J. and Lutz, J. (2008). Profile convexities in bedrock and alluvial streams. *Geomorphology*.

Phillips, J., McCormack, S., Duan, J., Ruso, J., Schumacher, A., Triparthi, G., Brockman, R., Mays, A., and Pulugurtha, S. (2010). Origin and interpretation of knickpoints in the Big South Fork River basin, Kentuchy-Tenessee. *Geomorphology*, 14:188–198.

Pike, R. (2000). Geomorphometry -diversity in quantitative surface analysis. *Progress in Physical Geography*, 24(1):1–20.

Pike, R. and Wilson, S. (1971). Elevation-Relief ration, hypsometric integral and geomorphic area-altitude analysis. *Geological Society of America Bulletin*, 82:1079–1084.

Pratt-Sitaula, B., Burbank, D., Heimsath, A., and Ojha, T. (2004). Landscape disequilibrium on 1000-10,000 year scales Marsyandi River, Nepal, central Himalaya. *Geomorphology*, 58:223–241.

R Development Core Team (2009). *R: A Language and Environment for Statistical Computing*. R Foundation for Statistical Computing.

Reinhardt, L., Bishop, P., Hoey, T., Dempster, T., and Sanderson, D. (2007a). Quantification of the transient response to base-level fall in a small mountain catchment: Sierra Nevada, southern Spain. *Journal of Geophysical Research*, 112(F03S05).

Reinhardt, L., Hoey, T., Barrows, T., Dempster, T., Bishop, P., and Fifield, L. (2007b). Interpreting erosion rates from cosmogenic radionuclide concentrations measured in rapidly eroding terrain. *Earth Surface Processes and Landforms*, 32:390–406.

Reusser, L., Bierman, P., Pavich, M., Zen, E.-a., Larsen, J., and Finkel, R. (2004). Rapid late pleistocene incision of Atlantic Passive-Margin river gorges. *Science*, 3:499–502.

Rice, R. (1977). *Fundamentals of Gemorphology*. Longman, New York.

Rigon, R., Rodriguez-Iturbe, I., Maritan, A., Giacometti, A., Tarboton, D., and Rinaldo, A. (1996). On Hack's law. *Water Resources Research*, 32(11):3,367–3,374.

Rosenbloom, N. and Anderson, R. (1994). Hillslope and channel evolution in a marine terraced landscape, Santa Cruz, California. *Journal of Geophysical Research*, 99(B7):14013–14029.

Safran, E., Bierman, P., Aalto, R., Dunne, T., Whipple, K., and Caffe, M. (2005). Erosion rates driven by channel network incision in the Bolivian Andes. *Earth Surfaces Processes and Landforms*, 30:1007–1024.

Schaller, M., Hovius, N., Willet, D., Ivy-Ochs, S., Synal, H., and Chen, M. (2005). Fluvial bedrock incision in the active mountain belt of Taiwan from in-situ produced cosmogenic nuclides. *Earth Surface Processes and Landforms*, 30:955–971.

Schoenbohm, L., Whipple, K., and Burchfiel, B. (2004). Geomorphic constrains on surface uplift, exhumation and plateau growth in the Red River region, Yunnan Province, China. *Geological Society of America Bulletin*, 116(7-8):895–909.

Schumm, S. and Stevens, M. (1973). Abrasion in place: a mechanism for rounding and size reduction of coarse sediment in rivers. *Geology*, 1:37–40.

Seidl, M., Dietrich, a., and Kirchner, W. (1994). Longitudinal profile development into bedrock: An analysis of Hawaiian channels. *Journal of Geology*, 102:457–474.

Seidl, M. and Dietrich, W. (1992). The problem of channel erosion into bedrock. In Schmidth, K. and de Ploey, J., editors, *Functional Geomorphology*, volume 23 of *Catena Supplement*, pages 101–124. Catena Verlag.

Seidl, M., Finkel, R., Caffe, M., Bryant, G., and Dietrich, W. (1997). Cosmogenic isotope analysis applied to river longitudinal profile evolution: problems and interpretations. *Earth Surface Processes and Landforms*, 22:125–209.

Sejrup, H., Hjelstuen, B., K.I., T. D., Haflidason, H., Kuijpers, A., Nygard, A., Praeg, D., Stoker, M., and Vorren, T. (2005). Pleistocene glacial history of the NW European continental margin. *Marine and Petroleum Geology*, 22:1111–1129.

Selby, M. (1985). *Earth's Changing Surface: An Introduction to Geomorphology*. Oxford University Press, Great Britain.

Seong, Y., Owen, L., Bishop, M., Bush, A., Clendon, P., Copland, L., Finkel, R., Kamp, U., and Shroeder, J. (2008). Rates of fluvial bedrock incision within an actively uplifting orogen: Central Karakoram Mountains, northern Pakistan. *Geomorphology*, 97:274–286.

Shackleton, N. and Opdyke, N. (1973). Oxygen isotope and palaeomagnetic stratigraphy of equatorial Pacific core V28-238: Oxygen isotope temperatures and ice volumes on a 10000 year and 1000000 year scale. *Quaternary International*, 3:39–55.

Sharma, V. (1984). The Fennoscandian uplift and glacial isostasy. *Tectonophysics*, 105:249–262.

Shennan, I., Hamilton, S., Hillier, C., Hunter, A., Woodall, R., Bradley, S., Milne, G., Brooks, A., and Bassett, S. (2006). Relative sea-level observations in western Scotland since the Last Glacial Maximum for testing models of glacial isostatic land movements and ice-sheets reconstructions. *Quaternary Science*, 21:601–613.

Shennan, I. and Horton, B. (2002). Holocene land and sea-level changes in Great Britain. *Journal of Quaternary Science*, 17(5-6):511–526.

Shennan, I., Peltier, R., Drummond, R., and Horton, B. (2002). Global to local scale parameters determining relative sea-level changes and the post-glacial isostatic adjustment of Great Britain. *Quaternary Science Reviews*, 21:397–408.

Shepherd, R. (1972). Incised river meanders: Evolution in simulated bedrock. *Science*, 178:409–411.

Shepherd, R. and Schumm, S. (1974). Experimental study of river incision. *Geological Society of America Bulletin*, 85:257–268.

Sinha, S. and Parker, G. (1996). Causes of concavity in longitudinal profile of rivers. *Water Resources Research*, 32(5):1417–1428.

Sissons, J. (1974). Late-glacial marine erosion in Scotland. *Boreas*, 3:41–48.

Sissons, J. (1979). The Loch Lomond Stadial in the British Isles. *Nature*, 280(199-203).

Sissons, J. (1981a). British shore platforms and ice-sheets. *Nature*, 291:473–475.

Sissons, J. (1981b). The last Scottish ice-sheet: facts and speculative discussion. *Boreas*, 10:1–17.

Sissons, J. (1982). The so-called high 'interglacial' rock shoreline of Western Scotland. *Transactions of the Institute of British Geographers*, 7(2):205–216.

Sissons, J. (1983). The Quaternary geomorphology of the Inner Hebrides: a review and reassesment. *Proceedings of the Geological Association*, 94(2):165–175.

Sissons, J. and Cornish, R. (1982). Differential glacio-isostatic uplift of crustal blocks at Glen Roy, Scotland. *Quaternary Research*, 18:268–288.

Sissons, J. and Dawson, A. (1981). Former sea-levels and ice limits in part of Wester Ross, northwest Scotland. *Proceedings of the Geological Association*, 92(2):115–124.

Sissons, J., Smith, D., and Cullingford, R. (1966). Late-Glacial and Post-Glacial shorelines in South-East Scotland. *Transactions of the Institute of British Geographers*, 39:9–18.

Sjöberg, L., Pan, M., Asenjo, E., and Erlingsson, S. (2000). Glacial rebound near Vatnajójull, Iceland, studied by GPS campaigns in 1992 and 1996. *Journal of Geodynamics*, 29(63-70).

Sklar, L. and Dietrich, W. (1998). River longitudinal profiles and bedrock incision models: stream power and the influence of sediment supply. In Tinkler, K. and Wohl, E., editors, *Rivers Over Rock: Fluvial Processes in Bedrock Channels*, number 107 in Geophysical Monograph. American Geophysical Union, USA.

Sklar, L. and Dietrich, W. (2001). Sediment and rock strength controls on river incision into bedrock. *Geology*, 29(12):1987–1090.

Sklar, L. and Dietrich, W. (2004). A mechanistic model for river incision into bedrock by saltating bed load. *Water Resources Research*, 40.

Sklar, L. and Dietrich, W. (2006). The role of sediment in controlling steady-state bedrock channel slope: Implications of the saltation-abrasion incision model. *Geomorphology*, 82:58–83.

Small, E., Anderson, R., Repka, J., and Finkel, R. (1997). Erosion rates of alpine bedrock summit surfaces deduced from insitu ^{10}Be and ^{26}Al. *Earth and Planetary Science Letters*, 150:413–425.

Smith, D., Cullingford, R., and Firth, C. (2000). Patterns of isostatic lands uplift during the Holocene: evidence from mainland Scotland. *The Holocene*, 10(4):489–501.

Smith, D., Cullingford, R., Mighall, T., Jordan, J., and Fretwell, P. (2007). Holocene relative sea level changes in glacio-isostatic area: New data from south-west Scotland, United Kingdom. *Marine Geology*, 242:5–26.

Smith, D., Fretwell, P., Cullingford, R., and Firth, C. (2006). Toward improved empirical isobase models of Holocene land uplift for mainland Scotland, UK. *Philosofical Transactions fot the Royas Society A*, 364:949–972.

Snow, S. and Slingerland, R. (1987). Mathematical modeling of graded river profiles. *Journal of Geology*, 95:15–33.

Snyder, N., Whipple, K., Tucker, G., and Merrits, D. (2000). Landscape response to tectonic forcing: Digital elevation model analysis of stream profiles in the Mendocino triple junction region, northern California. *Geological Society of America Bulletin*, 112(8):1250–1263.

Snyder, N., Whipple, K., Tucker, G., and Merrits, D. (2002). Interactions between onshore bedrock-channel incision and nearshore wave-base erosion forced by eustasy and tectonics. *Basin Research*, 14:105–127.

Snyder, N., Whipple, K., Tucker, G., and Merrits, D. (2003). Channel response to tectonic forcing: Field analysis of stream morphology in the Mendocino triple junction region, northern California. *Geomorphology*, 53:97–127.

Stamp, D. and Beaver, S. (1971). *The British Isles: A Geographic and Economic Survey*. Longman, London.

Stark, C., Foufoula-Georgiou, E., and Ganti, V. (2009). A non local theory of sediment buffering and bedrock channel evolution. *Journal of Geophysical Research*.

Stock, G., Anderson, R., and Finkel, R. (2005a). Rates of erosion and topographic evolution of the Sierra Nevada, California, inferred from cosmogenic ^{26}Al and ^{10}Be concentrations. *Earth Surface Processes and Landforms*, 30:985–1006.

Stock, J. and Montgomery, D. (1999). Geologic constrains on bedrock river incision using the stream power law. *Journal of Geophysical Research*, 104(B3):4983–4993.

Stock, J., Montgomery, D., Collins, B., Dietrich, W., and Sklar, L. (2005b). Field measurements of incision rates following bedrock exposure: Implications for process controls on the long profiles of valley cut by rivers and debris flow. *Geological Society of America Bulletin*, 117(11-12):174–194.

Stolar, D., Willet, S., and Montgomery, D. (2007). Characterization of topographic steady state in Taiwan. *Earth and Planetary Science Letters*, 261:421–431.

Stone, J. (2000). Air pressure and cosmogenic isotope production. *Journal of Geophysical Research*, 105(B10):23753–23759.

Stone, J., Lambeck, K., Fifield, L., Evans, J., and Cresswell, R. (1996). A lateglacial age for the main rock platform, western Scotland. *Geology*, 24:707–710.

Strahler, A. (1952). Hypsometric (area-altitude) analysis of erosional topography. *Bulletin of the Geological Society of America*, 63:1117–1142.

Summerfield, M. (1991). *Global Geomorphology.* Pearson Prentice Hall, Great Britain.

Synge, F. and Stephens, N. (1966). Late and Post-Glacial shorelines, and ice limits in Argyll and north-east Ulster. *Transactions of the Institute of British Geographers*, 39:101–125.

Tarboton, D., Bras, R., and Rodriguez-Iturbe, I. (1991). On the extraction on channel networks from digital elevation data. *Hydrological Processes*, 5:81–100.

Tarboton, D., Bras, R., and Rodriguez-Iturbe, I. (1992). A physical basis for drainage density. *Geomorphology*, 5:59–76.

Thorn, C. (1988). *An Introduction to Theoretical Geomorphology.* Unwin Hyman, Great Britain.

Thorp, P. (1981). A trimline method for defining the upper limit of Loch Lomond Advance glaciers: examples from the Loch Leven and Glen Coe areas. *Scottish Journal of Geology*, 17:49–64.

Tinkler, K. and Wohl, E. (1998). A primer on bedrock channels. In Tinkler, K. and Wohl, E., editors, *Rivers Over Rock: Fluvial Processes in Bedrock Channels*, volume 107 of *Geophysical Monograph*, pages 1–18. American Geophysical Union.

Tomkin, J., Brandon, M., Pazzaglia, F., Barbour, J., and Willet, S. (2003). Quantitative testing of bedrock incision models for the Clearwater River, NW Washington State. *Journal of Geophysical Research*, 106(B6 2308).

Tucker, G. and Bras, R. (2000). A stochcastic approach to modeling the role of rainfall variability in drainage evolution. *Water Resources Research*, 36(7):1953–1964.

Tucker, G. and Hancock, G. (2010). Modelling lanscape evolution. *Earth Surface Processes and Landforms*, 34:28–50.

Tucker, G. and Whipple, K. (2002). Topographic outcomes predicted by stream erosion models: Sensitivity analysis and intermodel comparison. *Journal of Geophysical Research*, 107(B9 2179).

Turowski, J., Hovius, N., Wilson, A., and Horng, M. (2008). Hydraulic geometry, river sediment and the definition of bedrock channles. *Geomorphology*, 99:26–38.

Turowski, J., Lague, D., and Hovius, N. (2007). Cover effect in bedrock abrasion: A new derivation and its implications for the modelling of bedrock channel morphology. *Journal of Geophysical Research*, 112(F04006).

van der Beek, P. and Bishop, P. (2003). Cenozoic river profile development in the Uppler Lachlan catchment (SE Australia) as a test of quantitative fluvial incision models. *Journal of Geophysical Research*, 108(B6).

VanLaningham, S., Meigs, A., and Goldfinger, C. (2006). The effects of rock uplift and rock resistance on river morphology in a subduction zone forearc, Oregon, USA. *Earth Surface Processes and Landforms*, 31:1257–1279.

von Engeln, O. (1940). A particular case of knickpunkte. *Annals of the Association of American Geographers*, 30:268–271.

Walcott, R. (1973). Structure of the Earth from X100001 glacio-isostatic rebound. *Annual Review of Planetary and Science Letters*, 1:15–37.

Walker, J. and Willgoose, G. (1999). On the effect of digital elevation model accuracy on hydrology and geomorphology. *Water Resources Research*, 35:2,259–2,268.

Wegmann, K. and Pazzaglia, F. (2002). Holocene strath-terraces, climate change and active tectonics: The Clearwater River basin, Olympic Peninsula, Washington State. *Geological Society of America Bulletin*, 114(6):731–744.

Whipple, K. (2001). Fluvial landscape response time: how plausible is steady-state denudation? *American Journal of Science*, 301:313–325.

Whipple, K. (2004). Bedrock rivers and the geomorphology of active orogens. *Annual Review Earth Planetary Sciences*, 32:151–185.

Whipple, K., Hancock, G., and Anderson, R. (2000a). River incision into bedrock: Mechanics and relative efficacy of plucking, abrasion and cavitation. *Geological Society of America Bulletin*, 112(3):490–503.

Whipple, K., Snyder, N., and Dollenmayer, K. (2000b). Rates and processes of bedrock incision by the Upper Ukak River since the 1912 Novarupta ash flow in the Valley of Ten Thousand Smokes. *Geology*, 28(9):835–838.

Whipple, K. and Tucker, G. (1999). Dynamics of the stream-powr model: Implications for the height limits of mountain ranges, landscape response timescales and research needs. *Journal of Geophysical Research*, 104(B8):17661–17674.

Whipple, K. and Tucker, G. (2002). Implications of sediment-flux-dependent river incision models for landscape evolution. *Journal of Geophysical Research*, 107(B2).

Whittaker, A., Attal, M., and Allen, P. (2010). Characterising the origin, nature and fate of sediment sorted from catchments perturbed by active tectonics. *Basin Research*, 22:809–828.

Whittaker, A., Attal, M., Cowie, P., Tucker, G., and Roberts, G. (2008). Decoding temporal and spatial patterns of fault uplift using transient river long profiles. *Geomorphology*, 100:506–526.

Whittaker, A., Cowie, P., Attal, M., Tucker, G., and Roberts, G. (2007). Bedrock channel adjustment to tectonic forcing: Implications for predicting river incision rates. *Geology*, 35(2):103–106.

Willemin, J. (2000). Hack's law: sinuosity, convexity, elongation. *Water Resources Research*, 36(11):3,365–3,374.

Willet, S. (1999). Orogeny and orography: The effecs of erosion on the structure of mountain belts. *Journal of Geophysical Research*, 104(B12):28,957–28,981.

Willgoose, G., Bras, R., and Rodriguez-Iturbe, I. (1991). A phyisical explanation of an observed link area-slope relationship. *Water Resources Research*, 27(7):1697–1702.

Wobus, C., Crosby, B., and Whipple, K. (2006a). Hanging valleys in fluvial systems: Controls on the occurrence and implications for landscape evolution. *Journal of Geophysical Research*, 111(F02017).

Wobus, C., Kean, J., Tucker, G., and Anderson, R. (2008). Modeling the evolution of channel shape: Balancing computational effiency with hydraulic fidelity. *Journal of Geophysical Research*, 113.

Wobus, C., Whipple, K., Kirby, E., Snyder, N., Johnson, J., Spyropolou, K., Crosby, B., and Sheenan, D. (2006b). Tectonics from topography: Procedures, promise and pitfalls. In Willet, S., Hovious, N., Brandon, M., and Fisher, D., editors, *Tectonics, climate and landscape evolution*, number 398 in Special Paper, pages 55–74. Geological Society of America.

Wohl, E. (2004). Limits to downstream hydraulic geometry. *Geology*, 35(10):897–900.

Wohl, E. (2008). The effect of bedrock jointing on the formation of straths in the Cache la Pouldre River drainage, Colorado Front Range. *Journal of Geophysical Research*, 113(F01007).

Wohl, E. and Ikeda, H. (1997). Experimental simulation of channel incision into a cohesive substrate at varying gradients. *Geology*, 25(24):295–298.

Wohl, E. and Ikeda, H. (1998). Patterns of bedrock channel erosion on the Boso Peninsula, Japan. *Journal of Geology*, 106:331–345.

Wohl, E. and Merritt, D. (2001). Bedrock channel morphology. *Geological Society of America Bulletin*, 113(9):1205–1212.

Wolman, G. (1954). A method of sampling coarse river-bed material. *Transactions Americal Geophysical Union*, 35(6):951–956.

Wolman, G. (1987). Sediment movement and knickpoint behaviour in a small piedmont drainage basin. *Geografiska Annaler*, 69(1):5–14.

Wright, W. (1911). On a preglacial shoreline in the western isles of Scotland. *The Geological Magazine*, 3:97–107.

Wyrick, R. and Pasternack, G. (2008). Modeling energy dissipation and hydrulic jump regime responses to channel nonuniformity at river steps. *Journal of Geophysical Research*, 113(F03003).

Yanites, B. and Tucker, G. (2010). Controls and limits on bedrock channel geometry. *Journal of Geophysical Research*, 115(F04019).

Yatsu, E. (1955). On the longitudinal profile of a graded river. *Transactions Americal Geophysical Union*, 36(4):211–219.

Zhang, W. and Montgomery, D. (1994). Digital elevation model grid size, landscape representation, and hydrological simulations. *Water Resources Research*, 30:1019–1028.